20 May 2005

Science

Vol. 308 No. 5725
Pages 1073–1208 $10

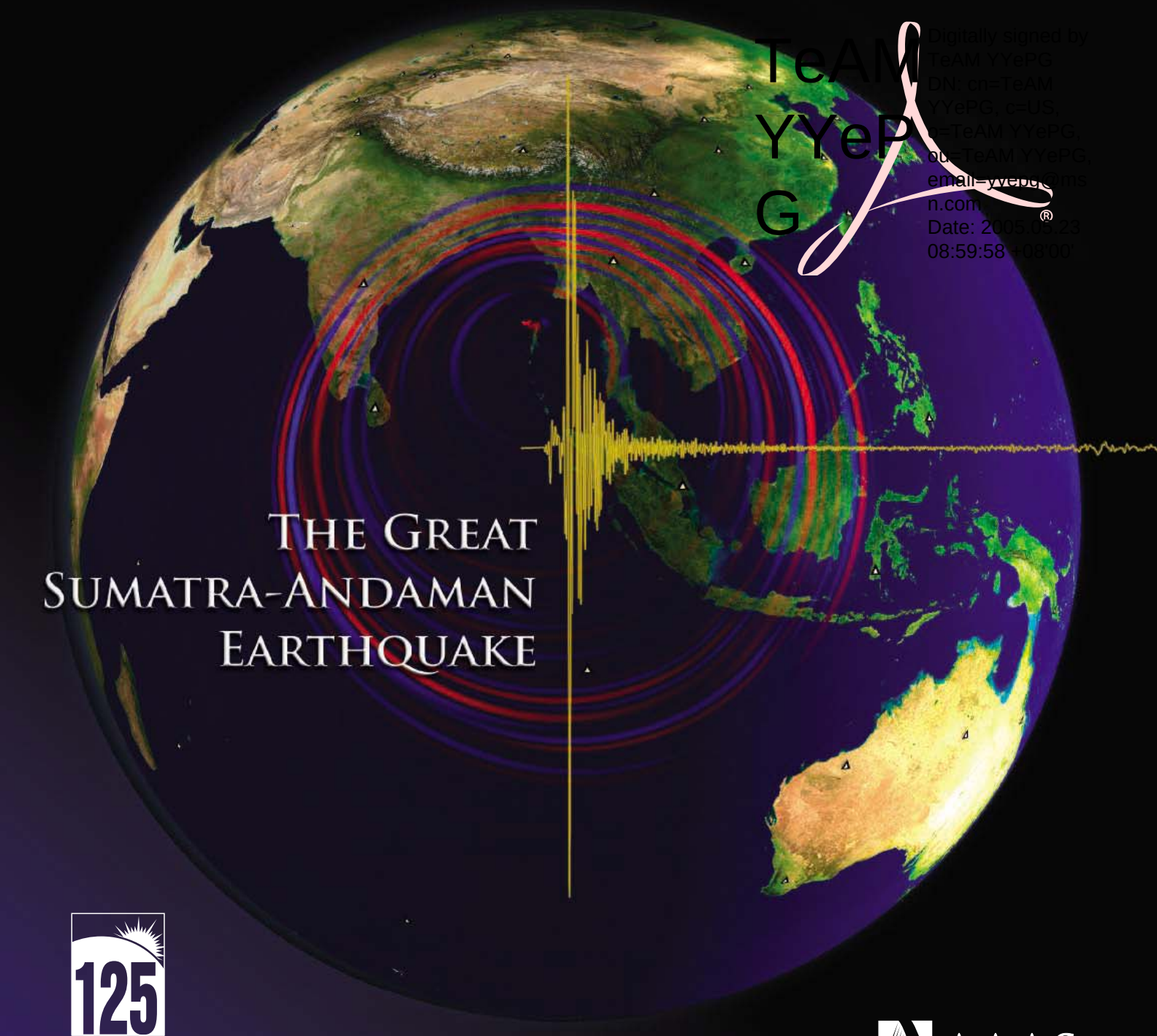

The Great Sumatra-Andaman Earthquake

125 YEARS OF GLOBAL Science

AAAS

The perfect assortment.

With GeneMorph® mutagenesis kits, a balanced spectrum of mutations is right at your fingertips.

GeneMorph® random mutagenesis kits* feature our patented Mutazyme® II DNA polymerase, which delivers a balanced mutational spectrum with more robust yields than *Taq* polymerase under error-prone PCR conditions. This allows you to discover more key residues responsible for protein function easier and faster than before, thus enhancing the evolution of your protein.

- **Simple protocol to control mutation frequency**
- **Efficient mutagenesis rates of 1 to 16 bases per kb**
- **Overcome poor PCR yield and mutational bias of *Taq* polymerase**

Our GeneMorph® II Kits include Mutazyme® II Polymerase, which delivers a balanced mutational spectrum.

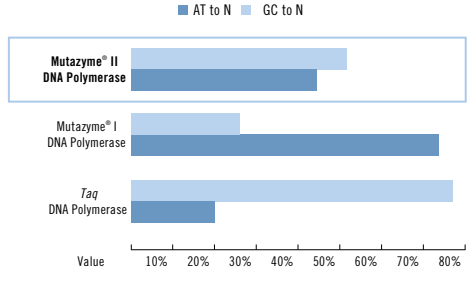

Need More Information? Give Us A Call:

Stratagene USA and Canada
Order: (800) 424-5444 x3
Technical Services: (800) 894-1304

Stratagene Europe
Order: 00800-7000-7000
Technical Services: 00800-7400-7400

Stratagene Japan K.K.
Order: 03-5159-2060
Technical Services: 03-5159-2070

* U.S. Patent No. 6,803,216 and patent pending

www.stratagene.com

Ask us about these great products:

GeneMorph® II Random Mutagenesis kit	30 rxns	200550
GeneMorph® II EZClone Domain Mutagenesis kit	10 rxns	200552

Purchase of these products is accompanied by a license to use them in the Polymerase Chain Reaction (PCR) process in conjunction with a thermal cycler whose use in the automated performance of the PCR process is covered by the up-front license fee, either by payment to Applied Biosystems or as purchased, i.e., an authorized thermal cycler.

STRATAGENE

TrueClone™ Collection

Over 24,000 *Authentic* Full-Length Human cDNA Clones

Authenticity stands the test of time. Is a copy compromising the value of your research?

Largest Collection	The most comprehensive source of over 24,000 individual full-length human genes including important gene families (560 protein kinases, 340 GPCRs, 68 NHRs, etc.)
Authentic Clone	Isolated directly from primary human cDNA libraries with no PCR artifacts
Expression-Ready	All genes are cloned downstream of a CMV promoter, ready for transfection and protein expression in mammalian cells
Quick Delivery	cDNA clones typically delivered within 72 hrs as purified plasmid DNA

Recent discovery made via HTP screening of over 10,000 genes from OriGene's TrueClone collection:

Identification of the Wnt Signaling activator leucine-rich repeat in Flightless interaction protein 2 by a genome-wide functional analysis. *Proc. Natl. Acad. Sci. 2005*

ORIGENE TECHNOLOGIES, INC.

888-267-4436 • www.origene.com

GE Healthcare

Ni Sepharose™

4x greater binding capacity in histidine-tagged protein purification

Ni Sepharose™ products from GE Healthcare give you the highest binding capacity available for histidine-tagged protein purification. With up to four times the binding capacity, it's no longer pure imagination to dramatically increase your yield, while saving time and costs. Maximum target protein activity is assured, thanks to tolerance of a wide range of additives and negligible nickel ion leakage. The flexibility to use a variety of protocols ensures the highest possible purity. Ni Sepharose 6 FF is excellent for manual procedures such as gravity/batch and easy scale-up, while the HP version is designed for high-performance in automated purification systems – both are available in different formats, including prepacked columns. Outstanding performance has never been easier to achieve.

www.amershambiosciences.com/his

imagination at work

GE10-05

Science

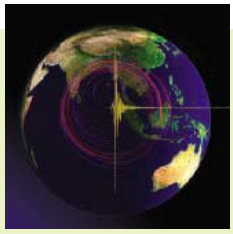

Special Issue

The Great Sumatra-Andaman Earthquake

Volume 308
20 May 2005
Number 5725

Spectral-element simulation of surface ground velocities (red up, blue down) 15.8 minutes after rupture initiation of the great 2004 Sumatra-Andaman earthquake. Seismogram shows 160 minutes of actual-amplitude vertical ground displacement recorded at Pallekele, Sri Lanka. See page 1127. [Image: S. Lombeyda, Caltech Center for Advanced Computing Research; V. Hjorleifsdottir and J. Tromp, Caltech Seismological Laboratory; R. Aster]

Departments

1104

News of the Week

1115

News Focus

Letters

Books *et al.*

Policy Forum

Contents continued

eppendorf PhysioCare Concept criteria 1 and 2

- Highest level of precision and ergonomics
- Pipettes for any application and budget
- Ceramic pistons
- Ergonomics approved by TÜV

A complete picture.

Integrated systems – Exceptional durability

PhysioCare Concept pipettes.
In this highly developed world shouldn't you be afforded the best possible work environment, one that is highly efficient and also satisfies your physiological needs? Absolutely.

Eppendorf helps you give it your best every day with optimum pipetting systems. Shorter work processes, reduced stress and low error rates will contribute to your total satisfaction with the new eppendorf **PhysioCare Concept**.

TÜV Rheinland approved our manual pipettes as: ergonomic, user-friendly and user tested.

PhysioCare concept

Check out how good your pipette really is!
PhysioCare Concept™ website
www.physiocare-concept.info

eppendorf

In touch with life

Your local distributor: www.eppendorf.com/worldwide · Application Hotline: +49 180-3 66 67 89
Eppendorf AG · Germany · +49 40 538 01-0 • Eppendorf North America, Inc. 800-645-3050

Perspectives

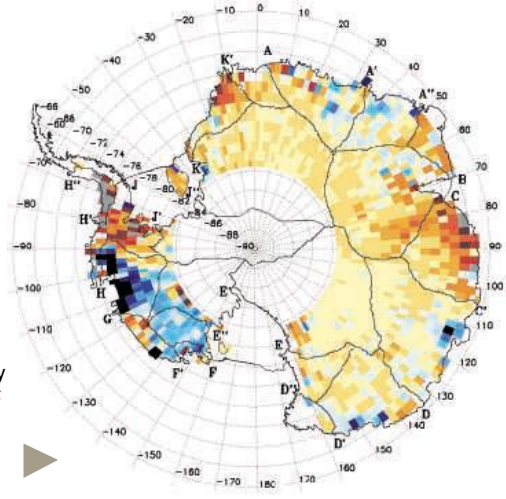

Science Express www.sciencexpress.org

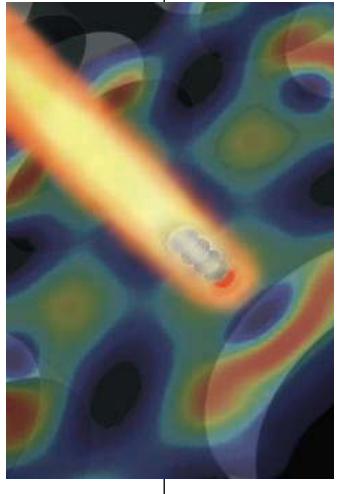

1122 &1158

Technical Comment Abstracts

Brevia

Research Article

Contents continued

GetInfo

science.labvelocity.com

Get the lab product info you need — FAST

Science announces a new online life science product information system, **GetInfo**, powered by **LabVelocity**

- Quickly find and request free information on products and/or services found in the pages of *Science* magazine
- Ask vendors to contact you with more information
- View detailed product information
- Link directly to vendors' websites

Visit GetInfo today at
science.labvelocity.com

Science
AAAS

Science

Reports

1103 &1161

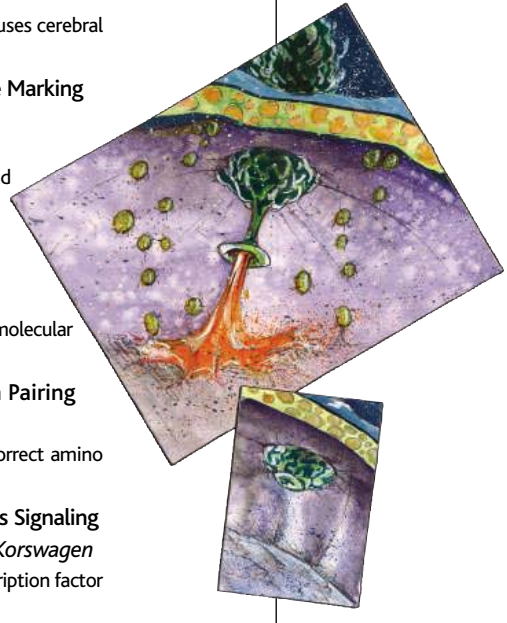

1174

AAAS
ADVANCING SCIENCE, SERVING SOCIETY

SCIENCE (ISSN 0036-8075) is published weekly on Friday, except the last week in December, by the American Association for the Advancement of Science, 1200 New York Avenue, NW, Washington, DC 20005. Periodicals Mail postage (publication No. 484460) paid at Washington, DC, and additional mailing offices. Domestic individual membership and subscription (51 issues): $135 ($74 allocated to subscription). Domestic institutional subscription (51 issues): $550; Foreign postage extra: Mexico, Caribbean (surface mail) $55; other countries (air assist delivery) $85. First class, airmail, student, and emeritus rates on request. Canadian rates with GST available upon request, GST #1254 88122. Publications Mail Agreement Number 1069624. **Printed in the U.S.A.**

Change of address: allow 4 weeks, giving old and new addresses and 8-digit account number. **Postmaster:** Send change of address to *Science*, P.O. Box 1811, Danbury, CT 06813–1811. **Single copy sales:** $10.00 per issue prepaid includes surface postage; bulk rates on request. **Authorization to photocopy** material for internal or personal use under circumstances not falling within the fair use provisions of the Copyright Act is granted by AAAS to libraries and other users registered with the Copyright Clearance Center (CCC) Transactional Reporting Service, provided that $15.00 per article is paid directly to CCC, 222 Rosewood Drive, Danvers, MA 01923. The identification code for *Science* is 0036-8075/83 $15.00. *Science* is indexed in the *Reader's Guide to Periodical Literature* and in several specialized indexes.

Contents continued ▶

iQ™5 Multicolor Real-Time PCR Detection System

Pass the iQ Test

What do all these images have in common? The answer is 5. Introducing the iQ5 real-time PCR detection system, bringing true five-color detection capabilities to all of your real-time PCR applications.

Five reasons why the iQ5 is the ultimate system for value and flexibility.

- **Powerful thermal gradient**
- **Open-platform optical system with user-changeable filter sets**
- **PCR sample quantitation with statistical summary for replicates**
- **Gene expression analysis by relative quantity (ΔC_T) or normalized expression ($\Delta\Delta C_T$)**
- **Customizable software reports that offer comprehensive summaries of assay run conditions, data graphs and tables, and data analysis parameters**

For more information, visit us on the Web at
www.bio-rad.com/products/iQ5/

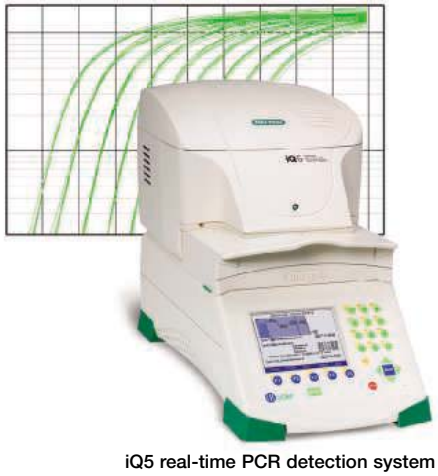

iQ5 real-time PCR detection system

Visit us on the Web at **discover.bio-rad.com**
Call toll free at 1-800-4BIORAD (1-800-424-6723);
outside the US, contact your local sales office.

BIO-RAD

Science
www.scienceonline.org

sciencenow www.sciencenow.org Daily News Coverage

Congress Can't Hide from Math
Network theory highlights partisanship in House of Representatives.

Drug Protects Injured Brains
Experimental treatment reduces postconcussion scarring in rats.

Sodium Has a Meltdown
Metal has bizarre properties at high pressures.

Breaking into science journalism.

science's next wave www.nextwave.org Career Resources for Young Scientists

Global: Starting a Career in Science Writing—Feature Index *A. Fazekas*
Next Wave explores issues that researchers face when trying to break into a career in science journalism.

Global/US: Some Thoughts on Becoming a Science Writer *J. Austin*
Our editor offers tips on making the transition from the scientific bench to published authorship.

Global/UK: Breaking into the Media—Do You Need Formal Training? *E. Pain*
To become a science writer in the U.K., should one go back to university?

Global/EU: Markets to Explore *A. Forde*
The media's interest in science ranges from newspapers and books to internal company reports.

US: Tooling Up—Managing Your Mentor for Career Sustainability *D. Jensen*
A recent book offers suggestions for managing the supervisor-subordinate relationship.

MiSciNet: FACES—Diversifying Engineering and Science *R. Arnette*
The Facilitating Academic Careers in Engineering and Science program aims to increase the number of African-American students receiving doctorates in engineering and science.

science's sage ke www.sageke.org Science of Aging Knowledge Environment

Perspective: MiMage—A Pan-European Project on the Role of Mitochondria in Aging
C. Scheckhuber and H. D. Osiewacz
European researchers focus on mitochondria to pinpoint conserved mechanisms of aging.

News Focus: Spring Forward *R. J. Davenport*
March babies hit menopause earliest.

Mitochondria and aging.

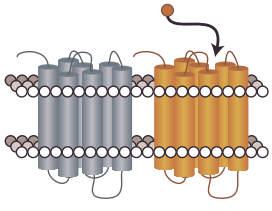

Odorant receptors.

science's stke www.stke.org Signal Transduction Knowledge Environment

Perspective: Class-3 Semaphorin Signaling—The End of a Dogma *V. Potiron and J. Roche*
A new twist in the complex path of semaphorin signaling suggests that SEMA3E signaling may be neuropilin-independent.

Perspective: One Neuron, Multiple Receptors—Increased Complexity in Olfactory Coding?
M. Spehr and T. Leinders-Zufall
Insect odor sensing breaks the one receptor–one neuron rule.

Teaching Resource: Proteases and Signaling *S. Wilk*
Use these materials to prepare a graduate-level class on the role of proteolysis in cell signaling.

Teaching Resource: Apoptosis *S. Wilk*
Use these materials to prepare a graduate-level class on programmed cell death.

Separate individual or institutional subscriptions to these products may be required for full-text access.

edited by Stella Hurtley and Phil Szuromi

Mapping the Human Transcriptome

Our understanding of the human genome is continually being improved and we are only now beginning to understand the complexity of the human transcriptome. **Cheng *et al.*** (p. 1149, published online 24 March 2005) used high-density oligonucleotide arrays to map the sites of transcription for 30% of the human genome (encoded on 10 chromosomes). The distribution of polyadenylated (polyA+) and nonpolyadenylated (polyA–) RNAs varied within the cell nucleus and cytosol. A much higher percentage of the genome is transcribed either as polyA–, polyA+, or bimorphic (found as polyA– and polyA+) sequences than had been assumed. For example, in the HepG2 cell line, up to 15% of the genome is transcribed. Many of the transcripts identified have not been annotated, and come from the sense and antisense strands or are overlapping. These findings further point out the complexity of the human transcriptome.

Splashy Surface Electrons

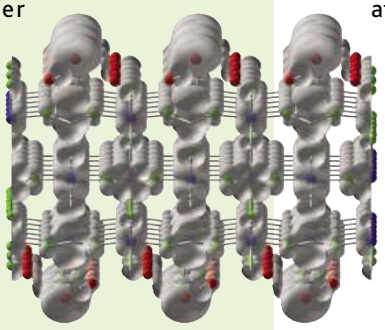

Many electron transfer processes occur at metal oxide surfaces, and water can play a key role by providing local trap states that open up lower energy pathways for reactions. **Onda *et al.*** (p. 1154) studied the (110) surface of titanium oxide at various levels of hydration, both with two-photon photoemission studies and density functional calculations. They find evidence for an excited electronic state on partially hydroxylated surfaces that is 2.4 electron volts above the Fermi level. The calculations indicate that the electrons' environments resemble those of electrons in water clusters, rather than those for electrons on water-covered metal surfaces. This "wet-electron" state relaxes back into the conduction band on time scales less than 15 femtoseconds.

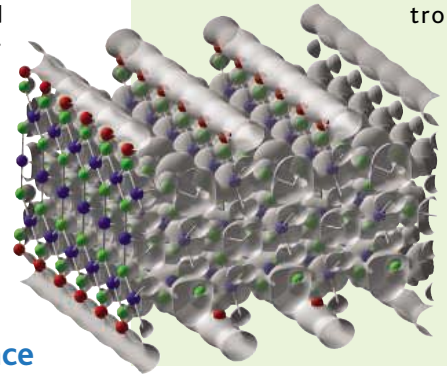

Marked Influence on Stem Cells

Replication-defective retroviral vectors are often used to mark and track stem cell progeny without, it has been assumed, influencing the regulation of the stem cells or conferring any selective advantage or disadvantage. **Kustikova *et al.*** (p. 1171) examined the insertion sites present in dominant and long-term repopulating mouse hematopoietic stem cells. They observed a pronounced competitive inequality after insertional deregulation of randomly hit alleles. The genes in question each have recognized roles in the self-renewal, or survival, of hematopoietic stem cells. The findings have implications for clinical gene therapy, and suggest a possible need to revise conclusions generated by genemarking studies.

Interfering with RNA Interference

RNA interference (RNAi) is central to a number of natural RNA-based silencing processes and is becoming a common tool used in a wide range of studies in eukaryotes. It is also being explored for its therapeutic potential. **Kim *et al.*** (p. 1164, published online 24 March 2005) carried out a genome-wide screen in *Caenorhabditis elegans* for components of the RNAi pathway using RNAi. Although apparently a "circular" methodology, the screen identified 90 viable and lethal genes involved in RNAi, most of which were not previously linked with the process. Classes of factors include RNA binding and processing factors, chromatin-associated factors, and nuclear import and export factors. The screen also provides insight into the degree of overlap between different RNAi-based silencing pathways.

Catch the Monkey

Discoveries of new species of mammal are increasingly rare, and discoveries of new primates even more so. **Jones *et al.*** (p. 1161; see the news story by Beckman) report the almost simultaneous discovery of two populations of a new species of African monkey in the highlands of southern Tanzania. The new species, named the highland mangabey, is believed to number only a few hundred individuals. Its discovery underscores the importance of the montane woodlands of Tanzania as a conservation focus for primates.

Collagen's Cerebral Side

Porencephaly is a rare brain disorder that typically is manifested in newborns and that is characterized by degenerative cavities in the cerebral cortex. **Gould *et al.*** (p. 1167) characterized mutant mice with phenotypic features reminiscent of human porencephaly. Half of the mutant mice died of cerebral hemorrhage within 1 day of birth, and the surviving pups showed focal disruptions in the vascular basement membrane that was accompanied by porencephaly in a subset of the animals. The causative mutation mapped to the gene encoding procollagen type IV α 1. The mutation led to the inhibition of collagen secretion into the basement membrane. Mutations in the same gene were subsequently identified in two families with inherited forms of porencephaly and cerebral hemorrhage. These results raise the possibility that mutations compromising vascular integrity may increase susceptibility to more common disorders, such as stroke.

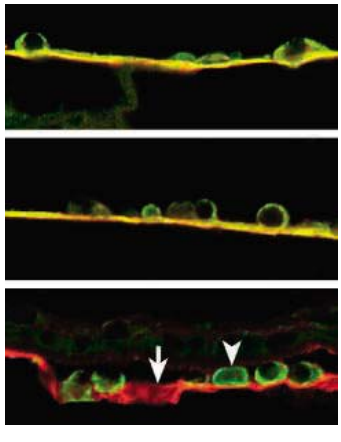

CREDITS: (TOP TO BOTTOM) ONDA *ET AL.*; GOULD *ET AL.*

Putting Quantum Dots into Cavities

Cavity quantum-electrodynamics (QED) experiments have been a key tool in understanding and controlling the dynamics of single quantum systems. Although there are advantages, both practical and basic, in carrying out cavity-QED experiments with solid-state emitters, experimental realization has been difficult to achieve. **Badolato *et al.*** (p.1158; see the Perspective by **Krauss**) present a technique for deterministically coupling an excitation level in a single quantum dot to a single mode of an optical cavity. In their three-step process, they first identify the quantum dot of interest and characterize its excitation spectrum. Next, using the dot itself as a registration marker, they fabricate a two-dimensional photonic crystal cavity that is specially designed with the quantum dot's excitation spectrum in mind, and then place it in a near-optimal position relative to the quantum dot. Finally, they optimize the coupling between the dot and photonic crystal cavity by a series of etch-steps that fine-tune the physical dimensions of the photonic crystal. The observed strong coupling between the quantum dot and the cavity should put the system in the regime for probing cavity-QED in a solid-state environment.

Stress Response, Aging, and Cancer Predisposition

The activity of FOXO transcription factors is associated with increased life span. **Essers *et al.*** (p. 1181; see the Perspective by **Bowerman**) find that in both *Caenorhabditis elegans* and mammalian cells, FOXO and β-catenin are associated in a protein complex. In *C. elegans*, β-catenin promotes the transcriptional activity of FOXO in response to oxidative stress. β-catenin mediates developmental effects of the wingless or Wnt pathway and is implicated in promoting excess cell proliferation in certain cancers. β-catenin's stimulation of FOXO, on the other hand, inhibits progression through the cell cycle. Thus, a critical balance between β-catenin signaling through FOXO or other transcription factors regulated by the Wnt pathway may influence stress responses, aging, and disposition to cancer.

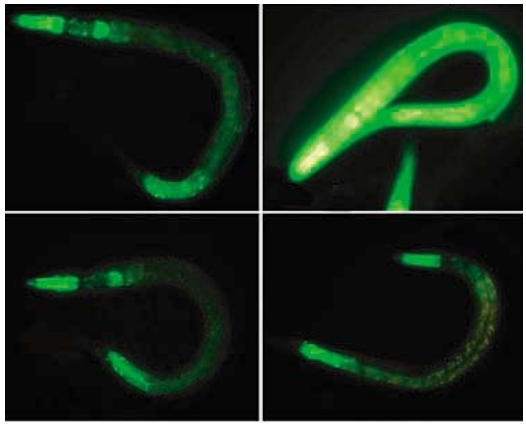

CREDIT: ESSERS *ET AL.*

Membrane Engineering

The intracellular pathogen *Salmonella enterica* resides in a vacuole from which it translocates effector proteins into the host cell. These bacterial effectors manipulate eukaryotic functions. SifA is a key *Salmonella* effector protein, and *sifA*$^-$ mutants are highly attenuated in virulence in mice. **Boucrot *et al.*** (p. 1174) now describe how *Salmonella* uses secreted effectors to negatively regulate the binding of the microtubule-associated kinesin motor onto the bacterial vacuole. SifA targets a host protein, SKIP, that down-regulates the recruitment of kinesin. In this manner, *Salmonella* controls the kinesin activity associated with its vacuole membrane and, in turn, the dynamics of membrane exchange.

Not Lost in Translation

The ribosome uses kinetic proofreading and induced-fit mechanisms to ensure the fidelity of the translation reaction. **Cochella and Green** (p. 1178; see the Perspective by **Daviter *et al.***) analyzed a mutant transfer RNA (tRNA) molecule that promotes mis-incorporation of amino acids. It appears that the tRNA molecule in itself can transmit structural information from the codon:anticodon decoding center to other regions of the ribosome that promote guanosine triphosphate hydrolysis and accommodation of the tRNA in the ribosome acceptor site. Thus, tRNA is more than a passive player in the translation reaction.

Wanted: Better Benchmarks

How much should a nation spend on science? What kind of science? How much from private versus public sectors? Does demand for funding by potential science performers imply a shortage of funding or a surfeit of performers? These and related science policy questions tend to be asked and answered today in a highly visible advocacy context that makes assumptions that are deserving of closer scrutiny. A new "science of science policy" is emerging, and it may offer more compelling guidance for policy decisions and for more credible advocacy.

All developed and many developing nations today have accepted the need to support technical education and research as keys to future economic strength. Studies from the 1990s show that U.S. investment in R&D development led to greater economic productivity, and that information technology, in particular, has been a major factor in sustaining U.S. productivity growth. The question is not whether R&D investments are important, but what investment strategies are most effective in the rapidly changing global environment for science. Here, ideas diverge.

Take the issue of the technical workforce. Sharply differing opinions exist regarding the production of U.S. scientists to meet possible impending shortages.* The differences turn on the interpretation of "benchmark" data regarding the numbers of degree holders produced in the United States and other countries, particularly China and India. In the latter countries, the rates of growth in the numbers of scientists are high, although actual numbers are small relative to those in the United States. Advocates for increased production of U.S. scientists point to our low graduation rates, whereas critics emphasize limited short-term job opportunities for graduates and postdocs. Resolution of this issue requires a broader understanding of socioeconomic factors in a number of nations that would allow us to attach probabilities to different future scenarios. Optimal strategies for large mature economies such as that of the United States will doubtless differ from those for smaller or developing economies. Here, as elsewhere in policy debates, the benchmarks do not speak for themselves.

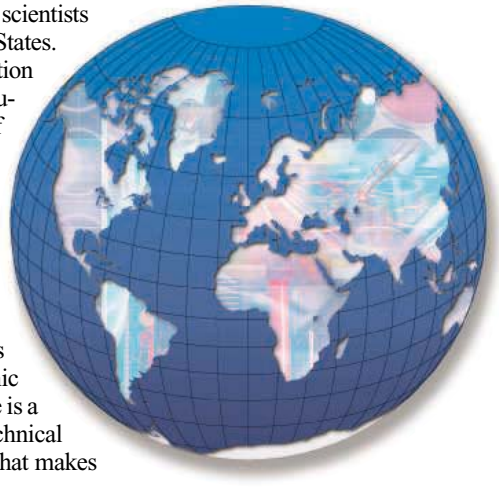

The data we choose to collect do say something about the framework in which we understand the relations among science, government, and society. Our customary reliance on historical trends in national data, however, creates an inertia that causes data categories to lag far behind changes in the dynamic socioeconomic framework, now evolving internationally. We know that there is a complex linkage between workforce issues and other economic variables. Technical workforces in different countries are increasingly interdependent in a way that makes single-country data unreliable for workforce forecasts.

Globalization and changing modes of science that have blurred disciplinary distinctions have undermined the value of traditional science and engineering data and their conventional interpretations. The old budget categories of basic and applied R&D, still tracked by the U.S. Office of Management and Budget, do not come close to capturing information about the highly interdisciplinary activities thought to fuel innovation. A 1995 U.S. National Research Council (NRC) committee chaired by Frank Press took a step toward data reform when it introduced the combined category of "federal science and technology," declaring that "the linear sequential view of innovation is simplistic and misleading." More attention, however, is needed to definitions and models that suit current needs of policy. A recent report from the NRC Committee on National Statistics found that "the structure of . . . data collection is tied to models of R&D performance that are increasingly unrepresentative of the whole of the R&D enterprise." Further, "It would be desirable to devise, test and, if possible, implement survey tools that more directly measure the economic output of R&D in terms of short-term and long-term innovation."†

Relating R&D to innovation in any but a general way is a tall order, but not a hopeless one. We need econometric models that encompass enough variables in a sufficient number of countries to produce reasonable simulations of the effect of specific policy choices. This need won't be satisfied by a few grants or workshops, but demands the attention of a specialist scholarly community. As more economists and social scientists turn to these issues, the effectiveness of science policy will grow, and of science advocacy too.

John H. Marburger III

John H. Marburger III is director of the Office of Science and Technology Policy, Executive Office of the President of the United States, in Washington, DC.

*D. Kennedy, J. Austin, K. Urquhart, C. Taylor, *Science* **303**, 1105 (2004). †*Measuring Research and Development Expenditures in the U.S. Economy*, L. D. Brown, T. J. Plewes, M. A. Gerstein, Eds. (National Academies Press, Washington, DC, 2005).

10.1126/science.1114801

edited by Gilbert Chin

IMMUNOLOGY

From Walkabout to Wanderlust

Cells of the immune system are highly motile and use chemotaxis in navigating to and within different regions of the body. Communication between B cells and T cells is needed for antibody production and in the deployment of armed T cells to sites of infection. During development, immature immune cells must also find their way from their site of origin toward peripheral lymphoid organs.

Using two-photon microscopy of lymph nodes, Okada *et al.* followed the fate of antigen-specific B cells. After activation, the cells within the follicular B cell zone awoke from a relatively sluggish, random motion and began to steer a steady course toward the neighboring region of the lymph node containing T cells. This process depended on the surface chemokine receptor CCR7, linking the gradient of the chemokine CCL21 within the follicle to the directional behavior. Once inside the T cell zone, B cells coupled with T cell partners in a multidirectional dance, with the B cells appearing to take the lead.

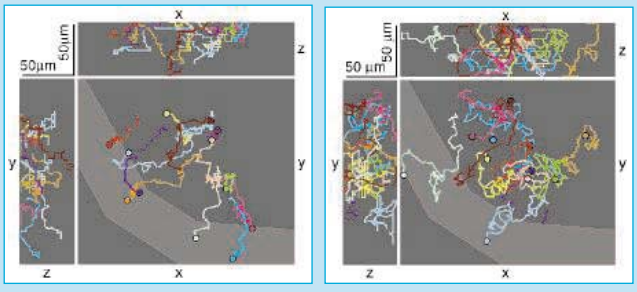

Antigen-engaged B cells (left) end up (circles) in T cell zones (light gray), whereas naïve B cells (right) simply wander about.

In a study of developing T cells within the thymus, Witt *et al.* observed that thymocytes located within the cortical region altered their behavior after they had undergone positive selection. Similarly to follicular B cells, selected thymocytes switched from a random walk to directed migration toward the thymic medulla, through which they transit as they exit the thymus. Again, this suggests that long-distance cues induce the urge to travel in newly selected T cells. — SJS

PLoS Biol. **3**, e150; e160 (2005).

GEOCHEMISTRY

Up From the Depths

Recent geological and chemical evidence supports the conclusion that in the distant past, Earth's oceans were repeatedly stratified, so that an anoxic layer formed at depth, as in the Black Sea of today. During these periods, bacterial metabolism would have used sulfate (instead of oxygen) as an electron acceptor, and the deep oceans would have become enriched in hydrogen sulfide as a consequence.

Kump *et al.* show that the upward flux of the accumulated hydrogen sulfide would have been quenched by the mixing of atmospheric oxygen into the surface of the oceans. They go on to infer that at times when the atmospheric oxygen level was low, large-scale upwelling of hydrogen sulfide gas might have taken over and that, in extreme cases, this could have resulted in the release of significant amounts of this toxic gas into the atmosphere. Biomarkers indicative of a high abundance of nonoxygenic photosynthetic green sulfur bacteria have been found, corresponding to the times of several mass extinctions and most recently for the end-Permian extinction (see Grice *et al.*, Reports, 4 February 2005, p. 706), which is broadly associated with low oxygen levels and extensive ocean anoxia. — BH

Geology **33**, 397 (2005).

CHEMISTRY

House of Triangles

Atomic clusters often adopt cage-like geometries with triangular faces, such as the tetrahedron, octahedron, and icosahedron. Goicoechea and Sevov have extended this series by constructing a germanium cluster composed of 32 triangles. The Ge_{18} ellipsoid has approximate threefold symmetry and a charge of 4^-, and was crystallized with four charge-balancing potassium ions that were sequestered inside cryptand ligands. The cluster encapsulates two palladium atoms, which appear to stabilize the large cage from within by overlapping with the Ge orbitals. The synthesis fuses the two cluster halves together from a solution of K_4Ge_9 and tetrakis(triphenylphosphine) palladium precursors. Although a similar geometry has been seen in extended solid lattices, mass spectrometry confirmed that these structures are stable as discrete species in solution. — JSY

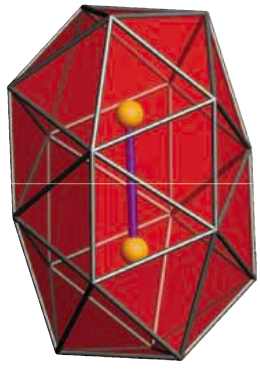

The 18-vertex deltahedron and the palladium dimer (orange).

J. Am. Chem. Soc. 10.1021/ja051224q (2005).

BIOMEDICINE

Staying Hydrated

The peptide vasopressin (antidiuretic hormone) is critical for maintaining fluid homeostasis. Its receptor, V2R, is located at the surface of epithelial cells lining the kidney's collecting duct. Receptor activation increases water permeability through aquaporin, leading to the retention of water. Mutation of an arginine residue to histidine at position 137 of V2R blocks receptor activation, resulting in nephrogenic diabetes insipidus, in which patients suffer from severe dehydration due to excessive water excretion. The critical arginine is located within a motif that is highly conserved in the family of G protein–coupled receptors.

Feldman *et al.* find that if the arginine is mutated to either cysteine or leucine, the opposite condition occurs—excessive water retention—and they refer to this condition as nephrogenic syndrome of inappropriate antidiuresis. The mutations were identified in two infants who displayed the abnormal water overload characteristic of hyperactivated V2R, even though both patients lacked detectable vasopressin. It remains to be determined how mutations at

CREDITS: (TOP) OKADA *ET AL.*, *PLOS BIOL.* **3**, E150 (2005); (BOTTOM) GOICOECHEA *ET AL.*, *J. AM. CHEM. SOC.* 10.1021/JA051224Q (2005)

the same position either activate or inactivate the receptor, causing genetic disorders of opposite character. — LDC

N. Engl. J. Med. **352**, 1884 (2005).

MICROBIOLOGY

Feeling Dehydrated

Bacteria monitor their environment and change their behavior to exploit that environment most effectively. Wang *et al.* have discovered an unanticipated player that bacteria use to sense environmental wetness: the bacterial flagellum. One key ingredient for continued growth is a source of water; at a hydrated surface, bacteria form large colonies that swarm across the surface via flagella-driven motility. Mutants in the bacterial chemotaxis signaling pathway exhibit fewer and shorter flagella when grown on a surface and are less hydrated than wild-type cells. It seems that the flagella sense external wetness, and when external hydration is limiting, the flagella inhibit their own growth by blocking the secretion of flagellin subunits and the export of the transcriptional inhibitor FlgM, thereby switching off the synthesis of further flagellum components. The specialized secretion systems responsible for the export and assembly of flagella and for the secretion of bacterial virulence factors are jointly regulated by this sensing system. — SMH

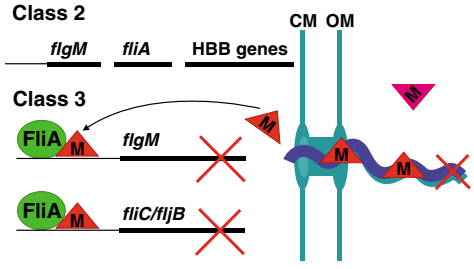

Model for how FlgM blocks transcription of late-stage flagellin genes.

EMBO J. 10.1038/sj.emboj.7600668 (2005).

CHEMISTRY

DNA as a Chiral Catalyst

Chemists have long explored the use of biocatalysts such as proteins and RNA in their syntheses; the handedness of these molecules is particularly useful for the selective synthesis of individual enantiomers (the two mirror-image forms of chiral molecules).

Roelfes and Feringa show that intercalation of a suitable catalyst into DNA enables enantioselective synthesis. Because the catalyst itself is nonchiral, the chirality of the DNA is responsible for the chiral selectivity. Through judicious choice of catalyst, the authors can even prepare both enantiomers of the product. The catalyst is noncovalently bound to the DNA, allowing the system to be optimized and adapted rapidly for new reactions. Furthermore, the product can be separated easily from the reaction mixture. — JFU

Angew. Chem. Int. Ed. 10.1002/ange.200500298 (2005).

HIGHLIGHTED IN *SCIENCE*'S SIGNAL TRANSDUCTION KNOWLEDGE ENVIRONMENT

Science's stke www.stke.org

Methylation Outside the Nucleus

Ezh2 is a member of the polycomb group of proteins and functions in development by catalyzing the methylation of lysine residues on histone proteins, thereby causing changes in gene expression. However, Ezh2 exists in the cytoplasm as well as the nucleus, and Su *et al.* have explored whether the enzyme might have functions apart from its role in modifying chromatin structure. Ezh2 has been reported to associate with the guanine nucleotide exchange factor Vav1, which is an important component of T cell signaling and mediator of changes in actin polymerization in response to stimulation of the T cell receptor (TCR). T cells lacking Ezh2 were defective in TCR-induced actin polymerization and showed an impaired proliferative response. Similarly, fibroblasts lacking Ezh2 showed decreased actin polymerization in response to platelet-derived growth factor, and this deficiency could be rescued by expressing a cytoplasmically localized form of Ezh2. The methylation target of Ezh2 is not known but appears to lie between TCR activation and activation of the guanosine triphosphate Cdc42; Vav1, though, appears not be modified by Ezh2. These findings indicate that posttranslational modification by methylation has key regulatory roles outside of the nucleus, with implications for immune responses to the TCR and cancer biology, where increased expression of Ezh2 in cancer cells is associated with increased metastatic capacity. — LBR

Cell **121**, 426 (2005).

CREDITS: WANG *ET AL.*, *EMBO J.* 10.1038/SJ.EMBOJ.7600668 (2005)

GE Healthcare

What do you call making protein purification easy right from the start?

Pure imagination brought to life.

GE Healthcare is the one name behind all the leading tools in biomolecular research. Our focus is on providing protein purification systems, columns and media that make drug discovery simpler and faster from the outset to help you compete more effectively. Innovations like HiTrap™ and HisTrap™ columns, which offer outstanding convenience and reproducibility. Or the ÄKTAdesign™ platform, combined with the seamless control of UNICORN™ software, which gives you speed, ease and confidence whatever your application or scale.

At GE Healthcare we never stand still. We're constantly working to improve our offering – finding new ways of bringing pure imagination to life, to give you even better performance in tomorrow's race.

Visit www.amershambiosciences.com/pureimagination

imagination at work

Sepharose™ Sephadex™

GE08-05

www.sciencemag.org

Science

1200 New York Avenue, NW
Washington, DC 20005
Editorial: 202-326-6550, FAX 202-289-7562
News: 202-326-6500, FAX 202-371-9227

Bateman House, 82-88 Hills Road
Cambridge, UK CB2 1LQ
+44 (0) 1223 326500, FAX +44 (0) 1223 326501

SUBSCRIPTION SERVICES For change of address, missing issues, new orders and renewals, and payment questions: 800-731-4939 or 202-326-6417, FAX 202-842-1065. Mailing addresses: AAAS, P.O. Box 1811, Danbury, CT 06813 or AAAS Member Services, 1200 New York Avenue, NW, Washington, DC 20005

INSTITUTIONAL SITE LICENCES please call 202-326-6755 for any questions or information

REPRINTS Ordering/Billing/Status 800-635-7171; Corrections 202-326-6501

PERMISSIONS 202-326-7074, FAX 202-682-0816

MEMBER BENEFITS Bookstore: AAAS/BarnesandNoble.com bookstore www.aaas.org/bn; Car purchase discount: Subaru VIP Program 202-326-6417; Credit Card: MBNA 800-847-7378; Car Rentals: Hertz 800-654-2200 CDP#343457, Dollar 800-800-4000 #AA1115; AAAS Travels: Betchart Expeditions 800-252-4910; Life Insurance: Seabury & Smith 800-424-9883; Other Benefits: AAAS Member Services 202-326-6417 or www.aaasmember.org.

science_editors@aaas.org (for general editorial queries)
science_letters@aaas.org (for queries about letters)
science_reviews@aaas.org (for returning manuscript reviews)
science_bookrevs@aaas.org (for book review queries)

Published by the American Association for the Advancement of Science (AAAS), *Science* serves its readers as a forum for the presentation and discussion of important issues related to the advancement of science, including the presentation of minority or conflicting points of view, rather than by publishing only material on which a consensus has been reached. Accordingly, all articles published in *Science*—including editorials, news and comment, and book reviews—are signed and reflect the individual views of the authors and not official points of view adopted by the AAAS or the institutions with which the authors are affiliated.

AAAS was founded in 1848 and incorporated in 1874. Its mission is to advance science and innovation throughout the world for the benefit of all people. The goals of the association are to: foster communication among scientists, engineers and the public; enhance international cooperation in science and its applications; promote the responsible conduct and use of science and technology; foster education in science and technology for everyone; enhance the science and technology workforce and infrastructure; increase public understanding and appreciation of science and technology; and strengthen support for the science and technology enterprise.

INFORMATION FOR CONTRIBUTORS

See pages 135 and 136 of the 7 January 2005 issue or access www.sciencemag.org/feature/contribinfo/home.shtml

EDITOR-IN-CHIEF **Donald Kennedy**
EXECUTIVE EDITOR **Monica M. Bradford**
DEPUTY EDITORS **R. Brooks Hanson, Katrina L. Kelner**
NEWS EDITOR **Colin Norman**

EDITORIAL SUPERVISORY SENIOR EDITORS Barbara Jasny, Phillip D. Szuromi; SENIOR EDITORS Gilbert J. Chin, Lisa D. Chong, Pamela J. Hines, Paula A. Kiberstis (Boston), Beverly A. Purnell, L. Bryan Ray, Guy Riddihough (Manila), H. Jesse Smith, Valda Vinson, David Voss; ASSOCIATE EDITORS Marc S. Lavine, Jake S. Yeston; ONLINE EDITOR Stewart Wills; CONTRIBUTING EDITOR Ivan Amato; ASSOCIATE ONLINE EDITOR Tara S. Marathe; BOOK REVIEW EDITOR Sherman J. Suter; ASSOCIATE LETTERS EDITOR Etta Kavanagh; INFORMATION SPECIALIST Janet Kegg; EDITORIAL MANAGER Cara Tate; SENIOR COPY EDITORS Jeffrey E. Cook, Harry Jach, Barbara P. Ordway; COPY EDITORS Cynthia Howe, Alexis Wynne Mogul, Sabrah M. n'haRaven, Jennifer Sills, Trista Wagoner; EDITORIAL COORDINATORS Carolyn Kyle, Beverly Shields; PUBLICATION ASSISTANTS Chris Filiatreau, Joi S. Granger, Jeffrey Hearn, Lisa Johnson, Scott Miller, Jerry Richardson, Brian White, Anita Wynn; EDITORIAL ASSISTANTS Ramatoulaye Diop, E. Annie Hall, Patricia M. Moore, Brendan Nardozzi, Michael Rodewald; EXECUTIVE ASSISTANT Sylvia S. Kihara; ADMINISTRATIVE SUPPORT Patricia F. Fisher

NEWS SENIOR CORRESPONDENT Jean Marx; DEPUTY NEWS EDITORS Robert Coontz, Jeffrey Mervis, Leslie Roberts, John Travis; CONTRIBUTING EDITORS Elizabeth Culotta, Polly Shulman; NEWS WRITERS Yudhijit Bhattacharjee, Jennifer Couzin, David Grimm, Constance Holden, Jocelyn Kaiser, Richard A. Kerr, Eli Kintisch, Andrew Lawler (New England), Greg Miller, Elizabeth Pennisi, Charles Seife, Robert F. Service (Pacific NW), Erik Stokstad; Amitabh Avasthi (intern); CONTRIBUTING CORRESPONDENTS Marcia Barinaga (Berkeley, CA), Barry A. Cipra, Adrian Cho, Jon Cohen (San Diego, CA), Daniel Ferber, Ann Gibbons, Robert Irion, Mitch Leslie (NetWatch), Charles C. Mann, Evelyn Strauss, Gary Taubes, Ingrid Wickelgren; COPY EDITORS Linda B. Felaco, Rachel Curran, Sean Richardson; ADMINISTRATIVE SUPPORT Scherraine Mack, Fannie Groom BUREAUS: Berkeley, CA: 510-652-0302, FAX 510-652-1867, New England: 207-549-7755, San Diego, CA: 760-942-3252, FAX 760-942-4979, Pacific Northwest: 503-963-1940

PRODUCTION DIRECTOR James Landry; SENIOR MANAGER Wendy K. Shank; ASSISTANT MANAGER Rebecca Doshi; SENIOR SPECIALISTS Vicki J. Jorgensen, Jessica K. Moshell; SPECIALISTS Jay R. Covert, Stacey Ferebee; **PREFLIGHT** DIRECTOR David M. Tompkins; MANAGER Marcus Spiegler; SPECIALIST Jessie Mudjitaba;

ART DIRECTOR Joshua Moglia; ASSOCIATE ART DIRECTOR Kelly Buckheit; ILLUSTRATOR Katharine Sutliff; SENIOR ART ASSOCIATES Holly Bishop, Laura Creveling, Preston Huey, Julie White; ASSOCIATE Nayomi Kevitiyagala; PHOTO RESEARCHER Leslie Blizard

***SCIENCE* INTERNATIONAL**

EUROPE (science@science-int.co.uk) EDITORIAL: INTERNATIONAL MANAGING EDITOR Andrew M. Sugden; SENIOR EDITOR/PERSPECTIVES Julia Fahrenkamp-Uppenbrink; SENIOR EDITORS Caroline Ash (Geneva: +41 (0) 222 346 3106), Stella M. Hurtley, Ian S. Osborne, Peter Stern; ASSOCIATE EDITOR Stephen J. Simpson; EDITORIAL SUPPORT Emma Westgate; Deborah Dennison ADMINISTRATIVE SUPPORT Janet Clements, Phil Marlow, Jill White; NEWS: INTERNATIONAL NEWS EDITOR Eliot Marshall DEPUTY NEWS EDITOR Daniel Clery; CORRESPONDENT Gretchen Vogel (Berlin: +49 (0) 30 2809 3902, FAX +49 (0) 30 2809 8365); CONTRIBUTING CORRESPONDENTS Michael Balter (Paris), Martin Enserink (Amsterdam and Paris); INTERN Mason Inman

ASIA Japan Office: Asca Corporation, Eiko Ishioka, Fusako Tamura, 1-8-13, Hirano-cho, Chuo-ku, Osaka-shi, Osaka, 541-0046 Japan; +81 (0) 6 6202 6272, FAX +81 (0) 6 6202 6271; asca@os.gulf.or.jp JAPAN NEWS BUREAU: Dennis Normile (contributing correspondent, +81 (0) 3 3391 0630, FAX 81 (0) 3 5936 3531; dnormile@gol.com); CHINA REPRESENTATIVE Hao Xin, + 86 (0) 10 6307 4439 or 6307 3676, FAX +86 (0) 10 6307 4358; haoxin@earthlink.net; SOUTH ASIA Pallava Bagla (contributing correspondent +91 (0) 11 2271 2896; pbagla@vsnl.com); CENTRAL ASIA Richard Stone (+7 3272 6413 35, rstone@aaas.org)

EXECUTIVE PUBLISHER **Alan I. Leshner**
PUBLISHER **Beth Rosner**

FULFILLMENT & MEMBERSHIP SERVICES (membership@aaas.org) DIRECTOR Marlene Zendell; MANAGER Waylon Butler; SENIOR SPECIALIST Pat Butler; SPECIALISTS Laurie Baker, Tamara Alfson, Karena Smith, Andrew Vargo; MARKETING ASSOCIATE Deborah Stromberg

BUSINESS OPERATIONS AND ADMINISTRATION DIRECTOR Deborah Rivera-Wienhold; BUSINESS MANAGER Randy Yi; SENIOR FINANCIAL ANALYST Lisa Donovan; BUSINESS ANALYST Jessica Tierney; FINANCIAL ANALYST Farida Yeasmin; RIGHTS AND PERMISSIONS: ADMINISTRATOR Emilie David; ASSOCIATE Elizabeth Sandler; MARKETING: DIRECTOR John Meyers; MEMBERSHIP MARKETING MANAGER Darryl Walter; MARKETING ASSOCIATE Julianne Wielga; RECRUITMENT MARKETING MANAGER Allison Pritchard; ASSOCIATES Mary Ellen Crowley, Amanda Donathen, Catherine Featherston; DIRECTOR OF INTERNATIONAL MARKETING AND RECRUITMENT ADVERTISING Deborah Harris; INTERNATIONAL MARKETING MANAGER Wendy Sturley; MARKETING/MEMBER SERVICES EXECUTIVE: Linda Rusk; JAPAN SALES AND MARKETING MANAGER Jason Hannaford; SITE LICENSE SALES: DIRECTOR Tom Ryan; SALES AND CUSTOMER SERVICE Mehan Dossani, Catherine Holland, Adam Banner, Yaniv Snir; ELECTRONIC MEDIA: INTERNET PRODUCTION MANAGER Lizabeth Harman; ASSISTANT PRODUCTION MANAGER Wendy Stengel; SENIOR PRODUCTION ASSOCIATES Sheila Mackall, Amanda K. Skelton, Lisa Stanford; PRODUCTION ASSOCIATE Nichele Johnston; LEAD APPLICATIONS DEVELOPER Carl Saffell

PRODUCT ADVERTISING (science_advertising@aaas.org); MIDWEST Rick Bongiovanni: 330-405-7080, FAX 330-405-7081 • WEST COAST/W. CANADA B. Neil Boylan (Associate Director): 650-964-2266, FAX 650-964-2267 • EAST COAST/E. CANADA Christopher Breslin: 443-512-0330, FAX 443-512-0331 • UK/SCANDINAVIA/FRANCE/ITALY/BELGIUM/NETHERLANDS Andrew Davies (Associate Director): +44 (0)1782 750111, FAX +44 (0) 1782 751999 • GERMANY/SWITZERLAND/AUSTRIA Tracey Peers (Associate Director): +44 (0) 1782 752530, FAX +44 (0) 1782 752531 JAPAN Mashy Yoshikawa: +81 (0) 33235 5961, FAX +81 (0) 33235 5852 ISRAEL Jessica Nachlas +9723 5449123 • TRAFFIC MANAGER Carol Maddox; SALES COORDINATOR Deiandra Simms

CLASSIFIED ADVERTISING (advertise@sciencecareers.org); U.S.: SALES DIRECTOR Gabrielle Boguslawski: 718-491-1607, FAX 202-289-6742; INTERNET SALES MANAGER Beth Dwyer: 202-326-6534; INSIDE SALES MANAGER Daryl Anderson: 202-326-6543; WEST COAST/MIDWEST Kristine von Zedlitz: 415-956-2531; EAST COAST Jill Downing: 631-580-2445; LINE AD SALES Emnet Tesfaye: 202-326-6740; SENIOR SALES COORDINATOR Erika Bryant; SALES COORDINATORS Rohan Edmonson, Christopher Normile, Joyce Scott, Shirley Young; INTERNATIONAL: SALES MANAGER Tracy Holmes: +44 (0) 1223 326525, FAX +44 (0) 1223 326532; SALES Christina Harrison, Suitlana Barnes; SALES ASSISTANT Helen Moroney; JAPAN: Jason Hannaford: +81 (0) 52 789 1860, FAX +81 (0) 52 789 1861; PRODUCTION: MANAGER Jennifer Rankin; ASSISTANT MANAGER Deborah Tompkins; ASSOCIATE Amy Hardcastle; SENIOR TRAFFICKING ASSOCIATE Christine Hall; SENIOR PUBLICATIONS ASSISTANT Robert Buck; PUBLICATIONS ASSISTANT Natasha Pinol

AAAS BOARD OF DIRECTORS RETIRING PRESIDENT, CHAIR Shirley Ann Jackson; PRESIDENT Gilbert S. Omenn; PRESIDENT-ELECT John P. Holdren; TREASURER David E. Shaw; CHIEF EXECUTIVE OFFICER Alan I. Leshner; BOARD Rosina M. Bierbaum; John E. Burris; John E. Dowling; Lynn W. Enquist; Susan M. Fitzpatrick; Richard A. Meserve; Norine E. Noonan; Peter J. Stang; Kathryn D. Sullivan

AAAS
ADVANCING SCIENCE, SERVING SOCIETY

NetWatch

edited by Mitch Leslie

COMMUNITY SITE

Feeding Africa

Africa is the continent with the fastest-growing population, and researchers working on ways to hike food production there will find plenty to chew on at African Crop Improvement. The home page of a Rockefeller Foundation research grants program, the site offers a bumper crop of information on the needs of African agriculture, biotechnology, and related topics. Backgrounders on important crops such as bananas, cassava, and sorghum (above) describe the plant's origins and uses and identify research priorities. For example, the main limit on cassava production comes from the virus-caused cassava mosaic disease. Links include the bean and millet genome projects. A news section posts media reports and press releases on the latest developments, and you can share ideas with fellow researchers on the new message board.

www.africancrops.net

LINKS

Garden of Cyber Delights

It's a jungle out there on the Web, especially if you're hunting for good plant resources. This federal government portal cuts a path to hundreds of quality botany Web sites. The annotated links—from a single page on paleobotany to an algae taxonomy database—include many useful sites for teachers and researchers. Check out the anatomy of a fern's leaf, learn about the diseases of forage crops, or read Gregor Mendel's original 1865 paper on plant hybridization that revolutionized genetics.

www.nbii.gov/disciplines/botany/index.html

EDUCATION

Death by Design

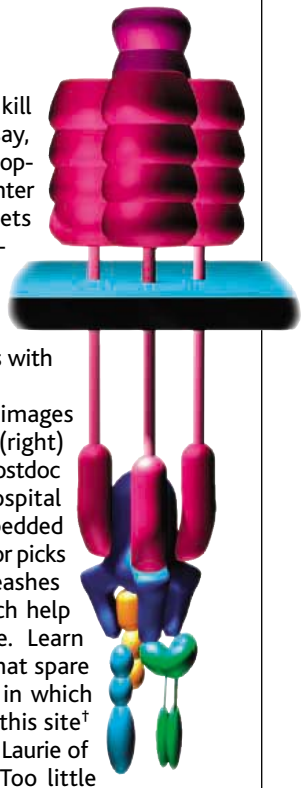

Every day millions of our cells kill themselves and biologists say, "Thank goodness." Known as apoptosis, this methodical self-slaughter helps defend against cancer, lets the brain make the right connections during development, and contributes to many other body activities. Newbies can absorb the basics of the process with this pair of tutorials.

Videos of suicidal cells and images such as this "death receptor" (right) add panache to the primer* by postdoc Phil Dash of St. George's Hospital Medical School in London. Embedded in a cell's membrane, the receptor picks up the suicide signal and unleashes enzymes called caspases, which help orchestrate the cell's demise. Learn about the survival pathways that spare cells and read about diseases in which control of apoptosis falters at this site† from graduate student Alasdair Laurie of the University of Leeds, U.K. Too little apoptosis lets tumors run amok, and too much depletes needed cells in Huntington's disease and AIDS.

* www.sgul.ac.uk/depts/immunology/~dash/apoptosis
† fbspcu01.leeds.ac.uk/users/bmbatrl/atrl_topic.htm

IMAGES

The Art of the Small

Are these shapes the latest fashion in southern California roof tiles, or maybe something from a lizard's back? Neither. The multicolored objects are the delicate scales on a butterfly's wing, which refract light to create an iridescent sheen. This shot is one of many striking photos hanging in the online galleries of the Micropolitan Museum. The site, hosted by the British portal Microscopy-UK, displays the work of Wim van Egmond, an artist and photographer in the Netherlands. He has trained his camera on everything from pond-dwelling water mites to the glasslike skeleton of a sponge to mats of cyanobacteria. Learn more about some of these creatures by linking to the magazine *Micscape*, which features articles written by enthusiasts of the small.

www.microscopy-uk.org.uk/micropolitan/index.html

FUN

Inside the Box

If you're wondering what goes on in a CD burner or how the drug Botox erases wrinkles, check out How Stuff Works. The commercial site is packed with ads, but beyond them you'll find hundreds of brief articles on autos, electronics, health, and science (mostly written by nonscientists). Brush up on how fuel cells work, read about the chemicals inside fireworks, or get a quick overview of diabetes. Unlike CDs you buy, which have tiny bumps indicating 0s and 1s, a home CD burner encodes data by relying on a layer of material that turns dark when a laser passes over it.

www.howstuffworks.com

Send site suggestions to netwatch@aaas.org. Archive: www.sciencemag.org/netwatch

CREDITS (TOP TO BOTTOM): SEBASTIAN BOLESCH/PETER ARNOLD INC.; PHIL DASH/ST. GEORGE'S HOSPITAL MEDICAL SCHOOL; WIM VAN EGMOND

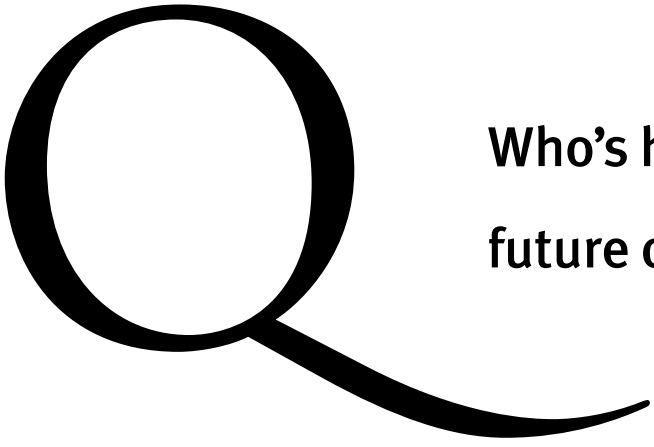

Who's helping build the future of science?

"I read my *Science* on the work site. Formerly a chemist, I found my true calling in woodworking, but I still try to keep up with advances in science. Reading *Science* also helps me answer questions from colleagues in the building trades about the safety and efficacy of the diverse materials we encounter."

Milton Trimitsis, carpenter and AAAS member

To see other member photos, please visit: http://promo.aaas.org/memberpics.shtml

AAAS

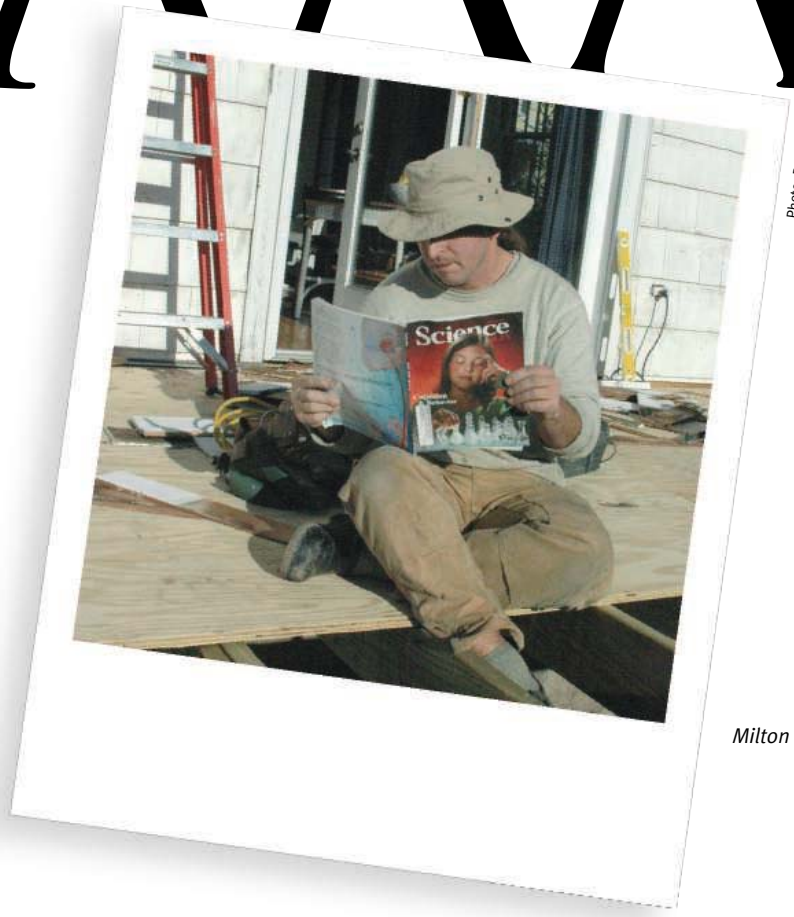

Photo: David Doyle

Milton Trimitsis

AAAS is committed to advancing science and giving a voice to scientists around the world. We work to improve science education, promote a sound science policy, and support human rights.

Helping our members stay abreast of their field is a key priority for AAAS. One way we do this is through *Science*, which features all the latest breakthroughs and groundbreaking research, and keeps scientists connected wherever they happen to be. Members like Milton find it essential reading.

To join the international family of science, go to www.aaas.org/join.

AAAS

ADVANCING SCIENCE, SERVING SOCIETY

www.aaas.org/join

This Week

PAGE 1100
NASA chief details his plans

1103
Glimpse of a new species

CELL BIOLOGY

Korean Team Speeds Up Creation Of Cloned Human Stem Cells

With speed and efficiency that will make waves in laboratories and legislatures around the world, scientists have created nearly a dozen new lines of human embryonic stem (ES) cells, ones that for the first time carry the genetic signature of diseased or injured patients. Last year, a group led by veterinarian Woo Suk Hwang and gynecologist Shin Yong Moon of Seoul National University reported the first—and until now the only—derivation of ES cells from human nuclear transfer experiments (*Science*, 12 March 2004, p. 1669). Those efforts yielded just one cell line from more than 200 tries, but the researchers report online in *Science* this week (www.sciencemag.org/cgi/content/abstract/1112286) that they can consistently derive a cell line in fewer than 20 tries.

The dramatic increase in efficiency suggests that creating genetically matched ES cell lines for patients needing some kind of cell transplant might not be impractical. "It's a breakthrough that I didn't think would happen for decades," says developmental biologist Gerald Schatten of the University of Pittsburgh in Pennsylvania, an adviser to the Korean team and an author on the paper. Developmental biologist George Daley of Harvard University calls the work "spectacular." And the work may influence the ongoing political debate over whether research with human ES cells, whether cloned or not, is ethically justified. "Some people will hate it, others will love it," says Rudolf Jaenisch of the Massachusetts Institute of Technology. "But it puts the discussion on a very firm footing now. People will have to rethink the argument that it's not efficient."

The new ES cell lines were created by replacing an oocyte's nucleus with one from a somatic cell and then chemically kick-starting development of the egg. Scientists similarly created Dolly the sheep in 1996 and since then have used nuclear transfer to clone thousands of cattle, mice, and other animals. Hwang and his colleagues had no intention of cloning a person, however. They only allowed the human embryos to develop for 6 days, just long enough to derive stem cells that, in theory, can form any cell type in the body.

Fast pace. Through practice with cow eggs (*above*) and other means, Korean researchers have increased their efficiency at cloning human embryos to create stem cells (*inset*).

One important factor in his team's success, Hwang says, was the use of freshly harvested oocytes from fertile women instead of ones left over from fertility treatments. The age of donors may also be key. Whereas oocytes from women in their 30s yielded on average one ES cell line for every 30 tries, those from younger donors yielded one line for every 13 tries. In nine cases, it took only a single donation of oocytes from a woman to produce a new line. (Each donation yields about 10 oocytes.)

The Korean team developed several techniques to improve their efficiency. For example, instead of using a needle to suck out the egg's nucleus, they make a small tear in the egg and gently squeeze out the chromosomes. They then insert a skin cell through the tear and apply an electric shock to fuse the two cells.

Most ES cells are derived by applying antibodies to a blastocyst-stage embryo that kill its outer cell layer and leave the inner cell mass. Hwang, Moon, and their colleagues simply put a blastocyst on a layer of human feeder cells and found that the blastocysts naturally formed colonies of ES cells. They exhibited key markers of ES cells and could form skin, muscle, and bone cells, among others.

Last year, because they had used a cell from the ovary of the oocyte donor as the nucleus donor, the Korean team could not rule out that the ES cell line was the result of parthenogenesis: an unfertilized egg starting to divide on its own. This time, except for one line, the oocyte and skin cell donors were different. In all 11 cases, the genetic fingerprint of each line matched that of the skin cell donor.

Nine of the 11 cell lines are derived from people, ranging in age from 10 to 56, who have suffered spinal cord injuries. The team has begun to test some of the lines in animal models of spinal cord injury, but Hwang cautions that they remain years away from transplanting the cells into people. "We have to be overconvinced" that the cells are safe, he says.

Another line is derived from a 2-year-old boy who has congenital hypogammaglobulonemia, a genetic immune deficiency. In theory, scientists could correct the genetic defect in the stem cells and then reinject them into the boy. Indeed, Jaenisch, Daley, and their colleagues have used such a strategy to treat mice with a similar genetic defect. Nevertheless, Hwang stresses that the boy's parents and the spinal cord patients were explicitly told that the team's research was unlikely to help them directly—even though the informed consent form used was, by Korean law, mandated to suggest such a possibility.

Although also unlikely to be employed for treatment, another ES cell line, derived from a 6-year-old type 1 diabetes patient, should interest scientists. "The possibility of being able to study disease in a culture dish is very exciting," says Douglas Melton of Harvard University, who has recently received permission from the school's ethics committee to derive ES cells from diabetes patients. "If we could make T cells and β cells in a dish—we're not there yet, but we're getting closer—then we could compare the diabetic cells to wild-type cells and ask what goes wrong," he explains. "For ▶

CREDITS (TOP TO BOTTOM): LEE JIN-MAN/AP; HWANG *ET AL.*

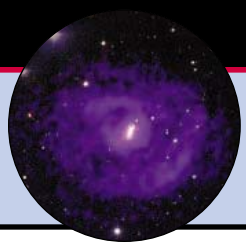

the first time we will have a chance to study the root causes of the disease."

The improved skills of the Korean group nevertheless raise difficult ethical questions (see www.sciencemag.org/cgi/content/abstract/1114454). For example, there may be increased demand among scientists for fresh oocytes from young, fertile women. Oocyte donation is usually a safe surgical procedure, but serious complications can arise. The hormones given to trigger production of extra eggs can also cause vomiting, headaches, mood swings, and hot flashes, and the long-term consequences of superovulation aren't well understood.

In the United States, a National Academies panel recently recommended that donors of oocytes should not be paid (*Science*, 29 April, p. 611). In Korea, the researchers were allowed to cover travel costs of donors, but they say that no one requested reimbursement and that no payments were made.

Bioethicist Norm Fost of the University of Wisconsin, Madison, says the team's efforts to inform oocyte and cell donors was sound, but he questions using children as skin cell donors. "The [skin biopsy] that they're doing is of almost no risk and trivial discomfort," he says. "But the default position is that when you're doing nontherapeutic research, you should use adults first."

The new results may heat up the political debate over human ES cells. Congress is expected to vote on expanded funding for ES cell research this summer, and in Massachusetts, home to Melton's group, Governor Mitt Romney has said he will veto a new law that would specifically allow human nuclear transfer experiments. (The legislature is expected to override the veto.)

Jaenisch notes that the Koreans' successes don't change the poor odds of cloning a person: As animal cloners have found, only a tiny percentage of blastocysts develop to term when implanted in surrogate mothers. "Reproductive cloning is not safe, and it will not work," he says. Most scientists agree, but given the unregulated nature of many infertility clinics, that may not be enough to stop renegade doctors from trying. What is certain, however, is that the new results will accelerate the already-racing stem cell field.

–GRETCHEN VOGEL

COLLABORATIONS

Japan Bars Indian Physicists From Lab

TOKYO—Several Indian physicists have been blocked from visiting a Japanese research lab in the past year because of what appears to be an overzealous interpretation of rules aimed at restricting the spread of nuclear weapons. Two Japanese ministries are at odds over the unofficial policy shift, which is slowing research and raising questions about future collaborations between the two countries.

The snafu mostly involves visas for Indian scientists hoping to work at Japan's High Energy Accelerator Research Organization (KEK) in Tsukuba, although there are reports of problems visiting other labs. KEK is the site of Belle, a 13-nation experiment to explore why the universe has more matter than antimatter. Last May, after making two trips to KEK, graduate student Garima Gokhroo of the Tata Institute of Fundamental Research in Mumbai learned that her visa application had been rejected. Over the next several months, at least one Tata colleague and at least three researchers from Punjab University in Chandigarh were also denied visas to visit KEK. Their plight has recently come to light.

KEK closed? Indian scientists have been refused visas to work on the Belle experiment at Tsukuba's KEK facility.

CREDIT: KEK

The Indian scientists say they were never given a reason for their rejections, and Masanori Yamauchi, a KEK physicist and spokesperson for the Belle collaboration, says he has been unable to get an explanation from Japan's Ministry of Foreign Affairs, which decides on visas. Contacted by *Science*, a spokesperson for the ministry declined to describe the criteria for granting or denying visas or say if Indian physicists are receiving special scrutiny.

But an official at the Ministry of Education, which recently started its own investigation, says the problem stems from concerns that India has declined to sign the Nuclear Non-Proliferation Treaty and other agreements intended to control the flow of sensitive weapons technologies. A change in personnel in the visa office has apparently resulted in a new hard line.

Yamauchi emphasizes that there is no connection between weapons technologies and the particle physics being studied at KEK. Tariq Aziz, a physicist in Tata's Department of High Energy Physics, notes that scientists visit Europe's high-energy physics lab CERN and the U.S. Fermi National Accelerator Laboratory "with no problem."

Japan's Education Ministry, which sponsors KEK and is promoting greater scientific cooperation across Asia, is embarrassed by the flap. "We are struggling to get appropriate visas for Indian scientists," says the official, who did not want to be identified. He says there could be a resolution "soon."

KEK's Yamauchi says that the 400-member Belle collaboration can continue without its Indian colleagues, but their absence is hurting data analysis from the experiments. "We are suffering there," he says. Tata's Gokhroo says her doctoral work "has definitely been delayed."

There could also be long-term consequences, including Tata's ability to play a role on a Belle upgrade and on the proposed Next Linear Collider. "I won't be able to ask for funding if our researchers aren't going to get visas," says Aziz.

–DENNIS NORMILE

NEW ENGLAND BIOLABS

Antarctic Phosphatase

RECOMBINANT AND 100% HEAT LABILE — A BETTER ENZYME THAN SAP AT A BETTER PRICE

For many years, BAP, CIP and SAP were the only options for dephosphorylation protocols. Now, New England Biolabs introduces Antarctic Phosphatase – a superior reagent that saves time because you can ligate without purifying vector DNA, and since it's recombinant, you are guaranteed the quality and value you've grown to expect from New England Biolabs.

To Order:

M0289S ..... 1,000 units ..... $58 ($US)
M0289L ..... 5,000 units ..... $232 ($US)

Advantages:

- 100% heat inactivated in 5 minutes
- ligate without purifying vector DNA
- recombinant enzyme for unsurpassed purity and consistency; no nuclease contamination
- active on DNA, RNA, protein, dNTPs and pyrophosphate
- active on all DNA ends: blunt, 5´ and 3´ overhangs

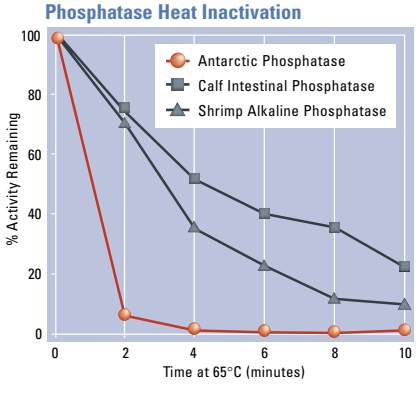

10 units of each phosphatase were incubated under recommended reaction conditions (including DNA) for 30 minutes and then heated at 65°C. Remaining phosphatase activity was measured by p-nitrophenyl-phosphate (pNPP) assay.

PRODUCTS YOU TRUST. TECHNICAL INFORMATION YOU NEED. www.neb.com

- **New England Biolabs Inc.** 32 Tozer Road, Beverly, MA 01915 USA 1-800-NEB-LABS Tel. (978) 927-5054 Fax (978) 921-1350 info@neb.com
- **Canada** Tel. (800) 387-1095 info@ca.neb.com
- **Germany** Tel. 0800/246 5227 info@de.neb.com
- **UK** Tel. (0800) 318486 info@uk.neb.com
- **China** Tel. 010-82378266 beijing@neb-china.com

NEW ENGLAND BioLabs® Inc.
the leader in enzyme technology

DISTRIBUTORS: Argentina (11) 4372 9045; Australia (07) 5594-0299; Belgium (0800)1 9815; Brazil (11) 3622 2320; Czech Rep. 0800 124683; Denmark (39) 56 20 00; Finland (09) 584-121; France (01) 34 60 24 24; Greece (010) 5226547; Hong Kong 2649-9988; India (044) 220 0066; Israel (3) 9021330; Italy (02) 381951; Japan (03) 5820-9408; Korea (02) 556-0311; Malaysia 603-80703101; Mexico 52 5525 5725; Netherlands (033) 495 00 94; Norway 23 17 60 00; Singapore 2731066; Spain 902.20.30.70; Sweden (08) 30 60 10; Switzerland (061) 486 80 80; Taiwan (02) 28802913

NANOTECHNOLOGY

Color-Changing Nanoparticles Offer A Golden Ruler for Molecules

ANAHEIM, CALIFORNIA—For researchers looking to monitor the nanoscale movement of biomolecules, good techniques are hard to come by. One that's been widely popular among biologists is to tag molecules of interest with different fluorescent dyes and hit them with a burst of light. Because of the way the dyes absorb and re-emit each other's light, tags very close together glow a different color from those farther apart. Unfortunately, the technique—known as fluorescent resonance energy transfer (FRET)—works only if the dye molecules are less than 10 nanometers apart, and the tags typically wink out after less than a minute of light exposure. Now a group at the University of California (UC), Berkeley, has come up with a novel molecular ruler that solves both problems at once.

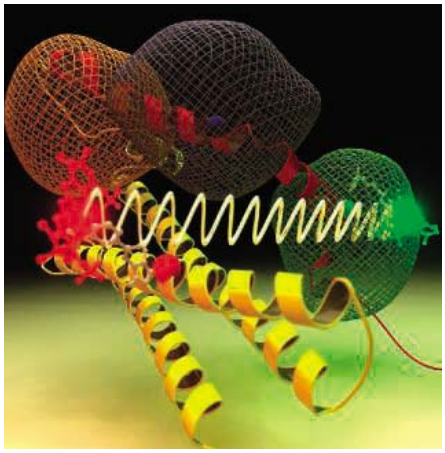

Space balls. In conventional FRET, interactions between organic dye tags (red and green) are used to measure distance.

At a meeting* here last week, UC Berkeley chemist Paul Alivisatos reported a way to use pairs of gold nanoparticles to measure distances out to 70 nanometers and keep track of their targets indefinitely. "It's really cool," says Thomas Kipps, a cancer cell biologist at UC San Diego. By extending the length of the ruler, Kipps says, nanoparticles—also known as quantum dots—offer the opportunity to gauge the proximity of molecules across stretches equivalent to large complexes of proteins. That, in turn, may make it possible to track events from the binding of DNA strands to one another to the ability of proteins called transcription factors to bind with and initiate genetic transcription.

Gold nanoparticles have been used for sensing since 1997, when a team at Northwestern University developed a scheme for detecting specific snippets of DNA with a simple color-change test. The researchers attached gold nanoparticles to single-stranded DNAs designed to home in on target DNA sequences. As the DNA strands bound to their quarries, they pulled the gold particles together tightly enough to change the way their electrons moved—a property known as plasmon resonance. The shifting electronic behavior altered the wavelengths of light the particles scattered, changing their color (*Science*, 22 August 1997, p. 1036). The experiment used hordes of nanoparticles to create a color change that was visible to the naked eye. But other studies suggested that even two particles should produce a shift visible through a microscope.

Alivisatos, Carsten Sönnichsen, Björn Reinhard, and Jan Liphardt—all colleagues at UC Berkeley and Lawrence Berkeley National Laboratory—decided to see for themselves. First, using a pair of proteins as molecular glue, they bound 40-nanometer gold nanoparticles to a glass slide. When they shined white light on the slide, far-apart particles scattered green light most strongly, with wavelengths of about 540 nanometers; light scattering from particles closer together shifted to the red end of the spectrum by about 20 nanometers. Between those two extremes, wavelength changed steadily with distance.

With their new molecular ruler in hand, Alivisatos and his colleagues set out to track the binding and unbinding of DNA. They started with a solution of pairs of gold nanoparticles tethered by snippets of single-stranded DNA. Under white light, the particles scattered light at about 550 nanometers. The researchers then added DNA strands that were complementary to the tethers. The newly introduced DNA strands bound to the tethers, stiffening them enough to push the nanoparticles apart by about 2 nanometers. As that happened, the wavelength of light scattered by the nanoparticles shifted toward the blue end of the spectrum by a few nanometers.

Alivisatos says he hopes the longer-lived, longer-range nanoparticle-based FRET will eventually overtake its organic cousin for measurements in which background light-scattering is low. That is already happening in the world of quantum dots, he notes, in which tiny inorganic nanoparticles are beginning to replace organic fluorescent dyes in a wide range of applications.

–ROBERT F. SERVICE

* NSTI Nanotech 2005, Anaheim, California, 8–12 May 2005.

CREDITS (TOP TO BOTTOM): LAWRENCE LIVERMORE NATIONAL LABORATORY; © 2004 G. F. SCHRÖDER

ScienceScope

UC Beefs Up Team Eyeing Bid to Run Los Alamos

The University of California (UC) has moved closer to competing for the management of Los Alamos National Laboratory (LANL) by announcing a major partner and a team leader. University officials said this week that Michael Anastasio, now director of Lawrence Livermore National Laboratory in California, would head the New Mexico nuclear weapons lab if it won the Department of Energy (DOE) contract. Last week the university said it was aligning with industrial giant Bechtel in advance of the DOE contract specifications, due out this week.

If UC submits a bid, it will be the third industry-academic alliance to enter the fray to manage the $2.2 billion lab, created in 1943. Sandia National Laboratories manager Lockheed Martin has already announced its decision to join with the University of Texas on a bid, with Sandia Director C. Paul Robinson as the would-be head. A third defense contractor, Northrup Grumman, plans to bid in collaboration with an as-yet-unnamed academic partner.

Anastasio, a weapons designer, has run the Livermore weapons lab since 2002. San Francisco–based Bechtel, which runs several government nuclear facilities, bolsters the university's safety and management skills. "They needed a partner like that if they were to have a chance," says former LANL assistant director Tom Meyer. But he worries that a culture of scientific freedom at Los Alamos could suffer if Bechtel became "a dominant partner."

–ELI KINTISCH

Global Network for Health Data

A global coalition of foundations, countries, and development agencies has formed to improve the collection of health data in the world's poorest countries. The Health Metrics Network, announced at the World Health Assembly in Geneva, Switzerland, this week, aims to strengthen disease reporting, tracking, and analysis.

Many countries don't even fully record births, deaths, or causes of death. Better health information would also guide international efforts to fight disease, says David Fleming, director of Global Health Strategies at the Bill and Melinda Gates Foundation, which is supporting the initiative with $50 million. "It's about making sure that every life counts and is counted," Fleming says.

–MARTIN ENSERINK

NASA BUDGET

Griffin Names Winners and Losers in Cost Squeeze

Declaring that NASA "can't afford to do everything on its plate," the agency's new chief last week laid out sweeping changes to the U.S. civilian space program—including the $5.5 billion science program. Michael Griffin says he plans to scale back space station research, defer work on a future Mars robotic mission, inject more cash into NASA's struggling earth science effort and servicing and safe deorbiting of the Hubble Space Telescope, and back a mission to Jupiter's moon Europa using a conventional rather than nuclear system. He also pledged to protect the science budget from the cost of sending humans to the moon and Mars.

Under scrutiny. Michael Griffin wants to defer the Mars Science Lab as part of cost-saving plan at NASA.

Griffin's plans for the $16.2 billion agency were laid out in a bulky budget document for the current year sent to Congress 11 May and reinforced at a Senate hearing the next day. "We have tried to be sensitive to the priorities of the affected research communities and have listened carefully to their input," he wrote.

Griffin was blunt about NASA's fiscal crisis, which includes $500 million in overruns on projects from the Mars Reconnaissance Orbiter to the Pluto mission slated for launch next year, more than $400 million in congressional pork, and the increased costs to get the space shuttle flying again. The new operating plan shaves $53 million this year from a $4 billion space and earth sciences budget. Bigger savings, he says, would come from deferring work on human exploration technologies, reducing the number of contractors involved in building a new human exploration vehicle, and scaling back the Prometheus nuclear system championed by his predecessor Sean O'Keefe (*Science*, 30 January 2004, p. 614).

Spending $270 million rather than $431 million this year on the system would torpedo plans for a probe to Jupiter to examine that planet's array of icy moons. But Griffin, appearing for the first time before the new Senate Appropriations Subcommittee on Commerce, Justice, and Science, assured legislators that a mission to Europa "remains a very high priority" and promised a detailed plan for a flight using standard chemical propulsion. Cost overruns killed an earlier proposed Europa mission.

Although overall spending on space and earth sciences remains largely unchanged, the shifts within that budget have big implications for individual projects. For example, NASA intends to defer launch of the Mars Science Laboratory from 2009 to 2011 and scale back funding for the Space Interferometry Mission and the Terrestrial Planet Finder—two missions slated for launch later in the next decade and designed to seek extrasolar planets. Some of that money would be diverted to earth science, and another portion would be used to ensure potential Hubble servicing and, eventually, a safe deorbiting of the massive telescope. "We have heard the response of the science community, and we in turn are being responsive," Griffin said. A final decision on a Hubble servicing mission is expected after the second shuttle mission, now slated for September. ▶

U.S. NUCLEAR WEAPONS

Bunker Buster Shot Down in Opening Volley

Opponents of nuclear "bunker buster" weapons have scored a victory in the first round of the annual fight over U.S. nuclear policy.

Stung by a congressional defeat last fall of its request for $27 million for a feasibility study of the Robust Nuclear Earth Penetrator (RNEP), the Bush Administration this year sought only $4 million for research by the Department of Energy's National Nuclear Security Administration (NNSA) and $4.5 million for the Air Force to devise a delivery system that would be carried by the stealth B-2 bomber. But the Administration's scaled-back strategy for the weapon, which would target facilities deep underground, did not fare well last week.

Representative David Hobson (R–OH), chair of the House spending panel, again zeroed out the NNSA funds from his bill. And for the first time, a House panel that authorizes defense programs voted to move RNEP from the energy department to the Pentagon, which is not permitted to conduct nuclear research. By "taking the 'N' out of RNEP," as a House staffer put it, legislators were expressing a preference for conventional approaches to rooting out entrenched foes. Members of the equivalent authorization panel in the Senate split the Administration's request, rejecting the B-2 component while approving the NNSA funds.

"It was very surprising. [House Armed Services] is a fairly conservative group of members," says David Culp, a lobbyist for the Friends Committee on National Legislation, a Quaker advocacy group. A House aide described the agreement as a face-saving way for the Republican-led committees to oppose the White House without excluding any chance of future development of nuclear penetrators. But although opponents of the proposed weapon are worried about that prospect, they are counting on Hobson to remain vigilant.

Supporters of the idea say that the concept needs to be part of the country's arsenal. "Are we proposing a specific weapon? No. We are proposing a study," Defense Secretary Donald Rumsfeld told Congress last month. Senator Jeff Sessions (R–AL) has said that the weapon adds "credibility" to the U.S. deterrent. Last month a report by the U.S. National Academies concluded that a bunker-buster weapon could result in heavy casualties because the bombs "cannot penetrate to depths required" for total fallout containment.

The spending and authorization bills must be approved by each body and then any differences reconciled. That schedule gives both sides plenty of time to dig in before the next battle. **–ELI KINTISCH**

CREDITS (TOP TO BOTTOM): ALEX WONG/GETTY IMAGES; JPL/NASA

Griffin also suggested "alternative configurations" that would allow NASA to complete the space station with fewer than the 28 shuttle flights now planned. "Some of the research [to be done] on the utilization flights could be deferred," he suggested. NASA's operating plan cuts $106 million from the $1-billion-a-year biological and physical research effort and assigns a lower priority to basic research using organisms such as cells and rats, as well as fundamental research with no link to human exploration. "Research [on the station] is valuable and must be done," Griffin said, "but if it is delayed a very few years … then … that delay would be worth it." He also promised legislators that exploration would trump the overall science budget only "under the most extreme budget pressure."

Despite their concerns about individual projects, legislators seemed to welcome Griffin's direct approach to the agency's fiscal troubles. "Some of the things you've said give us heartburn," said Senator Barbara Mikulski (D–MD). But "thank you for your candor." Given the difficult choices Griffin must make, that is high praise. **–ANDREW LAWLER**

U.S. MILITARY FACILITIES

Pathology Institute Hit in Base-Closing Plan

The U.S. Department of Defense (DOD) plans to create new research centers of excellence as part of an effort to shore up biodefense and other medical areas. But in doing so, it would close one of DOD's most venerable research institutions: the Armed Forces Institute of Pathology (AFIP) in Washington, D.C.

The changes are part of the Base Realignment and Closure 2005, the latest in the military's periodic effort to streamline its vast network of facilities (www.defenselink.mil/brac). DOD estimates the plan would save up to $50 billion over 20 years by realigning 29 bases and closing 33, including AFIP's host, the Walter Reed Army Medical Center campus in northwest Washington, D.C.

One beneficiary would be the U.S. Army Medical Research Institute of Infectious Diseases (USAMRIID) at Fort Detrick, Maryland. Already slated for a $1 billion facilities expansion in the president's 2006 budget request, USAMRIID stands to gain staff from other facilities and join a DOD center of excellence in biodefense. Five other joint Army, Navy, and Air Force centers will study topics such as chemical defense and infectious diseases.

Keeper. DOD's plan to close AFIP would move its registry of soldiers' DNA to Delaware.

The pathology institute, with a current 820-member staff that includes about 120 scientists, would, however, get lost in the shuffle. It began in 1862 as a museum for specimens from Civil War casualties. In 1946, Congress created AFIP, which specializes in diagnosing difficult disease cases for both military and civilian doctors. Its experts were "among the giants," and educational training there was "legend," says pathologist Fred Gorstein of Thomas Jefferson University in Philadelphia. Recently, AFIP scientists fingered the virus that caused the 1918 pandemic influenza, identified victims of the 9/11 terrorist attacks, and helped investigate the 2001 anthrax poisonings.

Staffers have known for a few years, however, that DOD might close AFIP as part of efforts to eliminate civilian services, and some have moved on. Under the plan, only AFIP's renowned tissue repository and the flagship National Museum of Health and Medicine, with its displays on Civil War medicine and preserved body parts and fetuses, will remain. Diagnostic pathology tasks will be outsourced, and DOD will shift AFIP's work on a DNA registry and forensics to Dover Air Force Base in Delaware.

Several AFIP scientists declined to comment. But pathologist William Travis, who left in January for Memorial Sloan-Kettering Cancer Center in New York City, called it "a tragedy" to close "a national medical treasure." He would like to see Congress rescue the institute, possibly by contracting it out to the American Registry of Pathology, a nonprofit organization chartered by Congress that links AFIP to civilians. Travis also worries about the fate of the tissue repository, which includes unique specimens of rare tumors and infectious diseases. "It loses its value if separated from pathology expertise," he says.

The base closure plan must be approved by an independent, nine-member commission and then by Congress, which is not allowed to tinker with its recommendations.

–JOCELYN KAISER

CREDIT: KAREN KASMAUSKI/CORBIS

ScienceScope

Battey Staying at NIH

The odds that the National Institutes of Health (NIH) will soften its strict rules on stock ownership improved this week after an institute director heading out the door decided to stay put and a senior scientist with qualms about becoming an institute director agreed to take the job.

James Battey, director of the National Institute on Deafness and Other Communication Disorders, had declared this spring that a prohibition on senior staff owning biomedical stock was forcing him to leave because he manages a family trust (*Science*, 8 April, p. 197). Battey had applied for a post at the new California Institute for Regenerative Medicine. But this week he said in an e-mail that he has dropped his job search and is "confident" that he can "fulfill my obligations to my family while remaining at NIH." He will also be reinstated as director of the NIH Stem Cell Task Force.

David Schwartz, incoming National Institute of Environmental Health Sciences director, said this week he will join NIH on 23 May because "my concerns about the conflict-of-interest rules have been heard and are being seriously considered." Schwartz, now at Duke University, had said earlier that the stock ban was a deterrent to his taking the new job.

–JOCELYN KAISER

U.S. Mineral Research Spared the Ax

The House appropriations committee last week took the first step in restoring funding to a $54 million program on mineral research that the Bush Administration wants to gut.

Run by the U.S. Geological Survey, the mineral resources program surveys imports, exports, and production of economically important and strategic minerals and predicts their future availability. Program scientists also research basic questions such as how microbes influence the geochemistry of mercury, arsenic, and other harmful minerals.

Faced with a loss of revenue from a malfunctioning LANDSAT satellite, the Bush Administration proposed a 53% cut for 2006 in the program and the elimination of 240 positions. The House committee "strongly disagrees" with that move, says report language, and recommends that the program be fully funded. The Senate is expected to take up the bill in the next few weeks.

–ERIK STOKSTAD

HIGHER EDUCATION

Harvard Pledges $50 Million To Boost Diversity on Campus

Harvard University plans to spend at least $50 million over the next decade to create a more diverse academic community in all disciplines, including throughout the sciences. President Lawrence Summers announced the outlay this week after receiving two reports commissioned in February following his comments about the ability of women to do science, which triggered a national debate.

The initiative will tackle all aspects of gender and minority issues, from the safety of women working late at night at research labs to the need for a high-level advocate within the Harvard administration. Such a comprehensive strategy is essential, say the chairs of the two task forces that reported to Summers. "Women need to see careers in science as desirable and realistic life choices," says Barbara Grosz, a computer scientist who led one of the task forces that focused on science and engineering. A second task force, led by science historian Evelynn Hammonds, examined challenges facing all women faculty.

Outside researchers are impressed with the breadth of the recommendations. "This is very encouraging," says Donna Nelson, a chemist at the University of Oklahoma, Norman, who tracks the status of women and minority academic scientists. "If they can implement this, they can take a leadership role."

Harvard has long been criticized for its lack of diversity of science faculty in several disciplines, a situation made worse by Harvard's decentralized structure and its policy not to grant tenure to junior faculty, task force members said. Last year, for example, four women and 28 men in the school of arts and sciences received tenure offers. But the long-simmering issue did not come to a head until Summers's comments at a January workshop on women in science became public (*Science*, 28 January, p. 492). The resulting outcry triggered a faculty vote of no confidence in Summers, who apologized repeatedly.

Raising awareness. Harvard Dean Drew Gilpin Faust (*left*) with task force chairs Evelyn Hammonds and Barbara Grosz.

Hammonds's committee called for a senior provost for diversity and faculty development to work with Harvard deans to promote gender and ethnic equity. Harvard Provost Steven Hyman hopes to name that person—who likely would come from within Harvard—by September. The panel also proposed two funds, one to provide partial salary support for hiring scholars who increase diversity, the second to fund their labs. It said Harvard should begin to gather systematic data on faculty hiring, retention, and other measures and make the academic culture more family-friendly, through enhanced maternity leave practices, child-care support, and adjustments to the tenure clock. Grosz's panel urged the university to set up summer research programs for undergraduates, expand mentoring for all students, and provide research money for faculty juggling family and career.

Funding will not be a problem, Summers assured reporters, referring to the likelihood of "more resources allotted down the road." The biggest challenge Harvard faces, he said, is to overcome "issues of culture" within a university created "by men for men." Harvard is accepting comments on the report through the end of June, and academics around the country will be watching closely to see how well Harvard succeeds in transforming that culture.

—ANDREW LAWLER

GENOMIC MEDICINE

Gene Sequence Study Takes a Stab at Personalized Medicine

COLD SPRING HARBOR, NEW YORK—Since its beginning 15 years ago, the Human Genome Project was sold to the public and to Congress as a biomedical effort that would ultimately bring a person's unique DNA sequence data to bear on preventing and treating disease. Now the National Human Genome Research Institute (NHGRI), which led the U.S. public sequencing effort, is about to take a controversial step toward that goal.

At the Biology of Genomes meeting here last week, NHGRI's Eric Green announced that NHGRI will launch a pilot study in which researchers will sequence a portion of DNA from 400 seemingly healthy volunteers and try to discern each person's unique genetic risk factors for disease. They also plan to study the reactions of the volunteers to learning these results. "[NHGRI] is doing a reality check: Do people really want personalized medicine?" says Kelly Frazer, a genomicist at Perlegen Sciences in Mountain View, California.

The project, dubbed clinENCODE, promises to jump-start the transition from basic biological studies to clinical genomics, and that "is what the genome project is all about," says Richard Wilson, director of the sequencing center at Washington University in St. Louis, Missouri. But both Bruce Roe of the University of Oklahoma, Norman, and Evan Eichler of the University of Washington, Seattle, call the study as described a "terrible idea," in part because the sequence information from each individual may not provide much relevant biomedical information.

The 400 volunteers will donate DNA and undergo a battery of tests, including blood pressure measurements and white blood cell counts. Green and his colleagues will sequence the same 1% of each person's genome, regions that are already being intensely studied by basic researchers. Green's team plans to report back any variations spotted, including ones that may explain a person's current and future health status.

It's not clear how people will react to such results. Previous studies involving genetic testing for specific diseases have suggested that people can handle bad health news. Still, many fear that this genetic information will lead to discrimination by employers and insurance companies.

Many genome scientists argue that clinENCODE is not the best way to explore the future of personalized medicine. "There are so many genes whose function and link to disease is unknown that the information we are going to give is of dubious nature" and may overwhelm the participants, says Frazer. If the chief goal is to test how the public reacts to personalized genome information, then why not simply do surveys or present mock sequencing results rather than incur the expense of sequencing, she and others wonder.

Even if the study provides little biomedical data, it will still be worthwhile, contends Robert Waterston, a geneticist at the University of Washington, Seattle. "We have to understand what the issues [of personalized medicine] are," he says. "[The study] begins to challenge us to think about these things."

—ELIZABETH PENNISI

CREDIT: KRIS SNIBBE/HARVARD NEWS OFFICE

ECOLOGY

Biologists Find New Species of African Monkey

When conservation biologist Trevor Jones peered last year through his binoculars at the shape flitting through Tanzania's Ndundulu Forest Reserve, he saw something unexpected. Out searching for a gray, pink-faced monkey called the Sanje mangabey, he instead spotted a brown, black-faced mangabey sporting an upright crest on his forehead that made the animal look "punky." Speechless and shaking, Jones sat down. "I was gobsmacked," says Jones, who works for the Udzungwa Mountains National Park in Tanzania.

Monkey see. Two research groups almost simultaneously spotted this new monkey species (artist's illustration).

About the same time, 350 kilometers away in Tanzania's Southern Highlands, researchers led by zoologist Tim Davenport of the Wildlife Conservation Society in Tanzania had been trying to track down an animal called the Kipunji. Local hunters often talked about the unusual monkey, but they were known to speak of spirit animals too. But real it was: Davenport first spotted the unique mangabey almost a year after his team started looking. The two groups heard about each other's findings in October, and now, on page 1161, they together describe the new species, dubbed *Lophocebus kipunji*.

"This is big news for Africa," says primatologist Scott McGraw of Ohio State University, Columbus. "The chances of finding a large, noisy monkey that no one's ever [scientifically] described before makes this a rare event," agrees primatologist John Fleagle of Stony Brook University in New York. In addition, the forest in which the teams found the species is one of the most globally significant regions for biodiversity—the now heavily threatened animal and plant species living there go back 30 million or 40 million years in history, says biologist Neil Burgess of the United Nations Development Programme and the World Wildlife Fund–USA.

Although the researchers still need a DNA sample to determine how closely related the new species is to other mangabeys, the highland mangabey looks and sounds quite different from its cousins. It utters a softer "honk-bark" compared to the louder "whoop-gobble" call of other tree-dwelling mangabeys, says Jones. Kipunji are also shy, he says, and exhibit some unusual behaviors: "Just before he flees, the male does this fantastic head-shaking behavior as if he's admonishing you."

Mangabeys belong to two groups. One group, which includes the Sanje mangabey, wanders the forest floors and is related to mandrills. The other lives in the trees and is more closely related to baboons; *L. kipunji* is the third species in this group. Some researchers consider the area in which the animals were found to be the "epicenter" of baboon and mangabey evolution. McGraw hopes the kipunji will help researchers reconstruct how the two primate species, and another called the gelada, radiated out from a common progenitor.

But the new mangabey is already threatened. Preliminary estimates of its range encompass just 120 square kilometers total, and the research teams predict that no more than 500 animals exist in each forest. Davenport says conservation efforts need to be stepped up to prevent the animals in the Southern Highlands from being hunted to extinction. Burgess adds that the highland mangabey and another recently discovered shrew in the Ndundulu Forest Reserve might be the push that gets the small piece of forest rolled into Udzungwa Mountains National Park. But ultimately, he says, Tanzania is a poor country: "If we want to keep these [animals], the global community has to provide money until the country becomes a richer place." Otherwise it may become poorer in monkeys. **–MARY BECKMAN**

Mary Beckman is a writer in southeastern Idaho.

CREDITS (TOP TO BOTTOM): ZINA DERETSKY/NATIONAL SCIENCE FOUNDATION; JOHN ROWE ANIMATIONS

PHYSICS

Neutron Stars Could Test Quantum Effect

It's one of the stranger predictions of quantum electrodynamics: In a strong magnetic field, the vacuum of space might behave like a crystal. In the 29 April issue of *Physical Review Letters*, Italian and French physicists argue that a peculiar star system might provide an unprecedented chance to test this prediction. "It's a really unique opportunity," says Michael Kramer, an astrophysicist at Jodrell Bank Observatory in Manchester, U.K. "Just speculating about the possibility is very exciting."

The excitement surrounds a binary pulsar: two neutron stars orbiting each other, discovered late in 2003. The neutron stars in the system both emit powerful beams of radiation that zap Earth at predictable intervals. This means that the system, known as J0737-3039, provides a pair of clocks to measure how the gravitational fields of the massive stars warp time and space, as the general theory of relativity predicts. Now physicists say they have found a new use for the stars.

Beam team. Binary system J0737-3039 might shed new light on light.

Quantum theorists consider the vacuum to be full of particles constantly winking in and out of existence. Where those "virtual particles" encounter the powerful magnetic fields near a neutron star, light passing through should slow down and bend, just as it does inside a hunk of glass or crystal. "The index of refraction changes with magnetic field," says Carlo Rizzo, a physicist at the Institute for Research on Atomic Systems and Complex Molecules in Toulouse, France. "And different frequencies of light have different velocities."

Rizzo and colleagues in France and Italy hope J0737-3039 will help them measure this subtle effect. "It's like somebody in the cosmos set up a system to do the sort of experiment we want to do in the lab," Rizzo says. At times during the stars' orbit, the beam from one pulsar passes right through the other pulsar's intense magnetic field. If x-ray astronomers observe for a long enough time, Rizzo says, they might see a bending of light rays that exceeds that due to the gravitational distortion of spacetime.

It won't be easy. "You have to observe for a long time if you want to have enough statistics," Rizzo says. Indeed, Alice Harding, a physicist at NASA's Goddard Space Flight Center in Greenbelt, Maryland, doubts that the bending will be seen anytime soon. Not only is the phenomenon small compared to gravitational lensing, but if the neutron star's spin axis is pointing even slightly in the wrong direction, "that will wipe out any detectable effect," she says.

But whether or not J0737-3039 is a good spot to find quantum-theoretic vacuum lensing, the system is already a laboratory for new physics. "It has almost become an industry on its own," Kramer says. **–CHARLES SEIFE**

Astronomers are learning how to find the barest sprinklings of stars, which trace unseen pockets of dark matter in our cosmic neighborhood

The Hunt for Stealth Galaxies

If grand spiral galaxies are the photogenic pinups of astronomy, then the faint smudges of stars called dwarf galaxies are the bit players that few fans will recognize. Telescopes can barely see them, and no one knows how many dwarfs inhabit the bleak gulfs between galaxies like the Milky Way and Andromeda. But just as minor actors can steal a scene, dwarf galaxies are earning respect from astronomers who take time to stare away from the lights.

Sensitive searches of space are unveiling a growing population of "little pathetic things," in the words of astronomer Liese van Zee of Indiana University, Bloomington. Although their stars are meager, dwarfs appear to be embedded within dense cocoons of unseen dark matter—the same mysterious stuff that composes the bulk of the universe's mass. Tracing the numbers and locations of dwarfs is giving theorists a better grasp of how dark matter has shaped the growth of larger galaxies and is revealing the smallest coherent clumps of matter within which stars can form.

Meanwhile, radio telescopes are tuning in to the faint murmurs of other small galaxies and finding huge amounts of matter—ordinary hydrogen gas—that never coalesced into stars. Some of this matter may date to the earliest history of the cosmos, giving astronomers a chance to study pristine gas unprocessed by the fires of stellar fusion. In one disputed case, researchers may have found a true "stealth galaxy," a massive whirling disk of hydrogen that has spawned no stars at all.

These galactic shreds may have been the first substantive knots of matter to assemble in the universe. Astrophysicists think most of them collided over the eons to create big galaxies like our own—mergers that continue on a minor scale today. In that picture, today's dwarfs are the last remnants of those ancient structural seeds.

"Dwarf galaxies are our best way to figure out what the building blocks of our galaxy would have looked like," says doctoral student Alan McConnachie of the University of Cambridge, U.K. "The dwarfs we can see are special. They are the ones that survived."

Imprints of tides

Astronomers must look close to home to find those survivors: Most dwarfs are too insubstantial to be seen at great distances. By studying dwarfs within our cosmic suburb, called the Local Group, astronomers can make deductions about the environs of any mature galaxy, says astronomer Michael Merrifield of the University of Nottingham, U.K.: "The immediate neighborhood of the Milky Way is a representative bit of the universe."

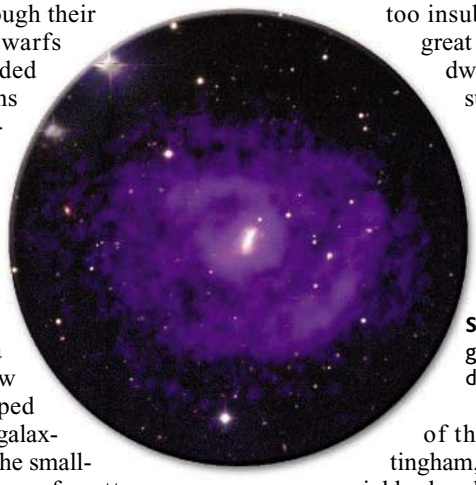

Starless gas. A vast hydrogen disk (purple) envelops dwarf galaxy UGC 5288.

The Milky Way and Andromeda dominate the Local Group, which spans about 10 million light-years of space. The group also contains a few midsize galaxies and about three dozen known dwarfs. Roughly a dozen of these dwarfs appear to orbit the Milky Way; Andromeda has a slightly bigger retinue. The rest are scattered spritzes of stars doing their own thing, with no apparent ties to the Local Group's giants.

These minigalaxies are not inert nubs. Rather, astronomers think they have histories as dynamic as those of their bigger neighbors. "They have been evolving chemically and structurally for the entire history of the universe," says McConnachie. That evolution critically depends on a dwarf's path through space.

Most isolated dwarfs in the middle of the Local Group are "irregulars," misshapen patches with some younger stars and rich clouds of gas. But when a dwarf approaches a big galaxy, it transforms. Hot matter on the outskirts of a massive galaxy may strip some gas out of the dwarf as it orbits, like a fresh wind clearing fog out of a city. Moreover, the big galaxy exerts gravitational tides on the dwarf. Those motions set off waves of star formation, exhausting the dwarf's remaining supply of gas—the fuel for creating new stars.

What's left is a so-called spheroidal, a barren fuzzball of old stars. These objects are ripe for cannibalism by the bullies of the Local Group, a process that astronomers can now trace from start to finish. It begins with telltale tidal distortions within the dwarfs, such as S-shaped patterns of stars in spheroidals near Andromeda. Within a few billion years, such dwarfs are doomed—sure to be dragged ever inward through the galaxy's extended halo of gas and its pervasive shroud of dark matter.

When a dwarf starts slogging through the visible outskirts of a big galaxy, gravitational tides tear it apart. Astronomers see this happening today to a stretched-out dwarf called Sagittarius, on the far side of the Milky Way. Similarly, thick streams of stars lacing around Andromeda are the sole remains of dwarfs that the galaxy recently absorbed.

Astronomers believe this process happened often in the early universe, as major galaxies assembled within dense pockets of dark matter. Dwarf galaxies have far "darker" pockets than big galaxies have, on a star-by-star basis. For instance, a nearby dwarf spheroidal called Draco may pack 200 times more mass in invisible matter than in its stars. That's an order of magnitude higher than the ratio of dark matter to luminous matter in the Milky Way. Dwarf galaxies are nuggets of dark matter, it seems, with stars sprinkled in as an afterthought.

CREDITS (TOP TO BOTTOM): D. ZUCKER/MPIA AND SLOAN DIGITAL SKY SURVEY (ANDROMEDA GALAXY); L. VAN ZEE, INDIANA UNIVERSITY AND NOAO/NRAO/AUI/NSF

Look closely. Most faint stars sprinkled throughout this photo belong to Andromeda IX, a satellite of the neighboring Andromeda galaxy (facing page).

CREDIT (INSET OF DWARF SATELLITE): D. ZUCKER/MPIA AND SUBARU/NAOJ

Calling all satellites

That blackness poses a vexing challenge. Theorists crave an accurate census of the dwarfs that populate our local cosmos to help solve a puzzle they first noted in 1999, called the "missing satellites problem." But astronomers can't yet tell how many they've missed.

According to cosmological models, a vast web of dark matter formed in the early universe. Astrophysicists see that embryonic pattern in the subtle ripples of the cosmic microwave background, the remnant glow of the big bang itself. The web controls where and how galaxies arise. Big clumps of dark matter attract smaller ones, thanks to their powerful gravity. And ordinary matter, such as hydrogen gas, settles within the clumps and sparks the birth of stars when its density gets high enough.

But the process is messy. Small knots of dark matter can swarm for eons without merging, like leaves circling an eddy. Simulations predict that enough of these leftover dark-matter "subhalos," as the knots are known, should fleck the Local Group to seed many hundreds of dwarfs. Where are they?

In the past 3 years, theorists have found a possible explanation: Many subhalos probably didn't stay calm enough to form stars. As hot young stars began to shine in bigger galaxies, they irradiated space with ultraviolet light. This energy would have excited hydrogen gas in the nascent dwarfs, preventing the gas from cooling enough to collapse into new stars. If stars did form, they might have wreaked havoc in the puniest subhalos. "The [gravitational] binding energies of these galaxies are so small that one supernova could disrupt the whole thing," says Merrifield.

If this scenario is correct, surveys with optical telescopes won't find hundreds of nearby dwarfs after all. However, observers and theorists agree that some dwarfs surely await detection. For instance, new simulations by a group based at the University of Durham, U.K., point to as many as 70 visible dwarfs near the Milky Way. The galaxy's 12 known dwarfs may yet be "the tip of the iceberg," says graduate student Noam Libeskind of the Durham team.

Astronomers are hot on the trail. Teams rely on surveys that span sweeping chunks of the sky—notably the Sloan Digital Sky Survey, based at Apache Point Observatory in Sunspot, New Mexico. The survey classifies stars by color and brightness so accurately that computers can select light from stars of a uniform type. For instance, all galaxies contain a percentage of bloated red giant stars. A surplus of such stars in a small patch of sky might trace the faint wisps of an unknown dwarf. Daniel Zucker of the Max Planck Institute for Astronomy in Heidelberg, Germany, compares this method to "finding forests by their trees."

> "The dwarfs we can see are special. They are the ones that survived."
>
> —Alan McConnachie, University of Cambridge

A team led by Zucker used Sloan data in 2004 to find a new companion to Andromeda, a barely-there dwarf called Andromeda IX. The stars are so sparse that even a detailed image from Japan's 8.2-meter Subaru Telescope in Hawaii, shown on this page for the first time, hardly reveals the galaxy. "You would have to stare at one place in the sky with a large telescope for an incredibly long time just to see some fuzziness," Zucker says.

Andromeda IX is an anemic galaxy of old stars, according to a study led by astronomer Daniel Harbeck of the University of California, Berkeley, in the 10 April *Astrophysical Journal*. The dwarf must have lost its gas early on, Harbeck says, preventing a new generation of stars from forging iron and other heavy elements. And the first analysis of the motions of stars within the dwarf hints at a dominant nugget of dark matter similar to the one found in Draco, reports a team led by astronomer Scott Chapman of the California Institute of Technology in Pasadena. The fast-moving, widely spaced stars would disperse into space without the dark matter's hefty gravity. The new paper will appear in *Astrophysical Journal Letters*.

Less than a year after the discovery of Andromeda IX, a new Milky Way dwarf—a smattering of about 100,000 stars in Ursa Major, or the Big Dipper—took its place as the least luminous known galaxy. The new runt could keep its dubious honor for a while, says astronomer Beth Willman of New York University, whose team announced the find in March. "This object is close to the limit of what we can detect with Sloan," Willman says, and Zucker adds that it probably wouldn't be visible with current data if it orbited Andromeda. Both Zucker and Willman see other potential dwarfs lurking in their images, but they say more-thorough surveys will be needed to find most galactic satellites and to make observations jibe with theory.

Making waves with radio

To do more, astronomers must turn a different set of eyes onto the heavens: radio telescopes. When tuned to a certain wavelength, these dishes pick up subtle signals from small galaxies—not from stars, but from gas.

That wavelength is the famous 21-centimeter line spontaneously emitted by cool, neutral hydrogen atoms. Radio astronomers have studied that line for decades, but only recently have they outfitted telescopes with the right tools to conduct broad surveys for gas-rich dwarf galaxies and other as-yet-unseen objects.

The most ambitious program is now under way at the 305-meter Arecibo radio telescope in Puerto Rico. With a sensitive new compound detector, built in Australia, the Arecibo team plans to image hydrogen emissions over 1/6 of the sky within 4 to 5 years. The survey officially began in February, but the team had already detected 165 galaxies and other objects during a commissioning run last fall.

"If a galaxy has any hydrogen gas in it, we will see it," says radio astronomer Martha Haynes of Cornell University in Ithaca, New York, who leads the survey with Cornell colleague Riccardo Giovanelli. Among the survey's main quarries are dwarfs in or near our Local Group that have retained their gas by virtue of avoiding interactions with big galaxies.

Indiana University's van Zee found one such object serendipitously with the Very Large Array of 27 radio telescopes in Socorro, New Mexico. Among five galaxies in van Zee's study was UGC 5288, a nondescript dwarf about 16 million light-years away. Radio emissions revealed an extraordinary disk of gas, extending seven times farther into space than the galaxy's stars. "It's a huge amount of hydrogen, but it's spread out like a pancake," says van Zee. She described the dwarf in January at a meeting of the American Astronomical Society in San Diego, California.

According to van Zee's analysis, the hydrogen is rotating peacefully. That suggests the gas was not expelled by supernovas or captured during a merger. She suspects the hydrogen is a relic of the galaxy's birth, making the disk a potentially rare sample of the gas from which galaxies arose—and relatively uncontaminated by nuclear fusion in stars.

UGC 5288 is "density-challenged," Haynes says. "It did not have enough gravity to form in a normal way. These galaxies have a much slower process of converting their gas into stars, if at all." Van Zee notes that UGC 5288 does contain a lot of dark matter, but some process—perhaps rapid spin at birth—spread most of its gas too diffusely.

Astronomers have long hoped to find an even more extreme object: a galaxy consisting only of gas, in which stars have never burst forth. A team led by astronomer Robert Minchin of Cardiff University in the United Kingdom made just such a claim in the 20 March *Astrophysical Journal Letters*. Using radio data from the Jodrell Bank Observatory in the U.K., the team found a "dark hydrogen cloud" about 1/10 as massive as the Milky Way on the margins of the heavily populated Virgo Cluster of galaxies. The starless cloud shows evidence of galaxylike rotation, Minchin says.

The observations drew worldwide attention, but few other astronomers were convinced. Nottingham's Merrifield noted that the pattern Minchin's team ascribed to a rotating disk—closely tied regions of hydrogen, some moving away from us and others toward us—could also arise from smaller blobs of gas moving in different directions. Haynes also is skeptical: "The Virgo Cluster is a tricky place to work. It's a dynamic environment," she notes, with galaxies milling about and perhaps casting off shreds of gaseous debris.

New detailed images might settle the issue. Minchin's team used the Westerbork Synthesis Radio Telescope, an array of 14 antennas in the Netherlands, to zero in on the mystery object in late April. The team has not yet settled on an explanation for the patterns it sees. "We're working on what it means," Minchin told *Science*. "It's certainly more complex than just a [dark] galaxy on its own. I still think it's a bona fide galaxy," he says, although it may have interacted with a neighbor.

The astronomers also will use the Hubble Space Telescope later this year to scour the dark patch for hints of stars. "Watch this space," Minchin says with a chuckle. His slogan applies equally well to those who scan the depths between giant galaxies, looking for feeble companions to help complete the tale of cosmic assembly.

–ROBERT IRION

Nonproliferation

A Radioactive Ghost Town's Improbable New Life

The city of Pripyat, abandoned after the Chornobyl explosion 19 years ago, offers a unique trove of data for modeling a dirty bomb attack

PRIPYAT, UKRAINE—A rusted Ferris wheel groans in a stiff breeze, the only sound in Pripyat's central square. In April 1986, this attraction and the adjacent bumper cars were newly built and preparing to open for the First of May holiday. Then on 26 April, reactor number four of the Chornobyl Nuclear Power Plant exploded, spreading radionuclides across Europe. Most of the 50,000 residents of Pripyat, within eyesight of the reactor, were power plant workers and their families; everyone was evacuated. They were told to pack for a 3-day trip, but their relocation to other parts of Ukraine ended up being permanent. Nineteen years later the abandoned town is frozen in time, the dilapidated little amusement park still waiting for opening day.

Dead end. Entry to the city of Pripyat, near the Chornobyl nuclear plant, has been barred since the evacuation of 1986.

CREDIT: R. STONE/*SCIENCE*

In a bizarre twist brought about by the 11 September 2001 terrorist attacks, Pripyat is getting a new lease on life. People will never move back into the deteriorating Soviet-era apartments. Instead, scientists are planning to use the radioactive ghost town as a unique laboratory for modeling the dispersal of radionuclides by the detonation of a dirty bomb or an attack with chemical or biological agents. "Pripyat offers an unparalleled opportunity to fully understand the passage of radioactive debris through an urban area," says a nonproliferation official with the U.S. State Department. Modeling in Pripyat, he says, also "can be extended to preparing us against biological and chemical aerosols."

The surreal city's resurrection as a test bed for catastrophes gained backing at a workshop on aerosol dynamics held last month at the International Radioecology Laboratory (IRL) in nearby Slavutych, a town built to replace Pripyat. The workshop was sponsored by the U.S. Civilian Research and Development Foundation, an Arlington, Virginia–based nonprofit that funds nonproliferation efforts in the former Soviet Union. There, radioecologist Ronald Chesser of

Texas Tech University in Lubbock described new models of the radioactive plumes from the burning reactor. In addition to giving a sharp picture of the accident, they can be adapted to predict the spread of aerosols in a hypothetical terrorist attack.

Two years ago, a team led by Chesser, Brenda Rodgers of West Texas A&M University in Canyon, and IRL's Mikhail Bondarkov measured radioactivity at hundreds of spots in the so-called Red Forest, a swath of dead pines west of the reactor that received lethal radiation doses from the first plume, known as the western trace. (It's called the Red Forest because the needles turned an auburn color.) Sampling 17 years after the accident, Chesser had expected a blurry approximation. "To our surprise," he says, "we saw a very good picture of the plume" as reconstructed from particle density and deposition data: a 660-meters-wide, 290-meters-tall bell-shaped column.

Fortunately, the western trace missed Pripyat, which lies about 3 kilometers north of the reactor, but it "probably wiped out most wildlife in the Red Forest," Chesser says. By the time the winds began pushing the plume northward, it was about half as dense, he says. To reconstruct how badly Pripyat was hit, last summer his group measured radioactivity at more than 1700 spots in and around the city. They found that the heart of the northern trace barreled just east of Pripyat (see graphic, right). If the city had absorbed a direct hit, Chesser estimates that the toll would have been roughly 6000 cancer deaths. "The winds were very, very fortunate," he says.

The U.S. Defense Threat Reduction Agency (DTRA) intends to build on this work to forecast what would happen if a dirty bomb were to explode in a city. "We can't directly simulate this kind of attack, so we use various means to obtain representative data," says John Pace, a meteorologist with DTRA's Chem-Bio Defense Program in Fort Belvoir, Virginia. "The advantage of Pripyat is that the radioactivity is already there." In the city's central square, moss growing in cracks in the pavement sends Geiger counters galloping; it will be another decade before half the radiocesium deposited here will have decayed. Although Pace notes that there are "huge differences" in the consequences of a dirty bomb compared to those of the Chornobyl explosion, by focusing on the spread of material, "we can still obtain useful data that we can use to improve our capabilities to respond to urban terror attacks."

Studying surface contamination can give clues to how aerosol deposition is affected by a town's layout, construction materials, and building positions relative to prevailing winds. "What's particularly interesting with Pripyat is that there are a number of rather tall buildings, up to 16 stories, so we can go back and gather exposure data from different levels above the ground," Pace says. Vertical mixing of contaminants in cities, he says, "is an area where we don't have as much data as we'd like."

Realistic model. Simulating a dirty bomb in Pripyat could yield valuable defense information, researchers say.

Down the road, benign gases could be released in Pripyat to model dispersal. DTRA has supported similar studies. In 2001, 120 shipping containers were set up to model release scenarios in the Mock Urban Setting Test at the Dugway Proving Ground in Utah (*Boundary-Layer Meteorology*, June 2004, p. 363). In Oklahoma City in 2003, DTRA and the Department of Homeland Security sponsored a study in which an inert tracer gas was released downtown. A similar experiment is planned for Madison Square Garden in New York City this summer.

In living cities, however, constraints on sensor placement and on release locations and times can limit the range of data collected. "A site like Pripyat would offer more freedom in that regard," says Jeremy Leggoe, a chemical engineer at Texas Tech who has modeled the influence of vegetation on aerosol dispersal. Pripyat has disadvantages: For example, vegetation that has gradually been engulfing the city would have to be cut back. "That's particularly important, since in a real event, a large proportion of the exposure that you're concerned about—initial victims and emergency responders—will take place at ground level," Leggoe says.

Faced with such obstacles, DTRA for now would prefer to harvest existing data. "In any other city exposed to radiation, there would have been cleanup efforts that disturbed the exposure patterns, but that's not the case with Pripyat," Pace says. DTRA has asked scientists who work in Pripyat to collect samples and report the results to the agency. Initial studies will not involve tracer gases. "Nor would we intentionally release radioactive materials," says Pace.

A measure of good may yet come out of Pripyat's eldritch fate. "Pripyat is not a mockup. It is not a sterile façade of buildings erected for the purpose of blasting particles through its empty spaces," says Chesser. "Bicycles, pianos, libraries, and baby dolls decaying through 19 winters are there to remind us that learning from this event really matters." Pripyat would be a good laboratory, he says, precisely because it is real.

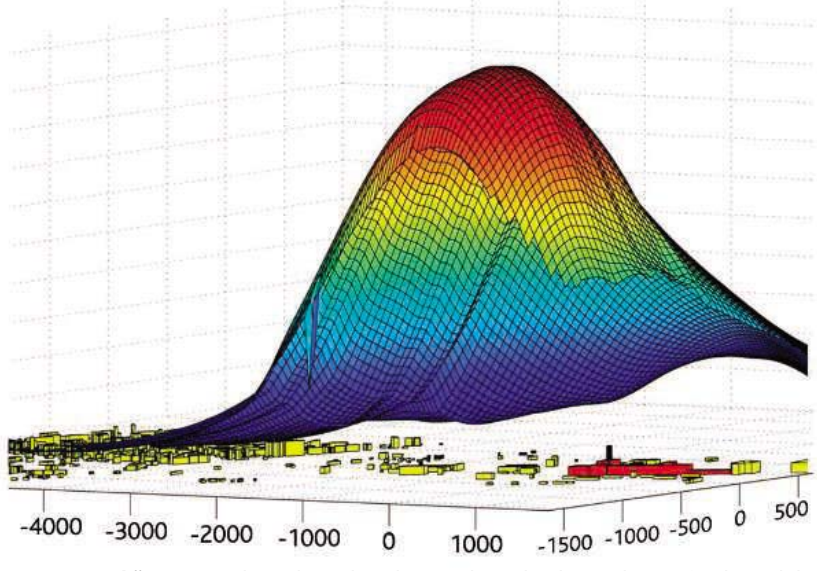

"Fortunate wind." A new analysis shows how breezes kept the dense plume of radionuclides from Chornobyl (in red) away from Pripyat's center.

–RICHARD STONE

CREDITS (TOP TO BOTTOM): R. STONE/*SCIENCE*; R. CHESSER

Attention, Class: A Departing NAS President Speaks His Mind

Bruce Alberts may be stepping down as president of the U.S. National Academy of Sciences. But he's a long way from retiring

Bruce Alberts came to the National Academy of Sciences (NAS) hell-bent on improving U.S. science and math education. Twelve years later, as he wraps up his second term as the academy's 20th president, Alberts admits that the country's educational system is still broken. But he hasn't stopped trying to fix it.

Along the way, he's also strengthened the academy's position as a respected, independent source of advice to the U.S. government by reducing the turnaround time on many of the 200-odd reports churned out every year by the National Research Council (NRC) that he heads. Says presidential science adviser John Marburger about NRC's 2001 report on climate change, "It gave them credibility with the Bush Administration and increased their inclination to use the academy more often." Former Clinton science adviser Neal Lane says the country "is indebted to Bruce … for his dogged determination to improve American science and math education, and for his commitment to international cooperation in science."

On 1 July, Alberts will return to his beloved University of California, San Francisco (UCSF), where he'll reclaim his old job as professor of biochemistry and biophysics, sans department chair. And in case anyone thinks that the 67-year-old biochemist has lost any of the spark that brought him to the nation's capital in 1993, his official portrait unveiled last week (p. 1109) should put such notions to rest. Its most prominent feature is a tie festooned with bright yellow pie faces with protruding tongues that depict a range of moods. The neckwear pokes fun at the people in this town who take themselves far too seriously. It's also a sign that Alberts is leaving NAS older and wiser—but with his spirit intact.

On 6 May, on the heels of his final annual NAS meeting, Alberts sat down with *Science* to discuss his accomplishments and failures as head of the self-elected meritocracy that stands as the country's most prestigious scientific organization. He spoke of the threat to science from advocates of intelligent design, of the need to better manage the U.S. scientific enterprise, and of the prospects for China and India becoming the next great scientific superpowers. Here are excerpts from that interview with Deputy News Editor Jeffrey Mervis.

Table talk. Alberts, shown here during a 1996 visit to the lab school at Smith College in Northampton, Massachusetts, enjoys spreading the gospel of hands-on science.

• **On the debate over teaching evolution:** "It says we've failed as scientists and science educators to convey the nature of science and its values to the American public, despite our world leadership in science and technology. … We've got to pay more attention to the education of young people and completely transform the way we teach introductory science at the college level. We are failing to make people understand what science is, or why they should care about it. … We all fear that this movement toward a biblical interpretation of scientific facts will eventually make us look like some of the countries in the Middle East. If we're going to remain a world leader, we're going to need all the scientific rationality that we can muster."

• **On why education reform is so difficult:** "We all think we understand education because we did well ourselves. It worked for us, and we think it should work for everybody else. But that's a big mistake. Half the brilliant students who come to Harvard planning to major in science drop out in the first year or two, because they don't get real science in their intro courses. Instead, they get huge amounts of knowledge that they must memorize before they can get to the good stuff, the hands-on and interactive courses.

We know what to do, and many of the small liberal arts colleges are doing it. But many of the large universities, with some notable exceptions, are not taking it seriously. … The incentives are wrong. Someone has to tell the department chairs that getting the resources they want—for equipment, graduate students, and so on—is going to depend on how they teach undergraduates. If you take away the money, the faculty will respond. I've learned that from spending 30 years in academia."

• **On advising the government:** "The Bush Administration [in 2001] asked us 14 specific questions about climate change, and I give them credit for asking. They didn't have to. … There are other problems that have arisen, and we're trying to help with them. For example, people keep saying that climate change isn't real, and that the science isn't there. We've answered that question, and we're going to continue to insist on those answers, whether they like it or not. … There are many things we'd like to do that we haven't been able to. We'd like to do a major study on nuclear power—the safety issues and where we as a country should go. But none of us have been successful, over four administrations [two for Clinton, two for Bush], in getting anybody to ask us to do that. And I don't know why they're not interested. … It's obvious that the Department of Energy has to ask us to do it. Otherwise, it doesn't make any sense because they won't listen to what we've come up with.

One big mistake I made as NAS president was to hold a competition within the academy for topics that we should study. We came up with lots of good ideas. But there was no client for them, so they had little effect. Getting an agency to put up even a little money for a study makes a big difference in their interest."

• **On recreating an Office of Technology Assessment (OTA):** "After Congress abolished OTA, we became the only show in town. We didn't like it, and we've tried to fill the gap, but we can't do everything. [At the same time], the idea of recreating it doesn't seem to have any political capital around here. We're not opposed to it, but you want to fight the battles that you think you can win."

• **On open access to journals:** "I think that the community should push for access to scientific information as quickly as possible. We tried [with the *Proceedings of the*

CREDIT: CAROL LOLLIS

National Academy of Sciences] to see how short we could make it. We actually tried only a 2-month delay. But the next year a number of librarians told us that they would wait the 2 months and not subscribe, saving the money for other journals. And so with regrets, our publication committee decided to let it slip to 6 months. It's an experiment, and maybe someday we'll move it ahead to 5 months. But 6 months has allowed us to maintain our subscription base. In fact, for 146 countries it's free immediately. But for scientists in the countries that can afford it—U.S. and Europe and Japan—we ask them to pay."

• **On changing the way the academy does business:** "We've tried to experiment, including some studies where the committees didn't even meet. But it doesn't work. The kind of thing we do needs that personal interaction. We get people together who don't know each other, and we create something different. For example, we did a report on the future of developmental toxicology, and we had scientists from both camps. … The first meeting was like Greeks talking to Romans. They didn't have a common language. It takes a couple of meetings, and some meals, before people get comfortable. And in the end they produced something unique. But you can't do that on the Internet.

There are a lot of tricks to the trade. A good chair knows how to call a coffee break when things aren't going well so that people can work out their differences. People want to see body language. … We've been pushing the envelope to do things faster, and we're going to keep trying."

• **On the impact of 9/11 on scientific openness:** "I think it's been a disaster. We've hurt security by not giving visas to leading foreign scientists, insulting our friends, and sending their students to other countries. Our tremendous scientific vitality is based on mixing the best talent from around the world. Twenty-five percent of the NAS members were born in another country, and they are our best diplomats. We're jeopardizing that by creating barriers that make no sense, like requiring students to promise that they won't stay here. It should be the reverse.

We have this broken system, and after 9/11 we're enforcing these rules in the name of national security. But what we're doing is the opposite of national security. I can't imagine a more effective way of losing our scientific leadership than closing down this country to scientific exchange. … And if and when we do get the problem straightened out, all our university presidents will have to go to India and China and solicit students, and tell them that they are now welcome. That's crazy."

• **On the rise of science in Asia:** "It seems likely to me that China or India will become the dominant scientific power. They take science and technology seriously, their young people are hungry to learn it, and they have such large numbers of people. But as we all know, there are many ways to make a mess of it. My favorite example is the recent science strike in France. They want more resources for science, which is good. But at the same time, you'd hope that they could adjust their system to make it more merit-based. Now, after your Ph.D., the first job gives you lifetime tenure. That's nuts. That's the perfect way not to run a scientific system. So I think the countries that will lead the world in science and technology are not just those with the most people. That's important. But you also need a system that allows the most talented people to have access to what they need to function effectively. Encourage the collision of ideas, and reward risk-taking and innovation. The United States is trying to do those things, too, but not well enough."

The ties have it. Bruce Alberts and his portraitist, Jon Friedman, during last week's unveiling at NAS's Keck Center.

CREDIT: CHRIS MADDALONI

• **On his future:** "My first year here was really hard. It was overwhelming. It was only after 4 years that I even started to think about staying. I hoped that in my second term I could do a lot, including fixing education. But I ended up spending most of my second term on international science. Now I hope to remedy that, starting in July, when I go back to UCSF. I'll be paid to focus on educational issues. One thing I want to do is stimulate better science by mixing people up, exposing them to new ideas, and helping them make new connections. As a young scientist, you have to be dragged out of your hole. But at the academy we've been doing that with our Frontiers of Science program and Keck Futures Initiative. I don't see why that sort of thing can't be done on the UCSF campus, or in the Bay Area.

I'm also trying to think of new models for scientists at the end of their careers. Continuing to run a lab and competing for grants until my third renewal is turned down and I have to leave in disgrace is not the way to go. We can't maintain an innovative system unless the old scientists become mentors and make way for the next generation. How do I get credit for this? I was president of the academy, so I don't need the credit. The worse way is to put your name on their paper. But why can't there be a second way, that also goes into the database, for people who really helped make things happen? I'd be proud if, after 10 years, you could find 30 papers that I had helped people to do good science."

Random Samples

Edited by Constance Holden

Neandertal Bite Not Incisive

There's no mistaking the jutting face of a Neandertal, with its swept-back cheekbones, big nose, and long mandible. Because teeth were important tools for early hominids, some believe the Neandertal mug evolved to maximize biting power, especially at the front teeth, which in many Neandertals show signs of extreme wear. Modern humans' more delicate features may have been made possible by innovations such as cooking and more sophisticated tools.

But a new study takes the bite out of this proposition. A team led by anthropologist Robert Franciscus of the University of Iowa in Iowa City used a biomechanical model that estimated the maximum forces generated at numerous points on the teeth and jaws to compare three Neandertal skulls with those of 29 anatomically modern humans. The team reports in the June *American Journal of Physical Anthropology* that there was no significant difference in jaw power between the two species. The authors speculate that the heavy tooth wear in Neandertals was due to more repetitive use rather than greater biting power.

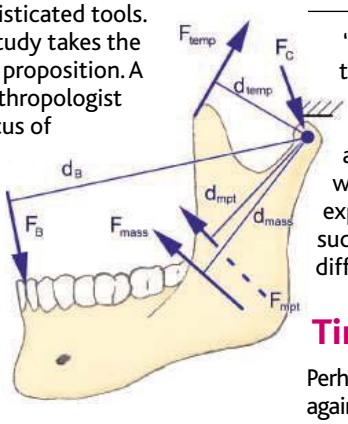

"This study puts some numbers to these hypotheses and finds them wanting," says New York University anthropologist Susan Anton. The authors suggest that researchers would do better to chew on alternative explanations for the Neandertal face, such as adaptation to cold climate or differences in respiratory physiology.

Primal Art

On the block at Bonhams auction house in London, alongside a Renoir sculpture and a William Wegman photo of a dog in a flight suit, are three abstract paintings by an artist named "Congo the Chimp."

Congo did the work in the mid-1950s under the tutelage of zoologist Desmond Morris, who was studying primates' sense of aesthetics. When Morris got the paintings displayed in London's Institute of Contemporary Art, some felt the exhibit mocked modern art.

"The art world should take these seriously," says primatologist Franz de Waal of the Yerkes Regional Primate Research Center at Emory University in Atlanta, Georgia. "I always felt Congo had it down. He had a sense of color, composition, and completion." Qualities of his work show neurological commonalities with humans, de Waal says, such as a sense of symmetry. It's estimated the trio will fetch $1100 to $1500 at the 20 June auction.

Time's Up on Time Travel

Perhaps the best experimental evidence yet against the feasibility of going back in time is that no one from the future showed up at a convention on time travel on 7 May at the Massachusetts Institute of Technology (MIT).

The gathering sprang from a late-night idea of MIT graduate student Amal Dorai, who read in a comic strip that only one such meeting would be needed because any future time travelers could attend.

Theoretical physicist Alan Guth of MIT filled in roughly 500 conventioneers on the leading proposals for time travel. The best that can be offered is a limited deal, he said. One scenario involves traveling through a wormhole, a tube through spacetime. By swirling one end of the hole at near the speed of light, time inside would slow down so a round trip could be made in a split second. But to keep a wormhole open would require a negative energy density—a state seen only at the quantum level.

The other proposal, said Guth, involves circling around two infinitely long cosmic strings, theorized tight wrinkles in spacetime with intense gravitational fields. In this scenario, you could return to the exact place and time you left, but you would be able to kill your departing self, creating a paradox that is at the heart of objections to time travel. Another problem is that such cosmic strings could take half the energy of the universe to create. MIT theoretical physicist Ed Farhi regretfully concluded: "It does look like the laws of physics conspire to prevent time travel."

Three Faces of Tut


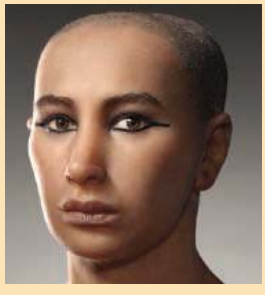


National Geographic has unveiled three independent attempts to reconstruct the face of the boy pharaoh Tutankhamen, who died 3300 years ago. The three teams—French, U.S., and Egyptian—based their reconstructions on 1700 computed tomography (CT) scans of the mummy that were made by the Egyptians early this year (*Science*, 28 January, p. 511).

The reconstructions differ on details of soft tissue, such as the end of the nose. One team was headed by New York University anthropologist Susan Anton, working with artist Michael Anderson of Yale University's Peabody Museum (right). The French effort (middle) was headed by Jean-Noel Vignal, a forensic anthropologist at the National Gendarmerie in Paris, with the help of anthropological sculptor Elisabeth Daynes. Antiquities chief Zahi Hawass led the Egyptian team. The Eygptian and French teams worked with the CT scans knowing they belonged to Tut; the NYU team didn't know.

CREDITS (TOP TO BOTTOM): BONHAMS AUCTIONEERS; ROBERT FRANCISCUS; SUPREME COUNCIL OF ANTIQUITIES, EGYPT AND NATIONAL GEOGRAPHIC SOCIETY, 2005

Edited by Yudhijit Bhattacharjee

IN THE NEWS

Fatal translation. Scientists usually like having their studies cited, but Harvard epidemiologists Wafaie Fawzi and David Hunter were distressed to see their research mentioned last week in advertisements in the *New York Times* and the *International Herald Tribune*. The two researchers allege that the ads, placed by European vitamin salesman and physician Matthias Rath (above), misrepresented their work on nutrition and HIV/AIDS to support Rath's view that antiretroviral therapy (ART) is ineffective against AIDS. Rath has been aggressively marketing vitamins to HIV-infected patients in South Africa.

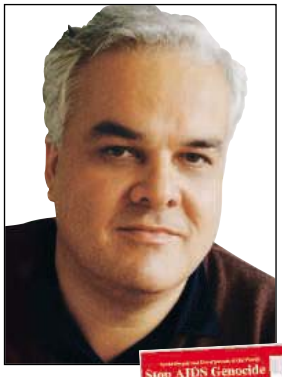

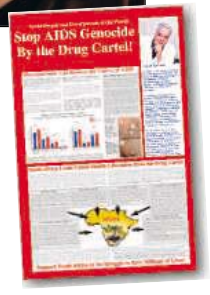

The study in question, published last year in the *New England Journal of Medicine*, found that multivitamins can delay HIV's progression and increase the time span before ART is needed. "However, it is important to underscore that the multivitamin supplements should not be considered as an alternative to ART, but as a complementary intervention that is part of a comprehensive care package," Fawzi and Hunter said in a statement last week.

Rath also has been sued for defamation by the Treatment Action Campaign in Cape Town, South Africa, which raises public awareness of HIV treatments. "We obviously believe that we have a very strong case and that we'll win," says Don Karn, spokesperson for the Dr. Rath Health Foundation, insisting that the ads describe Fawzi and Hunter's work accurately.

THE INSIDE STORY

Blog on. For months, Doug Roberts's Web log has given scientists at Los Alamos National Laboratory in New Mexico a chance to complain anonymously about their boss, George "Pete" Nanos. But Nanos's departure earlier this month (*Science*, 13 May, p. 936) doesn't mean the blog is obsolete, says Roberts, a computer scientist who has worked at Los Alamos for 20 years. The blog (lanl-the-real-story.blogspot.com) will continue to discuss the lab's woes, he says, from wasteful expenditures to the improper handling of classified information. "Dr. Nanos wasn't the only problem we have at Los Alamos," Roberts says.

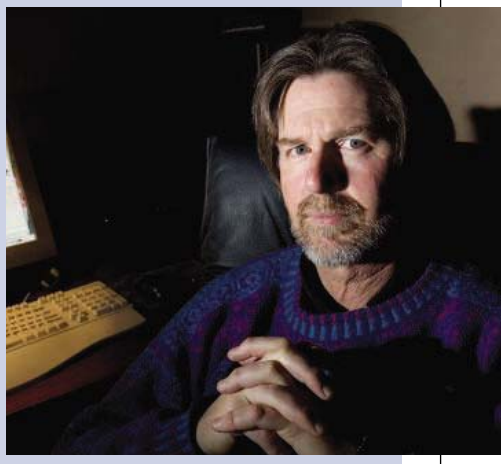

POLITICS

Rebuilding Iraqi science. A 44-year-old female biochemist will become Iraq's science and technology minister in the first elected government in decades. Bassima Yousef Boutros, currently a professor at Salah Eldin University in northern Iraq, is a Chaldo-Assyrian Christian.

Boutros told a Christian Web site, Answers in Action, that she would do her best "to use science and technology as the basis to build a civilized Iraq." Iraq's prime minister, Ibrahim Jaafari, has promised to name seven women to a 36-member cabinet.

AWARDS

Developmental biology prize. Geneticist Mario Capecchi of the University of Utah School of Medicine in Salt Lake City and pathologist Oliver Smithies of the University of North Carolina, Chapel Hill, have together won the $250,000 March of Dimes Prize in Developmental Biology for helping to develop gene targeting. The technique allows researchers to disable or modify the function of specific genes in lab mice. This is the 10th year of the prize, which is awarded annually to investigators whose work has contributed to the understanding of birth defects.

Got any tips for this page? E-mail people@aaas.org

TWO CULTURES

Embodying Einstein. It's not often that a dance choreographer has to think about the theories of Albert Einstein. But for his latest work, Mark Baldwin, the new director of the London-based Rambert Dance Company, has taken Einstein's 1905 papers on special relativity and Brownian motion as inspiration. The fruits of his labor, six dances called *Constant Speed*, premiere next week in London as part of the Institute of Physics' Einstein year celebrations.

Baldwin leaned on Ray Rivers, a theoretical physicist at Imperial College, London, to grasp the essence of the papers. "What I discovered during this process is just how compatible dance and physics are," says Baldwin.

For his interpretation of Brownian motion, all 22 members of the dance company will jitter on stage in the manner of microscopic particles being bombarded from all directions. The performance will be preceded by talks on Einstein's theories.

CREDITS (TOP TO BOTTOM): DR. RATH HEALTH FOUNDATION; AP; ANTHONY CRICKMAY

LETTERS

Meetings with Mentor

ARCHIMEDES, ARISTOTLE, HIPPOCRATES, AND Pythagoras would have known who Mentor was. Today the name of this legendary character is usually a prosaic noun or verb, used for a variety of great and small roles in people's lives, such as teacher, professional benefactor, thesis advisor, corporate role model, or sports coach.

In the *Odyssey* of Homer, Mentor is an old friend of Odysseus to whom that island king had entrusted his household when he departed his home, Ithaca, to fight in the Trojan War. The goddess Athena often assumes Mentor's shape and voice when she acts publicly on behalf of Odysseus and his son, Telemachus, leading them to display their inherent strengths. At the epic's conclusion, Athena, appearing to be Mentor, prevails upon the Ithacan factions to restore civic harmony. To residents of Ithaca, therefore, Mentor could be their elder neighbor, or he could actually be the disguised Athena. In Book IV of the *Odyssey*, an Ithacan local is puzzled that he had seen Mentor in Ithaca the previous morning but had also seen him depart on a ship with Telemachus several days earlier.

In legend and myth, there have been many other loyal neighbors and deities championing their favorite heroes. I believe that the ambiguity of who Mentor is when we come across him (or her) has contributed to this eponymous term. That is, Mentor may be merely the familiar elder friend, or Mentor may personify the principles for which Athena was the patron: wisdom (particularly strategizing intelligence), defense and guardianship of the city-state, and useful crafts.

In the 17th-century novel, *Les Aventures de Telemaque* by Fenelon, Athena, disguised as Mentor, is a prominent character as Telemachus' protector and advisor on exotic travels in training for his kingship. That novel's popularity contributed to our common use of Mentor's name.

Forgetting the origin of Mentor is a prime example of how we can lose the numinous depth of a word when we lose its original reference. The protégé of a mentor has sometimes even been called a "mentee." Appreciation of the original meanings of Mentor can enhance the experience of "mentoring" for the counselor and protégé.

When we come upon our Mentor on our life's Odyssey, we may be meeting both an elder guide and an exemplar of the crafts, wisdom, and guardianship of civilized society. In turn, the classic tradition of "mentoring" involves generous guidance of one's protégé toward personal accomplishments, career skills, and civic responsibility.

JUDITH B. KLOTZ
Department of Epidemiology, School of Public Health, University of Medicine and Dentistry of New Jersey, 720 Valley Forge Avenue, Lawrenceville, NJ 08648, USA.

Suction Feeding in a Triassic Protorosaur?

ALTHOUGH I ENJOYED SEEING A NEW AQUATIC tanystropheid described, the hypothetical methods suggested by the authors for locomotion and prey acquisition seem implausible ("A Triassic aquatic protorosaur with an extremely long neck," C. Li *et al*., Brevia, 24 Sept. 2004, p. 1931). Hyoids are known to expand the throat or throat skin in other reptiles, but cervical ribs are not. In this taxon, the cervical ribs are so well overlapped and bound to one another that only slight longitudinal sliding would have been permitted, not lateral expansion to suck prey into an expanding esophagus.

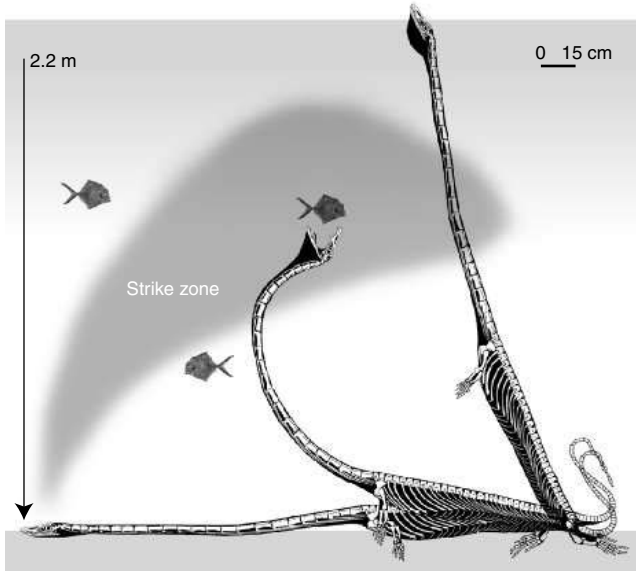

A reconstruction (see figure) suggests that this protorosaur, with its very small limbs, would have been a poor swimmer. More likely, it would have been a sit-and-wait predator, like its more terrestrial sister taxon, *Tanystropheus*. Hiding in bottom silt, in waters only deep enough to rise for a breath, *Dinocephalosaurus* could have snatched passing fish from below. The orbits were more open dorsally than in sister taxa, making this possible. The only problem with this scenario is the issue of lung inflation under hydrostatic pressure. This could have been solved by gulping a small bubble of air and carrying it to the bottom in the throat sac before passing it to the lungs under equalized pressure.

DAVID PETERS
1247 Highland Terrace, St. Louis, MO 63117–1712, USA.

IN THEIR BREVIA "A TRIASSIC AQUATIC PROTOrosaur with an extremely long neck" (24 Sept. 2004, p. 1931), C. Li *et al*. describe a new specimen of a Triassic protorosaur (*Dinocephalosaurus orientalis*) from marine deposits in southern China and suggest that its long and presumably expandable neck was an adaptation to explosive suction feeding. This form of feeding is not uncommon among aquatic vertebrates (*1*). Most marine suction feeders are fish that can expel the saltwater sucked in with the prey items through gill slits. Some sea turtles use moderate suction as they feed on plant material or less elusive prey. They have glands to dispose of the salt that is taken in (*2*).

Li *et al*. imply that *D. orientalis* swallowed the pressure wave created as its head plunged forward. The requisite pressure differential was supposedly generated by neck expansion. Muscles running from cervical ribs across intervertebral joints would have simultaneously straightened the neck and expanded its volume. Such a feeding mechanism that involves intake of large amounts of saltwater is unknown among marine reptiles. It would require physiologic adaptations to dispose of large amounts of saltwater swallowed and/or some mechanism of secondary water expulsion. It would also require large and rapid volumetric expansion of the esophageal cavity. It is unlikely that the hypothesized musculoskeletal arrangement in the neck, especially considering the slenderness of the ribs, would have served this purpose. In addition, long and slender cervical ribs are not uncommon among long-necked sauropod and theropod

dinosaurs, which are clearly not suction feeders (*3*). Without demonstration of osteological correlates for physiological removal of salt [e.g., large salt glands (*4*)] and some musculoskeletal adaptation for forceful volumetric increase in the neck (e.g., a large hyoid apparatus, "bucket-handle," or "spreading-caliper" mechanism of ribs) to create suction, there is no basis for the extraordinary feeding adaptation inferred for *D. orientalis*.

BRIGITTE DEMES AND DAVID W. KRAUSE
Department of Anatomical Sciences, Stony Brook University, Stony Brook, NY 11794–8081, USA.

References
1. G. V. Lauder, in *Functional Vertebrate Morphology*, M. Hildebrand, D. M. Bramble, K. F. Liem, D. B. Wake, Eds. (Belknap Press, Cambridge, MA, 1985), p. 210.
2. J. Wyneken, *The Anatomy of Sea Turtles* (NOAA Technical Memorandum NMFS-SEFSC-470, National Oceanic and Atmospheric Administration, Washington, DC, 2001).
3. D. B. Weishampel, P. Dodson, H. Osmólska, Eds., *The Dinosauria* (Univ. of California Press, Berkeley, 2004).
4. R. Hirayama, *Nature* **392**, 705 (1998).

Response

PETERS PRESENTS A RECONSTRUCTION OF *Dinocephalosaurus* and suggests that the relative size of the limbs indicates a "poor swimmer." We disagree. Two pairs of 30-cm-long, flipper-shaped fins seem more than adequate to drive a 1-m-long body. Living sea lions (*Zalophus californianus*) have a similar ratio of flipper to body length (*1*). We think it unlikely that *Dinocephalosaurus* was a benthic ambush predator. First, we would expect that the eyes in a benthic ambush predator would be dorsally located to monitor the overlying water (as seen in living frogfish and flatfish); the eyes of *Dinocephalosaurus* are anterior-laterally positioned, apparently to monitor regions to the sides and in front of the snout. In addition, Peters' reconstruction would have *Dinocephalosaurus* capture prey by sweeping its neck through the water. We find this unlikely because (i) the cervical vertebrae lack neural processes that would improve the mechanical advantage of the (necessarily small) neck muscles to drive dorsiflexion, and (ii) such motion would generate high drag forces on the neck that would tend to drag the body of the animal along the substrate in the direction opposite to the motion of the head. (The neck would act as an oar.)

Peters rejects our hypothesis that *Dinocephalosaurus* may have employed suction feeding (driven by expansion of the cervical ribs) as a mode of prey capture on the basis that the cervical ribs are "bound to one another." We know of no evidence to suggest that the cervical ribs were bound to each other; indeed, the dispersal of the cervical ribs in the only available specimen would seem to indicate that tissues that surrounded the cervical ribs were quite liable to decay and thus unlikely to have been collagenous or cartilagenous.

Demes and Krause object to our hypothesis on the grounds that most marine vertebrates that suction feed expel the water captured with the prey through a second opening (typically the gill openings); they imply that such water would have to be swallowed and object that no salt glands have been demonstrated in *Dinocephalosaurus*. First, because the reptilian kidney is unable to concentrate urine to osmolarities above that of sea water (*2*), some form of salt gland can be assumed to be present in all marine reptiles regardless of whether osteological evidence for the presence of salt glands is available. Second, although fish have a morphology that makes it easier for them to separate prey items from the surrounding fluid in suction feeding and suspension feeding, other vertebrates have found ways around the handicap of the lack of a second large opening into the oral cavity. Lauder (*3*, *4*) distinguished two categories of suction feeding vertebrates: those with a unidirectional flow through the buccal cavity and those with bidirectional flow. Turtles that use a bidirectional suction feeding strategy immobilize the prey after capture with the jaws or tongue; excess water stored in the buccal cavity or the esophagus is expelled through a small oral gape (*5*, *6*) or the nares. Similarly, with fang-like teeth in its jaws, *Dinocephalosaurus* seem well equipped to retain prey when expelling excess water. Most vertebrate suction feeders use the hyoid to depress the floor of the mouth, but the Australian snake-necked turtle (*Chelodina longicollis*) also uses elements from the first and second branchial arches (the ceratobranchials) to expand the pharynx (*7*). We have no direct evidence that *Dinocephalosaurus* used the cervical ribs to expand the throat, but that hypothesis is consistent with the observed morphology and we continue to search for additional tests of the hypothesis. If cervical ribs were used to power suction feeding in this animal, that function was certainly an exaptation.

MICHAEL LABARBERA[1] AND OLIVIER RIEPPEL[2]
[1]Department of Organismal Biology & Anatomy, University of Chicago, 1027 East 57th Street, Chicago, IL 60637, USA. [2]Department of Geology, The Field Museum, Chicago, IL 60605–2496, USA.

References
1. S. D. Feldkamp, *J. Zool. Lond.* **212**, 43 (1987).
2. K. Schmidt-Nielsen, *Animal Physiology* (Cambridge Univ. Press, Cambridge, 1997).
3. G.V. Lauder, in *Functional Vertebrate Morphology*, M. Hildebrand, D. M. Bramble, K. F. Liem, D. B. Wake, Eds. (Belknap Press, Cambridge, MA, 1985), p. 210.
4. G. V. Lauder, X. Shaffer, *Zool. J. Linn. Soc.* **88**, 277 (1986).
5. G. V. Lauder, X. Prendergast, *J. Exp. Biol.* **164**, 55 (1992).
6. X. Lemell *et al.*, *J. Exp. Biol.* **205**, 1495 (2002).
7. J. Van Damme, P. Aerts, *J. Morphol.* **233**, 113 (1997).

Letters to the Editor

Letters (~300 words) discuss material published in *Science* in the previous 6 months or issues of general interest. They can be submitted through the Web (www.submit2science.org) or by regular mail (1200 New York Ave., NW, Washington, DC 20005, USA). Letters are not acknowledged upon receipt, nor are authors generally consulted before publication. Whether published in full or in part, letters are subject to editing for clarity and space.

Ancestry of Photic and Mechanic Sensation?

IN THEIR REPORT "CILIARY PHOTORECEPTORS with a vertebrate-type opsin in an invertebrate brain" (29 Oct. 2004, p. 869), D. Arendt *et al.* offer an interesting perspective on the ancestry of vertebrate and invertebrate opsins and their associated receptors. Here, we offer an even broader perspective indicating that photic and mechanic sensation may share a common ancestry prior to the formation of Urbilateria (defined as the last common ancestor of insects and vertebrates).

Mechanosensors and opsins require expression in cells specialized to alter their resting potential upon stimulation and to project this information to effectors. Moreover, we assume that such cells function best if grouped into organs dedicated to the extraction of the specific stimuli. Achieving this requires not only the evolution of the specific mechano- or phototransducer molecules, but also the evolution of the cells expressing those molecules and the evolution of a transcription factor system that orchestrates the organ formation that houses such cells.

Recent progress on the issue of molecular basis of organ formation showed that the *Pax* genes are not only relevant for the formation of eyes (*Pax6*) and ears (*Pax2*) across phyla, but that an ancestral *Pax2/6* gene, *PaxB*, exists in cnidarians (*1*, *2*) and even in sponges (*3*). This suggests that eye and ear evolution may use paralogs of a single ancestral *Pax* gene dedicated to organize organ development, no matter what shape, cell types, and transducer molecules are used (*4*, *5*). A number of common cell-determining transcription factors are co-utilized in eyes and ears of different species; examples include the *bHLH* gene *atonal/Atoh1/Atoh5* (*6*, *7*), and the Pou domain factor Pou4f3 (*8*, *9*). The selective co-expression pattern of these genes, which appear to be situated downstream of the *Pax2* gene regulating development of the optic nerve and ear (*10*), is specialized for the formation of these two sensory systems. For example, *atonal/Atoh1/Atoh5* expression is

seen in mechanosensors and eyes in insects, and in vertebrates, the paralogs are in the hair cells of the ear and ganglion cells of the retina (*11*), the site for the melanopsin variation of the r-opsin (see Arendt *et al.*). Clearly, a number of these transcription factors and developmental cascades determining cellular fates are shared across phyla and across sensory organs.

Assuming that these similarities are more than coincidental and indicate a co-evolutionary history of eyes and ears, the present challenge is to trace the common origins of visual and balancing/auditory apparati to conserved cellular developmental programs. In keeping with the recently emerging concept of a "second code" for gene regulation (*12*), it is possible that enhancers orchestrating the development of opsin-containing and mechanosensory organs share motifs and properties that have led to the modular use of common cell-fate–determining transcription factors during evolution.

Thus, the elegant link between photoreceptors and opsins of invertebrates and vertebrates may be extended to include evolutionary connections between eyes and mechanoreceptors (*4*, *7*, *13*). This may contribute to clinical insights for the numerous diseases of both eyes and ears (*13*–*16*).

BERND FRITZSCH[1] AND JORAM PIATIGORSKY[2]

[1]Department of Biomedical Sciences, Creighton University, 2500 California Plaza, Omaha, NE 68178–0405, USA. [2]LMDB/NEI/NIH, 7 Memorial Drive, Building 7, Room 100A, Bethesda, MD 20892–0704, USA.

References

1. Z. Kozmik *et al.*, *Dev. Cell* **5**, 773 (2003).
2. H. Sun *et al.*, *Proc. Natl. Acad. Sci. U.S.A.* **94**, 5156 (1997).
3. D. Hoshiyama *et al.*, *J. Mol. Evol.* **47**, 640 (1998).
4. J. Piatigorsky, Z. Kozmik, *Int. J. Dev. Biol.* **48**, 719 (2004).
5. J. Piatigorsky, *Integr. Comp. Biol.* **43**, 492 (2003).
6. C. J. Lowe *et al.*, *Cell* **113**, 853 (2003).
7. N. Niwa, Y. Hiromi, M. Okabe, *Nat. Genet.* **36**, 293 (2004).
8. S. W. Wang *et al.*, *Development* **129**, 467 (2002).
9. W. Liu, Z. Mo, M. Xiang, *Proc. Natl. Acad. Sci. U.S.A.* **98**, 1649 (2001).
10. M. Torres, E. Gomez-Pardo, P. Gruss, *Development* **122**, 3381 (1996).
11. Y. Sun *et al.*, *Evol. Dev.* **5**, 532 (2003).
12. E. Pennisi, *Science* **306**, 632 (2004).
13. B. Fritzsch, K. W. Beisel, *Brain Behav. Evol.* **64**, 182 (2004).
14. T. Walsh *et al.*, *Proc. Natl. Acad. Sci. U.S.A.* **99**, 7518 (2002).
15. C. J. Starr, J. A. Kappler, D. K. Chan, R. Kollmar, A. J. Hudspeth, *Proc. Natl. Acad. Sci. U.S.A.* **101**, 2572 (2004).
16. Q. Xu *et al.*, *Cell* **116**, 883 (2004).

Response

THE EVOLUTIONARY LINK BETWEEN mechano- and photoreception put forward by Fritzsch and Piatigorsky is plausible and even extends to chemosensation. These senses most likely had a common origin early in animal evolution, and other senses should be added to this list. Given that photoreception based on animal-type opsins was in place at the dawn of Metazoa (*1*), we hypothesize that other sensory cell types are evolutionary derivatives of photosensory cells. Some caveats, however, have to be addressed.

First, cell types should be compared rather than entire organs. Organs are often composite structures made up of cell types with different evolutionary histories. For example, we have shown that the vertebrate eye is a composite structure comprising at least two different photoreceptor cell types (ciliary and rhabdomeric) of independent origin. Therefore, as also stated by Fritzsch and Piatigorsky, it is important to compare rhabdomeric photoreceptor cells of the eye and hair cells of the ear, rather than comparing eyes and ears.

Second, we would like to emphasize that the set of sensory cell types related by the shared combinatorial code of transcription factors (*pax6-pax2/5/8, atonal*, and POU IV class orthologs) extends to chemosensory cells as well, as documented for *pax6* (*2*–*4*), *pou4f3/acj6* (*5*, *6*), and *atonal/ath* (*7*, *8*). Notably, the specialized sensory structures (rhopalia) of several Cnidaria can contain photo- and mechano-, but also chemosensory cells in close proximity (*9*). Besides *paxB*, a cnidarian ortholog of the bilaterian *POU IV* genes is expressed in cnidarian rhopalia (*10*).

Third, this combinatorial code of transcription factors is shared only by subsets of photo-, mechano- and chemosensory cell types in the different phyla. For example, in *Drosophila*, only some peripheral nervous system mechanoreceptors depend on the activity of *atonal* orthologs; others are instead specified by genes of the *achaete-scute* complex (*as-c*) (*8*). In the vertebrates, numerous mechanosensory cells are specified by *atonal* orthologs (*8*); however, *as-c*-dependent mechanosensors should also exist, at least in the foregut (which is known to be mechanosensory, and lacking all neurons in *mash1-/-* mouse) (*11*). Since *atonal* and *achaete-scute* orthologs are distinctly expressed already in cnidaria (*12*–*14*), this mechanoreceptor dichotomy could well be older than Bilateria. Apparently, rhabdomeric PRCs and a subgroup of mechanosensory (and chemosensory) cell types are evolutionarily closer related to each other than to their respective functional cognates, indicating that functional classification does not always reflect evolutionary relatedness. This implies that in the course of evolution, sensory cells can shift their sensory modalities.

It is only recently that the molecular fingerprints of sensory cells in a variety of animal models, including the more ancestral polychaetes and cnidarians, start to be unravelled. These data allow reconstructing the diversification of the various types of sensory cells in the course of animal evolution and will elucidate the origin of our senses.

KRISTIN TESSMAR-RAIBLE, GÁSPÁR JÉKELY, KEREN GUY, FLORIAN RAIBLE, JOACHIM WITTBRODT, DETLEV ARENDT*

European Molecular Biology Laboratory, Developmental Biology Programme, Meyerhofstrasse 1, 69012 Heidelberg, Germany.

*To whom correspondence should be addressed. E-mail: arendt@embl.de

References

1. W. Deininger, P. Kroger, U. Hegemann, F. Lottspeich, P. Hegemann, *EMBO J.* **14**, 5849 (1995).
2. J. M. Collinson, J. C. Quinn, R. E. Hill, J. D. West, *Dev. Biol.* **255**, 303 (2003).
3. B. Hartmann *et al.*, *Mech. Dev.* **120**, 177 (2003).
4. D. Arendt, K. Tessmar, M. I. de Campos-Baptista, A. Dorresteijn, J. Wittbrodt, *Development* **129**, 1143 (2002).
5. D. A. Hutcheson, M. L. Vetter, *Dev. Biol.* **232**, 327 (2001).
6. P. J. Clyne *et al.*, *Neuron* **22**, 339 (1999).
7. C. J. Burns, M. L. Vetter, *Dev. Dyn.* **225**, 536 (2002).
8. B. A. Hassan, H. J. Bellen, *Genes Dev.* **14**, 1852 (2000).
9. T. H. Bullock, G. A. Horridge, *Structure and Function in the Nervous System of Invertebrates* (Freeman, San Francisco, 1965).
10. D. K. Jacobs, R. D. Gates, *Dev. Biol.* **235**, 241 (2001).
11. L. Lo, F. Guillemot, A. L. Joyner, D. J. Anderson, *Perspect. Dev. Neurobiol.* **2**, 191 (1994).
12. K. Seipel, N. Yanze, V. Schmid, *Dev. Biol.* **269**, 331 (2004).
13. P. Muller *et al.*, *Dev. Biol.* **255**, 216 (2003).
14. A. Grens, E. Mason, J. L. Marsh, H. R. Bode, *Development* **121**, 4027 (1995).

TECHNICAL COMMENT ABSTRACTS

COMMENT ON "The 1.2-Megabase Genome Sequence of Mimivirus"

David Moreira and Purificación López-García

Upon analysis of seven concatenated Mimivirus protein sequences, Raoult *et al.* (Research Articles, 19 Nov. 2004, p. 1344) suggested that Mimivirus defines a new branch in the tree of life. However, these proteins have incompatible evolutionary histories, and their individual phylogenies suggest that they have been acquired by the Mimivirus from amoebal hosts.

Full text at www.sciencemag.org/cgi/content/full/308/5725/1114a

RESPONSE TO COMMENT ON "The 1.2-Megabase Genome Sequence of Mimivirus"

Hiroyuki Ogata, Chantal Abergel, Didier Raoult, Jean-Michel Claverie

A handful of Mimivirus genes exhibit their most similar homologs in amoeba, which suggests that they may have been acquired from the virus host. However, global comparison of the Mimivirus predicted proteome with the recently completed *Entamoeba histolitica* genome sequence dismisses horizontal gene transfer as the dominant force in shaping the complexity of Mimivirus genome.

Full text at www.sciencemag.org/cgi/content/full/308/5725/1114b

ARCHAEOLOGY

Clearing the View of Our Foundations

David Wengrow

In his recent autobiography (*1*), Bob Dylan reflects on the wisdom of old songs. They teach us that societies have emerged, flourished, and declined, but during the 1960s he "had no idea which of these stages America was in." Protest is most forceful when expressed through traditional modes of communication. In *Myths of the Archaic State*, Norman Yoffee seeks to rescue the concept of social evolution from its critics—altering its shape, content, and meaning, while retaining its traditional goal of explaining, rather than simply describing, the emergence of early civilizations. Does he succeed?

Myths of the Archaic State
Evolution of the Earliest Cities, States, and Civilizations
by Norman Yoffee
Cambridge University Press, Cambridge, 2005. 291 pp. $75, £45. ISBN 0-521-81837-0. Paper, $34.99, £19.99. ISBN 0-521-52156-4.

First, a little background. In the 1960s, archaeologists on university campuses throughout the United States did a strange thing. They began to accept the terms of a debate on social evolution that threatened to undermine the very purpose of their discipline. Anthropologists at that time were arguing (again) that rules governing the long-term transformation of human societies are observable in the ethnographic record. Archaeologists could supply some antique window-dressing, but the actual dynamics of social evolution were to be transposed from the living present onto the dead past. By the 1980s, things had begun to change. Anthropologists became interested in history, the myth of "our contemporary ancestors" was exposed (again), and archaeologists were left to reinvent themselves. Today the theory of social evolution is undergoing another face-lift and students of ancient and prehistoric societies, weary after an overdose of deconstruction, are showing interest once again, this time on their own terms (*2*).

Like its author, a professor of Near Eastern studies at the University of Michigan whose research bridges archaeology, anthropology, and Assyriology, the book defies easy definition. Yoffee covers an extraordinary number of topics and regions, ranging from ancient Mesopotamian law to archaeological applications of complex adaptive systems theory (*3*), with forays into the ancient civilizations of Mesoamerica, South America, India, China, and Egypt. He does not question what has long been recognized as a basic family resemblance among these early hierarchical societies, but offers only a nominal definition of what constitutes an "early state." His position can be summarized as Yoffee's Rule: "If you can argue whether a society is a state or isn't, then it isn't." The search for essential properties of a state, the author argues, leads only to meaningless abstractions, thus divesting ancient cultures of precisely those features that make them instantly recognizable as "Egyptian," "Mayan," etc. (*4*). Instead, Yoffee seeks to get at the general through the particular, bringing archaeological and ancient textual evidence to bear on the question, where do varieties of social power come from?

Yoffee's answer is most clearly formulated in relation to ancient Mesopotamia, today's Iraq, where the world's first literate, urban societies took form some 6000 years ago. He proposed that early states were embedded within larger cultural systems ("civilizations") over which they exerted only limited control. Large-scale political structures were prone to collapse within centuries of their construction. The more durable elements of ancient civilizations—that is, the social groups capable of picking up the pieces and reworking them into new wholes—were smaller in scale: local assemblies, mercantile associations, craft experts, and extended families. Their authority was rooted in shared ties of identity and memory that crosscut more ephemeral political allegiances. The workings and failures of the ancient state are exposed from its margins, including documentation of the institutional lives of Babylonian women who (like medieval nuns) were cloistered to prevent the alienation of landed wealth. Here Yoffee goes furthest in unpacking the prevailing "myths about godly and heroic (male) leaders who planned and built prodigious monuments and cities, conquering their neighbors and making them powerless subjects of the ruling elites."

Like Teotihuacan (in the Valley of Mexico), Tikal (in the Mayan lowlands), and Mohenjo-Daro (in the Indus Valley), the earliest Mesopotamian cities were "supernovas that exploded from the environment of village life that preceded them." Yoffee cites estimates that in the third millennium BC the city-state of Lagash had held around 120,000 people. In considering such population figures, he might have asked more questions about the temporality of urban life, notably with regard to Egypt. Were state-sponsored settlements, such as the vast Old Kingdom "pyramid town" currently being excavated on the Giza Plateau, permanently occupied? Or did groups of workers, drawn from diverse backgrounds, take up temporary residence to participate in centrally organized projects of monumental construction? The latter possibility would strengthen Yoffee's observations concerning the fluidity of social identities and roles in ancient states.

Of particular interest to readers of *Science* will be the author's approach to the genesis of cities, which takes its cue from cross-disciplinary research into the adaptive logic of complex systems. Central to his account is a process that archaeologists are now calling "the evolution of simplicity," whereby everyday life in prehistoric villages—as represented by the remains of houses, decorated pottery, and other commonplace items—was divested of dense symbolic meanings and rendered fluid, predictable, and homogeneous. In later prehistory, this process was played out over vast geographical regions by tiny communities linked through dense trade networks. The components of these networks, villages often comprising just a handful of households, are perhaps analogous to the "small worlds" of complex systems theory (*5*): social time bombs, carrying within them the potential for sudden, dramatic mutation.

Earlier view of an early civilization. An 18th-century depiction of the ancient city of Babylon [from (*6*)].

The reviewer is at the Institute of Archaeology, University College London, 31-34 Gordon Square, London, WC1H 0PY, UK. E-mail: d.wengrow@ucl.ac.uk

Yoffee relates how early rulers styled themselves guardians of core cultural values, translating these values into the monumental images of authority that now populate our museums and have lost none of their capacity to enchant. He shows convincingly that ancient states were temporary situations, during which social relations became knotted into hierarchical patterns. The knots were reversible and much life went on in the spaces between them. Perhaps modern societies that claim equality, openness, and merit as the official values of organized power still need their myths of the archaic state—their ideas of a past form of domination more absolute than the dynastic and totalitarian systems of recent centuries. But that is a quite different problem, which the book does not address. Rather, *Myths of the Archaic State* clears away the cobwebs of an earlier generation of anthropological thought and, in its strongest moments, points toward a new configuration of global history.

References and Notes

1. B. Dylan, *Chronicles* (Simon and Schuster, New York, 2004), vol. 1.
2. For example, S. Shennan, *Genes, Memes and Human History: Darwinian Archaeology and Cultural Evolution* (Thames and Hudson, London, 2004).
3. R.A. Bentley, H. D. G. Maschner, Eds., *Complex Systems and Archaeology* (Univ. Utah Press, Salt Lake City, 2003).
4. For a contrasting approach, see B. G. Trigger, *Understanding Early Civilizations* (Cambridge Univ. Press, Cambridge, 2003).
5. D. Watts, *Six Degrees: The Science of a Connected Age* (William Heinemann, London, 2003).
6. G. Sievernich, H Budde, Eds., *Europa und der Orient, 800–1900* (Bertelsmann Lexikon Verlag, Gütersloh, Germany, 1989).

10.1126/science.1111129

PHILOSOPHY OF MIND

Seeing with the Mind's Eye

Phil Joyce

Written in a lively style, Colin McGinn's *Mindsight* is a philosophical investigation of the faculty of imagination that will appeal to a wide audience of informed readers. It takes its title from the author's theory that when we imagine "it is literally true that we see with our mind." According to McGinn (a professor of philosophy at Rutgers University), to imagine is to exercise the mind's eye—a hypothesized anatomical structure in the brain that provides genuine visual experiences about things of the external world. This claim may startle those scientists who doubt that philosophy, with its absence of experimental methods, has the credentials to advance our understanding of the mechanisms of the human mind and the structure of the brain. *Mindsight* dissolves such concerns by vividly demonstrating that philosophical enquiry, conducted with sufficient awareness of the cognitive sciences, can deepen our comprehension of the mind by eliminating unsatisfactory explanations of imagination, identifying promising alternatives, and posing the right questions for science to address.

What makes McGinn's study of the imagination distinctly philosophical is its use of phenomenology and conceptual analysis. The word "phenomena" stems from the Greek for appearances, and phenomenology is the study of the way things appear to us in conscious experience—of what it is like to have certain experiences. *Mindsight* is laden with introspective observations of the experience of imagining—descriptions of what it is like to imagine. Some of them remind us of familiar facts whose importance may be overlooked, but many describe features of the imagination that only the most careful introspection is likely to detect. These reflections provide phenomenological data that any theory of imagination must accommodate. Putting the point another way, if a theory fails to acknowledge these phenomenological insights, it is doubtful that the theory is talking about the imagination as experienced in our conscious mental lives. Furthermore, any theorician who accepts the challenge to explain the phenomenology of imagination must operate within certain logical constraints. It is in identifying these boundaries that McGinn deploys his second philosophical tool to great effect. For conceptual analysis makes explicit the logical connections between those key concepts on which any adequate theory will rely. (A general theory of mind, for example, is likely to draw on such concepts as representation, thought, experience, and action, and these will have complex interrelations that the theory must respect.) Phenomenology and conceptual analysis, working in harness, therefore promise to identify logical criteria that separate genuine explanations of the imagination from flawed theories.

Mindsight
Image, Dream, Meaning
by Colin McGinn

Harvard University Press, Cambridge, MA, 2004. 217 pp. $27.95, £18.95, €25.80. ISBN 0-674-01560-6.

McGinn lays the foundations for his theory of imagination by developing our understanding of two concepts that, he claims, will be central to any explanation of the phenomenological data: images and percepts. Roughly speaking, both images and percepts are conscious visual experiences. They differ primarily in their causes: images are the products of our imaginative faculty whereas percepts result from our perceptual systems. Percepts therefore put us reliably in touch with the world while images do not. In McGinn's view, if we can get our concepts of image and percept straight, then the logical structure of a satisfactory theory of imagination will fall into place.

The author amasses an array of argument to demolish the initially plausible suggestion, first advanced by the 18th-century Scottish philosopher David Hume, that images are, in all essential respects, simply faded relics of percepts. McGinn argues, for example, that images, but not percepts, are subject to the will: once we fix our gaze on something within our field of view, we cannot decide what visual percept consequently arises in consciousness. However, it seems that we frequently can decide what images we form. He also notes that percepts, unlike images, are informative in that images only contain what we put into them whereas the information content of percepts depends on what we perceive. In addition, images require our attention in order to persist. Percepts, by contrast, may remain in consciousness whether or not we attend to them. It is a familiar and alarming fact, for example, that we may drive our cars while our minds are elsewhere. But in those distracted moments we do not experience a blank visual field—we still see the road and other cars, it's just that we are not giving what we see the attention it deserves.

From these and other careful observations McGinn shows that images and percepts, contrary to Hume's plausible suggestion, are not variations of the same theme differing only in their intensity but are categorically different mental items. The early chapter in which he establishes this conclusion stands by itself as a paradigm example of the combined force of phenomenology and conceptual analysis in advancing our understanding of the mind.

Mindsight does far more than merely expose theoretical dead ends, however. It is a virtue of McGinn's approach that it brings alternative explanations into clearer focus. A case in point is his central claim that visual images result from an autonomous experience-producing organ in the brain, the mind's eye. Having established this foundation, McGinn carefully develops other intriguing theoretical possibilities in thought-provoking chapters on dreaming, delusion, and the connections among imagination, thought, and language.

Mindsight will be essential reading for philosophers with an interest in the imagination. Although it occasionally assumes familiarity with some philosophical concepts and theories, it will also amply reward any reader with an interest in the mechanisms of the mind.

10.1126/science.1110097

The reviewer is at the Department of Philosophy, University of Oxford, 10 Merton Street, Oxford, OX1 4JJ, UK. E-mail: phil.joyce@bigfoot.com

SCIENCE AND SOCIETY

High- and Low-Cost Realities for Science and Society

Helga Nowotny

Through the ongoing proliferation of images and symbols, information overload and hi-tech–driven media, science increasingly communicates with the public in ways that are deliberately designed and intended to meet the public (and political) imagination. At the same time, the public is led to imagine what the sciences and scientists mean and say. The appeal to the imagination can be pursued through different avenues. One is that of fiction, a recent example of which is Michael Crichton's blockbuster *The State of Fear* (*1*). In his plot, scientists are colluding with the environmental movement, making up facts when necessary, in order to support a common cause. In a shrewd move of having environmental lawyers rehearse possible arguments that the defense might use against them, he lectures extensively in the guise of the scientific graphs and footnotes and by presenting whatever else looks like scientific evidence, about all that is wrong with global warming. It is a mix of science, advocacy, and a vision of scientists whose idealism leads them astray. It has been on 37 best-seller lists with another book that looks at the impact of environmental change in a very different way: Jared Diamond's *Collapse* (*2*), which is based on a scholarly analysis of a series of case studies of ancient civilizations. If Crichton's book is taken not as a work of fiction, but becomes equated with one of fact, like Diamond's, do we not run the risk that trust in science will be decided by market forces and continuing sales figures? The public has become accustomed in a media-saturated world to switching between fact and fiction—but how far does this extend? The question I want to pose is whether in the desire to communicate with "society," "science" has contributed to a confusion between facts and fiction, or as the political analyst Yaron Ezrahi described it, between high-cost and low-cost realities (*3*). Ezrahi distinguishes between constructs of the world that require heavy investment of resources, such as time, money, efforts, and skills, and those which engage fewer resources on the part of those who consume these realities. Scientific knowledge constructs high-cost reality, usually based on a densely organized system of concepts, facts, rules, interpretation, methodological skills, equipment, and evidence. As such, the knowledge is not directly accessible to laypersons and remains esoteric. Low-cost realities may be expensive to produce, but are "cheap" to consume. They depend on the immediate experience of the flow of images and sounds. They become the shared means by which the public conceives, imagines, remembers, thinks, and relates or acts in politics. They allow the public to simulate the witnessing of real events without the trouble of being actually there. Low-cost reality is a spectacularly successful commercial product in our culture.

Richard Feynman once used the analogy (*4*) of a Mayan priest who had mastered the numerical concept of subtraction and other elaborate mathematical rules. He used them to predict the rising and setting of Venus. However, to explain his approach to an audience who did not know what subtraction is, the priest resorted to counting beans. The important thing, said Feynman, is that it makes no difference as far as the result is concerned: We can predict the rise of Venus by counting beans (slow, but easy to understand) or by using the tricky rules (which are much faster, but it takes years of training to learn them). However, we have not taken the public through the tedium of bean counting, nor—apart from some notable exemptions—focused on teaching the tricks. Instead, we have been proud to re-enact on the public stage the spectacle of the Maya priest stepping forward before the attentive crowd and announcing the rise of Venus—while Venus rises indeed under the applause and to the relief of the viewers. We have learned how to stage such events ourselves and have come to believe that we thereby render a public service. We have largely engaged in the construction of low-cost realities that appeal to emotions and the imagination. There have certainly been charges that selling science as sexy has gone too far (*5*), amusing as it may be to explain the magic in Harry Potter in scientific terms (*6*). Some have said that by turning the Year of Physics de facto into the Year of Einstein, the point is missed that physics, while central to our understanding of the Universe, is also central to making useful and practical things through engineering (*7*). Although it is exhilarating to think of science's role in extending the frontiers of our knowledge, it is critical that the public remembers how important science is to their day-to-day reality. There are critical issues that need to be discussed, although they are not especially glamorous, such as the ongoing shift between the public nature of sci-

Now that researchers are becoming more than 1% of the population, should their ways of interacting with society change?

The author is chair of EURAB, the European Research Advisory Board of the European Commission, and Fellow at the Wissenschaftszentrum Wien, A-1080 Vienna, Austria. E-mail: helga.nowotny@wzw.at

ence and the tendency toward its propertization (*8*) or the upcoming debate about security-oriented research and the potential clash between the public interest in scientific openness and its security interests. Sexy communication is not going to be enough to inform good decision-making.

Declining trust in science and scientific experts has been clear in public controversies like genetically modified organisms (GMOs) or the bovine spongiform encephalopathy (BSE) crisis, as well as in the rejection of scientific evidence regarding vaccination safety in the UK. The Euro-barometer, conducted as an EU-wide survey, probes the state of mind of EU citizens and how they view science and technology. The most recent data are expected to be published in mid-May and, for the first time, will be commented on by a panel of experts. The 2001 survey (*9*) revealed that two-thirds of the public do not feel well-informed about science and technology, and the number of people who believe in the capacity of science and technology to solve societal problems is declining. Trust in science in general seems to be on the decline in many national surveys, although scientists still come out way ahead of politicians or other public institutions.

There are currently clear examples of research on the frontiers of science clashing with human beliefs and values. From the United States, voices can be heard deploring the tendency of politicians to interfere with scientific agendas in teaching and in research (*10*) and faith-based opposition to the teaching of evolution and some forms of frontier research, like stem cells continue to raise serious concern. Luckily, creationism/evolution is not an issue in Europe, largely due to the centralized education systems in most countries. However, an analogous situation exists for stem cell research, with some countries, like Germany and Italy, completely opposed. There will be a referendum in Italy shortly on stem cell research. The Catholic church urges the public not to vote, in the hope that the necessary 50% quota will not be reached, and the referendum will be defeated.

Although we may welcome greater public interest in science, if only to avoid another backlash in fields like nanotechnology as occurred with GMOs, we must also confront the thorny issue of how contemporary democracies will deal with minorities who, on faith-based or other, value-related grounds, refuse any compromise. There is no reason to believe that Europe will be immune to an ascendancy of groups who oppose otherwise promising lines of research on the basis of their value system. If the values dimension is here to stay, it is far from certain that the usual response of setting up ethical guidelines and committees will suffice, let alone that any of the efforts to "better communicate science" will have any effect.

If the goal is a more research-friendly society, one in which research and innovation become embedded in society and an expression of "the capacity to aspire" (*11*), we have to explain what research is and how the process of research is actually carried out. We need to focus more on the processes of research; on the inherent uncertainty that is part and parcel of it; on how bottom-up and top-down approaches intersect; on the actual, and not only idealized, role that users play; and on how research funding agencies work, both on national and supranational levels. We should explain how research priorities are set, because it is not nature whispering into the ears of researchers, but an intricate mixture of opportunities and incentives, of prior investments and of strategic planning mixed with subversive contingencies. We would also be better poised to explain to the wider public the difference between claims or promises made on the part of researchers, depending on whether these claims have been peer-reviewed or not. How should the public know about these rules that play such an important part for the scientific community, see their significance as well as their limitations, unless we explain how they actually work? Or how should they know about the differences in scientific cultures, what counts as evidence, or how consensus is reached with criticism being an essential precondition for moving toward it, if nobody tells them?

To observe and explain what scientists are really doing requires that we make the multiple links of interaction between science and society transparent, as well as the institutions that mediate and shape science policies. The dialogue needs to be extended into the world of politics, economics, and culture, including how scientists are influenced by globalization. There is a need for additional capacity building so that civil society can become a partner in this encounter with science. Apart from patient groups or organizations that have sponsored research into orphan diseases, there has been little organized effort in Europe so far.

It is only fair to say that much has been accomplished. The initial notion of public understanding of science as a didactically conceived one-way street through which scientific literacy is diffused did not miraculously lead to increased public support for science. It is increasingly being replaced by concepts of public awareness of science and public engagement with science. Activities that have been undertaken in this more interactive and outreaching mode range from the "Physics for taxi drivers" in London (*12*) to the regular public science festivals occupying their place alongside other, cultural, festivals. The 16th International Science Festival which has recently occurred in Edinburgh (*13*), and the Swiss "Science et Cité" initiatives stand out (*14*) as good examples of forums that encourage discussion and debate. Almost all member states of the European Union now celebrate European Science Week (*15*). The European Science Open Forum (ESOF) was a highly successful European event in Stockholm in 2004 and will be held again in Munich in 2006.

The larger (and richer) research institutions, such as the Max Planck Society in Germany or the CNRS in France, have set up their own outreach and public relations units. The current Framework Programme of the EU foresees outreach activities as an integral part of the contract obligations, although it is regrettable that outreach is not considered a factor in evaluating research proposals. The European Commission's proposed 7th Framework Programme, published on 6 April 2005, foresees an expanded "Science in Society" action line with an increased provisional budget of €554 million (US$712 million) for 7 years.

Successful communication can begin to be measured through short-term indicators, such as improvements in public opinion polls on trust in science or increases in enrollment figures for undergraduate physics or chemistry programs. In the longer term, we will need to measure evolution in the direction of scientific citizenship, which presupposes rights and duties on the part of citizens as much as on the part of political and scientific institutions. Innovation is the collective bet on a common fragile future, and neither science nor society knows the secret of how to cope with its inherent uncertainties. It can only be accomplished through an alliance among the participants and a shared sense of direction.

References and Notes

1. M. Crichton, *The State of Fear* (HarperCollins, New York, 2004).
2. J. Diamond, *Collapse: How Societies Choose to Fail or Succeed* (Viking, New York, 2004).
3. Y. Ezrahi, in *States of Knowledge: The Co-Production of Science and Social Order*, S. Jasanoff, Ed. (Routledge, London, 2004), pp. 254–273.
4. R. P. Feynman, *QED: The Strange Theory of Light and Matter* (Princeton Univ. Press, Princeton, NJ, 1986), pp. 10–12.
5. P. Weinberger, *Falter*, 16 February 2005, p. 14.
6. R. Highfield, *Harry Potter: How Magic Really Works* (Penguin, London, 2003).
7. "Einstein is dead," *Nature* **433**, 179 (2005).
8. H. Nowotny, in *The Public Nature of Science Under Assault: Politics, Markets, Science, and the Law*, Helga Nowotny *et al.* (Springer Verlag, New York, 2005), pp. 1–28.
9. http://europa.eu.int/comm/public_opinion/archives/ebs/ebs_154_en.pdf
10. A. I. Leshner, *Science* **307**, 815 (2005).
11. A. Appadurai, in *Culture and Public Action*, V. Rao and M. Walton, Eds. (Stanford Univ. Press, Stanford, CA, 2004), pp. 59–84.
12. www.iop.org/news/860
13. www.edinburghfestivals.co.uk/science/
14. www.science-et-cite.ch/de.aspx
15. www.cordis.lu/scienceweek/home.htm

10.1126/science.1113825

CELL BIOLOGY

Oxidative Stress and Cancer: A β-Catenin Convergence

Bruce Bowerman

The Wnt signaling pathway often seems indefatigable, acting at numerous times and places throughout both invertebrate and vertebrate development. Its influence is broad, directing processes as diverse as body axis formation, organogenesis, cell migration, and stem cell proliferation (*1*, *2*). When Wnt ligands activate cell surface receptors, the proteolytic destruction of a remarkable cytoplasmic protein called β-catenin is halted. This key mediator of Wnt signaling is then free to move to the nucleus where it binds to and converts a family of transcriptional repressors called T cell factors (TCFs) into activators of gene expression (*1*, *2*). Malfunction of this pathway can result in the abnormal stabilization of β-catenin, a key causative step in some of the most common and deadly forms of cancer, including colon carcinoma and melanoma (*2*). Intriguingly, β-catenin is thought to influence the metastatic potential of tumor cells by affecting chromatin remodeling (*3*). It is also a key component of adherens junctions that hold epithelial cells together (*1*). Now a report by Essers *et al*. on page 1181 of this issue identifies yet another role for β-catenin, providing compelling evidence that it also is a cofactor for the FOXO subfamily of winged helix transcription factors (*4*). FOXO family members promote mammalian cell survival by inducing cell cycle arrest and quiescence in response to oxidative stress (*5*–*10*). They also regulate longevity in model organisms (*11*). Thus, β-catenin continues to surprise biologists with its multifarious and possibly related roles in development and cancer, and apparently in cell survival and longevity as well.

This most recent β-catenin insight comes from studies of the roundworm *Caenorhabditis elegans*. Essers *et al*. astutely noticed that *C. elegans* mutants lacking the function of BAR-1, a β-catenin homolog, exhibit defects not only in Wnt signaling but also in dauer formation. This alternative larval stage is a temporary response to unfavorable conditions such as starvation, stress, or high population density (*11*). It is exited when favorable growth conditions return. The route to the dauer state has received much attention recently because mutations that promote this fate in larvae also increase the life span of adult worms (*11*). Because the *C. elegans* FOXO family member DAF-16 is required for both dauer development and normal longevity, Essers *et al*. asked whether BAR-1/β-catenin is required for DAF-16/FOXO function. Like mammalian FOXO family members, DAF-16 is negatively regulated by an insulin-like receptor called DAF-2. When activated, this receptor triggers a signaling cascade that keeps DAF-16 out of the nucleus. Loss of DAF-2 function thus activates DAF-16, launching the dauer fate and increased longevity (*11*). Essers *et al*. found that this scenario requires BAR-1/β-catenin. Furthermore, overexpression of BAR-1/β-catenin promotes dauer fate in a manner that depends on DAF-16/FOXO. Loss of BAR-1/β-catenin function, like loss of DAF-16/FOXO, shortens life span. These genetic studies demonstrate that BAR-1/β-catenin is required for DAF-16/FOXO function. The authors also found that BAR-1/β-catenin binds to, and presumably augments the activity of, DAF-16/FOXO. Essers *et al*. further show that these β-catenin functions are conserved in mammals. Expression of β-catenin and FOXO4, in a mammalian cell line that lacks endogenous β-catenin, increased the expression of transcriptional reporter genes beyond the levels induced by FOXO4 alone. Similarly, stabilization of endogenous β-catenin in mammalian cells increased FOXO4-mediated activation of reporter genes. Finally, the two mammalian proteins potentially bind each other, as they were isolated in a complex from mammalian cells.

Both DAF-16 and mammalian FOXO family members are activated in response to stress caused by highly reactive oxygen species (*8*, *9*). This oxidative stress response results in increased expression of superoxide dismutase enzymes that eliminate reactive oxygen (*10*, *12*). Interestingly, another consequence of FOXO activation in mammalian cells is cell cycle arrest and entry into quiescence. This nonproliferative state (*5*–*7*) limits damage from reactive oxygen and promotes cell survival (*8*, *10*). Indeed, this mammalian cell cycle response may be related to dauer formation in *C. elegans*, as both involve physiological stasis (*7*). Essers *et al*. provide clear evidence that β-catenin is required for FOXO-mediated expression of superoxide dismutases in worms and mammalian cells, as well as for FOXO-mediated cell cycle arrest in mammalian cells. It is noteworthy that β-catenin therefore participates in two seemingly antagonistic processes: the conversion of TCF repressors into transcriptional activators to promote cell proliferation during development and tumorigenesis, and the activation of FOXO transcription factors to promote cellular dormance (see the figure).

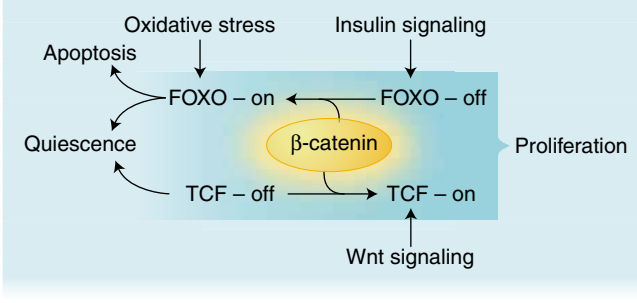

An overview of β-catenin–dependent regulation of cell proliferation versus cell quiescence. β-catenin interacts with FOXO transcription factors to promote exit from the cell cycle and entry into quiescence. Oxidative stress activates this function of FOXO, while insulin signaling inhibits it. β-catenin also promotes cell proliferation through its interactions with TCF transcription factors (*1*, *2*). These two opposing functions of β-catenin may influence cancer progression and might be manipulated as a therapeutic approach.

These new findings raise intriguing questions about the involvement of β-catenin in cancer. Although it is not clear how these opposing effects influence cancer cells, Essers *et al*. do find endogenous β-catenin and FOXO4 in a complex in a colon carcinoma cell line. If both effects of β-catenin are operative in precancerous cell lineages, perhaps subsequent mutations in other genes negate the cell cycle arrest promoted by β-catenin's interaction with FOXO, thereby favoring tumor formation. Perhaps shifting the balance of β-catenin's interactions with TCF and FOXO could be used to favor quiescence over proliferation.

The author is in the Institute of Molecular Biology, University of Oregon, Eugene, OR 97403, USA. E-mail: bbowerman@molbio.uoregon.edu

Indeed, a recent study shows that FOXO transcription factors are acetylated, and that deacetylation promotes cell cycle arrest and quiescence over programmed cell death. (*8*). Modifiers of TCF, FOXO, or β-catenin that can shift the balance of their interactions to favor quiescence would have potential implications for cancer therapy. It is also curious that despite epidemiological evidence indicating that antioxidants lower cancer risk, these new findings suggest that activating the oxidative stress response might promote quiescence and thereby antagonize cancerous cell proliferation. Thus, the oxidative stress response may not only promote cell survival and longevity, but also may prove useful in the development of cancer therapies.

References

1. C. Y. Logan, R. Nusse, *Annu. Rev. Cell Dev. Biol.* **20**, 781 (2004).
2. T. Reya, H. Clevers, *Nature* **434**, 843 (2005).
3. J. H. Kim *et al.*, *Nature* **434**, 921 (2005).
4. M. A. G. Essers *et al.*, *Science* **308**, 1181 (2005).
5. R. H. Medema *et al.*, *Nature* **404**, 782 (2000).
6. G. J. Kops *et al.*, *Mol. Cell. Biol.* **22**, 316 (2002).
7. B. M. T. Burgering, G. J. Kops, *Trends Biochem. Sci.* **27**, 352 (2002).
8. A. Brunet *et al.*, *Science* **303**, 2011 (2004); published online 19 February 2004 (10.1126/science.1094637).
9. M. A. Essers *et al.*, *EMBO J.* **23**, 4802 (2004).
10. G. J. Kops *et al.*, *Nature* **419**, 316 (2002).
11. C. Kenyon, *Cell* **120**, 449 (2005).
12. Y. Honda, S. Honda, *FASEB J.* **13**, 1385 (1999).

10.1126/science.1113356

PLANETARY SCIENCE

The Interior of Mars

Yingwei Fei and Constance Bertka

The planetary core is the engine of a planet: It drives convection of the mantle, shapes the planet's surface, and—if the core contains convective molten metal that creates a dynamo—generates a global magnetic field. Based on its mean density and the bulk chemistry of terrestrial planets, Mars is believed to have a dense metallic core and a silicate mantle. However, because no seismic data exist for Mars, the density profile of its interior and the depth of the core-mantle boundary are not known precisely, and it remains unclear whether the martian core is solid or liquid.

Enhanced online at www.sciencemag.org/cgi/content/full/308/5725/1120

For the past decade, space missions to Mars have provided important constraints on the physics and chemistry of its interior, although these missions were primarily designed to map and understand surface or near-surface features of the planet. From a combined analysis of Mars Global Surveyor tracking data and Mars Pathfinder and Viking Lander range and Doppler data, the planet's moment of inertia—an important geophysical parameter for understanding the planet's internal density distribution—has been determined at high precision (*1*, *2*). Topography and gravity data collected by Mars Global Surveyor have constrained the global average thickness of the martian crust to between 30 and 80 km (*3*, *4*).

Models that combine these data with a range of possible core compositions allow the boundaries for mantle density to be defined. The results indicate that the martian mantle is more iron-rich than that of Earth (*5*, *6*). Interpretations of the chemistry and mineralogy of martian meteorites (*7*) and of the basaltic rocks at the landing sites of the Mars Exploration Rover Mission (*8*), although model dependent, are consistent with this conclusion.

Several lines of independent evidence suggest that the martian core has been liquid throughout its history. The first line of evidence comes from the discovery of strongly magnetized ancient crust by Mars Global Surveyor (*9*, *10*). The magnetization was acquired more than 4 billion years ago, implying a short-lived (~0.5 billion years) early martian core dynamo (*11*). Such a core dynamo may be driven either by compositional convection (which is set in motion by a composition gradient) in a liquid outer core due to solidification of an inner core, or by thermal convection in a fully liquid core due to high heat flux out of the core (*11*).

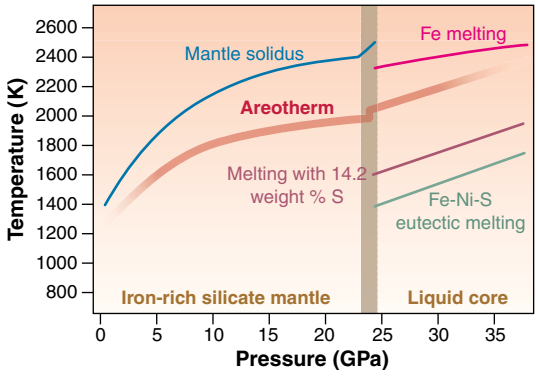

Evidence for a liquid core. Melting curves of putative martian mantle and core materials are compared with the estimated temperature profile (areotherm) for the martian interior. The martian mantle is expected to be solid, because its temperature is lower than the mantle solidus (the temperature at which melting begins). The minimum melting temperature in the Fe-Ni-S system (the eutectic melting temperature) at martian core pressures is also shown. Given an estimated core temperature of 2000 K, Mars has an entirely liquid core for a model core composition with 14.2 weight % sulfur.

Thermal evolution models of the martian core indicate that core solidification would have generated a long-lived (>1 billion years) dynamo (*12*). This scenario is not consistent with the observed martian magnetic field history. The short-lived early martian dynamo may have been caused by an initially superheated core after rapid core formation (*12*) or by mantle processes such as overturning of a chemically or mineralogically distinct layer (*13*), resulting in an increased heat flux out of the core. These models require a liquid core to initiate a dynamo. Evidence for a subsequent short-lived (<0.4 billion years) martian core dynamo around 3.75 billion years ago (*14*) would further strengthen the case for a liquid core, because it is difficult to produce a short-lived dynamo with multiple episodes if the core starts to solidify. The second line of evidence for a liquid martian core comes from measurements of the solar tidal deformation of Mars, obtained by analyzing Mars Global Surveyor radio tracking data (*2*). The measurements indicate that at least the outer part of the core is liquid and are also consistent with an entirely liquid core.

High-pressure experimental melting data for martian core materials at martian core pressures provide the third line of evidence for a liquid martian core (see the figure). At core pressures, the iron-nickel-sulfur system begins to melt at such a low temperature (~1400 K) that any amount of sulfur in the core would lead to at least a liquid outer core for any reasonable thermal model (*15*, *16*). Given an estimated present-day core temperature of 2000 K (*12*) and a model core composition containing 14.2 weight % sulfur, the martian core is most certainly liquid (see the figure).

The size of the martian core is the least-constrained physical parameter of the planet, but it has important implications for the chemical compositions of the core and the mantle. Space missions with multiple landers equipped

Y. Fei is with the Geophysical Laboratory, Carnegie Institution of Washington, Washington, DC 20015, USA. E-mail: fei@gl.ciw.edu. C. Bertka is with the Geophysical Laboratory, Carnegie Institution of Washington, Washington, DC 20015, USA and the American Association for the Advancement of Science, Washington, DC 20005, USA. E-mail: cbertka@aaas.org

with seismometers are required to precisely determine the size of the core. Such missions would also provide fundamental information on the structure and density profile of the martian interior, which is critical for understanding both the formation and evolution of Mars. This understanding is essential for providing a general context to explore the formation and evolution of terrestrial planets, including our own.

Previous and ongoing missions are providing a wealth of information about the martian surface and the role that water may have played throughout the history of the planet. However, the forces that have shaped the planet's surface are driven in large part by the evolution of its interior. A comprehensive understanding of the planet's history requires a greater understanding of its interior. A mission that focuses on the martian interior is overdue.

References and Notes

1. W. M. Folkner *et al.*, *Science* **278**, 1749 (1997).
2. C. F. Yoder *et al.*, *Science* **300**, 299 (2003).
3. M. T. Zuber *et al.*, *Science* **287**, 1788 (2000).
4. M. A. Wieczorek, M. T. Zuber, *J. Geophys. Res.* **109**, 10.1029/2003JE002153 (2004).
5. C. M. Bertka, Y. Fei, *Earth Planet. Sci. Lett.* **157**, 79 (1998).
6. C. M. Bertka, Y. Fei, *Science* **281**, 1838 (1998).
7. H. Wänke, G. Dreibus, *Meteoritics* **20**, 367 (1985).
8. H. Y. McSween *et al.*, *Science* **305**, 842 (2005).
9. M. H. Acuña *et al.*, *Science* **284**, 790 (1999).
10. J. E. P. Connerney *et al.*, *Science* **284**, 794 (1999).
11. D. J. Stevenson, *Nature* **412**, 214 (2001).
12. J.-P. Williams, F. Nimmo, *Geology* **32**, 97 (2004).
13. L. T. Elkins-Tanton *et al.*, *Lunar Planet. Sci.* **34**, 1479 (2003).
14. R. J. Lillis *et al.*, *Lunar Planet. Sci.* **36**, 1578 (2005).
15. Y. Fei *et al.*, *Am. Mineral.* **85**, 1830 (2000).
16. Y. Fei, C. M. Bertka, *Lunar Planet. Sci.* **34**, 1829 (2003).

17. We thank F. Nimmo for helpful discussions. Funding was provided by the NASA Cosmochemistry program and the Carnegie Institution of Washington.

10.1126/science.1110531

DEVELOPMENTAL BIOLOGY

Ignoratio Elenchi: Red Herrings in Stem Cell Research

Peter J. Quesenberry, Gerri Dooner, Mark Dooner, Mehrdad Abedi

According to recent reports, cells from bone marrow can incorporate into other tissues and take on the identity of the resident cells. This has been shown in vivo for liver, heart, brain, skin, lung, pancreas, and the gut. One dramatic report even showed reversal of fatal liver failure in mouse by bone marrow cells derived from purified stem cells (*1*). These reports have generated a lively, and at times divisive, debate. Overriding the discussion is a general perception that the published work is not reproducible. As stated in a recent review received by us: "It would be nice to know why and how highly competent scientists can repeatedly come up with completely contradictory results."

Some researchers in the field have developed specific criteria that, they argue, should be met before work on this problem can be accepted (*2*–*4*). Far from resolving the issues, these criteria have acted as diversions from the proper goals of this research. In essence, they present an argument that purports to prove one thing, but instead proves a different conclusion not at issue. This logical fallacy is known as ignoratio elenchi ("ignoring the issue"). Its most common form is the red herring. These criteria include a demonstration of the robustness of the phenomenon, of the clonal nature of the stem cells, and of definite determinations that the bone marrow cells have not fused with the target tissue cells.

There is no absolute way to assess "robustness." Nevertheless, quite high proportions of cells derived from bone marrow have been documented in lung (*5*), liver (*1*), and skeletal muscle (*6*). But tissues with less marrow-to-target cell conversion, namely the brain and heart, have been highlighted in the controversy. In fact, a wide variety of results have been reported in different tissues. For instance, the percentage of marrow-derived cells for skeletal muscle has varied from 0.2 to 12.5%; for lung, from 1 to 35%; and for liver, from none to 30 to 50%. The bone marrow cell type or host treatment differed among these reports. Injury, an important trigger of stem cell incorporation, ranged from none to radiation, to radiation plus exercise, bleomycin, cardiotoxin, or genetic injury. Human granulocyte colony-stimulating factor treatment was used in a few studies. The exact identity of the bone marrow cells also varied widely, from whole bone marrow, various subsets of bone marrow populations, cells recovered after transplantation, to cells from umbilical cord blood. Some studies were in mouse, some in human. The negative results (showing no marrow cell incorporation) have been mainly in cardiac and neural tissues, in which cell plasticity is less robust, although not nonexistent. With such diversity of experimental models, only one study has actually exactly duplicated another. Several papers have been touted as failing to reproduce plasticity results (*7*, *8*). But, in fact, even the authors of "Little Evidence for Plasticity of Adult Hematopoietic Stem Cells" (*7*) commented (*9*) that "our data are not directly comparable to those of Krause *et al.* (*5*) and do not implicitly refute their observations." Abedi and colleagues (*6*) have now established that there are at least eight variables that determine whether marrow cells differentiate into skeletal muscle: injury, cell type, timing of engraftment, chimerism with radiation, route of administration, number of cells administered, the functional state of the cells, and stem cell mobilization after engraftment. A single exception in which experimental details were replicated is the work of Murry *et al.* (*10*) on cardiac reconstitution. These authors attempted to reproduce previously reported studies but obtained different results. The discrepancy remains unexplained. Thus, there have been a large number of studies published with varied and provocative results, but in fact there have been virtually no attempts to precisely reproduce the work of others.

FACTORS INFLUENCING CELL PLASTICITY

- Injury*
- Cell type
- Timing of engraftment
- Chimerism with radiation
- Route of administration
- Number of cells administered
- Functional state of cells
- Stem cell mobilization after engraftment

*Most important

The second, often cited criterion is that the donor cells should all be derived from a single clone. This appears to be based on two misperceptions: that transdifferentiation (a change from one differentiated cell type to another) is the only valid route to clinical utility, and that defined bone marrow stem cell populations are homogeneous. Transdifferentiation has not been established in any system, and most investigators do not think that this process accounts for stem cell plasticity. Rather, directed differentiation from minor stem cell populations appears more likely. In addition, most stem cell populations that are defined as purified by their ability to renew hematopoiesis in vivo are quite heterogeneous when other criteria are

The author is in the Department of Research, The Center for Stem Cell Biology, Providence, RI 02908–4735, USA. E-mail: pquesenberry@rwmc.org

considered. For example, when a highly purified population of stem cells responds in vitro to cytokines, the resultant single-cell derived clones differ in size, configuration, and cell type (*11*). Such studies remind us of both the multipotentiality and the heterogeneity of the source cells. Thus, population studies may be more important than single (clonal) cell studies in defining the plasticity of stem cells.

Cell fusion has been the biggest red herring of all. Reports showed that embryonic stem cells could fuse with neural stem cells or whole marrow cells, at a low rate. Lagasse *et al.* (*1*) demonstrated replacement of up to 50% of liver cells due to fusion of donor bone marrow cells with host hepatocytes. In this case, fusion was the mechanism underlying therapeutically effective replacement of diseased liver cells. Fusion, then, can be a good thing, under some circumstances.

As with "robustness," the phenomenon of fusion is model dependent. Some reports of bone marrow cell plasticity show fusion and others indicate plasticity without fusion. Purified umbilical cord blood cells convert to fetal liver cells in sheep, without fusion (*12*). Studies by Harris *et al.* (*13*) with a Cre-lox transgenic approach showed that lung and skin conversions were not due to fusion. Thus, fusion may occur in some but not all models and can produce therapeutically beneficial results.

Should our ignorance of the mechanism of incorporation stop clinical trials from going forward? We think not. Many thousands of individuals have been cured by allogeneic transplantation for acute leukemia; yet our views on the underlying mechanisms continue to change. Recently, bone marrow cells have been used to treat acute myocardial infarction in nine clinical trials (involving more than 100 patients) (*14*). Approaches differed in each study, but various aspects of cardiac function were improved and there was little acute toxicity. In these studies, the mechanisms are unknown and long-term results are pending.

Despite the controversy, our knowledge of stem cells continues to advance. Studies on both basic mechanisms of plasticity and clinical utility should proceed in parallel. Let the good work go forward.

References

1. E. Lagasse *et al.*, *Nat. Med.* **6**, 1229 (2000).
2. D. J. Anderson, F. H. Gage, I. L. Weissman, *Nat. Med.* **7**, 393 (2001).
3. I. Lemischka, *Exp. Hematol.* **30**, 848 (2002).
4. A. J. Wagers, I. L. Weissman, *Cell* **116**, 639 (2004).
5. D. S. Krause *et al.*, *Cell.* **105**, 369 (2001).
6. M. Abedi *et al.*, *Exp. Hematol.* **32**, 426 (2004).
7. A. J. Wagers, R. I. Sherwood, J. L. Christensen, I. L. Weissman, *Science* **297**, 2256 (2002).
8. R. F. Castro *et al.*, *Science* **297**,1299 (2002).
9. A. J. Wagers *et al.*, *Science* **299**,1317 (2003).
10. C. E. Murry *et al.*, *Nature* **428**, 664 (2004).
11. G. A. Colvin *et al.*, *Blood* **104** (abstr. 3215) (2004).
12. G. Kogler *et al.*, *J. Exp. Med.* **200**, 123 (2004).
13. R. G. Harris *et al.*, *Science* **305**, 90 (2004).
14. A. Keating, *Biol. Blood Marrow Transplant.* **11**, 2 (2005).

10.1126/science.1104432

PHYSICS

Control at the Quantum Level

Thomas F. Krauss

The ability to control interactions between light and matter has led to many exciting technological developments, most notably the laser, which has enabled the information technology revolution as we know it. On page 1158 of this issue, Badolato *et al.* (*1*) demonstrate such control at the quantum level between a quantum dot (a nanometer-scale emitter of electromagnetic radiation) and a nanometer-scale optical resonator (nanocavity) in a photonic crystal. The approach allows multiple quantum interactions (see the figure) to be combined. The work is an important step toward the realization of solid-state quantum computers.

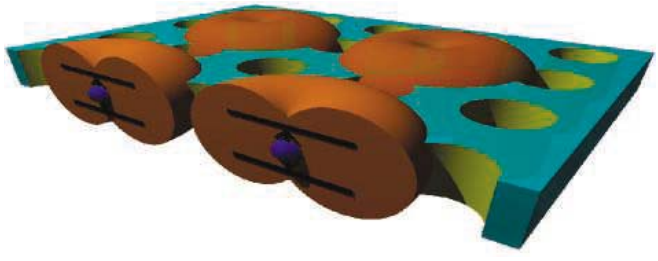

A multiple coupled quantum system. To realize a coupled quantum system—which may, for example, form a section of a quantum computer—one must control the relevant optical and electronic resonances accurately. Here, multipe strongly coupled nanocavity-quantum dot systems are shown to interact. Each Individual system is represented by the coupling between the oscillating electron states (horizontal lines linked by arrows) and the cavity resonance (orange torus).

There have been several recent demonstrations of strong light-matter interactions between quantum dots and optical nanocavities (*2*, *3*), but these studies relied on chance: Researchers fabricated large numbers of cavities and then searched for those that happened to incorporate quantum dots that emitted light at the right wavelength. Badolato *et al.* (*1*) add an unprecedented element of design and control that is essential for taking these concepts further toward the fabrication of practical devices such as single-photon emitters and quantum computers.

Strong interactions between an emitter and a cavity are at the heart of quantum information processing, for example, in single-photon emission, optical logic, and quantum computing. Groundbreaking experiments with quantum systems have been performed, for example, with atoms suspended in a free-space cavity between two mirrors (*4*). However, realizing these experiments in the solid state is crucial for practical applications and is similar to the step change caused by the replacement of vacuum tubes with solid-state transistors.

It is thus not surprising that the recent all-solid-state demonstration of strong coupling between a single "atom-like" quantum dot emitter and the optical nanocavity is embedded in (*2*, *3*) caused much excitement. How does this approach work?

An excited emitter (such as a quantum dot) will emit a photon after a characteristic spontaneous-emission lifetime. If the emitter is in a suitable environment (such as a nanocavity that is resonant at the emitter's wavelength), the emission will be enhanced. This "Purcell effect" reduces the spontaneous-emission lifetime, making the emission process more efficient. It is governed by the "Q/V factor" of the system: The closer together the emitter and the cavity are in space (small volume V) and frequency (high quality factor Q), the stronger the interaction.

This is where the photonic crystal environment comes in. Photonic crystals are periodic dielectric structures (represented by the array of holes in the figure) through which light of a certain wavelength range cannot propagate; this light is therefore reflected. The high reflectivity allows one to construct cavities with extremely high Q (*5*). Furthermore, these high-Q cavities can be made very small, on the length scale of an optical wavelength in the material, which is several times 100 nm (1 nm = 10^{-9} m). Photonic crystals offer the highest Q/V factor of any cavity type known to date.

In the Purcell regime, the system is weakly coupled, that is, the properties of the emitter are modified but not fundamentally altered by the presence of the cavity. As the Q/V factor increases, the system enters a new regime, where the emitter and the cavity are so strongly coupled that they

The author is at the School of Physics and Astronomy, University of St. Andrews, St. Andrews KY16 9SS, UK. E-mail: tfk@st-and.ac.uk

exchange energy and act like a coupled quantum system. In this strong-coupling regime, the system becomes sensitive to individual photons, that is, the cavity responds differently to an incoming photon depending on whether it is already occupied by a photon or not. This sensitivity opens up another new realm for photon-photon interactions, such as single-photon logic and single-photon emission. For comparison, photon-photon interactions in a conventional nonlinear optical device require ~10^6 or more photons.

However, because the cavity Q factors are so high (meaning very narrow spectral linewidths) and volumes so small, the strong coupling is difficult to control. To overcome this problem, most researchers fabricate so many cavities that the chance of finding one that contains a quantum dot of suitable resonance in the right place is high. Putting the dot in the right place is a rather important aspect that is easily overlooked; even though the cavity is small, the light is not evenly distributed in it, and for maximum effect, the dot must sit at a peak of the cavity mode. Badolato *et al*. achieve this through the use of "marker dots" that accurately indicate the dot position; with the use of alignment markers, the cavity can then be placed lithographically at the right position (*1*).

If several such strongly coupled systems can be brought into close proximity, they can interact and "entangle" their states in a quantum system, which forms the basis for quantum computing. Here lies the true strength of the deterministic approach: It is difficult enough in the "chance" approach to find a single cavity and dot in resonance, but the chances of finding two or more next to one another is vanishingly small; controlling the resonances is the only viable option.

Badolato *et al.* have not actually demonstrated strong coupling in their cavities, but they are very close. Much stronger interactions could easily be achieved through the use of cavity designs with higher Q (*5*). The strength of their result is therefore that two major mechanisms for controlling the coupling between quantum dot and cavity have been successfully demonstrated: the placement of the dot with respect to the cavity mode, and the tuning of the cavity resonance.

For the dream of quantum computers based on optical cavities (see the figure) to become reality, further control needs to be exercised, for example, in the creation of quantum dots with deterministic emission wavelength. The work by Badolato *et al*. is nonetheless a major step forward in exercising control over quantum systems in the solid state.

References

1. A. Badolato *et al*., *Science* **308**, 1158 (2005).
2. J. McKeever *et al*., *Science* **303**, 1992 (2004); published online 26 February 2004 (10.1126/science.1095232).
3. J. P. Reithmaier *et al*., *Nature* **432**, 197 (2004).
4. T. Yoshie *et al*., *Nature* **432**, 200 (2004).
5. B.-S. Song *et al*., *Nat. Mater.* **4**, 207 (2005).

10.1126/science.1113753

MOLECULAR BIOLOGY

A Renewed Focus on Transfer RNA

Tina Daviter, Frank V. Murphy IV, V. Ramakrishnan

Translation of the genetic code occurs through base-pairing interactions between the codon on messenger RNA and the anticodon on transfer RNA (tRNA) that are mediated by the ribosome, the molecular machine that catalyzes protein synthesis. Even before the complete elucidation of the genetic code, it was clear that the accuracy of protein synthesis is too high to be accounted for by codon-anticodon pairing alone (*1*). The discovery that it could be affected by antibiotics and ribosomal mutations suggested that the ribosome has a decoding site that inspects codon-anticodon interactions (*2*). Hence, the discovery of a mutant tryptophanyl tRNA ("Hirsh suppressor") that could supress the termination of protein synthesis was a puzzle (*3*). A G24A mutation on this tRNA, although quite distant from the anticodon at positions 34 to 36 (see the figure), nevertheless conferred on the mutant tRNA the ability to pair with the UGA stop codon in addition to the wild-type UGG codon. How does this tRNA recognize UGA and evade proofreading by the ribosome? Now, decades after the discovery of the Hirsh suppressor, its secrets are being revealed. On page 1178 in this issue, Cochella and Green (*4*) show how the kinetic properties of the mutant tRNA allow it to decode stop codons.

Aminoacyl-tRNA is initially brought into the ribosome as a complex with elongation factor Tu (EF-Tu) and guanosine 5′-triphosphate (GTP) (see the figure). Upon GTP hydrolysis, EF-Tu is released. In a view of decoding termed kinetic proofreading (*5*, *6*), incorrect tRNAs can dissociate from the ribosome either before or after EF-Tu release, with the overall selectivity being as much as the product of both selection steps. Experimental evidence for proofreading came when it was shown that near-cognate tRNAs (which contain a single subtle mismatch between codon and anticodon) require more GTPs hydrolyzed per amino acid incorporated than do cognate tRNAs (*7*, *8*). In this view, the ribosome merely provided a passive platform for tRNA selection, with mutations and antibiotics altering accuracy by affecting the rate of GTP hydrolysis by EF-Tu. In principle, mutations distant from the codon-anticodon pairing could also affect the rate of GTP hydrolysis.

More recent work points to a direct role for the ribosome and its associated players in tRNA selection. Careful studies on the stability of RNA helices show that the free-energy differences from a base-pairing mismatch can account for a factor of 5 to 10 in selectivity (*9*) rather than the factor of 100 assumed previously. This is too low to account for the accuracy of protein synthesis even with proofreading. Pre–steady-state kinetic experiments show that the forward rates of GTPase (guanosine triphosphatase) activation (the rate-limiting step in GTP hydrolysis) and accommodation (movement of tRNA into the peptidyl transferase center) are dramatically higher for cognate tRNA than for near-cognate tRNA (*10*, *11*). Thus, cognate tRNA is likely more efficient at inducing a productive ribosome conformation, consistent with results from nuclear magnetic resonance studies on a portion of the decoding site (*12*). Crystallographic studies on the 30*S* ribosomal subunit showed that, in the productive conformation, the ribosome directly monitors the geometry of base pairing at the minor groove of the first two positions (but interestingly not at the wobble position) between the codon and anticodon (*13*).

Several other key pieces of evidence helped to clarify things further. Kinetic studies showed that intact tRNA is required to transmit the signal from codon recognition in the 30*S* subunit to the GTPase center in the 50*S* subunit (*14*). Cryoelectron microscopy demonstrated that in the ribosome, the tRNA in complex with EF-Tu has a bend in the anticodon stem-loop: The region around the anticodon loop is in nearly the accommodated orientation, while the bend allows the rest of the tRNA to remain in the orientation presented by EF-Tu (*15*, *16*). Crystal structures revealed

MRC Laboratory of Molecular Biology, Hills Road, Cambridge CB2 2QH, UK. E-mail: ramak@mrc-lmb.cam.ac.uk

that conformational changes seen could only be induced in the 30*S* subunit by cognate and not near-cognate tRNA (*17*). Thus, the ribosome uses part of the additional binding energy from its interactions with the minor groove of the cognate codon-anticodon helix to induce a conformational change leading to a productive closed form, which involves a distorted tRNA. After GTP hydrolysis and dissociation of EF-Tu, the distorted tRNA, which has been described as a "molecular spring" (*18*), would be free to relax into the accommodated state. This would be faster in the cognate case where the anticodon end was constrained in a conformation close to the accommodated state (*17*).

This view made it possible to rationalize various mutations affecting the accuracy of translation that were spread throughout the ribosome or tRNA (*1*, *17*). These mutations would favor one or the other conformation, thus facilitating or inhibiting the closure of the ribosome or the distortion of the tRNA. A role for the dynamic property of tRNA in decoding was presaged long before the recent structural data (*19*). But decades after its discovery, there were still no hard data to explain exactly how the Hirsh suppressor tRNA increased the error rate.

Now, using rapid quench methods, Cochella and Green (*4*) have directly measured the rates of GTP hydrolysis and dipeptide formation for the Hirsh suppressor and its corresponding wild-type tRNA. These rates reflect the rate-limiting preceding step in each case, namely, GTPase activation and accommodation (*10*, *11*). Using a mutant EF-Tu that is defective in GTP hydrolysis, they also measured the rate of dissociation of tRNA from the ribosome. As might be expected for a mutation far from the anticodon, the dissociation rates of the Hirsh suppressor and the corresponding wild type are very similar on the various codons tested. However, the forward rates of both GTPase activation and accommodation are much higher for the Hirsh suppressor than for the wild type when a near-cognate codon is used. The increase in the rate of GTPase activation can be explained if the mutation makes the tRNA more easily deformable into the bent structure in the transition state. But what about the increase in the accommodation rate?

Based on the observation that forward rates of GTPase activation and accommodation were simultaneously affected by various agents (for example, codon-anticodon pairing or antibiotics such as paromomycin) (*11*), it was proposed that these two steps were both regulated by the domain closure in the 30*S* subunit (*17*). That the Hirsh suppressor also affects both these rates might appear to strengthen this notion. However, the Hirsh suppressor is the one case where one might not have expected these two rates to be coupled: If GTPase activation is accelerated because the tRNA is more deformable, then such a tRNA should be slower in relaxing into the undeformed state during accommodation. The "molecular spring" should be less stiff and therefore snap into place more slowly.

So where does this leave the molecular spring idea? Cochella and Green (*4*) propose that specific interactions between the ribosome and tRNA might be altered for the mutant tRNA. Interestingly, the mutation itself is close to helix 69 of the 50*S* subunit in both the bent and relaxed forms of tRNA. If the mutant tRNA makes stronger interactions with the ribosome, it could compensate for weaker codon-anticodon interactions. This in turn could help to distort the tRNA and place its anticodon stem-loop in approximately the accommodated orientation before EF-Tu release, and hold it in this orientation during its subsequent movement, just as with cognate tRNA. Perhaps holding the anticodon end in the accommodated orientation and thus restricting the movement of the tRNA (*17*) is more important in speeding up accommodation than the "stiffness" of a putative tRNA spring. To resolve these issues, we need similar kinetic data on other mutants, as well as higher resolution structures of wild-type and mutant tRNAs bound to the ribosome in these various states.

In the meantime, after a long period in which the focus has been on the ribosome, Cochella and Green have redirected attention toward the properties of the tRNA substrate itself. Interestingly, tRNA is one of the most heavily modified RNAs in the cell. These modifications may alter the dynamic properties of various tRNAs to ensure roughly similar rates and accuracies despite differences in the strength of the codon-anticodon interactions. Indeed, recent binding affinity data support this notion (*20*). In any case, it is becoming increasingly clear that far from being a rigid and passive substrate, tRNA has coevolved with the ribosome to allow the close and dynamic interplay required for the fidelity and speed of translation.

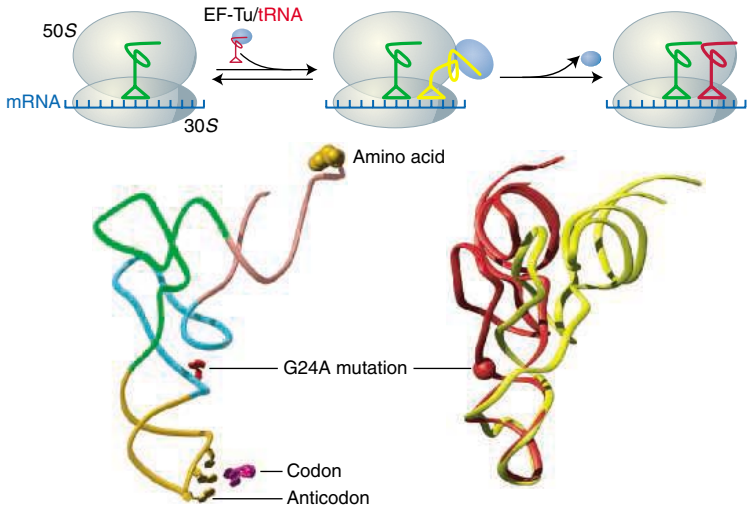

An active role for tRNA: (Top) A new aminoacyl-tRNA is brought into the A site of the ribosome in complex with elongation factor EF-Tu. Upon GTP hydrolysis, the aminoacyl-tRNA is released by EF-Tu, and swings into the peptidyl transferase center of the 50*S* subunit. The tRNA is distorted when bound with EF-Tu on the ribosome. **(Bottom)** A G24A mutation allows a tryptophanyl tRNA to read the UGA stop codon in addition to the UGG tryptophan codon. Strikingly, this mutation in the Hirsh suppressor tRNA is far from the anticodon, but close to the region of distortion in the tRNA when it first binds to the ribosome. The mutation allows GTP hydrolysis and the movement of tRNA into the peptidyl transferase center to proceed efficiently even on the stop codon (*4*).

References

1. J. M. Ogle, V. Ramakrishnan, *Annu. Rev. Biochem.* **74**, 129 (2005).
2. J. Davies, W. Gilbert, L. Gorini, *Proc. Natl. Acad. Sci. U.S.A.* **51**, 883 (1964).
3. D. Hirsh, *J. Mol. Biol.* **58**, 439 (1971).
4. L. Cochella, R. Green, *Science* **308**, 1178 (2005).
5. J. J. Hopfield, *Proc. Natl. Acad. Sci.* **71**, 4135 (1974).
6. J. Ninio, *Biochimie* **57**, 587 (1975).
7. R. C. Thompson, P. J. Stone, *Proc. Natl. Acad. Sci. U.S.A.* **74**, 198 (1977).
8. T. Ruusala, M. Ehrenberg, C. G. Kurland, *EMBO J.* **1**, 741 (1982).
9. N. Sugimoto, R. Kierzek, S. M. Freier, D. H. Turner, *Biochemistry* **25**, 5755 (1986).
10. T. Pape, W. Wintermeyer, M. V. Rodnina, *EMBO J.* **18**, 3800 (1999).
11. M. V. Rodnina, W. Wintermeyer, *Annu. Rev. Biochem.* **70**, 415 (2001).
12. D. Fourmy, S. Yoshizawa, J. D. Puglisi, *J. Mol. Biol.* **277**, 333 (1998).
13. J. M. Ogle *et al.*, *Science* **292**, 897 (2001).
14. O. Piepenburg *et al.*, *Biochemistry* **39**, 1734 (2000).
15. M. Valle *et al.*, *EMBO J.* **21**, 3557 (2002).
16. H. Stark *et al.*, *Nat. Struct. Biol.* **9**, 849 (2002).
17. J. M. Ogle, F. V. Murphy, M. J. Tarry, V. Ramakrishnan, *Cell* **111**, 721 (2002).
18. M. Valle *et al.*, *Nat. Struct. Biol.* **10**, 899 (2003).
19. M. Yarus, D. Smith, in *tRNA: Structure, Biosynthesis and Function*, D. Söll, U. RajBhandary, Eds. (American Society for Microbiology, Washington, DC, 1995), pp. 443–468.
20. R. P. Fahlman, T. Dale, O. C. Uhlenbeck, *Mol. Cell* **16**, 799 (2004).

10.1126/science.1113415

INTRODUCTION

Learning from Natural Disasters

The science of volcanology began with Pliny the Younger's observations of the devastating 79 A.D. Vesuvius eruption. The May 1980 Mount St. Helens eruption and its aftermath was the first major eruption observed and monitored systematically with a variety of modern instruments, and it revealed much about eruptive processes, leading in turn to the development of new monitoring instruments. These lessons were applied a decade later in responding to the much larger eruption of Mount Pinatubo in the Philippines. The science of hurricanes has improved from early observations in the same way. Our current ability to make useful estimates of hurricane course and strength derives from satellite and in situ observations. Data gathered from many prior storms, combined with computer modeling developed continually from a huge amount of weather data, have strengthened our prediction capacity. These are but two examples of how past observations, followed by detailed data obtained with modern instruments, have led to improved understanding of natural disasters and how to respond to them.

The Sumatra-Andaman earthquake of 26 December 2004, with its consequent tsunami, was the first great earthquake to be observed with modern instruments. These include a global seismic network equipped with seismographs capable of recording over a broad frequency range (which was partly set up for observing and understanding such earthquakes), satellites that can record changes in ocean height, and a worldwide Global Positioning System (GPS) network capable of recording subtle movements of Earth's crust. Great earthquakes have moment magnitudes of about 9 or greater, release an enormous amount of energy, and are usually caused by the rupture of a convergent plate boundary (where one plate is subducting beneath another). As was the case here, they can produce devastating tsunamis.

CREDIT: AMMON *ET AL.*

Four papers and a Viewpoint in this issue, and one Report published online on *Science* Express, describe the seismic, satellite, and GPS observations of this earthquake and some of its effects. As shown in these papers, such large earthquakes have important differences from smaller earthquakes. One is their huge rupture length, which is many times the width across the rupture. The Sumatra-Andaman earthquake ruptured about 1300 km of the plate boundary. The rupture itself took about 1 hour, moving mostly from south to north, and the GPS data indicate some additional deformation after that. It rang the earth much like a bell (it is still ringing), and it produced measurable deformations in Earth's crust—as recorded in GPS data—over nearly an entire hemisphere. This protracted and uneven release of energy complicates the determination of magnitude. These data, as well as observations of the geometry of the generated tsunami, can be inverted to show that the rupture progressed rapidly at first, producing displacements of up to 20 m, then more slowly farther north. Seismic waves from the Sumatra-Andaman earthquake, like some others, also triggered other earthquakes in distant volcanic areas; this time, however, possibly revealing the mechanism of that triggering. The earthquake also produced numerous aftershocks and was followed by another large temblor. These and other data provide a new basis for understanding these largest, rarest, and most destructive seismic events.

–BROOKS HANSON

CONTENTS

***See also* Science *Express Report by Banerjee* et al.**

Science

VIEWPOINT

A Flying Start, Then a Slow Slip

Roger Bilham

The human tragedy caused by the Sumatra-Andaman earthquake (moment magnitude 9.3) on 26 December 2004 and its companion Nias earthquake (moment magnitude 8.7) on 28 March 2005 is difficult to comprehend. These earthquakes, the largest in 40 years, have also left seismologists searching for the words and tools to describe the enormity of the geological processes involved. Four papers in this issue discuss aspects of a rupture process of surprising complexity, the first such event to test the sensitivity and range of many new technologies. A surprising feature of the earthquake is that after the initial rapid rupture, subsequent slip of the plate interface occurred with decreasing speed toward the north.

The Sumatra-Andaman earthquake on 26 December 2004 was the second largest earthquake in the instrumental record and the third most fatal earthquake ever. It released 4.3×10^{18} J, equivalent to a 100-gigaton bomb, or about as much energy as is used in the United States in 6 months. Shifts in the sea floor displaced more than 30 km^3 of seawater, generating a tsunami that traveled to the Antarctic, the east and west coasts of the Americas, and (with lessening amplitudes) the Arctic Ocean. The reduced volume capacity of the Bay of Bengal and the Andaman Sea, caused by a net uplift during the earthquake, has raised global sea level by about 0.1 mm. No point on Earth remained undisturbed at the centimeter level. As West *et al*. show, displacements in some volcanically active regions were sufficiently large to trigger small local earthquakes (*1*).

Cooperative Institute for Research in Environmental Sciences and Geological Sciences, University of Colorado, Boulder, CO 80309, USA. E-mail: roger.bilham@colorado.edu

Although unprecedented in area and magnitude, the Sumatra-Andaman earthquake and the resulting tsunami have historical analogs. In the last few hours of 1881, 6 years before the development of the world's first recording seismometer, an earthquake of moment magnitude (M_w) 7.9 on the Richter scale toppled chimneys in the Andaman Islands and pounded the hulls of ships coasting by the Nicobar Islands (*2*). Some 20 min after flooding the coast of Car Nicobar, the resulting tsunami ripped the paper chart from the Port Blair tide gauge; 2 hours later, it hit the coast of India. A 1-m wave elicited curiosity on the beach at Madras before curling invisibly around the southern and western coasts of Sri Lanka to be again recorded near the tip of India. Sixty years later, in June 1941, an earthquake of M_w 7.7 near Port Blair generated a smaller tsunami, damaging forests on the west coast of the Andaman Islands but leaving no numerical record of its run-up (*3*).

Yet the violence of these Andaman Island tsunamis was paltry compared to that of those tsunamis generated by earthquakes with $M_w > 8$ in 19th-century Sumatra. Earthquakes in 1833 and 1861 (*4*) are estimated to have generated waves 5 to 10 m high, causing massive damage on land but dissipating their energy southward and westward into a largely empty Indian Ocean. The amount of strain that has accumulated in Indonesia since these earthquakes recently prompted investigators at the California Institute of Technology to distribute posters educating local populations about their hazardous futures (*5*). Re-rupture of the historic rupture zones of 1833 and 1861 could destroy numerous Indo-

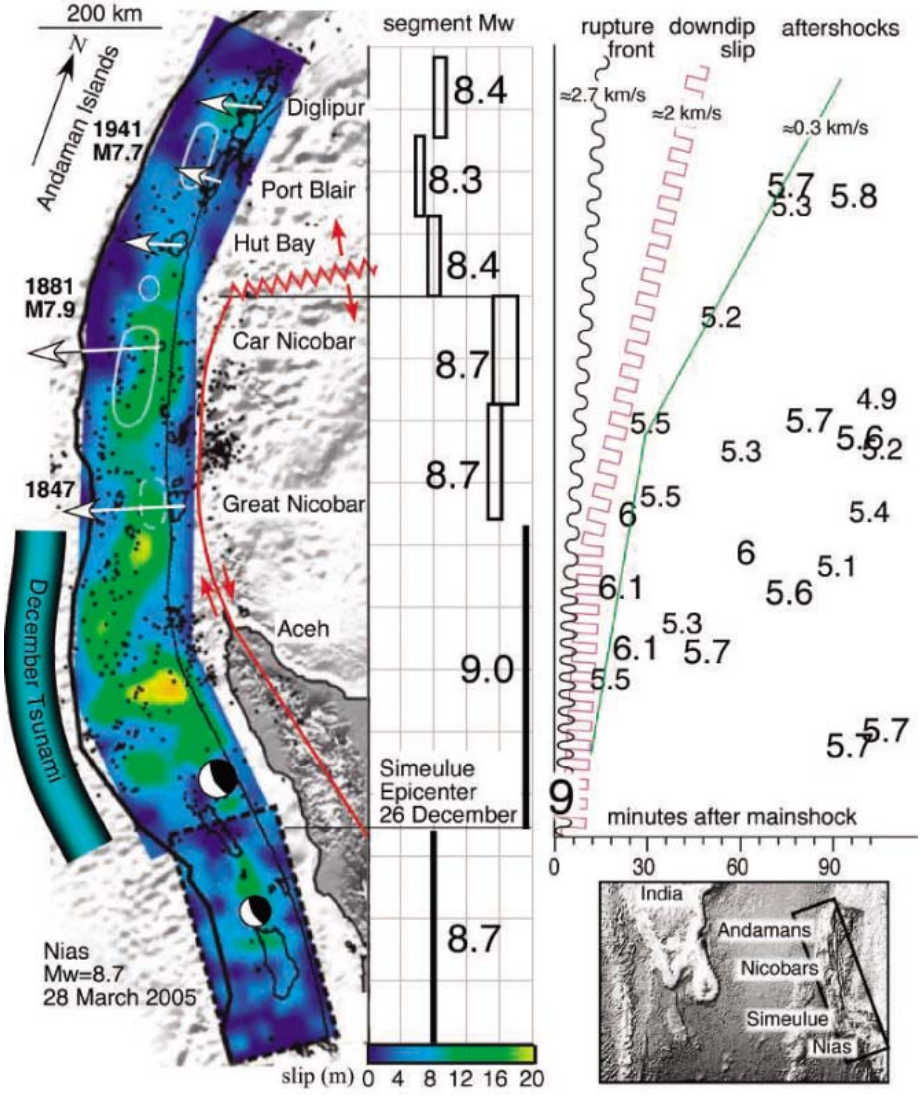

Fig. 1. Rupture zones and slip mechanisms for the Sumatra-Andaman earthquake of 26 December 2004 and the contiguous Nias earthquake of 28 March 2005. The total length of the two ruptures exceeds 1600 km. The outlines of historical earthquakes are shown in white, and the red line indicates the Andaman fault system terminated by the Andaman spreading center (sawtooth portion) (*13*). The damaging tsunami was generated by the southern 650 km of the M_w = 9.3 December quake. Seismic estimates of slip (*7*, *14*) are quite heterogeneous both along strike and down dip (**left**) (*6*), but they agree well with estimates of mean slip [white arrows (left) and black rectangles (**center**)] derived from GPS analysis (*11*, *15*). Representative magnitudes are calculated for various segments assuming uniform slip (center). (Right) The panel illustrates the northward-increasing delay between the fast rupture front (sine wave) (*6*), subsequent downdip slip (square wave), and aftershocks (smooth line) (*3*).

nesian villages and towns, and there is now grave concern that recent stress changes to their north and west will have moved each zone closer to rupture. The Nias earthquake on 28 March 2005 confirms that stress changes from the 26 December earthquake, though small (*6*), were sufficient to push this contiguous 300-km segment of plate boundary to the point of failure. The 3-month delay between the two earthquakes has awakened fears that a domino-like failure of the already highly stressed plate boundary to the south and east may follow.

Nobody familiar with the history or geology of the Sumatra/Andaman arc could have foreseen the magnitude of the 26 December 2004 earthquake, nor is there a precedent for its complexity (Fig. 1). The rupture initiated at 3.3°N near a blunt corner of the arc, where the almost-passive junction between the Indian and Australian plates plunges northeastward beneath the islands. Ammon *et al.* (*7*) report the analysis of *P* waves (the first-arriving and fastest waves that travel outward from an earthquake) digitally recorded by seismometers around the world. Their analysis reveals that during its first minute, the earthquake broke a 100-km patch of the plate boundary rather slowly northward. Had it stopped there, its magnitude would have perhaps reached a high 7, typical of historical events to the north. But instead of slowing, the rupture accelerated to 3 km/s for the next 4 min and thereafter maintained an average speed of about 2.5 km/s for a further 6 min.

The rupture front that marked the fracture of the Nicobar/Andaman plate boundary propagated like a noisy fire engine traveling to the northwest. Seismometers in Russia listening to its approach heard the sound at a higher pitch than did similar seismometers in Australia, which sensed the fracture receding from them [Lay *et al.* (*8*)]. In this sense, seismometers in Australia observed the rupture at longer wavelengths, just like the redshift of a receding galaxy caused by the Doppler effect in light waves. Ammon *et al.* note that the Doppler shift was not uniform in time. They attribute the changes in amplitude and wobbles in the Doppler shift to occasional acceleration and deceleration, or hesitation, of the rupture during its passage northward.

But the most remarkable feature of the earthquake was not the 8050-km/hour, 10-min urgency that characterizes the initial unzipping of the plate boundary; it was its slow subsequent slip. Slip occurred at typical rupture speeds in the south, sufficiently fast to propel the tsunami on its destructive worldwide journey. However, at its northern end, the surface between the Indian plate and the Andaman archipelago took more than half an hour to slide a distance of 7 to 20 m. It was this slow slip that tripled the quake's energy release from *M* 9 to a gigantic *M* 9.3. Slip occurred too slowly in the last 5 min to generate either tsunamis or sizable 20-s surface waves (the amplitudes of which are used to assign a Richter magnitude for an earthquake). After adjusting their computer codes, seismologists quantified this slow slip from the amplitude of waves with 20-min periods and longer, which circumnavigated the globe each hour for several days. Park *et al.* indicate that the longest-period waves were visible for weeks (*9*).

The slowness of this slip excited several of Earth's fundamental resonances. From these relative amplitudes, Park *et al.* surmise that the northern end of the rupture released one-third of the total energy in the earthquake, equivalent to an M_w 8.9 (*9*). This slow slip moved Global Positioning System (GPS) points on the Andaman Islands by more than 4 m toward southern India (*10*), sinking some shores and raising others. Tide gauge data recorded no subsidence for 30 min after seismic shaking, confirming the delayed timing of this slip (*3*, *11*).

It is sobering to realize that if this northern slip had not been slow, it would have generated tsunamigenic waves along the entire 1300-km-long rupture zone, causing more widespread and more severe damage on the coastlines of India, Myanmar, and Thailand. This aside, many seismologists are now wondering whether their past assessments of future seismic hazard elsewhere have been too conservative. Seismic hazards on numerous plate boundaries, such as the nearby Himalaya, have been assessed until now in terms of recent history, without the benefit of an extended record that may contain extreme events (*12*). The 2004 Sumatra-Andaman earthquake is a wake-up call that conservative seismic forecasts may not serve society well.

References and Notes

1. M. West, J. J. Sánchez, S. R. McNutt, *Science* **308**, 1144 (2005).
2. M. Ortiz, R. Bilham, *J. Geophys. Res.* **108**, 1029/2002JB001941 (2003).
3. R. Bilham, E. R. Engdahl, N. Feldl, S. P. Satyabala, *Seism. Res. Lett.*, in press.
4. P. Cummins, M. Leonard, *AusGeo News* No. 77 (March 2005).
5. These posters were distributed in field seasons before the 2004 earthquake (see www.tectonics.caltech.edu/sumatra/downloads/20040604SumatraPoster.ppt).
6. J. McCloskey, S. Nalbant, S. Steacy, K. Sieh, *Nature*, in press.
7. C. J. Ammon *et al.*, *Science* **308**, 1133 (2005).
8. T. Lay *et al.*, *Science* **308**, 1127 (2005).
9. J. Park *et al.*, *Science* **308**, 1139 (2005).
10. S. Jade, V. K. Gaur, M. B. Ananda, P. D. Kumar, S. Banerjee, *Current Sci.*, in press.
11. C. P. Rajendran, A. Earnest, K. Rajendran, R. Bilham, J. Freymueller, in preparation.
12. R. Bilham, K. Wallace, *Geol. Surv. India Spec. Pub.* **85**, 1 (2005).
13. J. Curry, *J. Asian Earth Sci.* **25**, 187 (2005).
14. M. Ishii, P. M. Shearer, H. Houston, J. E. Vidale, *Nature*, in press.
15. P. Banerjee, F. F. Pollitz, R. Bürgmann, *Science* 19 May 2005 (10.1126/science.1113746).

10.1126/science.1113363

RESEARCH ARTICLE

The Great Sumatra-Andaman Earthquake of 26 December 2004

Thorne Lay,[1,2]* Hiroo Kanamori,[3] Charles J. Ammon,[4] Meredith Nettles,[5] Steven N. Ward,[2] Richard C. Aster,[6] Susan L. Beck,[7] Susan L. Bilek,[6] Michael R. Brudzinski,[8,9] Rhett Butler,[10] Heather R. DeShon,[8] Göran Ekström,[5] Kenji Satake,[11] Stuart Sipkin[12]

The two largest earthquakes of the past 40 years ruptured a 1600-kilometer-long portion of the fault boundary between the Indo-Australian and southeastern Eurasian plates on 26 December 2004 [seismic moment magnitude (M_w) = 9.1 to 9.3] and 28 March 2005 (M_w = 8.6). The first event generated a tsunami that caused more than 283,000 deaths. Fault slip of up to 15 meters occurred near Banda Aceh, Sumatra, but to the north, along the Nicobar and Andaman Islands, rapid slip was much smaller. Tsunami and geodetic observations indicate that additional slow slip occurred in the north over a time scale of 50 minutes or longer.

The 26 December 2004 Sumatra-Andaman earthquake was the largest seismic event on Earth in more than 40 years, and it produced the most devastating tsunami in recorded history (*1*). Like other comparably sized great earthquakes—such as the 1952 Kamchatka, the 1957 Andreanof Islands in the Aleutians, the 1960 Southern Chile, and the 1964 Prince William Sound, Alaska, earthquakes—the Sumatra-Andaman event ruptured a subduction zone megathrust plate boundary. These giant earthquakes occur where large oceanic plates underthrust continental margins. They involve huge fault areas, typically 200 km wide by 1000 km long, and large fault slips of 10 m or more. Such events dwarf the contributions to plate motion of vast numbers of lower magnitude earthquakes. The high tsunami-

associated death toll appears to have been due to the dense population of the affected region. The tsunami magnitude, M_t, of the earthquake was 9.1 (*2*), as compared to M_t = 9.1 for the 1964 Alaska and M_t = 9.4 for the 1960 Chile earthquakes (*3*). The event ruptured 1200 to 1300 km of a curved plate boundary, with variations in direction of interplate motion and age of subducting lithosphere apparently affecting the nature of the faulting. The 28 March 2005 event ruptured an adjacent 300-km-long portion of the plate boundary (*4*). These two events are the largest to occur after the global deployment of digital broadband, high-dynamic-range seismometers (*5*, *6*), which recorded both the huge ground motions from the mainshocks and the tiny motions from ensuing free oscillations of the planet and from small aftershocks (*7*, *8*). In this and two companion papers (*9*, *10*), we report on the nature of faulting in these great earthquakes based on seismological analyses of the extensive, openly available seismogram data set from the international Federation of Digital Seismic Networks (FDSN) backbone network (*5*, *6*).

Plate geometry and setting. The 2004 and 2005 earthquakes ruptured the boundary between the Indo-Australian plate, which moves generally northward at 40 to 50 mm/year, and the southeastern portion of the Eurasian plate, which is segmented into the Burma and Sunda subplates (Fig. 1). East of the Himalayas, the plate boundary trends southward through Myanmar, continuing offshore as a subduction zone along the Andaman and Nicobar Islands south to Sumatra, where it turns eastward along the Java trench (*11*). As a result of the highly oblique motion between the Indo-Australian plate and the Burma and Sunda subplates (Fig. 1), a plate sliver, referred to as the Andaman or Burma microplate, has sheared off parallel to the subduction zone from Myanmar to Sumatra (*12*). Oblique, but predominantly thrust, motion occurs in the Andaman trench with a convergence rate of about 14 mm/year (*13*, *14*). The Andaman Sea ridge-transform system, an oblique back-arc spreading center, accommodates the remaining plate motion, joining with the Sumatra Fault to the south (*15*, *16*). Underthrusting along the Sunda trench, with some right-lateral faulting on the inland Sumatra Fault, accommodates interplate motion along Sumatra.

Historic great earthquakes along this plate boundary occurred in 1797 [magnitude (M) ~ 8.4], 1833 (M ~ 9), and 1861 (M ~ 8.5) (*17*, *18*), providing the basis for the long-recognized potential for great earthquakes along Sumatra (*11*, *19*). A smaller (M ~ 7.8) event in 1907 just south of the 2004 rupture zone produced seismic and tsunami damage in northern Sumatra (*11*). These events all occurred to the southeast of the 2004 rupture zone (Fig. 1). The 28 March 2005 event ruptured the same region as the 1861 and 1907 events (Fig. 1). Smaller events in the Andaman trench, also presumed to involve thrusting motions, occurred beneath the Nicobar Islands in 1881 (M ~ 7.9) and near the Andaman Islands in 1941 (M ~ 7.9). There is no historical record of a previous tsunamigenic earthquake in the Bay of Bengal comparable to the 2004 event (*12*).

In the 40 years preceding the 2004 event, little seismicity occurred within 100 km of the trench in the region between the 2004 and 1881 epicenters (figs. S1 to S3). Similarly, seismicity was low in the source region of the great 1861 earthquake before the 28 March 2005 event and is still low in the 1833 rupture region (fig. S2). Numerous earthquakes occurred near the 2004 epicenter in recent years, including a seismic-moment magnitude (M_w) = 7.2 event in 2002. These features are consistent with long-term strain accumulation in the eventual rupture zone and stress concentration in the vicinity of the mainshock hypocenter.

The mainshocks. The 2004 mainshock rupture began at 3.3°N, 96.0°E, at a depth of about 30 km, at 00:58:53 GMT (*1*). The Harvard centroid-moment-tensor (CMT) solution indicates predominantly thrust faulting on a shallowly (8°) dipping plane with a strike of 329° (*20*, *21*). The rake (110°) indicates a slip direction ~20° closer to the trench-normal direction than to the interplate convergence direction, consistent with some long-term par-

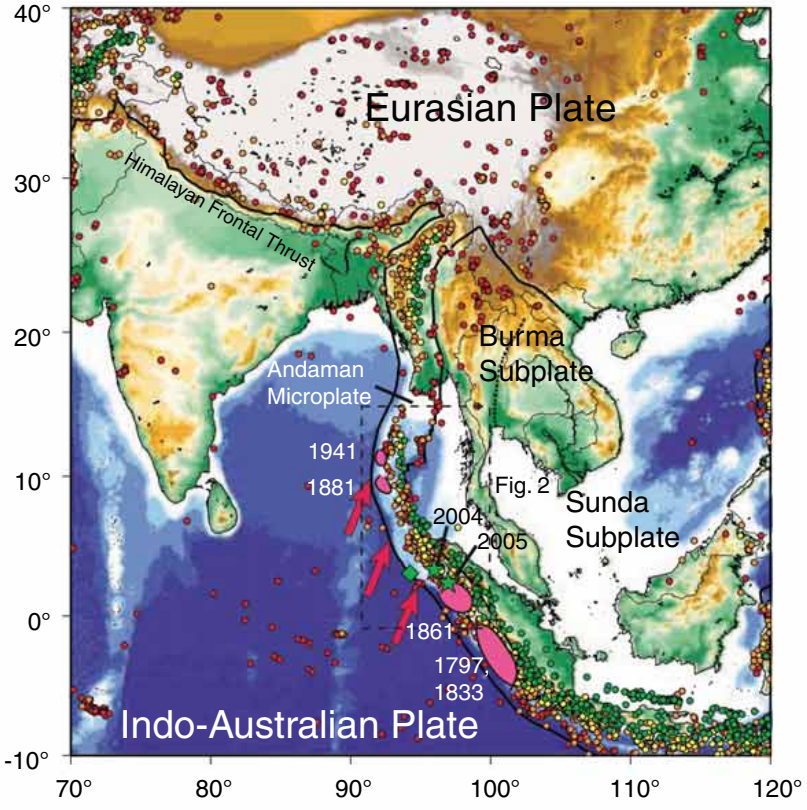

Fig. 1. Regional map showing earthquakes with magnitudes >5.0 from 1965 to 25 December 2004 from the earthquake catalog of the National Earthquake Information Center (NEIC). Red dots show events with depths <33 km; orange, depths of 33 to 70 km; yellow, depths of 70 to 105 km; and green, depths >105 km. Locations of previous large earthquake ruptures along the Sunda-Andaman trench system are shown in pink. Dashed box shows area of the map in Fig. 2. Green stars show the epicenters of the two recent great events; the green diamond shows the CMT centroid location for the 2004 Sumatra-Andaman event. The thick red arrows indicate the NUVEL-1 relative plate motions between the Indo-Australian and Eurasian plates.

[1]Earth Sciences Department and [2]Institute of Geophysics and Planetary Physics, University of California, Santa Cruz, CA 95064, USA. [3]Seismological Laboratory, California Institute of Technology, MS 252-21, Pasadena, CA 91125, USA. [4]Department of Geosciences, The Pennsylvania State University, 440 Deike Building, University Park, PA 16802, USA. [5]Department of Earth and Planetary Sciences, Harvard University, 20 Oxford Street, Cambridge, MA 02138, USA. [6]Department of Earth and Environmental Science and Geophysical Research Center, New Mexico Institute of Mining and Technology, Socorro, NM 87801, USA. [7]Department of Geosciences, The University of Arizona, Gould-Simpson Building #77, Tucson, AZ 85721, USA. [8]Department of Geology and Geophysics, University of Wisconsin–Madison, 1215 West Dayton St., Madison, WI 53706, USA. [9]Geology Department, Miami University, Oxford, OH 45056, USA. [10]IRIS Consortium, 1200 New York Avenue, NW, Washington, DC, 20005, USA. [11]Geological Survey of Japan, Advanced Industrial Sciences and Technology, Site C7 1-1-1 Higashi, Tsukuba 305-8567, Japan. [12]National Earthquake Information Center, U.S. Geological Survey, Golden, CO 80401, USA.

*To whom correspondence should be addressed. E-mail: thorne@pmc.ucsc.edu

titioning of right-lateral motion onto the Sumatra Fault, which is not reported to have ruptured during the 2004 event. The aftershock distribution (Fig. 2) gives a first-order indication of the extent of the mainshock ruptures. For the 2004 event, the distribution suggests a rupture length of 1300 km extending from northwestern Sumatra to the Andaman Islands. Along the northern extension of the aftershock zone, the strike of the fault rotates progressively clockwise (Fig. 2). The associated degree of right-lateral slip (rake >90°) on the megathrust fault should increase to the north unless that component of interplate motion is partitioned onto the back-arc transform system. Given the variation in the relative plate motion along the aftershock zone, it is surprising that the CMT solution is a nearly pure double-couple source, indicative of simple faulting geometry. The faulting solution favors a concentration of <500 s period seismic radiation in the southern portion of the aftershock zone, as does the location of the centroid, which lies about 160 km west of the epicenter (Fig. 2).

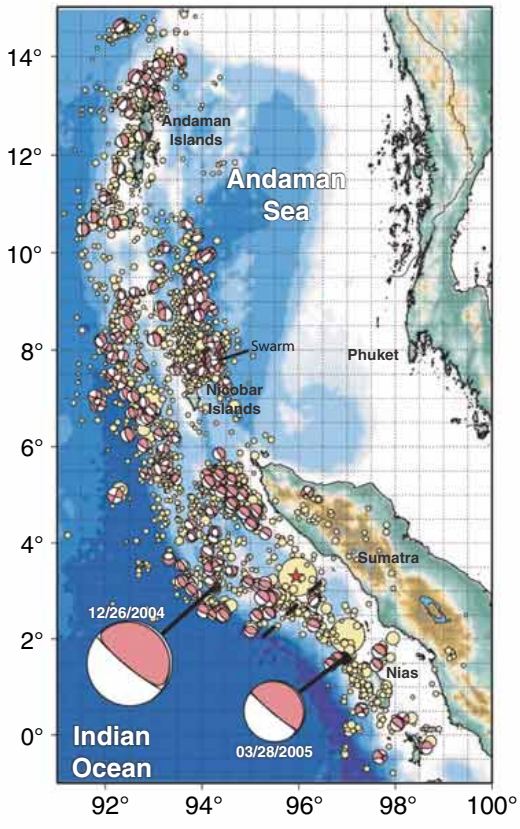

Fig. 2. Map showing aftershock locations for the first 13 weeks after the 26 December 2004 earthquake from the NEIC (yellow dots, with radii proportional to seismic magnitude). Moment-tensor solutions from the Harvard CMT catalog (*21*) are shown for the 26 December 2004 and 28 March 2005 mainshocks (large solutions at bottom, with associated centroid locations) and aftershocks. Star indicates the epicenter for the 2004 rupture obtained by the NEIC. Dashed line shows the boundary between the aftershock zones for the two events.

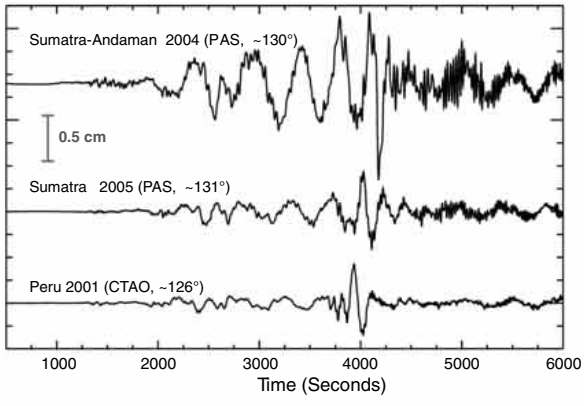

Fig. 3. Vertical-component ground displacements for periods <1000 s observed for the three largest earthquakes of the past 40 years. The upper trace shows the seismogram from the 26 December 2004 Sumatra-Andaman earthquake observed 130° away in Pasadena, California, USA; the middle trace is for the 28 March 2005 Sumatra earthquake observed 131° away in Pasadena, California, USA; the lower trace shows a seismogram for the 23 June 2001 M_w 8.4 earthquake off the coast of Peru, observed 126° away in Charters Towers, Australia. Additional waveforms are shown in fig. S4.

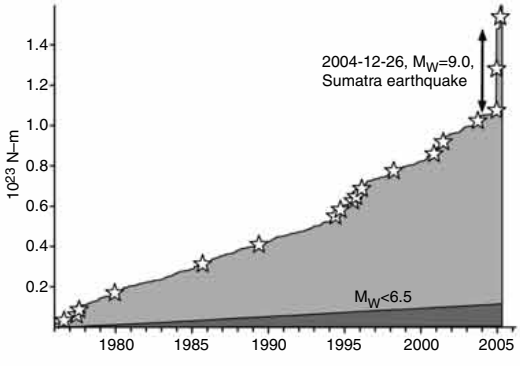

Fig. 4. Plot of cumulative seismic moment as a function of time for the 29-year history of the Harvard CMT catalog, which contains results for global earthquakes of magnitude larger than ~5.0, with great ($M_w \geq 8$) earthquakes indicated by stars. The 300- to 500-s period seismic moment for the 2004 event is comparable to the cumulative global earthquake seismic moment release for the preceding decade.

Peak-to-peak ground motions for the 2004 event exceeded 9 cm in Sri Lanka, 15.5° from the epicenter, and long-period surface-wave motions exceeded 1 cm everywhere on Earth's surface (*7*) (fig. S4). This giant event produced motions (Fig. 3) that dwarf those of the 2005 event and the 23 June 2001 Peru earthquake (M_w = 8.4), the largest earthquake previously recorded by global broadband seismometers (*22*). The high-quality global recordings enable seismological quantification of these great earthquakes (*23*).

Aftershock geometry. Harvard CMT focal mechanisms for aftershocks (Fig. 2) display a variety of geometries, including thrust faulting along the subduction zone and strike slip and normal faulting in the Andaman Sea back arc. These mechanisms are generally consistent with the expected slip partitioning along the boundary, with nearly arc-normal thrusting in the shallowly dipping subduction zone and right-lateral shearing in the back arc.

The most notable aftershock feature is a swarm of strike-slip and normal faulting events in the Andaman Sea back-arc basin (Fig. 2) involving more than 150 magnitude 5 and greater earthquakes that occurred from 27 to 30 January 2005 (*20*, *21*). Previous swarms of events have occurred in this region (e.g., July 1984), but this is the most energetic earthquake swarm ever observed globally. This swarm activity can be seen as part of the overall interplate motion partitioning.

Although aftershock mechanism variability and location uncertainty make it difficult to constrain the fault geometry in detail using

seismicity, the megathrust appears to be about 240 km wide along northwestern Sumatra, extending to a depth of about 45 km. Along the Nicobar and Andaman Islands, the megathrust fault plane appears to be no more than 160 to 170 km wide, extending to a depth of about 30 km.

Magnitude, source strength, and energy. The Harvard CMT solution for the 2004 earthquake, based on global FDSN recordings of 300- to 500-s period surface waves, has a seismic moment $M_o = 4.0 \times 10^{22}$ Nm (*24*), comparable to the cumulative seismic moment of all earthquakes for the preceding decade (Fig. 4). This moment yields $M_w = 9.0$, the widely quoted seismic magnitude for the mainshock. Uniform slip of about 5.0 m over a 1300-km-long fault varying in width from 240 to 160 km with rigidity $\mu = 3.0 \times 10^{10}$ N/m^2 would account for the CMT seismic-moment estimate. Larger slip on a smaller fault area in the south would also match the seismic moment. The CMT seismic moment for the 2005 mainshock is $M_o = 1.1 \times 10^{22}$ Nm ($M_w = 8.6$).

M_w is intended to characterize the earthquake process in terms of its final, static offset but is usually based on measurements of long-period seismic waves. For very large earthquakes, these measurements are typically made at periods of 100 to 300 s, the range of commonly observed seismic surface waves like those in Fig. 3. Magnitudes of the 1960 Chile ($M_w = 9.5$), the 1964 Alaska ($M_w = 9.2$), and the 2004 Sumatra-Andaman ($M_w = 9.0$) earthquakes were all estimated from measurements around 300 s (*25*–*27*). In this sense, their magnitudes can be directly compared. The 100- to 300-s period surface-wave amplitudes for the 1964 Alaska earthquake were about three times as large as those for the 2004 Sumatra-Andaman earthquake.

When an estimate of the seismic moment is made at periods too short to represent fully the earthquake source process, the result is an underestimate of the earthquake size. Given the high-quality seismic data available for the 2004 earthquake, the effective source strength (*28*) can be determined over a broad range of frequencies with relatively good confidence (Fig. 5). For an assumption of uniform faulting geometry, the strength of the seismic-wave excitation for periods >500 s was enhanced by a factor of 1.5 to 2.5 compared with that at 300 s (*9*, *10*). The moment magnitude of the Sumatra-Andaman earthquake may thus be larger than 9.0 by 0.1 to 0.3 units (*29*). The data for the Chile and Alaska earthquakes are insufficient to determine the magnitude at very long periods. Even at 300 s, considerable uncertainty is involved in the values of M_w for old events because of data limitations. As a result, comparison of M_w for these events to one or two tenths of a magnitude unit is not meaningful. These three earthquakes should instead be compared with respect to all aspects of their source characteristics (e.g., source spectrum, radiated energy, slip distribution, and rupture speed).

Short-period radiation is particularly important for ground accelerations and intensity of structural damage. Estimates of seismic intensity, based on relative measures of structural damage and vibration, indicate intensity IX in the vicinity of Banda Aceh, intensity VII in Port Blair in the Andaman Islands, and a relatively low intensity II to IV around the Bay of Bengal (*12*, *30*). The overprinting devastation from the tsunami complicates the estimation of high-frequency effects, but intensity IX is consistent with the short-period magnitudes $m_b = 7.0$ estimated by the USGS and $\dot{m}_b = 7.2$ reported here, the latter being about 0.3 magnitude units lower than for the 1964 Alaska earthquake (*31*, *32*) (fig. S5). These values imply that the 2004 event was not depleted in high-frequency radiation, unlike the notable 1992 Nicaragua tsunami earthquake (*33*).

The energy radiated by seismic waves, E_R, is an important macroscopic seismic parameter, because the amount of potential energy partitioned to E_R reflects the physical process of the source (*34*). Unfortunately, accurate estimation of E_R, especially for great earthquakes with long source durations, is difficult. An estimate of $E_R = 1.1 \times 10^{18}$ J is obtained for the 2004 event from *P* waves at 11 stations over a distance range of 45° to 95° (*35*–*37*). Energy estimates for earlier giant earthquakes are based only on magnitude-energy relationships, so meaningful comparisons are difficult. The radiated energy estimated here is about 10 times that of the

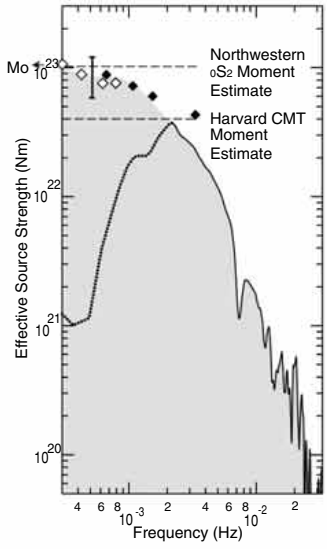

Fig. 5. Rayleigh-wave source-time function (STF) amplitude spectrum (solid and dotted line) computed by stacking more than 200 R_1 observations obtained by deconvolution of propagation effects in the frequency domain. We used a signal duration ranging from 750 to 2000 s (depending on source-receiver distance) zero-padded to 6000 s to estimate each spectrum. The dotted portion of the spectrum indicates frequencies for which the R_1 spectral amplitudes are not well resolved. White diamonds show estimates of moment from free oscillations ($_0S_2$, $_0S_3$, $_0S_4$, and $_0S_0$, from left to right) made by Northwestern University. Black diamonds show spectral levels estimated by comparison of filtered time-domain signals with synthetics for the Harvard CMT solution. Effective source strengths from the Harvard CMT solution (300 to 500 s) and that estimated from $_0S_2$, assuming the Harvard CMT faulting geometry, are indicated with dashed lines. The lowest frequency level, extrapolated to zero frequency, corresponds to the seismic moment, M_o. The approximate uncertainty for all of the low-frequency estimates is about a factor of 2. The bar indicates a corresponding range of uncertainty. The shaded region represents the composite source spectrum.

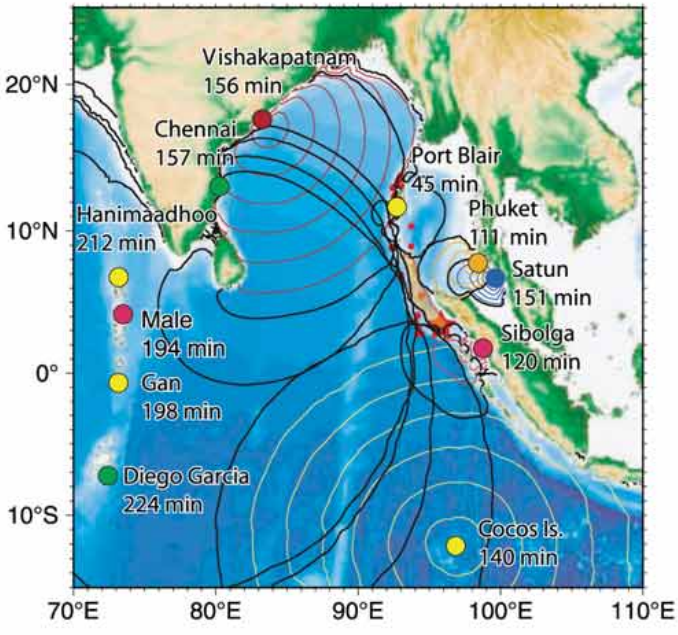

Fig. 6. Constraints on the tsunami source area obtained from the timing of tsunami arrivals at various locations around the Indian Ocean. Dark lines indicate the distance from the observing points from which tsunami might have generated at the event origin time. The tsunami source area outlined by these curves (brown region) appears to extend only 600 to 800 km north-northwest from the epicenter.

1994 deep Bolivia earthquake (M_w = 8.3) and about 40 times that of the 2001 Peru earthquake (M_w = 8.4) (Fig. 3).

Slip process of the 2004 event. The 2004 Sumatra-Andaman earthquake had the longest known earthquake rupture. Short-period seismic body waves (0.5 to 0.25 s) show azimuthally varying durations that indicate that the seismic rupture front propagated to about 1200 km north of the epicenter with a rupture velocity of about 2.0 to 3.0 km/s and that short-period radiation was generated for at least 500 s (*38*). Array analysis of 1- to 2-s period seismic waves from Hi-net stations in Japan yields compatible results (*39*). Analysis of longer period body waves and surface waves demonstrates that most of the slip that generated seismic waves was concentrated in the southern half of the rupture zone, with diminishing, increasingly oblique slip toward the north on the fault (*9*). The seismic moment of models that successfully match the long-period body- and surface-wave data is about 1.5 times as large as the CMT moment, consistent with free oscillation observations (*10*).

The seismic model does not, however, account for all observations. Geodetic constraints require two to three times more slip in the north (*40*). This suggests rupture of the northern region with a long source-process time that generated little or no seismic waves. Well-documented tilting in the Andaman and Nicobar Islands (*12*), with the western margins of the islands being uplifted and the eastern margins being submerged, can be accounted for by substantial slip of about 10 m on a 160-km-wide thrust plane in the northern half of the rupture zone or by less slip on more steeply dipping splay faults. Such large slip must have occurred on time scales longer than 1000 s, because it did not generate strong seismic-wave radiation late in the rupture.

Arrival times of tsunami waves around the Sea of Bengal provide additional constraints on the slip distribution in the north. Bounds can be placed on the location of ocean-bottom uplift due to faulting by back-propagating the initial tsunami wavefront from tsunami recording locations to the source region. The source region for strong initial tsunami excitation extends 600 to 800 km north of the epicenter, terminating near the Nicobar Islands (*41*) (Fig. 6 and fig. S6). The northern third of the aftershock zone appears not to have produced rapid vertical ocean-bottom displacements capable of generating large tsunami waves (fig. S7), but delayed slip cannot be ruled out. This estimate of the tsunami source region is consistent with satellite altimetry observations of the deep-water waves obtained by fortuitous passage of two satellites over the Indian Ocean 2 to 3 hours after the rupture occurred (*42*) (Fig. 7).

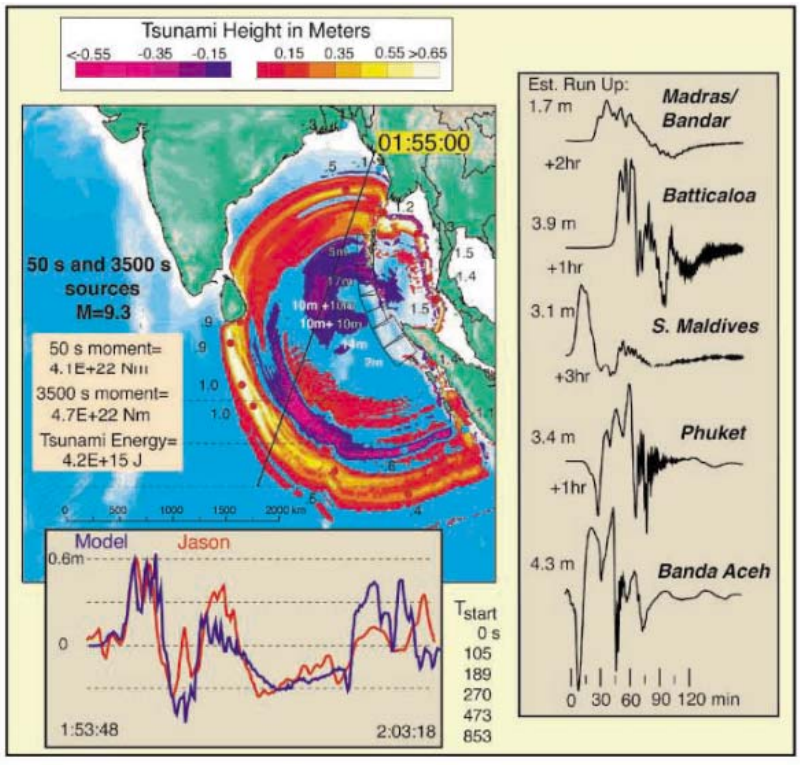

Fig. 7. (**Left**) Tsunami model at a time of 1 hour 55 min after earthquake initiation, computed for a composite slip model with fast slip (50-s rise time) in the southern portion of the rupture and slow slip (3500-s rise time) in the north. The northward propagating rupture velocity is about 2 km/s for the first 745 km, then slows to 750 m/s. The amplitude of fast and slow slip on the six fault segments are indicated by white numbers and outlined numbers, respectively. The overall seismic moment of 8.8 × 10^{22} Nm (μ = 3.0 × 10^{10} N/m^2) is divided fairly evenly between slow and fast contributions. Red colors in the map indicate positive ocean wave height, blue colors negative. The numbers along the wavefront give wave amplitudes in meters. Diagonal line is the track of the Jason satellite that passed over the region at about this time (10 min of actual transit time along the profile). The predicted (blue) and observed (red) tsunami wave are shown in the inset. The tsunami generated by the fast component of slip alone cannot explain the trough in the central Bay of Bengal (fig. S8 and Movie S1). (**Right**) Tsunami waveforms and estimated run-up heights for five locations around the Bay of Bengal. The first arrivals show water draw-down toward the east and inundation toward the west. Principal wave period is about 30 min.

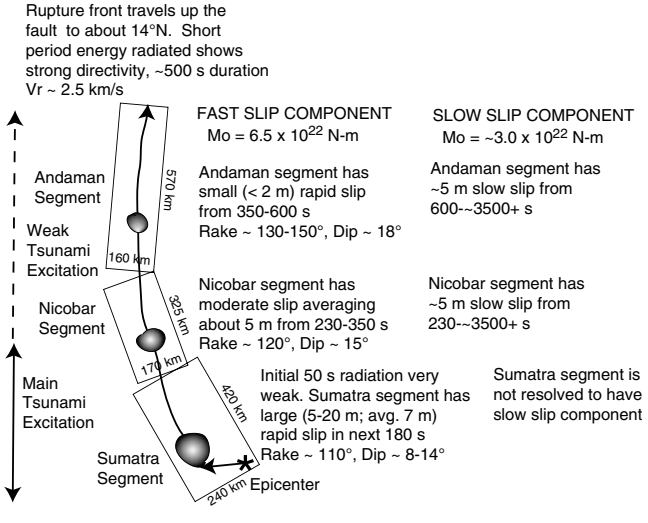

Fig. 8. Summary rupture scenario for the 2004 Sumatra-Andaman earthquake. We subdivide the rupture zone into three segments according to the inferred rupture process, not because of clear physical fault segmentation. The rupture begins at the southeastern edge of the Sumatra segment, with the initial 50 s of rupture characterized by fairly low energy release and slow rupture velocity. The rupture front then expands to the north-northwest at about 2.5 km/s, extending about 1300 km. Short-period radiation tracks the rupture front, with a total duration of about 500 s and clear north-northwest directivity. Large, rapid slip occurs in the Sumatra segment, with some patches having slip as great as 20 m during the first 230 s. The Nicobar segment has weaker slip during the next 2 min, and the Andaman segment fails with little (<2 m) rapid slip. Slow slip appears to continue in the Nicobar and Andaman segments, with a total duration of about 1 hour. The precise amount of slip and total moment of the slow-slip component are not well resolved, but about 10 m of slip under the Andaman Islands is required to account for the tilt experienced by the islands.

The tsunami calculation shown in Fig. 7, which provides a generally satisfactory fit to the satellite observations, uses a finite-fault model with the same geometry as that providing a good fit to the seismic data but with somewhat different slips, rise times, and start times on each segment (Movie S1). A broad trough in the ocean surface in the central Sea of Bengal 2 hours after the earthquake can be modeled well if slow slip occurred over ~1 hour under the Nicobar and Andaman Islands (fig. S8 shows the prediction for a model with no slow slip). This is currently the strongest constraint on the source-process time for the slow-slip component of the 2004 event. The tsunami energy computed for this composite model is 4.2×10^{15} J, less than 0.5% of the strain energy released by the faulting. Tsunami generation is not a very efficient process, but tremendous destruction can clearly result from this small component of the energy budget. No slow slip has yet been resolved for the 28 March 2005 event (*9*) (Movie S2).

Discussion. The 2004 Sumatra-Andaman earthquake rupture appears to have been a compound process of seismic-energy release, involving variable slip amplitude, rupture velocities, and slip duration. About 90 to 95% of the seismic observations can be accounted for with the rupture model (*9*, *10*) depicted schematically in Fig. 8.

The northern portion of the fault appears to have slipped 3 to 7 m more than accounted for by the seismic model, with a time scale of ~1 hour or longer. The cause of the compound slip behavior is not well-understood. It appears that the slow slip occurred only along the Nicobar and Andaman Islands segments of the rupture zone, where the plate convergence is increasingly oblique and slip is strongly partitioned. For the low convergence rate of 14 mm/year in the region, it would take 700 years to accumulate 10 m of slip potential in the region, which is consistent with the lack of historical great events in the northern part of the subduction zone.

The age of the subducting oceanic plate increases from about 60 million to 90 million years between Sumatra and the Andaman Islands, and this change may also influence mechanical coupling on the thrust plane. Subduction of younger lithosphere tends to result in interplate faults with shallow dips and broad contact areas that generate great earthquakes, whereas in locations where older lithosphere is subducted and back-arc spreading is observed, great earthquakes are rare (*43*–*45*). The strong lateral gradient in obliquity of interplate motion and the rapid increase in age of the subducting oceanic plate toward the north-northwest are distinctive features compared with the settings of previous great earthquakes. The most analogous tectonic environment may be the western Aleutians, where the 1965 (M_w = 8.7) Rat Island earthquake occurred along a curving plate boundary with increasing obliquity of interplate motion along the arc (*46*).

Logical regions for concern about future large earthquakes are along the Sumatra Fault and southeast of the 2005 event rupture; the adjacent region failed in 1833 and is likely to have accumulated substantial strain. International efforts to improve tsunami-warning capabilities in the Indian Ocean are warranted given the inevitability of future great thrust earthquakes along the Sumatra subduction zone.

References and Notes

1. The February 23, 2005 update on the U.S. Geological Survey (USGS) Web site http://earthquake.usgs.gov/eqinthenews/2004/usslav indicates 283,100 confirmed fatalities, 14,100 missing, and 1,126,900 displaced. The majority of the fatalities were in Indonesia (235,800), with 30,900 fatalities in Sri Lanka.
2. K. Abe, personal communication, 2005.
3. K. Abe, *J. Geophys. Res.* **84**, 1561 (1979).
4. http://earthquake.usgs.gov/eqinthenews/2005/usweax indicates more than 1300 fatalities on Nias, Simeulue, Kepulauen Banyak, and Meulaboh.
5. R. Butler *et al.*, *EOS Trans. Am. Geophys. Union* **85**, 225 (2004); http://www.iris.edu.
6. B. A. Romanowicz, D. Giardini, *Science* **293**, 2000 (2001).
7. J. Park *et al.*, *EOS Trans. Am. Geophys. Union* **86**, 57 (2005).
8. J. Park *et al.*, *Seismol. Res. Lett.*, in press (2005).
9. C. J. Ammon *et al.*, *Science* **308**, 1133 (2005).
10. J. Park *et al.*, *Science* **308**, 1139 (2005).
11. K. R. Newcomb, W. R. McCann, *J. Geophys. Res.* **92**, 421 (1987).
12. R. Bilham, E. R. Engdahl, N. Feldl, S. P. Satyabala Seism., *Seismol. Res. Lett.*, in press (2005).
13. Y. Bock *et al.*, *J. Geophys. Res.* **108**, 2367 (2003).
14. J. Paul *et al.*, *Geophys. Res. Lett.* **28**, 657 (2001).
15. R. McCaffrey, *J. Geophys. Res.* **97**, 8905 (1992).
16. K. Sieh, D. Natawidjaja, *J. Geophys. Res.* **105**, 28295 (2000).
17. J. Zachariasen *et al.*, *J. Geophys. Res.* **104**, 895 (1999).
18. D. H. Natawidjaja *et al.*, *J. Geophys. Res.* **109**, B04306, doi:10.1029/2003JB002398 (2004).
19. W. R. McCann, S. P. Nishenko, L. R. Sykes, J. Krause, *Pure Appl. Geophys.* **117**, 1082 (1979).
20. G. Ekström, A. M. Dziewonski, N. N. Maternovskaya, M. Nettles, *Phys. Earth Planet Inter.* **148**, 327 (2005).
21. Harvard CMT solutions can be accessed at http://www.seismology.harvard.edu/CMTsearch.html.
22. M. K. Giovanni, S. L. Beck, L. Wagner, *Geophys. Res. Lett.* **29**, 2018, doi:10.1029/2002GL015774 (2002).
23. Many stations of the Global Seismographic Network operated by the Incorporated Research Institutions for Seismology, the University of California, San Diego, and the USGS are connected by real-time telemetry to operational efforts of the USGS National Earthquake Information Center and the National Oceanic and Atmospheric Administration Pacific Tsunami Warning Center. These centers provide rapid earthquake location, seismic-magnitude, and tsunami-potential determinations (*8*).
24. Seismic moment is a measure of overall earthquake size, equal to the product of the rigidity of the material around the rupture zone, μ, the total fault area, A, and the average displacement across the fault, D ($M_o = \mu AD$).
25. For the Alaska and Chile events, the amplitude measurements are made at 300 s, but the zero-frequency seismic-moment value is estimated using a finite-source model.
26. H. Kanamori, *J. Geophys. Res.* **75**, 5029 (1970).
27. H. Kanamori, J. J. Cipar, *Phys. Earth Planet. Inter.* **9**, 128 (1974).
28. The amplitude spectrum in Fig. 5 is constructed as follows. The CMT solution has a specific moment-rate spectrum, $M_0^{CMT}(f)$, as a function of frequency, used to predict the displacement spectrum, $S_0^{CMT}(f)$, at a particular position. Let the observed spectrum at that position determined from normal modes or long-period surface waves be $S_0^{obs}(f)$. We define the relative moment-rate spectrum, $M_0^{obs}(f)$, by $M_0^{obs}(f) = \left(\frac{S_0^{obs}(f)}{S_0^{CMT}(f)}\right) M_0^{CMT}(f)$, yielding the effective source strength shown in Fig. 5. $M_0^{obs}(f)$ depends on $S_0^{CMT}(f)$, which in turn depends on the CMT source mechanism and depth and the modeling assumptions in the CMT solution.
29. If the dip angle increases toward the north, the moment determined here will be overestimated. A change in dip from 8° to 12° would reduce the estimated moment by 50%, and if the dip were 15° or more in the subduction zone along the Andaman Islands, the effect could be even larger. The increase in low-frequency source strength seen in Fig. 5 could thus be an artifact of using too shallow a dip for the northern portion of the rupture.
30. See http://pasadena.wr.usgs.gov/shake/ous/STORE/Xslav_04/ciim_display.html.
31. The standard seismic body-wave magnitude, m_b, involves the peak ground motion near a period of 1 s in the first few cycles of the *P* wave. For great earthquakes, the short-period energy usually continues to grow for some time, and a modified magnitude, $\hat{m}_b$, was introduced (*32*) to use the maximum ground motion of the short-period *P*-wave arrival. For events larger than $M_w = 6.5$, an empirical relation of $\hat{m}_b = 0.53\, M_w + 2.70$ has been observed. Comparisons of $\hat{m}_b$ with seismic moment are shown for many large earthquakes, including the Sumatra-Andaman event, in fig. S5.
32. H. Houston, H. Kanamori, *Bull. Seismol. Soc. Am.* **76**, 19 (1986).
33. H. Kanamori, M. Kikuchi, *Nature* **361**, 714 (1993).
34. H. Kanamori, *Proc. Jpn. Acad. Ser. B* **80**, 297 (2004).
35. E_R is estimated by the method of (*36*), using *P*-wave trains with a duration of 400 s. The contribution from later phases like *PP* and *PPP* is empirically estimated using the records of the 26 January 2001 India earthquake. For that event, the source duration is known to be shorter than 50 s. Thus, the ratio of E_R (1.4) estimated from the 400-s and 50-s records of the India earthquake represents the contribution of the later phases, and this ratio can be used to correct for the contribution of the later phases for the Sumatra-Andaman earthquake. The value of E_R, thus estimated, is 10 times as large as that listed by the USGS (*1*) (http://neic.usgs.gov/neis/eq_depot/2004/eq_041226/neic_slav_e.html). This difference is probably due to the difference in the durations of the records used for estimation. An estimate of E_R for the event can also be made based on the CMT seismic moment and conventional assumptions about the stress drop and the stress-release mechanism (*37*), which gives $E_R = 2 \times 10^{18}$ J (475 megatons energy equivalent), but this great rupture may not satisfy conventional assumptions. The 20-s-period surface-wave magnitude is $M_S = 8.8$, a measure that is expected to be low relative to magnitude measures at longer periods because of the long source duration relative to 20 s. Using this value in the Gutenberg M_S-E_R relationship gives $E_R = 1.0 \times 10^{18}$ J.
36. A. Venkataraman, H. Kanamori, *J. Geophys. Res.* **109**, B05302, doi:10.1029/2003JB002549 (2004).
37. H. Kanamori, *J. Geophys. Res.* **82**, 2981 (1977).
38. S. Ni, H. Kanamori, D. Helmberger, *Nature* **434**, 582 (2005).
39. M. Ishii, P. Shearer, H. Houston, J. Vidale, *Nature*, in press (2005).
40. P. Banerjee, F. F. Pollitz, R. Bürgmann, *Science* 19 May 2005 (10.1126/science.1113746).
41. The tsunami source region estimated in Fig. 6 and shown in greater detail in fig. S6 is based on back-projecting tsunami waves from arrival points with known arrival times to the origin time of the earthquake. This provides a lower bound of 600-km length

for the tsunami source area, based on assumptions of instantaneous rupture and total slip on the fault. If we allow for the delay in tsunami excitation due to finite rupture propagation time to the Nicobar region (~3 to 4 min), along with delay in excitation due to finite-slip rise time (1 to 5 min), the effective tsunami source area may extend to 10°N, giving a total source region about 800 km long.
42. J. Gower, *EOS Trans. Am. Geophys. Union* **86**, 37 (2005).
43. S. Uyeda, H. Kanamori, *J. Geophys. Res.* **84**, 1049 (1979).
44. L. Ruff, H. Kanamori, *Tectonophysics* **99**, 99 (1983).
45. R. Scholz, J. Campos, *J. Geophys. Res.* **100**, 22,103 (1995).
46. F. T. Wu, H. Kanamori, *J. Geophys. Res.* **78**, 6082 (1973).
47. This work was supported in part by the U.S. National Science Foundation under grants EAR-0125595, EAR-0337495, and EAR-0207608. Seismic waveform data from the Global Seismographic Network (funded by NSF under Cooperative Agreement EAR-0004370 and USGS) were obtained from the Incorporated Research Institutions for Seismology (IRIS) Data Management System. Jason data were provided by Lee-Lueng Fu of the Jet Propulsion Laboratory in Pasadena, CA.

Supporting Online Material
www.sciencemag.org/cgi/content/full/308/5725/1127/DC1
Figs. S1 to S8
Table S1
Movies S1 and S2

14 March 2005; accepted 25 April 2005
10.1126/science.1112250

RESEARCH ARTICLE

Rupture Process of the 2004 Sumatra-Andaman Earthquake

Charles J. Ammon,[1]* Chen Ji,[2] Hong-Kie Thio,[3] David Robinson,[4] Sidao Ni,[5,2] Vala Hjorleifsdottir,[2] Hiroo Kanamori,[2] Thorne Lay,[6] Shamita Das,[4] Don Helmberger,[2] Gene Ichinose,[3] Jascha Polet,[7] David Wald[8]

The 26 December 2004 Sumatra-Andaman earthquake initiated slowly, with small slip and a slow rupture speed for the first 40 to 60 seconds. Then the rupture expanded at a speed of about 2.5 kilometers per second toward the north northwest, extending 1200 to 1300 kilometers along the Andaman trough. Peak displacements reached ~15 meters along a 600-kilometer segment of the plate boundary offshore of northwestern Sumatra and the southern Nicobar islands. Slip was less in the northern 400 to 500 kilometers of the aftershock zone, and at least some slip in that region may have occurred on a time scale beyond the seismic band.

Seismic waves are excited by rapid and varying sliding motions that initiate with a frictional instability. Slip begins as the rupture front spreads across the fault with a velocity usually less than the ambient shear wave speed. Both rupture propagation and local slip history (the temporal variation and total slip at a particular position on a fault) influence the frequency and strength of radiated seismic waves. Different positions on the fault generally have different displacement histories, including variations in the rate and amount of slip. Seismic waves sense these differences, and by using ground motions observed far from the source seismologists can reconstruct the spatial and temporal slip history of faulting.

Several phenomena affect seismic wave excitation during faulting. One is the stress drop at the rupture front. As the rupture front expands, short-period P and S waves are generated from the local stress reduction. For large events, these waves can be used to map the earthquake's rupture expansion. The speed of rupture front propagation, which can be related to the energy partitioning during the faulting process, is an important quantity. The potential energy released during earthquakes is partitioned into seismic radiation, mechanical processes such as creation of fractures, and frictional heat (*1*). The amount of heat generated by frictional processes during the rupture depends on the absolute stress, total slip, and rupture area. The partitioning of energy between mechanical processes and seismic radiation varies from earthquake to earthquake and provides one method of classifying different faulting processes. Fast ruptures can be associated with a relatively large fraction of seismically radiated energy (*1*, *2*). For many well-studied earthquakes, the rupture speed is 70 to 95% of the shear wave velocity, but important variations have been observed as complex ruptures cross fault-segment boundaries (*3*). Another important observation is the spatial pattern of slip in large earthquakes. For many shallow earthquakes, slip near the hypocenter is relatively small, indicating to some extent that the earthquake began at a weak region and grew into a much larger event (*1*). These observations are extracted from analysis of the seismic wave field. The 26 December 2004 Sumatra-Andaman and the 28 March 2005 earthquakes (*4*) produced the most extensive high-quality broadband seismic data ever recorded for great earthquakes. Here, we exploit signals across a broad bandwidth and every part of the seismic wave field to construct an integrated seismic view of these earthquake ruptures. Our focus is on the first and larger of the two events.

Short-period *P*-wave directivity. Short-period P-wave radiation (*5*) for large earthquakes provides direct information about the rupture front propagation. The energy radiated by an expanding rupture front can be observed with the use of the global seismic networks (*6*) or regional seismic and hydroacoustic arrays (*7*–*9*). One of the simplest measures that can be made is the duration of short-period P-wave radiation from the source region (*10*, *11*). For a long-duration earthquake, a major challenge for P-wave analysis is the interference of later-arriving seismic waves reflected from the surface and discontinuities in the Earth with P waves radiated from later portions of the rupture. Fortunately, most secondary phases involve additional path segments in the highly attenuating upper mantle, and their short-period content is suppressed (*12*). Applying a high-pass filter can reduce the effects of secondary arrivals. The durations of short-period P waves will be shorter in the direction of rupture propagation and longer in the direction away from the moving source (the rupture front). Data for the Sumatra-Andaman earthquake (Fig. 1) indicate a north-northwest rupture propagation with a speed of about 2.5 km/s and an overall fault length of 1200 to 1300 km, a length consistent with the aftershock distribution (*4*).

The amplitude of the short-period waveforms generated during the rupture also varied about a relatively uniform level. At least three large (from 50 to 150 s, 280 to 340 s, and 450 to 500 s) and several additional seismic

[1]Department of Geosciences, Pennsylvania State University, 440 Deike Building, University Park, PA 16802, USA. [2]Seismological Laboratory, California Institute of Technology, MS 252-21, Pasadena, CA 91125, USA. [3]URS Corporation, 566 El Dorado Street, Pasadena, CA 91101, USA. [4]Department of Earth Sciences, University of Oxford, Parks Road, Oxford OX1 3PR, UK. [5]Chinese Academy of Sciences Key Laboratory of Crust-Mantle Materials and Environments, University of Science and Technology of China, Hefei, Anhui 230026, China. [6]Earth Sciences Department and Institute of Geophysics and Planetary Physics, University of California, Santa Cruz, CA 95064, USA. [7]Institute for Crustal Studies, Santa Barbara, CA 93106, USA. [8]National Earthquake Information Center, U.S. Geological Survey (USGS), Golden, CO 80401, USA.

*To whom correspondence should be addressed. E-mail: cammon@geosc.psu.edu

energy bursts are apparent (Fig. 1). For a uniform rupture speed, the large bursts are located near latitudes of 4° to 6°N, 8° to 10°N, and 12° to 13.75°N. Ishii *et al.* (*8*), with use of the Japanese Hi-net seismic network, identified two large bursts of *P*-wave energy at about 80 and 300 s after the origin time and a mean rupture speed of about 2.8 km/s. Their estimate of the rupture speed is slightly higher than the one we proposed, but the Hi-net bursts of energy are consistent with the first two features observed in the global network observations. Observations from three hydroacoustic arrays across the Indian Ocean were triangulated to identify the source of *T* phases excited by the Sumatra-Andaman rupture. The *T*-phase source propagated northward at a speed of about 2 km/s for the first 600 km of the rupture. A secondary more northern *T*-phase source began before the first had reached the Nicobar islands (*9*).

Long-period Rayleigh wave directivity. For earthquakes up to about magnitude 7.5, surface waves with periods greater than 20 s usually sense the entire rupture process, such that the surface wave magnitude, M_S, based on 20-s-period surface waves, is indicative of the entire slip event. But for the 2004 earthquake, even 500-s-period surface waves failed to sense the full slip process. Surface-wave phase velocities are close to rupture speeds, which enhances their sensitivity to rupture directivity (azimuthal time delays related to spatial and temporal source finiteness), so comparison of azimuthal patterns in the surface wave amplitudes at different periods provides useful constraints on the overall slip distribution on the fault. Surface waves disperse as they propagate, producing complex waveforms and amplitudes that depend on distance as well as source radiation pattern. For the 2004 event, the faulting geometry inferred from 300- to 500-s-period surface waves is nearly pure thrusting on a shallow plane (*4*), which produces a predominantly two-lobed azimuthal Rayleigh-wave radiation pattern (modified somewhat by the north-northwest rupture propagation), and a four-lobed Love-wave radiation pattern. We focus on Rayleigh waves because of their simpler pattern.

Rayleigh-wave amplitudes were measured with the use of R1 for shorter periods and R3 for longer periods (which are more robust when measured with longer time windows) (*13*). To keep the analysis straightforward, we account for effects of dispersion, fault geometry, and distance by making synthetic seismograms for Rayleigh waves. For periods shorter than 800 s, we used synthetic seismograms computed with the spectral-element method (*14*) for a three-dimensional (3D) Earth model composed of the mantle model s20rts (*15*), the model Crust 2.0 (*16*), and the topography from ETOPO5. For periods longer than 800 s, we used synthetics computed by summation of normal modes. The 3D simulations were performed on the Caltech Division of Geological and Planetary Sciences Dell cluster. Initially, the synthetics are for a point source model with no finiteness using the source parameters of the Harvard Centroid Moment Tensor (CMT) solution (*4*), and we simply measure the amplitude ratio (observed/predicted) and the time shift (observed – predicted) in various pass bands and plot them as a function of azimuth (Fig. 2, top left).

If there were no effects of finiteness, all the amplitude ratios would be unity for all periods. For a uniformly slipping fault with unilateral propagation, one would expect directivity effects to be stronger at shorter periods with larger amplitudes in the direction of rupture. For 150-s and 300-s waves, the amplitudes are enhanced along the rupture direction (around 330° N), as expected. However, the amplitude ratios and the strength of the azimuthal pattern unexpectedly do not decrease much at longer periods, up to at least 1500 s. This behavior cannot be interpreted by using uniform slip along the fault. Modeling of simple propagating ruptures suggests that the observations for periods shorter than 600 s are compatible with north-northwest propagation of a rupture at about 2.5 to 3 km/s for 400 to 600 km from the southern end of the fault, with overall slip averaging about 9 m. This slip accounts for the seismic moment of the Harvard CMT solution (*4*). But, longer-period surface wave amplitudes are only partly accounted for by this model. The pattern of time shifts (Fig. 2, top) supports this conclusion. At periods of 150 and 300 s, the time shift is relatively small, but, at periods longer than 600 s, the time shift is systematically positive; i.e., observed waves are later than predicted by the CMT. These observations suggest that additional slip extended in either time, space, or both is required to explain the surface-wave data.

Surface-wave moment rate functions. Intermediate-period surface waves (80 to 500 s) were the dominant signals globally recorded from this earthquake (*4*, *17*). Here, we remove the dispersive wave propagation effects by deconvolving the data by point-source normal-mode synthetic seismograms computed for the fault strike and rake of the CMT solution (*4*), but with a slightly larger dip (11°) (*18*, *19*). We assumed a standard Earth model (*20*), the USGS origin time and epicenter (*4*), and a source depth of 15 km. We used two different deconvolution approaches, a frequency-domain method (*21*) and a time-domain method (*22*). The results are similar, so we discuss the time-domain results here [see (*12*) for the frequency-domain estimates]. The result of each deconvolution is a source time function,

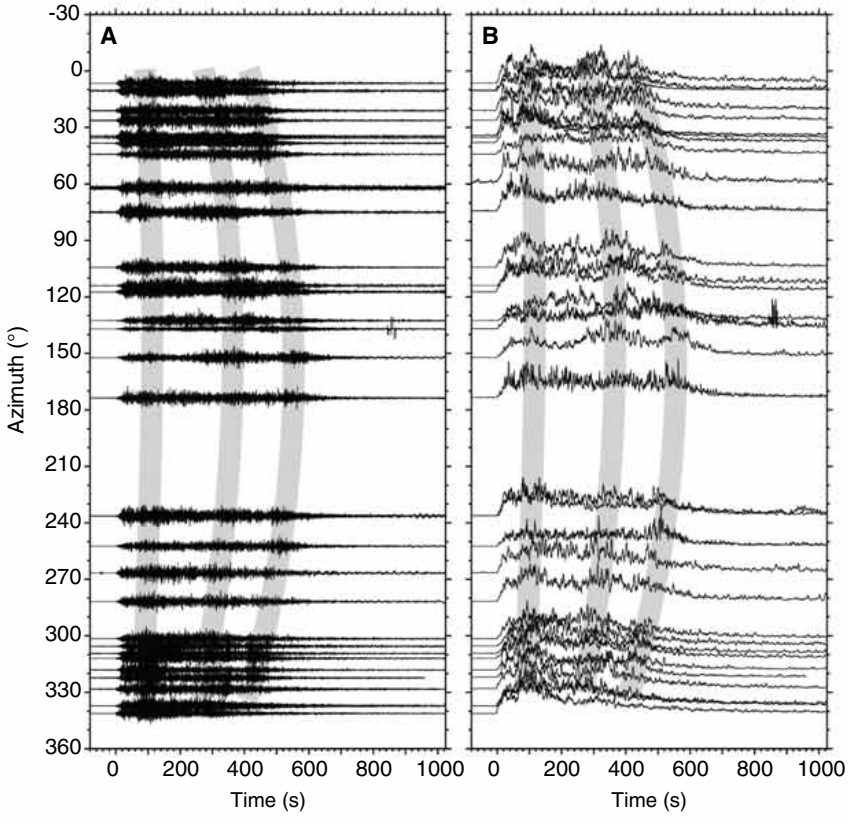

Fig. 1. High-frequency seismograms (**A**) and envelopes (**B**) as a function of azimuth from the epicenter. The signal duration varies smoothly as a function of azimuth, and three relatively energetic amplitude bursts are identified with the gray shading.

indicating the time history of Rayleigh-wave radiation at the corresponding azimuth.

Rayleigh-wave source time functions strongly vary with azimuth relative to 330°N [the strike of the Harvard CMT mechanism (*4*)] (Fig. 3). We thus arranged the data by directivity parameter (*23*), which transforms features with a sinusoidal azimuthal moveout to a linear moveout. We combined 172 R1 source time functions into 30 average source time functions binned by directivity parameter. The observations are not uniformly distributed with azimuth and reflect the paucity of seismic stations in the Southern Hemisphere. For azimuths close to the direction of rupture (near the bottom of the plot), the observations show a relatively narrow, large-amplitude pulse, and the pulse width increases with decreasing directivity parameter. As the azimuth relative to rupture increases, several smaller amplitude pulses shift systematically to later relative times, the peak amplitude decreases, and the overall duration increases. These pulses are not observable on all the recordings but can be seen clearly on several. Their true temporal relation can be seen on the time functions nearly perpendicular to the rupture. The moveout and pulse shape changes are related to the spatiotemporal slip distribution and rupture propagation as sensed by these waves.

These intermediate-period surface-wave time functions can be formally inverted for a 1D model of slip distribution along the fault by using an inverse Radon transform (IRT) (*24*, *25*). This is a first step toward 2D maps of the seismic moment distribution but has the added flexibility that the time dependence of slip does not have to be prescribed. The results (Fig. 4) show that the initial 60 s of the rupture had little moment and that the largest moment occurred about 100 to 200 km northward, about 1 min later. Once the large slip event began, the slip radiating in this bandwidth propagated northward at about 3 km/s. After a few hundred kilometers, the seismic energy in this bandwidth began to decrease steadily, suggesting that most of the rapid slip occurred in the first 700 to 800 km of the rupture. Beyond about 800 km, some slip is imaged, but it is low amplitude (<2 m) and not well resolved. Given that the short-period energy and the longest-period surface wave amplitudes require a rupture propagating farther to the north, we infer that the slip continued on to the central Andaman islands region, about 1300 km north of the hypocenter, but that it ruptured smoothly and radiated relatively little energy in this bandwidth.

2D analyses. The rupture area outlined by reverse-faulting aftershocks (*4*) has a substantial width (150 to 200 km), and seismic data are sensitive to variable slip along both the strike and dip directions. We applied three different modeling approaches to estimate the 2D moment distribution of the Sumatra-Andaman earthquake. The use of three methods allows us to identify and to focus on the robust features of the rupture resolved by seismic observations and to assess the sensitivity of those features to necessary choices of fault parameterization, temporal moment distribution parameterization, and seismic data weighting. The results presented here build upon rapid determinations of faulting conducted soon after the event (*26*).

Each method involves a different parameterization of the source as a function of time, but all three parameterize the slip by using planar faults divided into a grid of subfaults ranging in area from 16 km by 20 km to 50 km by 50 km. Each method includes some constraints on the propagation of the rupture front, although we made efforts to reduce the impact of these on the results. To parameterize the history of sliding on the fault, we used a varying rise time for each subfault or multiple time windows during which slip at the node is allowed to accumulate. In all methods, we restricted slip to occur during a specified time window (up to 180 s long) after the rupture front passes. The slip direction was allowed to vary about the plate motion or the Harvard CMT rake direction. For each approach, we constructed a set of linear or linearized equations relating the moment rate history of each subfault as a function of time to the observed seismograms. Methods used include linear programming to minimize the robust L1 norm for *SH* waves (*27*) (model I), a least-squares inversion of group velocity–windowed intermediate-period (80 to 300 s) surface waves combined with regional long-period seismograms (*28*) (model II), and a search-based method to minimize wavelet coefficients of the observed teleseismic *P* and *SH* waves and complete long-period three-component regional seismograms (*29*–*31*) (model III). The nonlinear dependence on rupture propagation is handled with constraints on the rupture front velocity or by using a grid search specifying a rupture front propagation that is perturbed during the inversion. Waveform fits for each model are included in (*12*).

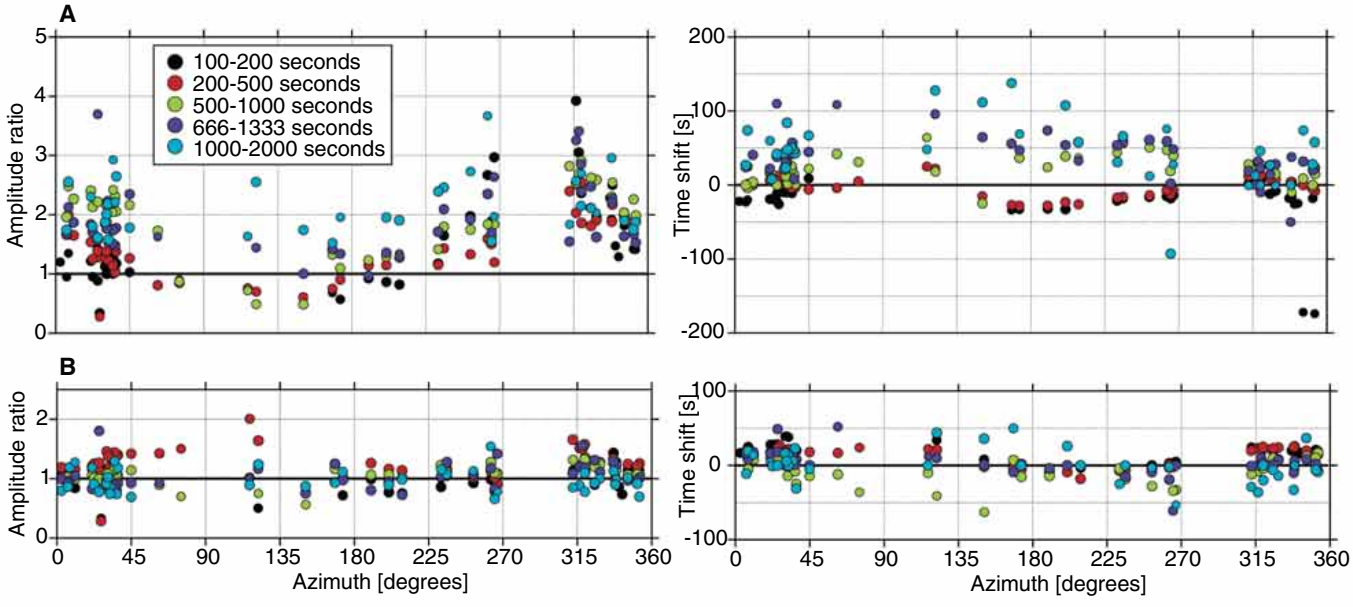

Fig. 2. Time-domain Rayleigh wave amplitude and phase-shift measurements as a function of azimuth from the epicenter. Observations for a period range of 150 to 1500 s are shown. All periods show the effects of directivity along the rupture direction of 310° to 330°N. (**A**) The observations are compared with predictions for the Harvard CMT solution for amplitude and time shift. (**B**) A similar comparison with predictions computed for model III. The smaller scatter for both amplitude and time shift indicates that model III can account for the first-order long-period surface wave observations.

The first model (Fig. 5A) was constructed with the use of the method described in (*27*) and 20 teleseismic *SH* waveforms, filtered to include periods shorter than 120 s. The rupture surface was parameterized as two fault segments: the first having a strike of 329° and a dip of 8° and the second having a strike of 333° and a dip of 7° (based on the mechanism of the 29 December 2004 M_W = 6.0 aftershock). Cells on each fault segment were 40 km by 40 km, and the source time function was divided into 15 12-s time steps. Each cell was allowed to slip in each time step except that the rupture front could not propagate faster than a *P* wave from the hypocenter. The total moment was constrained to be similar to the Harvard CMT moment of 4.0×10^{22} N·m; however, because the true rupture duration is longer than 180 s, any additional moment after 180 s is forced onto to the final time step, which is then discarded.

The solution favors at least 10 m of slip near the hypocenter. This amount is consistent with reported uplift of Simeulue Island (*32*). A second region of large slip, approaching 20 m, is located southeast and west of Great and Little Nicobar islands. A third patch of 5 to 10 m of slip is located near 4°N, but tests show that the data allow more slip in this region. In general, slip is concentrated along the deeper parts of the megathrust in this solution, suggesting that most of the seismic energy in the shorter period *SH* waves originated from relatively deep on the fault. The model's rupture started slowly near the hypocenter (~1.3 km/s) but accelerated up to 3.3 km/s toward the Nicobar islands in the north.

The second model (Fig. 5B) was obtained by using a least-squares inversion of regional long-period seismograms in the period range from 100 to 3000 s and regional and teleseismic surface waves in the period range from 80 to 300 s. The surface waves were modeled with use of aspherical Earth model corrections computed for the Harvard phase velocity model (*33*). The point-source grid spacing was 50 km by 50 km, each node having source time functions with a duration of 40 s. The largest slip predicted by the model was located between about 3° and 6°N, spread over much of the megathrust width, but with larger slip deeper. Slip near the hypocenter was relatively large but decreased quickly in the surrounding 100 km or so. As with the *SH* waveform results, a second area of larger slip was located northwest of Great and Little Nicobar islands. Slip decreased north of 9° to 10°N, but the model suggest that slip continued to the north into the Andaman islands region, and the total moment was about 6.5×10^{22} N·m, about 1.5 times larger than the Harvard CMT moment and approaching that estimated by using normal modes (*34*).

The third model (Fig. 5C) was constructed with the use of teleseismic body waves (20 to 200 s), intermediate-period three-component regional seismograms (50 to 500 s), and long-period teleseismic seismograms dominated by R1 and R2 phases (250 to 2000 s). The rupture surface was approximated with the use of three fault segments with strikes approximating the local trench axis. The fault segment dip angles were approximated with the use of seismicity-

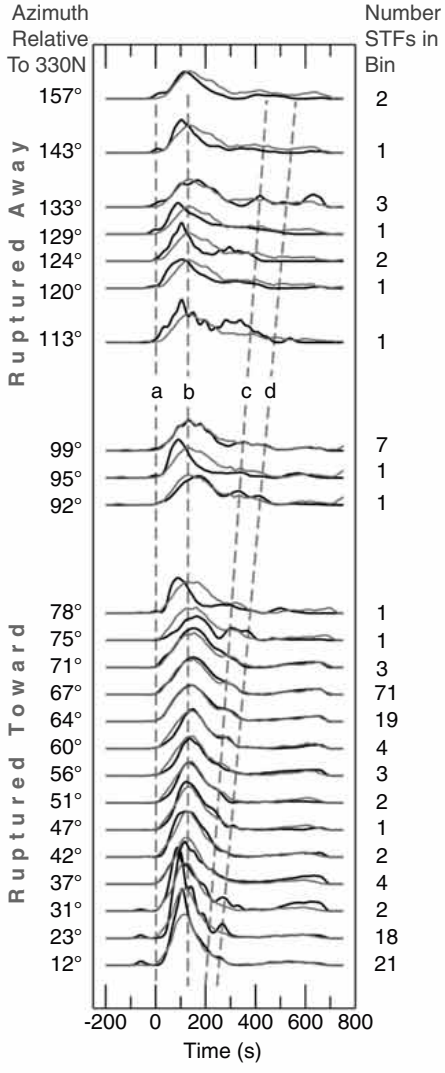

Fig. 3. Deconvolved Rayleigh wave source time function estimates (black lines). The source functions, obtained by water-level deconvolution, are arranged in order of increasing directivity parameter. The equivalent azimuth relative to the rupture direction (330°N) is shown to the left; the number of observations stacked in each bin is shown to the right. Lines a, b, c, and d identify discrete phases that can be tracked at least across as least several source functions. Predictions from the IRT inversion are shown in gray lines. The fits are best where the numbers of data are large. STFs, source time functions.

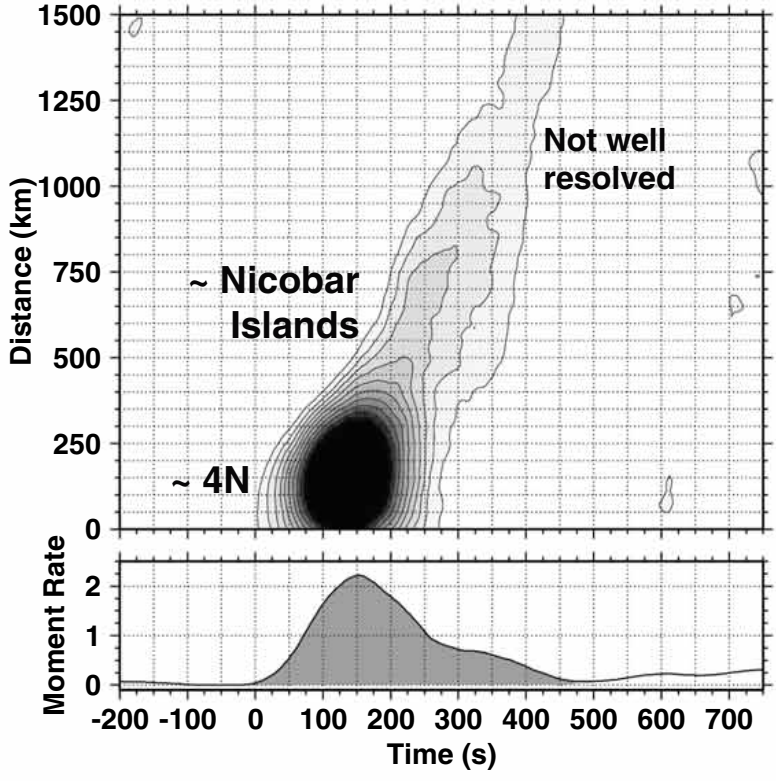

Fig. 4. (**Top**) Moment-rate density image showing the variation in seismic moment with time and with position along a 1D fault striking 330°N constructed with the use of Rayleigh waves (R1) in the period range from 80 to 400 s. (**Bottom**) Curve shows the moment-rate time function in units of 10^{20} N·m/s. The image is the result of 25 local search inversions, stacked to reduce truncated search artifacts. Stacking also smooths the image and moment-rate estimate. Slip radiating seismic energy in the intermediate-period surface wave band (80 to 100 s) clearly extends to about 750 km and was concentrated in the first 250 km. Fits are shown in Fig. 3.

based slab contours (*35*), which imply that the dip of the fault segments increases from south to north at 12°, 15°, and 17.5°. Subfault spacing was 20 km along strike and 16 km along dip. The intermediate- and long-period waveforms were computed by using normal mode summation but calibrated by spectral element synthetics computed as described above. A global optimization simulated annealing algorithm was used to estimate the slip amplitude and direction (the rake angle) as well as rupture initiation, rise, and rupture cessation times for each subfault. Rupture initiation times were allowed to vary up to ±150 s from the time that a rupture propagating at 2 km/s would pass the subfault. The 2 km/s average rupture speed was estimated with the use of multiple inversions but is not tightly constrained by the data.

In this model, the accumulated slip across the rupture surface composed of three planar faults (Fig. 5C) lasted for 550 s and produced a total moment of 6.5×10^{22} N·m, which gives a moment magnitude of $M_w = 9.1$. The model implies that slip was primarily concentrated south of 9.5°N, but slip extended northward into the Andaman Island regions. The area of largest slip is consistent with the surface-wave IRT results as well as model II, and these results all find a decrease in slip (radiating intermediate-band surface waves) along the first 750-km length of the rupture. The region of largest slip extends from about 3°N to about 6°N and includes substantial slip across the entire megathrust width. This is consistent with the large peak in the global surface-wave moment-rate functions. Slip is generally concentrated along the lower half of the megathrust, consistent with the other methods. In contrast with the *SH*-wave model (Fig. 5A), this model implies that slip near the hypocentral region was relatively low. A second region of strong slip is located west of northern Great Nicobar and Littler Nicobar islands, which matches the *SH* body-wave results. This model predicts uplift values between 1 to 5 m across a region with dimensions of 900 km by 100 km from the epicenter near 3°N to about 10°N. Uplift is a maximum near the trench between 4°N and 5°N (near-source surface displacement and movies of regional and global seismic velocities predicted by this model are included in the supplemental online material).

Slip maps for the 28 March 2005 (CMT $M_W = 8.6$) event are shown are shown in Fig. 5, B and C. The peak slip (~5 to 6 m) in both models is located near the hypocenter, and both models include rupture directed primarily to the southeast. The model slip is concentrated between about 20- to 40-km depth, which helps explain the smaller tsunami generated by

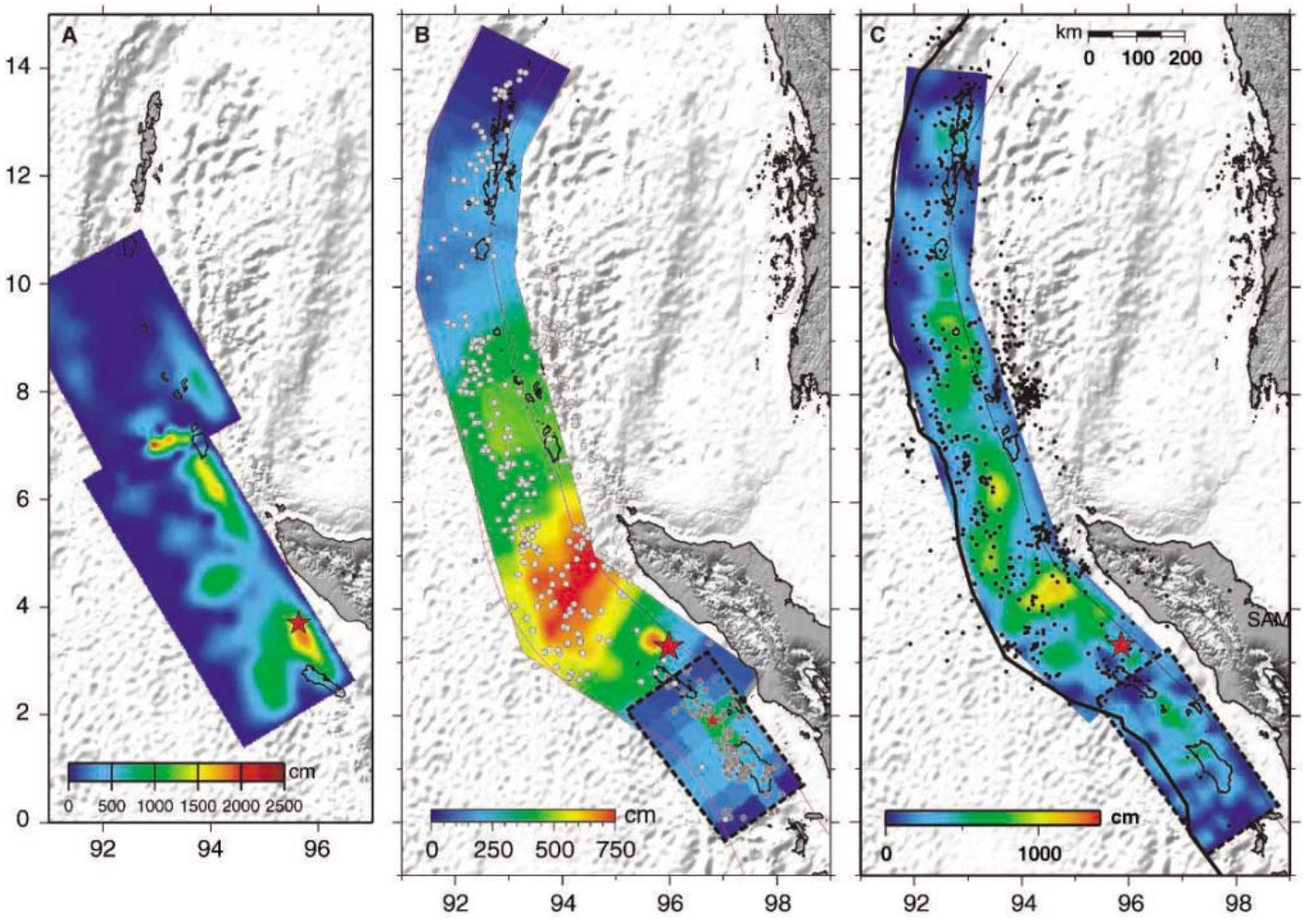

Fig. 5. (**A**) Fault slip 168s after rupture initiation estimated by using 20 azimuthally distributed teleseismic *SH* waveforms (Δ ~ 45° to 85°). The rupture models consists of two faults, the first having a strike of 329° and a dip of 8° and the second having a strike of 333° and a dip of 7° (based on the mechanism of the 29 December 2004 $M_W = 6.0$ aftershock). (**B**) Slip distribution from method II. The reliance on intermediate-period surface waves and long-period seismograms reduces the detail imaged in the rupture but provides a first-order view of the slip distribution. (**C**) Slip distribution of finite fault model III using teleseismic body waves (5 to 200 s), intermediate-period three-component regional waves (50 to 500 s), and long-period teleseismic waves (250 to 2000 s). The surface projections of three fault segments are colored on the basis of the slip amplitude. The black thick and thin lines delineate the trench mapped from the ETOPO2 and 50-km iso-depth slab contour. The aftershocks (Ml > 5) downloaded from the National Earthquake Information Center are indicated by black dots. Waveform fits for each model can be found in the electronic supplements. Slip of the 28 March 2005 event is outlined with a dashed line. Area ruptured during the 28 March 2005 event is outlined with a dashed line.

this event. The substantial outer arc high in this part of the subduction zone also likely played a role in the tsunami generation (*36*). The model rupture durations were ~150 s, and both models map the most substantial slip in the region previously identified at the 1861 earthquake rupture (*4*). Little, if any, slip penetrated into the 1833 rupture zone, which is a possible site for the next large event in the region.

Discussion. A number of general features are apparent from the directivity observations and fault rupture models. Like the 1960 Chile, the 1964 Alaska, and the 1952 Kamchatka earthquakes, the 2004 Sumatra-Andaman event ruptured largely unilaterally. Little aftershock activity penetrated south of the epicenter until the 28 March 2005 earthquake. Although there are differences in the rupture models described above, the first-order attributes of the rapid-slip faulting are well established. The moment rate functions (the combined effects of slip and rupture area expansion as a function of time) show that the fault sliding began relatively slowly but grew rapidly after about 40 to 60 s as large amounts of slip occurred off the west coast of Sumatra between 3°N and 4°N. The rapid increase in moment rate and the accompanying burst of short-period energy (Fig. 6) suggest the possible failure of a relatively strong section of the megathrust at that time. Slip amplitudes in the region are also the largest anywhere on the fault, approaching 15 m offshore of Sumatra. Rupture and slip continued to the north, but, after about 180 s, the moment rate decreased gradually to relatively low levels by about 450 to 600 s. The slip models obtained from inversions of body and surface waves (models 2 and 3) include gradually decreasing slip extending to 13° to 14°N. These models match the low-order normal-mode amplitudes to within about 10% (*34*). The lower panels in Fig. 2 show the predictions of model III (Fig. 5C) on the long-period Rayleigh wave directivity observations. The spread of the measurements in the top figures, both amplitude ratio and time shift, is greatly reduced, the amplitude ratios are relatively constant and close to unity, and the time shift is close to zero regardless of the period and azimuth (*12*). We conclude that the tapered slip between the Nicobar and Andaman islands is responsible for the observed azimuthal patterns of amplitude ratio and time shifts of Rayleigh waves.

This faulting model suggests a relationship between megathrust coupling and rupture velocity and/or slip rate: The results indicate that the fault was well-coupled in the south, somewhat less coupled in the central portion, and weakly coupled in the north of the rupture zone. The subducting slab dip angle, age, and plate motion obliquity all increase from the southern (Sumatra) segment to northern (Andaman) segments of the rupture (*4*), perhaps contributing to reduction of interplate coupling as a function of distance northward. The reduction of slip just north of the Great Nicobar Island coincides with a northward rotation of the trench, and the rupture terminated in a region where the trench is parallel with the interplate motion (or even extensional) (*4*).

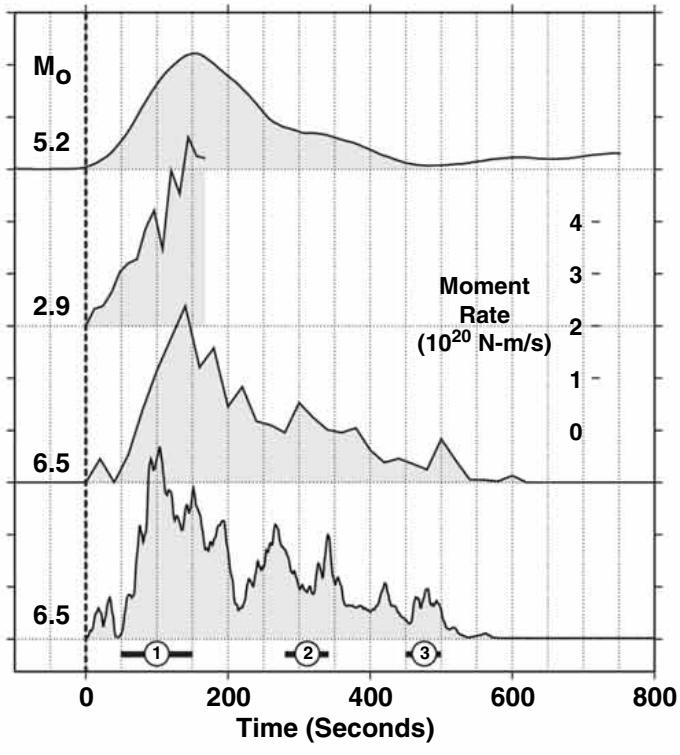

Fig. 6. Moment rate functions from each of the four rupture imaging methods in our analyses. From top to bottom, surface-wave IRT imaging and finite-fault inversion results using methods I, II, and III. All are presented on the same amplitude scale, and the seismic moment is listed above and to the left of each signal. For method I, the moment shown is the value reached 168 s after rupture commencement. Peak moment rates are in the range of 4×10^{20} N·m/s. Models constructed with the use of body waves are generally higher frequency. The surface-wave models recover only the smoother components of the rupture. The numbers at the bottom identify the apparent times of high-frequency energy bursts.

Although our models explain seismological data ranging from body waves to the gravest normal mode (period of 54 min) satisfactorily, the slip in the models to the north of 8°N is too small to explain global positioning system (GPS) displacements observed in the Nicobar Island (1 to 2 m vertical and 5 m horizontal) and the Andaman Island (1 to 2 m vertical and 3 m horizontal) (*37*). If we are to explain the deformation of the islands with the megathrust fault model estimated in slip inversions, we must increase the slip in the section north of 8°N by a factor of 2 to 3 (fig. S1). However, adding rapid slip of this magnitude considerably reduces the fit to the normal-mode amplitudes. Thus, most of this additional slip was probably slow and occurred at a time scale beyond the seismic band. More detailed analyses of tsunami, normal mode, and GPS data will be required to resolve the time scale of this additional slip.

References and Notes

1. H. Kanamori, *Proc. Jpn. Acad. Ser. B* **80**, 297 (2004).
2. Seismic efficiency can be defined as $ER/(ER + EG)$, where ER is the energy radiated seismically and EG is the energy mechanically dissipated during the fracture.
3. D. Wald, T. Heaton, *Bull. Seismol. Soc. Am.* **84**, 668 (1994).
4. T. Lay *et al.*, *Science* **308**, 1127 (2005).
5. Here, we are considering periods shorter than about 2 s as short periods.
6. Ni *et al.*, *Nature* **434**, 582 (2005).
7. A. Lomax, *Geophys. Res. Lett.*, in press.
8. M. Ishii, P. Shearer, H. Houston, J. Vidale, in preparation.
9. C. de Groot-Hedlin, in preparation.
10. J. Koyama, S. Zheng, *Phys. Earth Planet. Inter.* **37**, 108 (1985).
11. H. Houston, H. Kanamori, *Bull. Seismol. Soc. Am.* **76**, 19 (1986).
12. Materials and methods are available as supporting material on *Science* Online.
13. R1 is the fundamental mode Rayleigh wave that travels along the shorter great-circle arc connecting the source with the receiver; R2 travels along the longer arc. R3 leaves the source with the same azimuth as R1 but makes an additional transit around the Earth.
14. D. Komatitsch, J. Ritsema, J. Tromp, *Science* **298**, 1737 (2002).
15. J. Ritsema, H.-J. van Heijst, J. H. Woodhouse, *Science* **286**, 1925 (1999).
16. C. Bassin, G. Laske, G. Masters, *Eos* **81**, 897 (2000).
17. J. Park *et al.*, *EOS* **86**, 57 (2005).
18. C. J. Ammon, A. A. Velasco, T. Lay, *Geophys. Res. Lett.* **70**, 97 (1993).
19. A. A. Velasco, C. J. Ammon, T. Lay, *Bull. Seismol. Soc. Am.* **84**, 735 (1994).
20. A. M. Dziewonski, D. L. Anderson, *Phys. Earth Planet. Inter.* **25**, 297 (1981).
21. R. W. Clayton, R. A. Wiggins, *Geophys. J. R. Astron. Soc.* **47**, 151 (1976).
22. M. Kikuchi, H. Kanamori, *Bull. Seismol. Soc. Am.* **72**, 491 (1982).
23. The directivity parameter is an azimuth-corrected slowness defined by $\Gamma = \frac{\cos(\varnothing)}{c}$, where ø is the azimuth of the station relative to the rupture direction and c is the wave phase velocity. For the Rayleigh waves, we assumed a phase velocity of 4.75 km/s. The results do not change significantly if we vary the value by about 20%.
24. L. J. Ruff, *Geophys. Res. Lett.* **11**, 629 (1984).
25. L. Ruff, in *Seismic Tomography*, G. Nolet, Ed. (D. Reidel, Dordecht, Netherlands, 1987), pp. 339–366.
26. Early inversions of *P* waves included slip models on Web sites: http://neic.usgs.gov/neis/eq_depot/2004/eq_041226/neic_slav_ff.html (C.J), www.eri.u-tokyo.ac.jp/sanchu/Seismo_Note/2004/EIC161e.html (Y.Yamanaki) http://iisee.kenken.go.jp/staff/yagi/eq/Sumatra2004/

Sumatra2004.html (Y. Yagi), and www.geop.itu.edu.tr/%7Etaymaz/sumatra (T. Taymaz, O. Tan, S. Yolsal).
27. S. Das, B. V. Kostrov, *Phys. Earth Planet. Inter.* **85**, 293 (1994).
28. H. K. Thio, R. W. Graves, P. G. Somerville, T. Sato, T. Ishii, *J. Geophys. Res.* **109**, 10.1029/2002JB002381 (2004).
29. C. Ji, D. J. Wald, D. V. Helmberger, *Bull. Seismol. Soc. Am.* **92**, 1192 (2002).
30. C. Ji, D. J. Wald, D. V. Helmberger, *Bull. Seismol. Soc. Am.* **92**, 1208 (2002).
31. C. Ji, D. V. Helmberger, D. J. Wald, K.-F. Ma, *J. Geophys. Res.* **108**, 10.1029/2002JB001764 (2003).
32. K. Sieh, *Nature* **434**, 573 (2005).
33. G. Ekström, J. Tromp, E. W. F. Larson, *J. Geophys. Res.* **102**, 8137 (1997).
34. J. Park *et al.*, *Science* **308**, 1139 (2005).
35. O. Gudmundsson, M. A. Sambridge, *J. Geophys. Res.* **103**, 7121 (1998).
36. R. A. Kerr, *Science* **308**, 341 (2005).
37. Information about the Center for Earth Science Studies Seismology Research Group is available online at www.seires.net/content/view/123/52/.
38. We acknowledge the efforts of those associated with the collection of data made freely available through the Federation of Digital Broadband Seismographic Networks. Seismic waveform data were obtained from the Incorporated Research Institutions for Seismology (IRIS) Data Management System. This work was supported in part by NSF contracts EAR-0125595 and EAR-0337491, USGS contract 04HQGR0038, and the California Institute of Technology Tectonics Observatory. S.N. was supported in part by the Outstanding Young Scientists Program of the National Science Foundation of China (40425005).

Supporting Online Material
www.sciencemag.org/cgi/content/full/308/5725/1133/DC1
Materials and Methods
Figs. S1 to S13
Table S1
Movies S1 to S3

14 March 2005; accepted 27 April 2005
10.1126/science.1112260

RESEARCH ARTICLE

Earth's Free Oscillations Excited by the 26 December 2004 Sumatra-Andaman Earthquake

Jeffrey Park,[1] Teh-Ru Alex Song,[2] Jeroen Tromp,[2] Emile Okal,[3] Seth Stein,[3] Genevieve Roult,[4] Eric Clevede,[4] Gabi Laske,[5] Hiroo Kanamori,[2] Peter Davis,[5] Jon Berger,[5] Carla Braitenberg,[6] Michel Van Camp,[7] Xiang'e Lei,[8] Heping Sun,[8] Houze Xu,[8] Severine Rosat[9]

At periods greater than 1000 seconds, Earth's seismic free oscillations have anomalously large amplitude when referenced to the Harvard Centroid Moment Tensor fault mechanism, which is estimated from 300- to 500-second surface waves. By using more realistic rupture models on a steeper fault derived from seismic body and surface waves, we approximated free oscillation amplitudes with a seismic moment (6.5×10^{22} Newton·meters) that corresponds to a moment magnitude of 9.15. With a rupture duration of 600 seconds, the fault-rupture models represent seismic observations adequately but underpredict geodetic displacements that argue for slow fault motion beneath the Nicobar and Andaman islands.

The 26 December 2004 Sumatra-Andaman earthquake delivered a blow to our planet (*1*, *2*), exciting a plethora of vibrational free oscillations that, at periods $T > 1000$ s, remained observable for weeks in broadband seismic data from global networks. The frequencies and decay rates of Earth's free oscillations offer strong constraints (*3*–*5*) on our planet's interior composition, mineralogy, and dynamics (*6*–*15*), so analysis of long-period seismic data from this event should offer new perspectives on Earth structure. In this report, we discuss how seismic free oscillations also provide information on the size and duration of this earthquake.

[1]Department of Geology and Geophysics, Yale University, Post Office Box 208109, New Haven, CT 06520–8109, USA. [2]Seismological Laboratory, California Institute of Technology, MS 252–21, Pasadena, CA 91125, USA. [3]Department of Geological Sciences, 1850 Campus Drive, Evanston, IL 60208–2150, USA. [4]Departement de Sismologie, Institut de Physique du Globe de Paris (IPGP), 4 Place Jussieu, 75252 Paris Cedex 05, France. [5]Scripps Institution of Oceanography, University of California, San Diego, La Jolla, CA 92093–0225, USA. [6]Dipartimento di Scienze della Terra, Universita' di Trieste, Via Weiss 1, 34100 Trieste, Italy. [7]Royal Observatory of Belgium, Avenue Circulaire 3, B–1180 Bruxelles, Belgium. [8]Institute of Geodesy and Geophysics, Chinese Academy of Sciences, 174 Xudong Road, Wuhan 430077, China. [9]National Astronomical Observatory of Japan, 2–12 Hoshigaoka, Mizusawa, Iwate 023–0861, Japan.

Because Earth is roughly spherical, the geographical patterns of its free vibrational modes can be expressed in terms of the spherical harmonics, $Y_{lm}(\theta,\phi)$, and their vector gradients, where l is the angular degree, m is the azimuthal order, θ is colatitude, and ϕ is longitude. On a simple spherical planet (*16*), the free oscillations follow either a spheroidal (S) or toroidal (T) vibrational pattern and have spectroscopic notation ${}_nS_{lm}$ and ${}_nT_{lm}$, $m = -l,\ldots,l$, where n is the radial overtone number (Fig. 1). For a spherical reference model, all $2l + 1$ vibrations of ${}_nS_{lm}$ or ${}_nT_{lm}$ have identical frequency. On the real Earth, departures from the symmetries of a spherical reference model cause its free oscillations to couple, hybridize, and suffer fine-scale splitting of their vibrational frequencies (*17*–*20*). Frequency splitting of free oscillations with periods $T > 1000$ s is caused mainly by Earth's rotation, similar to Zeeman splitting of electron energies in an external magnetic field (*21*, *22*).

Earth's free oscillations were first reported after Fourier analysis of hand-digitized analog seismic records of the megathrust earthquakes of the middle 20th century (*23*–*26*), particularly the 22 May 1960 Chilean earthquake ($M_w = 9.5$). These huge events saturated most seismometers of the time, rendering many hours of data unusable. Frequency estimates from smaller, deeper earthquakes, more amenable to hand-digitization and Fourier analysis, led to accurate spherical-reference models for our planet's interior (*6*). Detailed study of free-oscillation attenuation, frequency splitting, and modal coupling was made feasible by digital recording (*7*, *8*, *27*, *28*) and by the advent of the Federation of Digital Seismic Networks (FDSN) with high-dynamic range induction-feedback sensors capable of recording faithfully the seismic waves from great earthquakes (*29*, *30*).

Broadband seismographic data. The 2004 Sumatra-Andaman earthquake tested broadband seismographic technology on a global scale. Peak ground motions exceeded 1 cm at all locations on Earth's solid surface (*31*). In one portion of the FDSN, 88% of the 125 stations of the Global Seismographic Network (GSN), operated by the U.S. Geological Survey and Project IDA of the University of California, San Diego (*32*, *33*), recorded data without interruption or distortion (*34*). Stations of the Geoscope network (*35*, *36*) had similar success.

In all, data records from more than 400 FDSN stations had sufficient quality to observe Earth's free oscillations with unprecedented signal-to-noise ratios. A broad distribution of stations facilitates the use of spherical harmonic-weighted stacks of data spectra to isolate individual Earth vibrations (fig. S2). The recent installation of a broadband seismometer in the South Pole quiet zone provides natural isolation of the $m = 0$ singlets of long-period modes (Fig. 2). Free oscillations can also be sought in complementary observations (Fig. 3) from strainmeters and tiltmeters (*37*–*40*), from superconducting gravimeters (*41*–*43*), and from continuously recording global positioning system (GPS) receivers (*44*, *45*). Superconducting gravimeter data offers an important

calibration for seismometer data at periods $T >$ 1000 s (*46*). The amplitude of the "breathing mode" ${}_0S_0$ is geographically constant to high accuracy; station-by-station comparisons of its amplitude in data from the IDA network suggest that a substantial minority of seismometers suffer 5 to 10% deviations from their nominal responses (*34*).

The largest earthquakes offer the most penetrating and long-lasting seismic probes of Earth's deep interior, revealing behavior predicted by theory but only rarely observed above ground noise. The coupling between spheroidal and toroidal modes associated with Earth's Coriolis force causes them to form hybrid vibrational patterns. The hybridized toroidal modes are predicted to acquire a vertical vibrational component, a feature nominally restricted to spheroidal modes. Although this behavior is readily observable for mode pairs ${}_0S_l - {}_0T_{l+1}$ in the 300- to 500-s period range that are close in frequency (*27*, *28*), at frequencies below 1 mHz the coupling is weaker and was not observed with seismometers before the 2004 Sumatra-Andaman earthquake (*47*) (Fig. 1 and fig. S3).

The geometry of low-degree modes allows us to constrain the long-period centroid of the earthquake (*8*, *23*). For a centroid at the equator, excitation of the $m = \pm 1$ vibrations of the mode ${}_0S_2$ would be zero for an earthquake on the east-dipping Sumatra-Andaman thrust fault. The amplitude of the $m = -1, +1$ vibrations of ${}_0S_2$ relative to the $m = -2$, 0, and $+2$ vibration indicates how far northward the Sumatra-Andaman earthquake ruptured (Fig. 4). The event hypocenter and Centroid Moment Tensor (CMT) location lie at 3.2°N and 3.1°N, respectively, displaced east-west by nearly 200 km. The relative excitation of the $m = \pm 1$ vibrational modes of ${}_0S_2$ is significantly underpredicted by this location centroid. Better agreement is obtained for a seismic source centroid closer to 7.5°N, suggesting a source process that extends into the northern half of the aftershock zone.

Earthquake size and duration. Since the late 1970s, seismologists have estimated magnitude M_w for large earthquakes in terms of the seismic moment M_o (*48*). As a measure of the average displacement integrated over the ruptured fault zone, M_o is associated with its behavior at zero frequency. It is therefore logical to estimate M_o from the amplitudes of the gravest Earth free oscillations, such as the modes ${}_0S_2$, ${}_0S_3$, ${}_0S_4$, ${}_0S_0$, and ${}_1S_0$. For nearly all earthquakes, these modes are excited too weakly for direct observation, but the Sumatra-Andaman event was different. The "football mode" ${}_0S_2$, the free oscillation with the longest observed period (53.7 min), is expressed strongly in vertical-component spectra computed from a large proportion of individual stations, as are many of the shorter-period modes. The amplitudes of several spheroidal free oscillations with periods $T >$ 1000 s were a factor of 1.25 to 2.6 larger than those predicted by the Harvard CMT source (*1*–*3*), reaching a maximum for the mode ${}_0S_2$ (Figs. 4 and 5). If this amplitude is related to fault motion with the same geometry as the CMT solution, i.e., thrusting on a shallow-dipping fault (8° dip), the estimated earthquake magnitude M_w increases from 9.0 to 9.3.

Source spectral amplitude is larger at long periods for earthquakes with long time durations. If seismic rupture progresses at a constant rate for a finite duration τ from a sharp onset to an equally abrupt termination, the source spectrum $M(f)$ equals $M_o(\sin \pi f\tau)/(\pi f\tau)$ as a function of cycle frequency f (*49*). The logarithm of $M(f)$ exhibits a low-frequency plateau that transitions to a power-law slope at a corner frequency $f_c = (\pi\tau)^{-1}$. Figure 5 graphs the source spectra implied by several spheroidal modes against $M(f)$ source spectra for constant-rupture durations $\tau = 800$ s and $\tau = 320$ s. Modal amplitudes do not follow the predictions of a constant-rate source spectrum, suggesting a variable rupture-propagation rate. For example, the rupture of two large fault

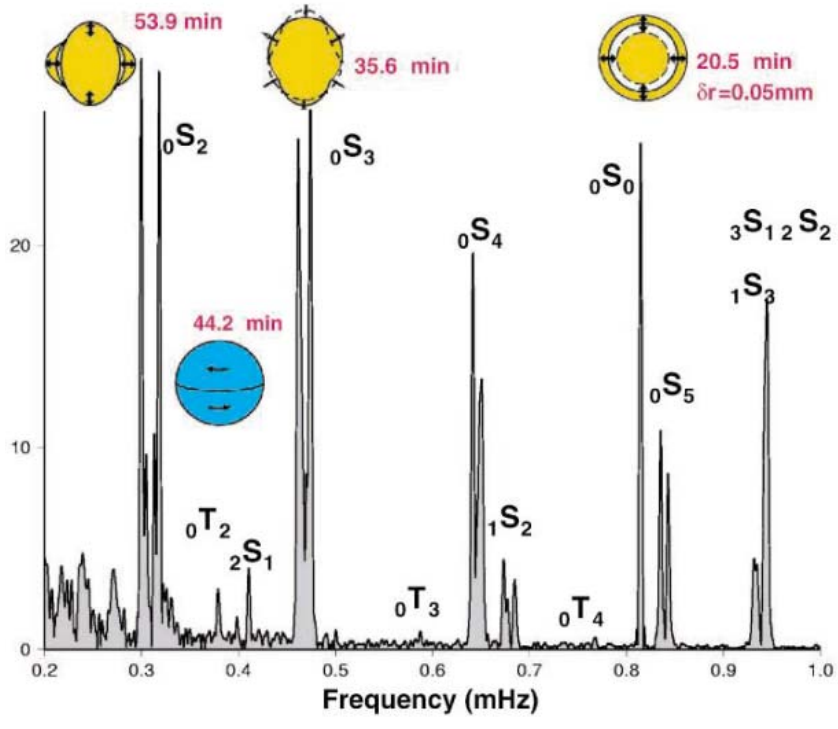

Fig. 1. Schematic of the motion of free oscillations ${}_0S_2$, ${}_0T_2$, ${}_0S_3$, and ${}_0S_0$ superimposed on a spectrum computed from 240 hours of vertical seismic motions recorded at the CAN (Canberra, Australia) station of the Geoscope Network. For comparison, fig. S1 plots the acceleration spectrum from the superconducting gravimeter collocated with CAN.

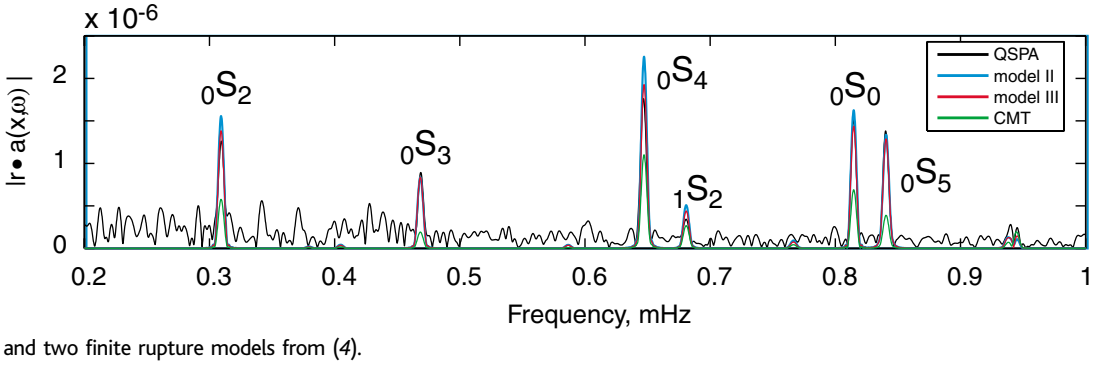

Fig. 2. Free-oscillation spectra for GSN station QSPA, whose sensor lies within an ice borehole in the quiet sector of the South Pole station. Only $m = 0$ free oscillations are nonzero at Earth's poles, leading to sharply defined single resonance peaks for modes ${}_nS_l$ and ${}_nT_l$ with period $T >$ 1000 s. A vertical-motion data series of 106 hours was analyzed. Predicted spectra are plotted with colored lines from Harvard CMT mechanism and two finite rupture models from (*4*).

segments with different orientations, onset times, and durations would cause spectral interference at long periods, as would a more complex rupture history. Such complexity aside, the trend of modal amplitudes is consistent with a rupture duration $\tau \leq 800$ s.

The initial phase of ${}_0S_0$ relative to the earthquake onset supports the inference of long-source duration τ. The initial phase of a free oscillation of period T aligns with the time centroid of the rupture process if the rupture duration is relatively small, i.e., $\tau \ll T$. Phase cancellation dampens the modal excitation if $\tau \geq T/2$, and the relation of modal initial phases with the source time centroid becomes complicated. We estimate the initial phase of ${}_0S_0$ to average 65° to 66° in the GSN and to average 61° over nine records from the Geoscope network (fig. S4). The initial displacement of ${}_0S_0$ is positive (0° phase), so this suggests a time centroid delayed 205 to 225 s relative to the earthquake onset. Rupture duration τ was between 400 and 450 s if the rupture rate were constant. The initial phase of ${}_1S_0$ is 115.7° averaged for nine Geoscope stations, consistent with a time centroid of 197 s. A variable rupture rate will cause scatter in time centroids estimated from different modes.

Free-oscillation observations constrain the Sumatra-Andaman earthquake source, but the constant-rupture model is too simple. A complex earthquake process is suggested by a number of observations, e.g., large bursts of high-frequency seismic radiation occurred in the first 200 s of rupture (*4*, *50*); aftershock locations spanned a 1300-km segment of plate margin (*5*), but in the northern 400 km of the zone the aftershocks commenced some 85 min after rupture onset (*51*); substantial surface-wave directivity at periods approaching 1000 s (*4*); the dip of the Sumatra-Andaman megathrust in its northern half tended to exceed the 8° dip of the Harvard CMT source mechanism (*5*); back-arc spreading in the Andaman Sea may have promoted the expression of strike-

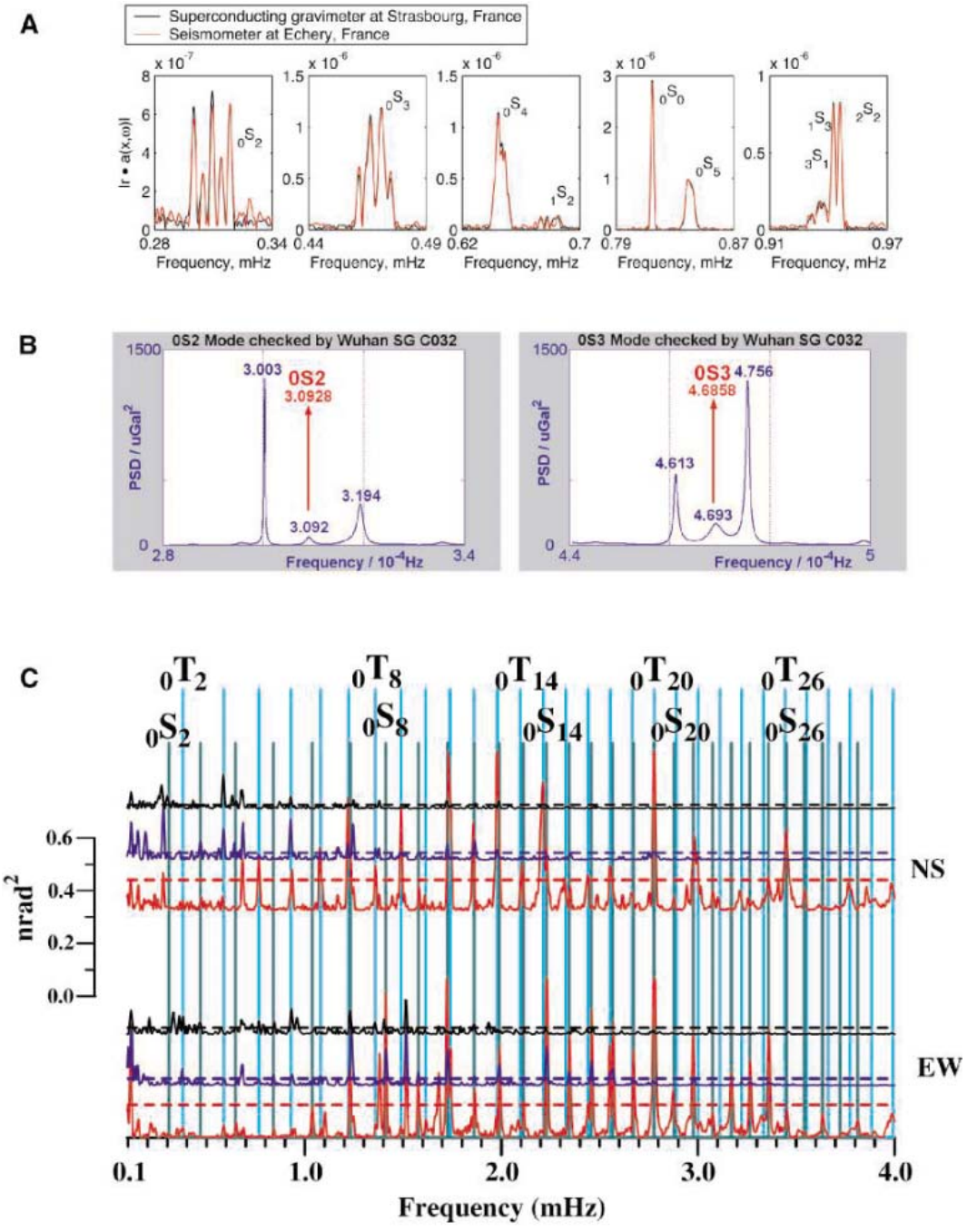

Fig. 3. Spectrum comparison for the 26 December 2004 Sumatra-Andaman earthquake. (**A**) Superconducting gravimeter (Strasbourg, France) and nearby vertical-component seismic data (Echery, France) have almost identical spectra. The multiple spectral peaks, e.g., of ${}_0S_2$, are caused by splitting associated with Earth rotation. A Hann taper has been applied to the 230-hours time series from both instruments before discrete Fourier transformation: (**B**) Burg-method spectrum estimates of data from the C032 superconducting gravimeter (SG) at Wuhan station, People's Republic of China, and (**C**) Blackman-Tukey-tapered spectral estimates of horizontal-component data from the Grotta Gigante pendulum tiltmeter, computed on three sliding time windows of 24 hours each, shifted by 12 hours. The red, blue, and black lines pertain to the windows starting at days 361.25, 361.75, and 362.25 of 2004, respectively. North-south motion is shown in top three traces; east-west motion is shown in the bottom traces. The broken line indicates the 95% confidence level at which a spectral peak is significant.

slip motion as the rupture progressed north (*5*); modeling suggests that the northern third of the fault zone contributed little to the observed tsunami (*5*). Many factors suggest that fault motion was larger and faster in the south of the fault zone, where rupture began, and was smaller and slower in the north.

Modeling the rupture. Drawing on inferences made from these data, we consider here two finite-rupture models based on body and surface waves [models II and III of (*4*)] in which rupture has longer duration (600 s versus 300 s), longer length (1300 km versus ~400 km), and larger moment (6.5×10^{22} N·m versus 4.0×10^{22} N·m) than that inferred from the CMT solution (Fig. 6). Both models prescribe a spatially varying fault geometry that is, on average, steeper than the CMT solution. A steeper fault is more efficient at exciting the long-period modes, and therefore the finite rupture models can greatly improve the match between predicted and observed modal amplitudes (*52*–*56*) with a far smaller M_o than inferred by (*3*). A transition to oblique thrust motion in the Andaman islands region improves the fit to long-period toroidal modes. Model III, which prescribes a peak rate of rupture propagation somewhat earlier than model II, is slightly more successful at predicting the absolute value of modal vertical-component spectral peaks, typically with an average misfit pf less than 10%, depending on the mode (Figs. 2, 7, and 8 and table S1).

Despite the rough success of a single seismic rupture model across the entire seismic spectrum, geodetic evidence for a slow component of Sumatra-Andaman displacement cannot be dismissed. A fault slip of ~1 hour in duration, as suggested by tsunami modeling for the Nicobar-Andaman fault segment (*5*), would excite seismic free oscillations inefficiently because of phase cancellation. Its signature would be expressed as a complex pattern of modal amplitude and phase anomalies. Modal spectra for the 2004 Sumatra Andaman earthquake are more difficult to predict with simple parameterized rupture models than modal spectra from the 28 March 2005 northern Sumatra earthquake ($M_w = 8.6$), despite higher signal-to-noise ratios in the larger event (Fig. 8). If amplitude and phase misfits leave unexplained 10% or more of the long-period free-oscillation amplitudes of the 2004 event, slow fault motion equivalent to at least $M_w = 8.4$ would be possible, a geophysical event larger than any earthquake between 1965 and 2001.

For both Sumatra earthquakes, modal amplitude and phase anomalies will constrain any additional long-term slip. In this context, the calibration and long-term resilience of global seismographic networks is paramount. A future megathrust earthquake ($M_w \geq 9.0$) is inevitable somewhere along Earth's plate boundaries but may occur after today's seismometers have begun to age and perhaps fail. The broadband vault seismometer most suitable for today's global seismographic networks, the Streckeisen STS-1 (*57*), is no longer manufactured. It is important for the international seismological community to consider designing the next-generation broadband seismic sensor.

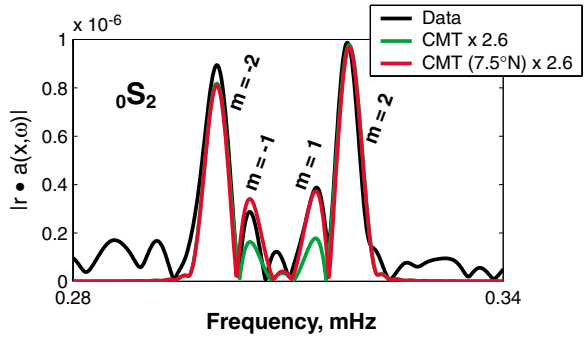

Fig. 4. Observed and predicted $_0S_2$ spectra at SCSN station OSI (Osito Adit, California). Black curve is data; red, prediction for the Harvard CMT mechanism and location but with scalar moment increased by a factor of 2.6. Note how the $m = 1$ and $m = -1$ singlets are too small, indicating that the CMT centroid is too close to the equator. Green curve is prediction for the CMT moment, increased by a factor of 2.6 and shifted to a centroid location at 7.5°N. This shift improves the fit to the $m = 1$ and $m = -1$ singlets. A Hann taper has been applied to the 144-hour time series.

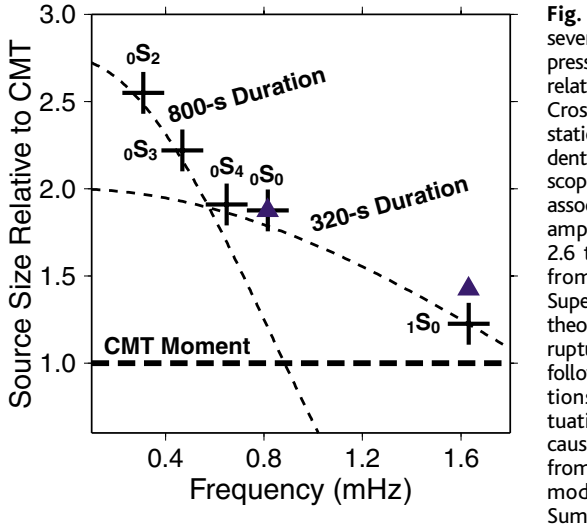

Fig. 5. The measured amplitudes of several long-period free oscillations, expressed in terms of their amplitude excess relative to the Harvard CMT solution. Crosses indicate estimates from GSN stations; triangles are estimated independently with the use of data from Geoscope stations. The largest amplification is associated with the mode $_0S_2$, whose amplitude seems to require roughly 2.6 times the CMT moment estimated from 300- to 500-s surface waves. Superimposed on the measurements are theoretical source spectra for constant-rupture sources of duration τ, which follow $\sin(\pi f\tau)/(\pi f\tau)$ dependence. Deviations in source geometry and fluctuations in rupture rate would cause cause the source spectrum to depart from this simple model. Nevertheless, modal excitation suggests that the Sumatra-Andaman earthquake involved fault slip on more than one time scale.

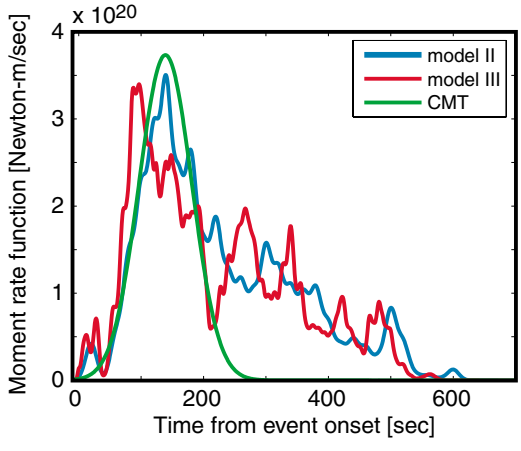

Fig. 6. Moment-rate functions (MRFs) for the 26 December Sumatra-Andaman earthquake. The MRF associated with the Harvard CMT is given by the green line, the MRF of finite-fault inversion II of (*4*) is denoted by the blue line, and the MRF of finite-fault inversion III of (*4*) is denoted by the red line.

References and Notes

1. G. Ekström, A. M. Dziewonski, N. N. Maternovskaya, M. Nettles, *Phys. Earth Planet. Inter.* **148**, 327 (2005).
2. Harvard CMT solutions can be accessed at www.seismology.harvard.edu/CMTsearch.html.
3. S. Stein, E. Okal, *Nature* **434**, 581 (2005).
4. C. J. Ammon *et al.*, *Science* **308**, 1133 (2005).
5. T. Lay *et al.*, *Science* **308**, 1127 (2005).
6. F. Gilbert, A. M. Dziewonski, *Philos. Trans. R. Soc. London Ser. A* **278**, 187 (1975).
7. R. Buland, J. Berger, F. Gilbert, *Nature* **277**, 358 (1979).
8. R. J. Geller, S. Stein, *Bull. Seismol. Soc. Am.* **69**, 1671 (1979).
9. J. P. Davis, *Geophys. Res. Lett.* **12**, 141 (1985).
10. D. Giardini, X. Li, J. H. Woodhouse, *Nature* **325**, 405 (1987).
11. M. Ritzwoller, G. Masters, F. Gilbert, *J. Geophys. Res.* **93**, 6369 (1988).
12. R. Widmer, G. Masters, F. Gilbert, *Geophys. J. Int.* **104**, 541 (1991).
13. G. Laske, G. Masters, *Nature* **402**, 66 (1999).

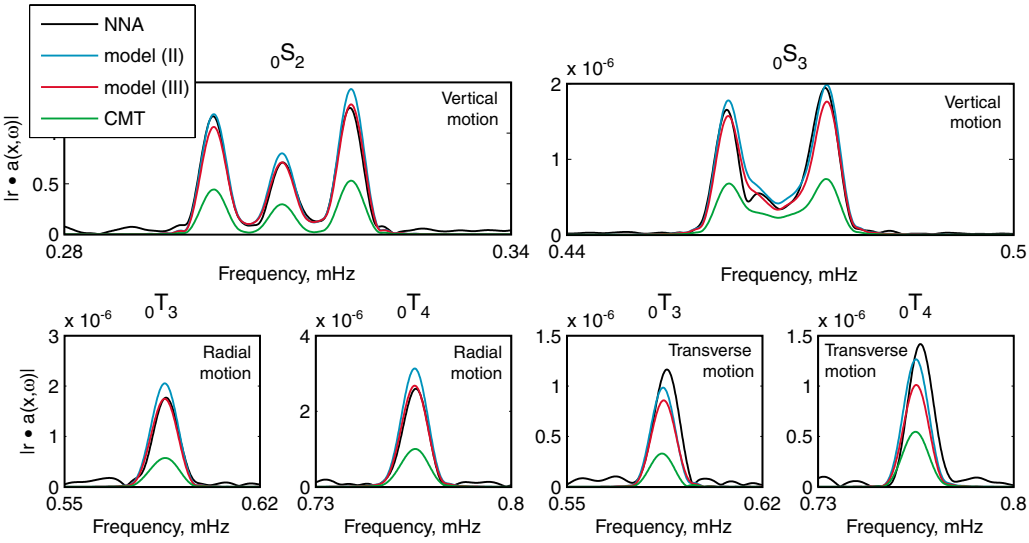

Fig. 7. Comparison of data (NNA, at Nana, Peru) and synthetics from various models. Low-order spheroidal modes $_0S_2$, $_0S_3$ at vertical component and toroidal modes $_0T_3$, $_0T_4$ at horizontal component are shown (**top**). A Hann taper is applied to 144-hours time series of vertical motion before discrete Fourier transformation. Similar tapering was performed on 44-hour time series of radial and transverse horizontal motion before discrete Fourier transformation.

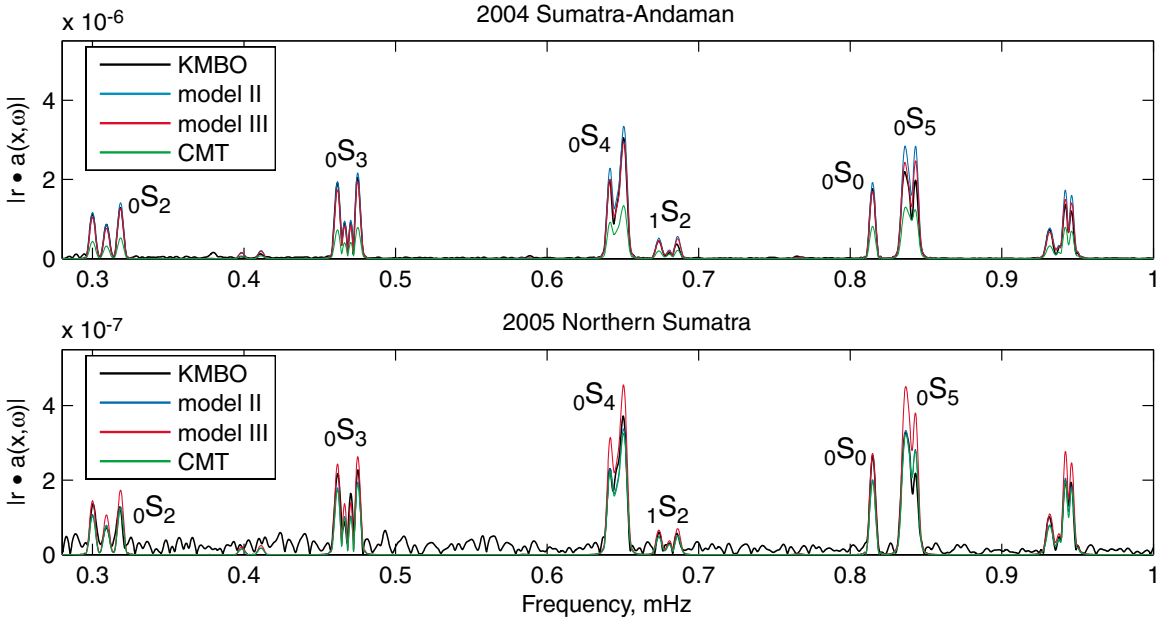

Fig. 8. Spectrum comparison for the 26 December 2004 Sumatra-Andaman and 28 March 2005 Northern Sumatra earthquakes using 127-hour records of vertical motion recorded at station KMBO (Kilima Mbogo, Kenya). Spectral predictions of the Harvard CMT solutions are graphed as well as spectra predicted from finite-rupture models from (*4*). Note the greater success of the CMT solution for the 2005 event, consistent with a smaller less complex rupture process.

14. M. Ishii, J. Tromp, *Science* **285**, 1231 (1999).
15. G. Roult, E. Clevede, *Phys. Earth Planet. Inter.* **121**, 1 (2000).
16. F. A. Dahlen, J. Tromp, *Theoretical Global Seismology* (Princeton Univ. Press, Princeton, NJ, 1998). A spherical reference model describes a nonrotating planet whose stress-strain relation is elastic and either is isotropic or else exhibits anisotropy with a radial axis of symmetry.
17. J. H. Woodhouse, *Geophys. J. R. Astron. Soc.* **61**, 261 (1980).
18. F. A. Dahlen, *Geophys. J. R. Astron. Soc.* **66**, 1 (1981).
19. J. Park, F. Gilbert, *J. Geophys. Res.* **91**, 7241 (1986).
20. P. Lognonne, B. Romanowicz, *Geophys. J. Int.* **102**, 365 (1990).
21. G. Backus, F. Gilbert, *Proc. Natl. Acad. Sci. U.S.A.* **47**, 362 (1961).
22. F. A. Dahlen, R. V. Sailor, *Geophys. J. R. Astron. Soc* **58**, 609 (1979).
23. H. V. Benioff, F. Press, S. W. Smith, *J. Geophys. Res.* **66**, 605 (1961).
24. N. F. Ness, J. C. Harrison, L. B. Slichter, *J. Geophys. Res.* **66**, 621 (1961).
25. L. E. Alsop, G. H. Sutton, M. Ewing, *J. Geophys. Res.* **66**, 631 (1961).
26. S. W. Smith, *J. Geophys. Res.* **71**, 1183 (1966).
27. G. Masters, J. Park, F. Gilbert, *J. Geophys. Res.* **88**, 10285 (1983).
28. W. Zürn, G. Laske, R. Widmer, F. Gilbert, *Geophys. J. Int.* **143**, 113 (2000).
29. B. A. Romanowicz, D. Giardini, *Science* **293**, 2000 (2001).
30. More information is available online at www.fdsn.org.
31. J. Park *et al.*, *Eos* **86**, 57 (2005).
32. R. Butler *et al.*, *Eos* **85**, 225 (2004).
33. More information is available online at www.iris.edu.
34. J. Park *et al.*, *Seism. Res. Lett.* **76**, 329 (2005).
35. G. Roult *et al.*, *Phys. Earth Planet. Int.* **113**, 25 (1999).
36. More information is available online at http://geoscope.ipgp.jussieu.fr.
37. N. R. Goulty, G. C. P. King, A. J. Wallard, *Nature* **246**, 470 (1973).
38. B. A. Bolt, R. G. Currie, *Geophys. J. R. Astron. Soc.* **40**, 107 (1975).
39. M. Zadro, C. Braitenberg, *Earth Sci. Rev.* **47**, 151 (1999).
40. The Grotta Gigante pendulum tiltmeter recorded both the 1960 Chile and the 2004 Sumatra-Andaman earthquakes.
41. M. Van Camp, *Phys. Earth Planet. Inter.* **116**, 81 (1999).
42. K. Nawa *et al.*, *Phys. Earth Planet. Inter.* **120**, 289 (2000).
43. X. Lei, H. Xu, H. Sun, *Chin. Sci. Bull.* **47**, 1573 (2002).
44. K. M. Larson, P. Bodin, J. Gomberg, *Science* **300**, 1421 (2003); published online 15 May 2003 (10.1126/science.1084531).
45. Free oscillations may be resolvable if GPS data from a global network are stacked and corrections for second-order ionospheric effects remove biases that are spatially broad; see (*58*).
46. To calibrate gravimeter and seismometer spectra, the free-oscillation spectral peaks must be corrected for the motion-induced gravitational forces on the seismic sensor (*16*). The breathing mode $_0S_0$ involves only motion parallel to Earth's radius, and the free-air correction to local gravity magnifies its apparent motion by 12%. For data from the Sumatra-Andaman earthquake, an apparent initial amplitude of 55 μm for $_0S_0$ shrinks to 49 μm after this correction. Similar corrections must be made for all modal amplitudes at frequencies f = 1000 s), including corrections for motion-induced accelerations associated with tilt and redistribution of Earth's mass. For instance, the true vertical motion of the football mode $_0S_2$ is 81.2% that computed from the seismometer response alone.
47. The instrumental self-noise of the broadband seismometers used in global seismic networks increases at low frequencies. Earth's gravest free oscillations have therefore been studied primarily with superconducting gravimeter data, not seismometer records, after correction for fluctuations in atmospheric pressure (*28, 59–61*). The signal-to-noise ratio for seismometer records of the 23 June 2001 Peru event (M_w = 8.4) was not high enough to allow the observation of hybridized toroidal modes on the vertical

seismic components, but they are evident for the 2004 Sumatra-Andaman earthquake.
48. T. C. Hanks, H. Kanamori, *J. Geophys. Res.* **84**, 2348 (1979).
49. S. Stein, M. Wysession, *An Introduction to Seismology, Earthquakes, and Earth Structure* (Blackwell Scientific, Malden, MA, 2003).
50. M. Ishii, P. Shearer, H. Houston, J. Vidale, *Nature,* in press.
51. R. Bilham, E. R. Engdahl, N. Feldl, S. P. Satyabala, *Seism. Res. Lett.,* in press.
52. Synthetics are computed according to normal-mode perturbation theory (*16*). Perturbations from a spherical nonrotating Earth model, such as rotation, ellipticity, and lateral heterogeneity are included. We adopt mantle model S20RTS (*53*) and crustal model crust2.0 (*54*) to account for lateral heterogeneity. The latest estimates of spheroidal and toroidal eigenfrequencies and quality factors are used in the calculation (*55*). Modal splitting and coupling due to rotation, ellipticity, and lateral heterogeneity are accounted for on the basis of a group coupling scheme using 36 subgroups of 117 modes below 3 mHz (*56*).
53. J. Ritsema, H. J. van Heijst, *Sci. Prog. (New Haven)* **83**, 243 (2000).
54. C. Bassin, G. Laske, G. Masters, *Eos* **81** (Fall Meeting Suppl.), F897 (abstr. S21A-03) (2000).
55. The Reference Earth Model Web site is at http://mahi.ucsd.edu/Gabi/rem.html.
56. A. Duess, J. Woodhouse, *Geophys. J. Int.* **146**, 833 (2001).
57. R. Pillet, N. Florsch, J. Hinderer, D. Rouland, *Phys. Earth Planet. Inter.* **84**, 161 (1994).
58. S. Kedar, G. A. Hajj, B. D. Wilson, M. B. Heflin, *Geophys. Res. Letts.*, *30*, 1829, doi:10.1029/2003GL017639 (2003).
59. W. Zürn, R. Widmer, *Geophys. Res. Lett.* **22**, 3537 (1995).
60. M. Van Camp, *Phys. Earth Planet. Inter.* **116**, 81 (2000).
61. S. Rosat, J. Hinderer, L. Rivera, *Geophys. Res. Let.*, *30*, 2111, doi:10.1029/2003GL018304 (2003).

62. This work was supported in part by NSF. Seismic waveform data from the Global Seismographic Network (funded by NSF and U.S. Geological Survey) were obtained from the Incorporated Research Institutions for Seismology (IRIS) Data Management System. Seismic waveform data was also obtained from the Geoscope Program (IPGP France) and the Southern California Earthquake Center.

Supporting Online Material
www.sciencemag.org/cgi/content/full/308/5725/1139/DC1
SOM Text
Figs. S1 to S5
Table S1

15 March 2005; accepted 29 April 2005
10.1126/science.1112305

REPORT

Periodically Triggered Seismicity at Mount Wrangell, Alaska, After the Sumatra Earthquake

Michael West,* John J. Sánchez, Stephen R. McNutt

As surface waves from the 26 December 2004 earthquake in Sumatra swept across Alaska, they triggered an 11-minute swarm of 14 local earthquakes near Mount Wrangell, almost 11,000 kilometers away. Earthquakes occurred at intervals of 20 to 30 seconds, in phase with the largest positive vertical ground displacements during the Rayleigh surface waves. We were able to observe this correlation because of the combination of unusually long surface waves and seismic stations near the local earthquakes. This phase of Rayleigh wave motion was dominated by horizontal extensional stresses reaching 25 kilopascals. These observations imply that local events were triggered by simple shear failure on normal faults.

After the great earthquake in Sumatra (*1*), local earthquakes spaced evenly in time occurred at Mount Wrangell, one of the world's largest andesite shield volcanoes. Located in south-central Alaska, Mount Wrangell anchors the eastern end of the Aleutian-Alaska chain of arc volcanoes (Fig. 1). Fumaroles, frequent seismicity, and historical steam plumes attest to Wrangell's active geothermal system (*2*). Because of its volcanic and seismic activity, a network of seismometers is jointly operated in the Wrangell area by the Alaska Volcano Observatory and the Alaska Earthquake Information Center. Surface waves from the moment magnitude (M_w) 9.0 Sumatra earthquake on 26 December 2004 propagated across the regional network and produced vertical trough-to-peak ground displacements of 1.5 cm. A swarm of 14 earthquakes near Mount Wrangell occurred during the passage of the Rayleigh waves (fig. S1), about 1 hour after the initial rupture in Indonesia (Fig. 2).

Six of the local events were large enough to be located. All of these were within 10 km of the summit caldera. The local signals were strongest near the summit at station WANC, suggesting even tighter clustering. Determination of precise locations and focal mechanisms was inhibited by the emergent waveforms and the modest four-station local network. With one exception, located events occurred at depths of 2 km or less. Magnitudes ranged up to local magnitude 1.9. The variation in waveforms and amplitudes, and the scatter in event locations, indicate that the triggered events were not coming from a single source but instead were dispersed around the summit. Some of the waveforms may be composites of more than one simultaneous event. Although 90% of the routinely located seismicity at Wrangell is of the long-period type (*3*), the events in the triggered cluster appear to have been high-frequency tectonic events (except for event 3, Fig. 2B).

Small earthquakes are common at Wrangell. A comparison to the two days before and after the Sumatra earthquake, however, shows a less than 1% probability of six randomly occurring events of any type in any 10-min window. This probability is further decreased by the requirement of magnitudes up to 1.9; high-frequency tectonic origin; even spacing between events; and coincident timing with teleseismic Rayleigh wave ground motion. Although these

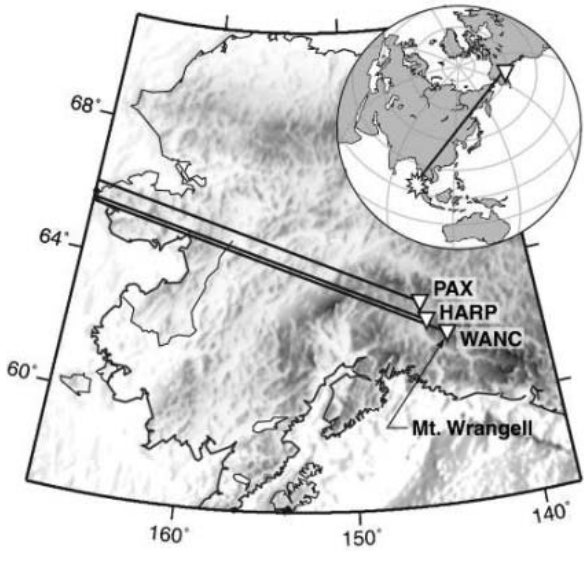

Fig. 1. Map with great circle paths from Sumatra to Mount Wrangell. Surface waves arrived at Wrangell from the west-northwest. Station WANC is at the summit of Wrangell. Three other short-period stations, including one three-component instrument (not shown), are located within 10 km of WANC. Stations PAX and HARP are nearby broadband instruments that are 115 and 72 km from WANC, respectively.

Alaska Volcano Observatory, Geophysical Institute, University of Alaska, Fairbanks, AK 99775, USA.

*To whom correspondence should be addressed. E-mail: west@gi.alaska.edu

additional constraints are hard to quantify formally, they remove any doubt about whether the timing of the local swarm and the Sumatran event could be coincidence.

Remotely triggered seismic swarms in volcanic and geothermal regions have been documented after numerous earthquakes. The first well-documented example of widespread triggering was the 1992 M_w 7.3 Landers earthquake, which initiated swarms at several locations in the western United States (*4*, *5*). The M_w 7.9 Denali earthquake in 2002 triggered swarms at distances up to 4000 km (*6*). The recent Wrangell episode demonstrates that great earthquakes can perturb geothermal and volcanic systems around the world.

The hydrothermal system at Wrangell has a history of being disturbed by earthquakes (*7*). The seismicity rate at Mount Wrangell dropped by 50% in the five months after the Denali earthquake (*3*). In the Denali case, static stress changes due to motion on the fault, less than 100 km away, present a plausible control on seismicity that cannot be invoked in the recent episode. No change in the seismicity rate has been observed since the Sumatra earthquake. Although different mechanisms may be at work in each period, the post-Denali changes indicate that the open hydrothermal system at Wrangell exists in a tenuous equilibrium.

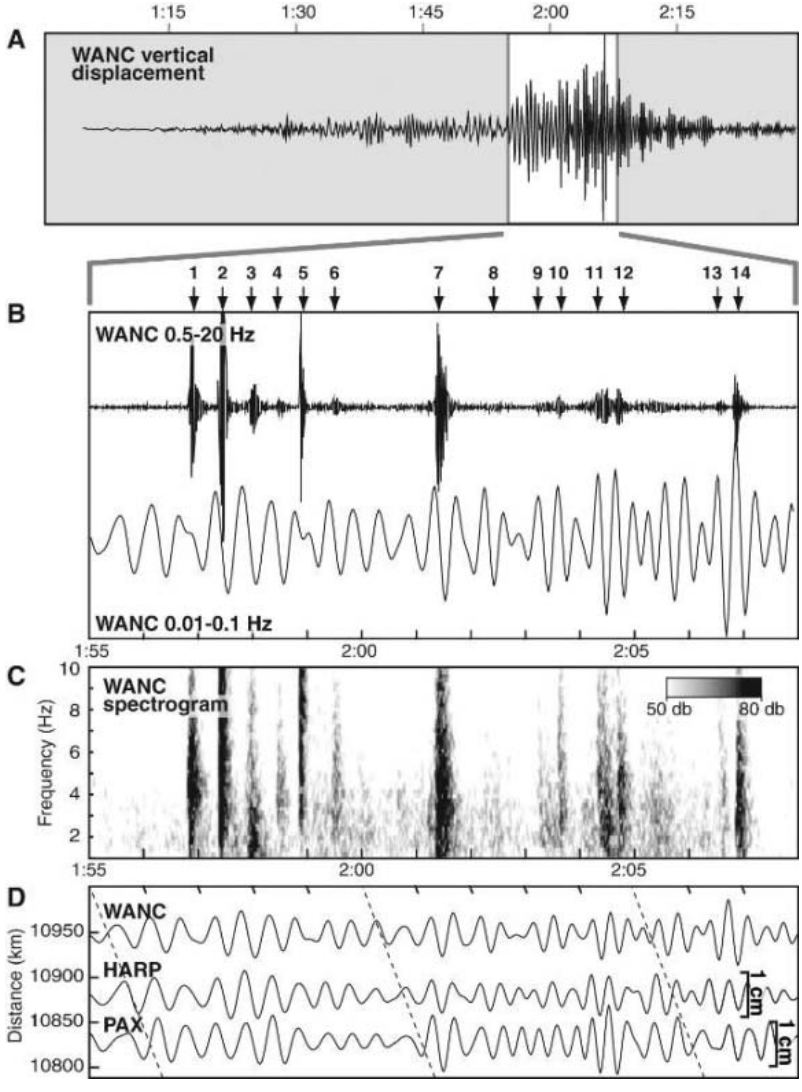

Fig. 2. Seismic records of the Sumatra earthquake and local events at Mount Wrangell. (**A**) Vertical component displacement record from short-period station WANC, plotted against universal time on 26 December 2004. Large-amplitude Rayleigh phases arrived in Alaska 1 hour after the Sumatra earthquake. (**B**) Expanded view of surface wave displacement at WANC. The upper record is filtered on 0.5 to 20 Hz to highlight high-frequency local earthquakes (indicated by numbers 1 to 14). The lower record is filtered instead on 0.01 to 0.1 Hz to show teleseismic ground motion. Large-amplitude vertical excursions of the teleseismic signal are correlated with the occurrence of local events. Estimates of true ground motion are unreliable at long periods for this short-period instrument. (**C**) Spectrogram showing frequency content of local events, obtained by applying a Fourier transform to 5-s windows of the WANC record. db, decibels. (**D**) Comparison of WANC displacement records to those from nearby broadband stations. Distances given are the distance to the station from the Sumatra earthquake epicenter. Dashed lines mark a time axis that has been skewed to adjust HARP and PAX records to appear as if they were recorded at WANC. HARP and PAX records are shifted by 24 and 37 s, respectively, corresponding to a velocity of 3.1 km/s. Scale bars mark the amplitude of displacement recorded at HARP and PAX. All three records show excellent phase correlation, affirming the reliability of short-period station WANC. The sensors at WANC, HARP, and PAX are a Mark Products L-4, a Güralp CMG-3T, and a Streckeisen STS-2, respectively.

The events at Mount Wrangell are distinguished from other remotely triggered swarms by the one-to-one correspondence between local earthquakes and cycles within the teleseismic wave train. All of the 14 Wrangell earthquakes that occurred during the passage of large-amplitude Rayleigh waves occurred during the same phase of the teleseismic waveform (Fig. 2B and fig. S2). The best comparison between local and teleseismic records was provided by station WANC (Fig. 2B). The 30-s surface waves were clearly recorded despite the 1-Hz natural frequency of the vertical short-period sensor. A formal instrument response correction was applied to the data. Conceptually, this correction consists of an amplification of several orders of magnitude and a phase shift of 180° for relatively long periods such as those described here (*8*). Because short-period instruments are not designed for interpreting teleseismic surface waves, we compared the corrected traces to nearby broadband instruments, each corrected for individual response. The broadband sensors were too far away to record the local swarm. They were essential, however, in verifying the short-period instrument response correction and providing more reliable ground motion amplitudes. This comparison demonstrates that the short-period instruments accurately captured the phase of the surface wave signal (Fig. 2D), despite a relative gain of less than 0.001 for 30-s periods relative to 1-s periods.

We compared the local events with the Sumatra earthquake by investigating the arrivals recorded at station WANC, with the caveat that event origin times may be 2 to 3 s earlier than their arrival times. A shift of 2 to 3 s will have a negligible effect on correlation with 20- to 30-s surface waves. We integrated the original velocity records to displacement for ease of visualization. All local events correlated with periods of positive vertical ground displacement. In addition, there is a correspondence between the amplitude of displacement and whether or not local events were triggered. Phases with amplitudes below 0.25 cm did not trigger events. Given the derivation described below, this corresponds to a threshold transient stress of ~8 kPa. An M_w 8.1 earthquake near the Macquarie Islands 3 days earlier produced stresses an order of magnitude lower and was not accompanied by anomalous earthquakes at Mount Wrangell.

The key to understanding these events was provided by nearby broadband, three-component seismometers that linked the events to teleseismic radial retrograde motion indicating Rayleigh waves (fig. S1). Shear and normal stresses work in tandem to promote faulting. Shear stresses alter the forces acting along fault planes, whereas normal stresses alter the confining pressure and friction across the faults. Alhough we do not know the orientation of faults deep within Mount Wrangell, analysis of the Rayleigh wave stress field can give insights into the faulting mechanism. We used a two-dimensional half-space model to estimate normal and shear stresses in the vertical and radial directions (*9*). We started with equations for particle displacement for a 30-s Rayleigh wave traveling with a phase velocity of 3.7 km/s. We calculated spatial derivatives to obtain strain and stress values across horizontal and vertical planes, using constitutive laws that assume a Poisson ratio of 0.25 and a shear modulus of 35 GPa (*10*) (figs. S1 to S3). The horizontal and vertical normal stresses, σ_{xx} and σ_{zz}, vary in phase with one another and are in phase with vertical ground displacement. Shear stresses σ_{xz} and σ_{zx} are out of phase by a quarter cycle and peak when the vertical displacement is 0. The exact stresses and depths vary greatly as a function of Rayleigh wave frequency and velocity structure. However, a few trends are clear. Near the surface, σ_{xx} is necessarily the only nonzero stress component (fig. S3). σ_{xx} diminishes with depth, whereas σ_{zz} increases until the two are equal in the mid-crust. The shear stresses, σ_{xz} and σ_{zx}, are zero at the surface and increase with depth. In a realistic Earth structure, stress concentrations will occur near subsurface boundaries; however, these basic trends remain. The events at Mount Wrangell occurred in the top few kilometers, suggesting that failure was controlled primarily by changes in the horizontal normal stress, σ_{xx}, which varied by up to ±25 kPa. Specifically, the events occurred during periods of extensional horizontal stress.

The apparent instantaneous initiation of earthquakes during periods of positive ground displacement constrains the possible mechanisms for triggered seismicity. The correlation suggests that triggering is not due to a cumulative stress effect over many cycles. Rather, the triggered events are the result of deformation over the preceding several seconds only. This is further confirmed by the observation that local events began immediately after the onset of large-amplitude Rayleigh wave displacements. Our favored explanation is simple shear failure. The correlation with extensional horizontal stress implies that the most favorable fault mechanisms are normal faults striking perpendicular to the direction of wave propagation (*11*). We do not have fault mechanism information to verify this possibility. However, the analysis of individual stress components provides a powerful tool for future studies in which fault mechanisms are known. Many different behaviors are encompassed under the broad label of triggering, and more than one mechanism is likely at work. In this case, however, the immediate failure of normal faults as a result of transient stresses can explain the features we observed.

An additional attraction to shear failure is its simplicity. In the case of Mount Wrangell, secondary effects involving fluid movement, bubbles, or crack weakening are not required. The events at Mount Wrangell occurred during phases of reduced confining pressure when faults were shifted closer toward failure. This does not explain how such minute stress changes are capable of stressing a fault to failure. After more than a decade of documented remote triggering episodes, it is clear that most occur in geothermal or volcanic systems, suggesting that high pore fluid pressures already maintain faults close to failure (*12–15*). The recent earthquakes are similar to prior triggering episodes in that high existing pore pressure may have primed fractures for failure in response to small transient stresses. The geothermal system at Mount Wrangell has a 50-year history of responding to large regional earthquakes and has demonstrated that small stress perturbations can drive substantial changes in fumarolic discharge (*7*).

Although the Mount Wrangell episode does not explicitly require the movement of pore fluids, a fluid pumping model may be compatible with our observations. In this model, a pressure increase squeezes fluids from interconnected pore space into nearby fault zones (*16*, *17*). The assumption of an extensive hydrothermal system is reasonable in light of persistent steam emissions from the summit of Mount Wrangell. Although increased pressure pumps the fluids according to Darcy's law, it is the total volume of fluid in the fault zone that would influence fault friction. The total fluid volume in the ensemble of fault zones is the integral of the flow. Thus, the maximum fluid content should lag roughly one-quarter phase behind the maximum pressure (Fig. 3). It is possible that such a fluid mechanism primes the fault zone, followed several seconds later by extensional stresses that trigger shear failure. The nonaligned phase relationship with triggered events, however, indicates that the fluid effect is a secondary factor, if it exists, and cannot solely explain the triggering.

The observations at Mount Wrangell are an especially clear case of what we suspect is a more general occurrence. The correlation was made clear by the unusually long-period surface waves and the close proximity of seismic stations. Analysis of existing data sets in light of this pattern may reveal phase correlation to be a powerful tool for identifying the mechanisms that control earthquake triggering.

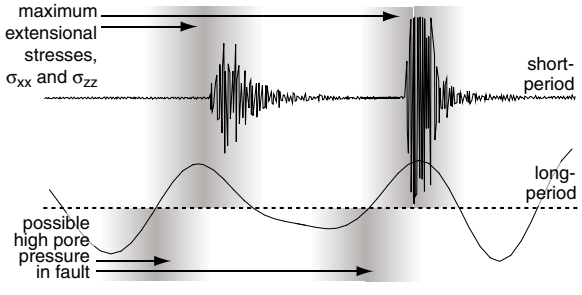

Fig. 3. Schematic showing the influence of trigger mechanisms relative to short- and long-period displacement records. The maximum extensional stresses are reached at the time of maximum vertical ground displacement. The secondary effect of high pore pressure due to fluid pumping into the fault zone may occur a quarter phase earlier. Although the flow into the fault zone peaks at the point of minimum displacement, the total volume of fluids in the fault would lag by roughly a quarter phase.

References and Notes

1. J. Park *et al.*, *Science* **308**, 1139 (2005).
2. G. M. Cross, G. K. C. Clarke, C. S. Benson, *J. Geophys. Res.* **94**, 7237 (1989).
3. J. J. Sanchez, S. R. McNutt, *Bull. Seismol. Soc. Am.* **94**, S370 (2004).
4. D. P. Hill *et al.*, *Science* **260**, 1617 (1993).
5. J. S. Gomberg, P. A. Reasenberg, P. Bodin, R. A. Harris, *Nature* **411**, 462 (2001).
6. S. G. Prejean *et al.*, *Bull. Seismol. Soc. Am.* **94**, S348 (2004).
7. C. S. Benson, G. Bender, R. J. Motyka, A. B. Follett, *Eos* **76**, 198 (1995).
8. K. Aki, P. Richards, *Quantitative Seismology* (University Science Books, Sausalito, CA, ed. 2, 2002).
9. J. Gomberg, S. Davis, *J. Geophys. Res.* **101**, 733 (1996).
10. Materials and methods are available as supporting material on *Science* Online.
11. C. Scholz, *The Mechanics of Earthquakes and Faulting* (Cambridge Univ. Press, Cambridge, ed. 2, 2002).
12. M. Cocco, J. R. Rice, *J. Geophys. Res.* **107**, 10.1029/2000JB000138 (2002).
13. S. Husen, S. Wiemer, R. B. Smith, *Bull. Seismol. Soc. Am.* **94**, S317 (2004).
14. J. E. Streit, S. F. Cox, *J. Geophys. Res.* **106**, 2235 (2001).
15. B. Sturtevant, H. Kanamori, E. E. Brodsky, *J. Geophys. Res.* **101**, 25 (1996).
16. E. E. Brodsky, E. Roeloffs, D. Woodcock, I. Gall, M. Manga, *J. Geophys. Res.* **108**, 10.1029/2002JB002321 (2003).
17. E. E. Brodsky, S. G. Prejean, *J. Geophys. Res.* **110**, 10.1029/2004JB003211 (2005).
18. This study was possible because of the combined seismic network efforts of the Alaska Volcano Observatory and the Alaska Earthquake Information Center. We also thank S. Prejean, J. Stachnik, J. Gomberg, S. Moran, and two anonymous reviewers. Supported by National Science Foundation grant no. EAR-0326083 and by the Alaska Volcano Observatory, a cooperative program between the U.S. Geological Survey Volcano Hazards Program, the Geophysical Institute at the University of Alaska Fairbanks, and the Alaska Division of Geological and Geophysical Surveys.

Supporting Online Material

www.sciencemag.org/cgi/content/full/308/5725/1144/DC1
Materials and Methods
Figs. S1 to S3

18 March 2005; accepted 25 April 2005
10.1126/science.1112462

Institutional Site License Available

Q What can *Science* SAGE KE give me?

A Essential online resources for the study of aging

SAGE KE – Science of Aging Knowledge Environment offers:

- Perspectives and Reviews on hot topics
- Breaking news stories
- A database of genes and interventions
- PDFs of classic papers

SAGE KE brings the latest information on aging related research direct to your desktop. It is also a vibrant virtual community, where researchers from around the world come together to exchange information and ideas. For more information go to www.sageke.org

To sign up today, visit promo.aaas.org/sageas

Sitewide access is available for institutions.
To find out more e-mail sagelicense@aaas.org

Science
SAGE KE
AAAS

A Cost of Long-Term Memory in *Drosophila*

Frederic Mery* and Tadeusz J. Kawecki

Two distinct forms of consolidated associative memory are known in *Drosophila*: long-term memory (LTM) and so-called anesthesia-resistant memory (ARM) (*1*, *2*). In the context of Pavlovian aversive olfactory learning, LTM will only form after repeated conditioning events separated by rest intervals (a spaced protocol), whereas ARM will also form if consecutive conditioning events immediately follow one another (a massed protocol) (*2*). LTM is more stable, but unlike ARM, its formation requires protein synthesis (*2*). LTM is thus likely to be energetically costly, but it is not clear if the additional energy demand has any effect on an animal's fitness.

We studied how induction of consolidated memory affects the resistance of adult flies to extreme stress imposed by an absence of food and water. We used an outbred wild-type *Drosophila melanogaster* line that has been artificially selected for improved memory and shows particularly good LTM (*3*). We trained the flies to associate an odor with an aversive mechanical shock (associative conditioning) (*4*). Five consecutive training sessions were either separated by 20-min intervals (the spaced protocol) or followed one another immediately (the massed protocol). Both protocols induced avoidance of the odor previously associated with the shock if flies were assayed 24 hours after conditioning (Fig. 1A). However, the response after the spaced protocol was dependent on protein synthesis (i.e., involved LTM), whereas the response after the massed protocol was not (Fig. 1A). In control experiments, other flies were either exposed to mechanical shocks without any odors (shock only) or exposed to both shocks and odors but not concurrently (nonassociative conditioning), which did not lead to formation of even short-term associative memory (Fig. 1A, red bars) (*4*).

We subjected each fly to one of seven conditions: associative massed conditioning (inducing ARM), associative spaced conditioning (inducing LTM), nonassociative conditioning (massed or spaced), shock only (massed or spaced), and untreated control. Directly afterwards, we assayed their individual desiccation and starvation resistance, measured as time until death in the absence of food and water (*4*). Despite exposure to the same shock and odors, flies conditioned in the associative spaced protocol died on average 4 hours (19%) earlier than flies subjected to nonassociative spaced conditioning ($F_{1,116} = 28.1$, $P < 10^{-3}$) (Fig. 1B). This effect was the same for males and females (interaction $F_{1,116} = 0.1$, $P = 0.74$). This difference might have been due to greater activity induced by associative conditioning, but video tracking of individual flies indicated no difference in locomotor activity (fig. S1). No difference in time to death under stress was observed for flies subject to associative versus nonassociative conditioning in the massed protocol, in which LTM is not formed ($F_{1,116} = 0.7$, $P = 0.42$) (Fig. 1B).

The earlier death of flies subjected to associative spaced conditioning, relative to those subjected to other conditioning treatments, is thus likely to reflect additional strain due to the formation and maintenance of LTM. Given the importance of resistance to desiccation and starvation in natural *Drosophila* populations (*5*, *6*), this result suggests that long-term memory has not only benefits but also ecologically relevant costs. Whether, and to what extent, natural selection favors improvements of memory will depend on the balance of the costs and benefits (*7*). Such costs may also help to explain why evolution has maintained ARM as another form of consolidated memory, distinct from LTM: Although LTM is more stable than ARM, it is also apparently more expensive.

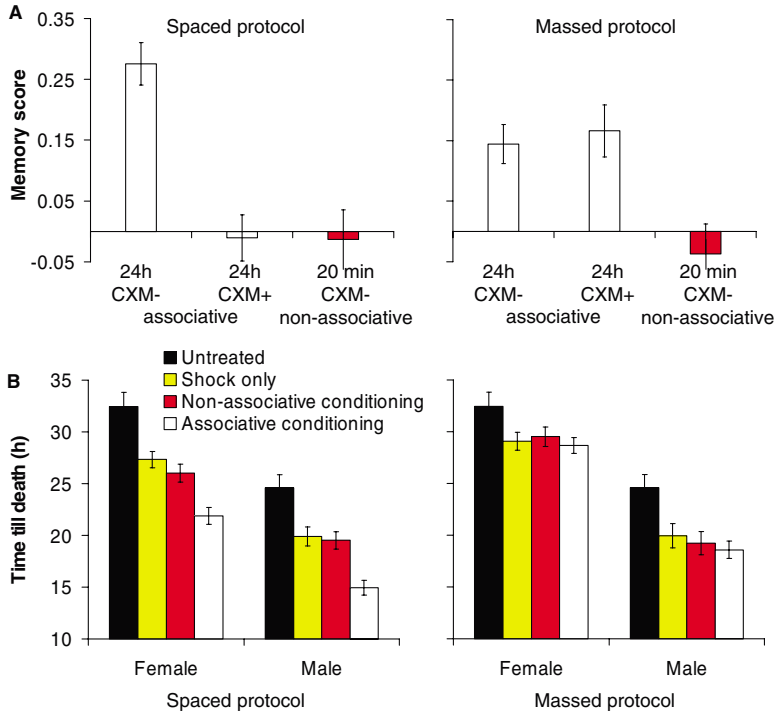

Fig. 1. (**A**) Olfactory memory (mean ± standard error; $n = 8$ replicate memory scores per treatment) induced by spaced and massed conditioning protocols. In both protocols, associative conditioning induced 24-hour memory in normal flies (CXM–), but treatment with the protein synthesis inhibitor cycloheximide (CXM+) erased the response after the spaced protocol only, showing that only this response is based on LTM. No associative memory was detectable 20 min after nonassociative conditioning (red bars). (**B**) Time until death in the absence of food and water (mean ± standard error) of flies subject to different conditioning treatments ($n = 30$ flies per treatment and sex).

References and Notes

1. G. Isabel, A. Pascual, T. Preat, *Science* **304**, 1024 (2004).
2. T. Tully, T. Preat, S. C. Boynton, M. Del Vecchio, *Cell* **79**, 35 (1994).
3. F. Mery, T. J. Kawecki, *Proc. Natl. Acad. Sci. U.S.A.* **99**, 14274 (2002).
4. Materials and methods are available as supporting material on *Science* Online.
5. D. Karan *et al.*, *Evolution* **52**, 825 (1998).
6. E. Nevo, E. Rashkovetsky, T. Pavlicek, A. Korol, *Heredity* **80**, 9 (1998).
7. J. E. Niven, M. Vähäsöyrinki, M. Juusola, *Proc. R. Soc. London Ser. B* (suppl.) **270**, S58 (2003).
8. We thank T. Preat and two reviewers for helpful comments and D. Meyer and S. Sutter for help with the video monitoring system. Supported by grant no. 3100A0-100387 from the Swiss National Science Foundation (T.J.K.).

Supporting Online Material
www.sciencemag.org/cgi/content/full/308/5725/1148/DC1
Materials and Methods
Fig. S1

22 February 2005; accepted 17 March 2005
10.1126/science.1111331

Section of Ecology and Evolution, Department of Biology, University of Fribourg, Chemin du Musée 10, CH-1700 Fribourg, Switzerland.

*To whom correspondence should be addressed. E-mail: frederic.mery@unifr.ch

Transcriptional Maps of 10 Human Chromosomes at 5-Nucleotide Resolution

Jill Cheng,[1]* Philipp Kapranov,[1]* Jorg Drenkow,[1] Sujit Dike,[1] Shane Brubaker,[1] Sandeep Patel,[1] Jeffrey Long,[1] David Stern,[1] Hari Tammana,[1] Gregg Helt,[1] Victor Sementchenko,[1] Antonio Piccolboni,[1] Stefan Bekiranov,[1] Dione K. Bailey,[1] Madhavan Ganesh,[1] Srinka Ghosh,[1] Ian Bell,[1] Daniela S. Gerhard,[2] Thomas R. Gingeras[1]†

Sites of transcription of polyadenylated and nonpolyadenylated RNAs for 10 human chromosomes were mapped at 5–base pair resolution in eight cell lines. Unannotated, nonpolyadenylated transcripts comprise the major proportion of the transcriptional output of the human genome. Of all transcribed sequences, 19.4, 43.7, and 36.9% were observed to be polyadenylated, nonpolyadenylated, and bimorphic, respectively. Half of all transcribed sequences are found only in the nucleus and for the most part are unannotated. Overall, the transcribed portions of the human genome are predominantly composed of interlaced networks of both poly A+ and poly A– annotated transcripts and unannotated transcripts of unknown function. This organization has important implications for interpreting genotype-phenotype associations, regulation of gene expression, and the definition of a gene.

The current classification of protein-coding and noncoding genomic regions is based on intron-exon structures of well-characterized protein-coding genes. Noncoding genomic regions, which account for 98% to 99% of the human genome, consist of introns found within protein-coding transcripts and the intergenic regions between them (*1*, *2*). Recent observations indicate that noncoding regions are transcribed into polyadenylated, stable RNAs that are transported into the cytosol during development (*3*–*8*). The ENCODE consortium has suggested transcripts of unknown function (TUFs) as an unofficial name for these unannotated transcribed regions (*9*). Transcribed fragments (transfrags) are used to denote array-detected regions of transcription (*3*–*5*) representing exons of both well-characterized protein-coding genes and TUFs.

Although our understanding of poly A+ cytosolic TUFs has increased, much less is known about the synthesis sites of transcripts lacking 3′ polyadenylation (poly A–). Replication-dependent histone genes are currently considered to be the only transcripts synthesized exclusively as poly A– transcripts (*10*). However, 30 years ago, Milcarek *et al.* reported that approximately 30% of rapidly labeled polysomal-associated RNA in actinomycin D–inhibited HeLa cells was poly A– (*11*). Similarly, Salditt-Georgieff *et al.* reported that there were three times as many transcripts with 5′ cap structures as poly A+-containing transcripts localized with polysomes of Chinese hamster cells (*12*). Later studies revealed that many genes are transcribed as poly A+ RNAs, which under specific conditions are processed to reduce or totally remove the 3′ poly A sequences. Such RNAs are called "bimorphic" transcripts (*13*). The distribution of poly A+ and poly A– transcripts between the nucleus and cytosol is also relatively unexplored.

In this report, we examined approximately 30% of the human genome encoded in 10 human chromosomes (6, 7, 13, 14, 19, 20, 21, 22, X, and Y) and mapped the sites of transcription for poly A+ cytosolic RNA derived from eight cell lines. For one cell line (HepG2), maps were constructed for cytosolic and nuclear poly A– and poly A+ transcripts. The full-length structures of many TUFs have been determined by employing a rapid amplification of cDNA ends (RACE) technique and resolving the RACE products by using high-density arrays. These studies indicate that previously considered "junk" genomic regions encode multiple overlapping poly A+ and poly A– coding transcripts and TUFs.

Overview of sites of transcription of cytosolic poly A+ RNAs along 10 human chromosomes. High-density arrays using 25-mer oligonucleotides spaced every 5 bp on average (i.e., 20-bp overlap) provided an interrogation resolution at least seven times as high as that of previous studies (*3*–*6*, *14*). The consequences of conducting array-based interrogations every 5 bp include increased likelihood of detecting exons of shorter length, increased statistical confidence in determining whether a region is transcribed, and identification of specific hybridization patterns characteristic of 3′ ends of transcripts (fig. S1).

Five male and three female cell lines were selected as sources for mature (i.e., post-spliced) cytosolic poly A+ RNA. Maps were constructed with the lowest likelihood of signals being derived from cross-hybridization. Transfrag sequences that overlapped with pseudogene sequences or contained low-complexity repeat sequences were removed (*15*).

Approximately 9% of 74,180,611 total probe pairs detected transcription per cell line and per chromosome. Average positive probe percentiles for individual chromosomes ranged from 7.1% [chromosome (chr) 13] to 14.6% (chr 19) (table S1A). This number increased to 16.5% for a cumulative map, referred to as a "1 of 8 map" in which a positive probe must appear in at least one of eight cell lines. This is consistent with our previous results from chromosomes 21 and 22 (*3*). The average number of transfrags found per cell line and per chromosome was observed to be 16,864 (table S1B). The average and median lengths of observed transfrags were 115 and 78 nucleotides, respectively (table S1C). The number of transfrags increases to 31,443 in the 1 of 8 map, yet the average length of a transfrag, 124 bp, remains approximately the same.

On average, 18,694,360 nucleotides (4.9% of interrogated genomic nucleotides) are transcribed as cytosolic poly A+ RNA derived from 10 chromosomes of each cell line. In the 1 of 8 map, the number of transcribed cytosolic poly A+ nucleotides increases to 38,656,627 (10.1%). The 2.1-fold difference (4.9% versus 10.1%) indicates that a considerable proportion of the detected transcription is cell-line specific. This observation is consistent with earlier findings (*4*).

Correlation of detected sites of transcription with current genome-wide annotations. Maps created by using poly A+ cytosolic RNA from eight cell lines were compared with annotations from the University of California–Santa Cruz (UCSC) genome browser database (*16*, *17*). We found that 56.7% of the detected cytosolic poly A+ sequences from the 1 of 8 map do not overlap with any well-characterized exon, mRNA, or expressed sequence tag (EST) annotation (Fig. 1). With the exception of chromosomes 13, 19, and Y, the remaining seven chromosomes have similar proportions of assignment

[1]Affymetrix Inc., Santa Clara, CA 95051, USA. [2]Office of Cancer Genomics, National Cancer Institute, Bethesda, MD 20892, USA.

*These authors contributed equally to this work.
†To whom correspondence should be addressed. E-mail: tom_gingeras@affymetrix.com

of transcribed nucleotides to the unannotated category. Annotation-dense chromosome 19 has a lower proportion of detected unannotated (33.4%) transcripts, with the smallest amount of detected transcribed unannotated sequences in the intergenic regions (13%). Chromosomes 13 and Y have higher proportions (69.5% and 80.3%, respectively) of unannotated transcribed sequences, most of which originate from intergenic regions. In general, the genomic positions of transcribed regions track with gene and exon densities for each of the chromosomes (fig. S2). With the exception of chromosomes Y and 19, 56.8% to 77.7% of detected transcribed regions (1 of 8 composite analysis) are derived from within genes (exons and introns). Overall, 31.8% of detected transcription originates from unannotated intergenic regions. The remainder of the 42% to 49% of the observed unannotated cytosolic poly A+ transcription is derived from the intronic regions within genes (26%) (Fig. 1).

Estimates of the fraction of positive probes interrogating well-characterized exons reveal a tendency toward a bimodal distribution with all probes being "on" (>90%) or "off" (<10%) (fig. S3). Approximately 68% of well-characterized exons (58,984) fall within one of the two peaks. Exons with partial positive probe coverage (i.e., >10% and <90%) may represent alternative exon structures compared with those described in the current annotation collections. Alternatively, the lack of correspondence between some of the exon annotations and detected transfrags may be attributed to inaccuracies in transfrag generation, sequencing errors, or misassembly of the human genome (*18*).

Figure S4 estimates the degree of cell-line-specific transcription by plotting the percentage of total nucleotides within known or novel transfrags against the number of cell lines expressing that transfrag. Two dominant populations of transfrags emerge: those expressed in one or two cell lines and those expressed in all cell lines.

Characterization and structure of transcripts containing unannotated transfrags. A combination of RACE, high-density arrays, and cloning/sequencing techniques was used to characterize transcripts containing unannotated transfrags (*15*) (fig. S5). Of 768 randomly selected unannotated transfrags, 634 (82.6%) yielded a set of 5′ and/or 3′ RACE products (table S2). Of these 768 regions, 438 (57.0%) yielded successful 5′ and 3′ RACE products on at least one genomic strand, and 467 (60.8%) show evidence of transcription on both strands. Thus, approximately 61% of surveyed loci show evidence of overlapping transcription on the positive and negative strands of the genome.

Among the 438 transfrags where 5′ and 3′ RACE were successful, 86 reside in intergenic regions, 145 reside in intronic regions, and 207 are adjacent to exons on either strand. To better understand the structure of putative novel transcripts found by RACE, 661 strand-specific RACE groups derived from the 438 index transfrags were analyzed against annotations of known genes and ESTs (Fig. 2) (*15*). Of these, 547 RACE groups contain transfrags that overlap annotations on the sense or antisense strand, 51 groups reside entirely within the intergenic regions, and 63 groups reside entirely within introns of known genes on the sense or antisense strand. Of the 547 RACE groups overlapping annotations, 118 groups contain transfrags that are nearly identical to annotated exons and, thus, are potential novel isoforms of known genes. The other 429 RACE groups contain transfrags that partially intersect annotations, representing transcripts that overlap with the well-characterized coding transcripts on either the sense or antisense strand. For RACE groups that overlap exons or reside within introns, approximately equivalent numbers were found to be sense or antisense to annotations. Overall, 44% of detected RACE-group transcripts are paired with at least one transcript present on the opposite strand. These results, combined with the entire RACE analysis, provide a consistent picture of overlapping transcription in the human genome (fig. S6).

Reverse transcription polymerase chain reaction (RT-PCR) was conducted on 250 (57%) of the 438 genomic loci that produced 5′ and 3′ RACE products from at least one genomic strand. A total of 217 (87%) regions yielded successful RT-PCR products, and 178 cDNA clones were isolated from 107 of the 217 regions. An example of one intergenic unannotated TUF is depicted in fig. S7.

The average length of the isolated transcripts is 680 nucleotides (range 173 to 4650 nucleotides), which are distributed over a range of 173 to 115,020 nucleotides in the genome. Of the 178 cloned transcripts, 114 (64%) are spliced, with an average of 3.2 exons per transcript and an average exon length of 238 nucleotides. Of the 178 characterized transcripts, 65% have a coding capacity of less than 100 amino acids.

Fifty-four percent of the spliced transcripts use canonical splice sites (GT/AG). Many of the noncanonical splice sites are previously characterized alternative splicing signals. However, a total of 26 (14.6%) of the spliced cDNAs were obtained from antisense transcripts, which are exact reverse complements of sense transcripts. Figure S8 illustrates three transcribed regions with mirror complementary sense and antisense transcripts pairings. Such

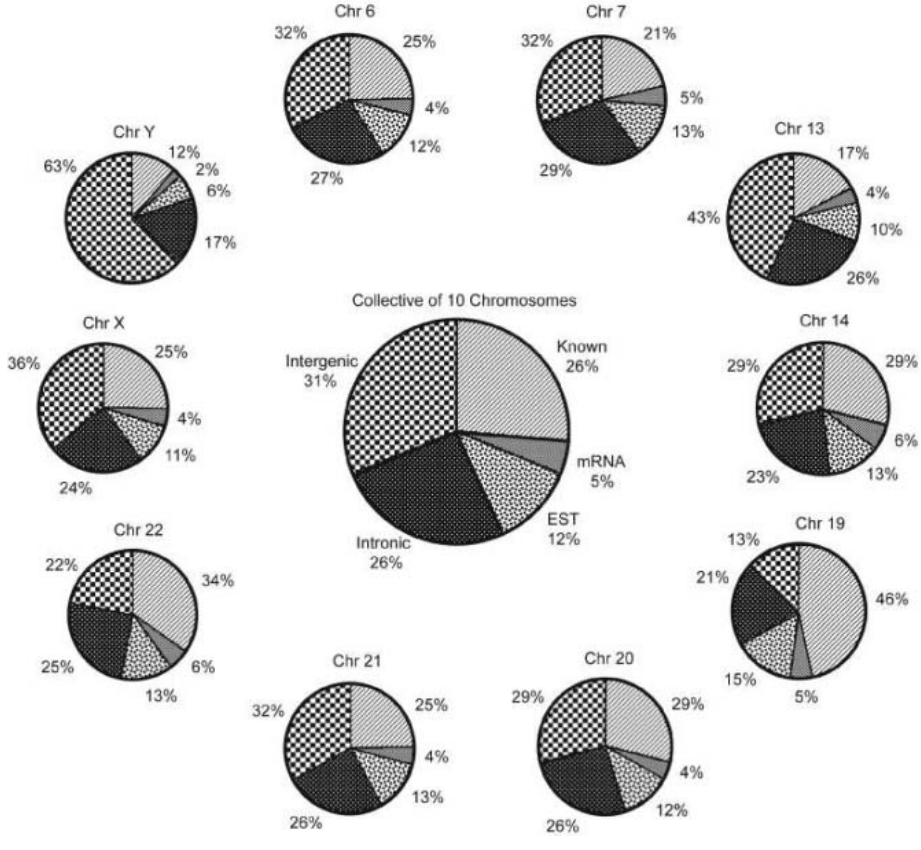

Fig. 1. The correlation of detected transcription in one of eight cell lines to annotations along each of the 10 chromosomes is shown for each chromosome individually and as a collective of all chromosomes. The detected transcription was determined using poly A+ cytosolic RNA from each of the eight cell lines. The annotations used in this correlation are defined in (*15*). The pattern code used in the central pie chart is used in all other pie charts.

complementary transcript pairs have been observed for well-characterized coding genes (*19*).

Poly A+ and A– transcripts and their distribution in the nucleus and cytosol. From the HepG2 cells, 58,874,113 (15.4%) nonredundant nucleotides were detected as transcribed and stable poly A+, poly A–, or bimorphic RNAs isolated from nuclear or cytosolic compartments. All analyses describing the proportions of poly A+, A–, and bimorphic transcribed sequences are based on 58,874,113 bp as a denominator, unless otherwise described. This percentage (15.4%) is nearly an order of magnitude greater than expected from the annotated exons and gene prediction. Fig. S9A illustrates the overlapping and nonoverlapping relationships among the four RNA samples. The comparisons of the four RNA samples result in 15 such relationships, of which 6 represent exclusive nuclear or cytoplasmic and poly A+ and poly A– groupings (Table 1A and fig. S9). The number of transcribed nucleotides and percentage of the total transcribed sequence of the nonrepeat sequences of 10 chromosomes is shown for each of the unique and overlapping poly A+ and A– categories of the relationships (Table 1A). Several of the overlapping relationships (2, 3, 6, 7, 8, 11, 12, 14, and 15) signify that the same detected sequences appear to be bimorphic with respect to the presence of poly A+ and A– sequences (Table 1B). The detected transcribed nucleotides present in poly A+ RNA samples (fig. S9B) and poly A– samples (fig. S9C) and the transfrag sequences found exclusively in the nucleus (fig. S9D) and cytosol (fig. S9E) reveal several characteristics of the composition and compartmentalization of the human transcriptome.

(i) Overall, there are about 2.2 times as many uniquely poly A– (43.7%) transcribed sequences as uniquely poly A+ (19.4%). Thus, 63.1% of the detected transcribed nucleotides are uniquely poly A+ or A– (Table 1B), with 36.9% comprising the bimorphic class of transcripts.

(ii) A large proportion of the sequences found in the nuclear and cytosolic compartments appears to be exclusive to these compartments. The amount of poly A+ sequences (9.7%) exclusively detected in the nucleus is less than one-third the amount of poly A– sequences (31.0%) (Table 1A). Bimorphic detected sequences found exclusively in the nucleus amount to 10.6%. Approximately 25% and 34% of poly A+ nuclear sequences (9.7%) are associated with well-annotated exons and introns, respectively (Fig. 3). The remaining 41% are associated with unannotated intergenic regions of the genome. In total, 75% of the exclusively nuclear-detected poly A+ sequences (9.7%) are unannotated. Similarly, 18% and 57% of poly A– exclusive nuclear sequences (31.0%) are associated with well-characterized exons and introns, respectively, whereas the remaining 25% are located in unannotated intergenic regions of the genome. These data indicate that 82.0% of the exclusive nuclear poly A– sequences are unannotated.

Poly A+ (3.1%) sequences exclusively detected in the cytosol are less than half as abundant as detected poly A– (6.5%) sequences (Table 1A). Bimorphic detected sequences found exclusively in the cytosol amount to 0.6%. About 43% and 22% of poly A+ cytosolic sequences (3.1%) are associated with well-annotated exons and introns, respectively (Fig. 3). The remaining 34% are associated with unannotated intergenic regions of the genome. In total, 56% of the exclusively cytosolic-detected poly A+ sequences (3.1%) are unannotated. We find that 16% and 36% of poly A– exclusive cytosolic sequences (6.5%) are associated with well-characterized exons and introns, respectively, whereas the remaining 48% are located in unannotated intergenic regions of the genome. A total of 84.0% of the exclusive cytosolic poly A– sequences are unannotated.

(iii) A comparison of exclusively nuclear or cytosolic transcribed nucleotides shows a five-

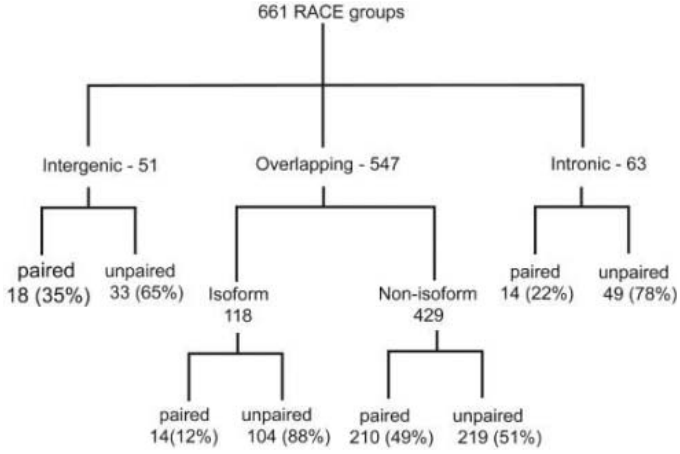

Fig. 2. A hierarchical tree describing the relationship among the RACE/array profiles derived from unannotated, array-detected regions and the annotations. A combined 5′ and 3′ RACE profile from each strand was treated as a separate RACE group. A RACE/array profile for each group is scored "intergenic" if it never overlaps the bounds of a known gene or any other annotation, including an EST; "overlapping" if it overlaps any annotation; or "intronic" if it is confined to the bounds of a known gene but does not overlap an annotation (*15*). "Paired" is defined as overlapping transcripts based on the RACE/array analysis. An overlapping group is further classified into "isoform" or "nonisoform" based on the precision of RACE/array alignment with the exon-intron boundaries of known genes. If a RACE/array profile resembles at least one annotated exon boundary, it is considered an isoform of a known gene.

Table 1. Number and percentage of transcribed nucleotides detected in nucleus and cytoplasm as poly A+ and A– RNA.

A.

Compartment	Description	Nucleotides	% Total
1	Unique to cytosolic A− (CyA−)	3,847,281	6.5%
9	Unique to nuclear A− (NuA−)	18,237,769	31.0%
13	Unique to cytosolic A+ (CyA+)	1,835,709	3.1%
5	Unique to nuclear A+ (NuA+)	5,706,194	9.7%
4	Unique to CyA− and NuA−	3,662,746	6.2%
15	Unique to CyA− and CyA+	349,320	0.6%
12	Unique to NuA− and CyA+	346,798	0.6%
10	Unique to CyA+ and NuA+	3,890,530	6.6%
14	Unique to NuA− and NuA+	6,263,761	10.6%
2	Unique to CyA− and NuA+	417,273	0.7%
8	Unique to CyA− and NuA− and CyA+	431,597	0.7%
3	Unique to CyA− and NuA− and NuA+	1,839,537	3.1%
11	Unique to NuA− and CyA+ and NuA+	3,219,788	5.5%
6	Unique to CyA− and CyA+ and NuA+	1,314,159	2.2%
7	Unique to Cy A− and NuA− and CyA+ and NuA+	7,511,651	12.8%
Grand total	All four compartments combined	58,874,113	100.0%

B.

Compartments	Description	% Total
1+13+15	Sequences detected only in cytoplasmic fraction	10.2%
5+9+14	Sequences detected only in nuclear fraction	51.3%
5+13+10	Sequences detected only in A+ RNA	19.4%
1+9+4	Sequences detected only in A− RNA	43.7%
15+12+14+2+8+3+11+6+7	Sequences detected in both A+ and A− RNA	36.9%

fold difference in sequence complexity detected in the nucleus (51.3%) compared with the cytoplasm (10.3%) of HepG2 cells (fig. S9, D and E). Such a difference is expected given the enrichment of transcribed intron sequences that appear to remain in the nucleus. The Werner (syndrome) helicase-interacting protein 1 (WHIP1) (*20*) on chromosome 6 illustrates how the intronic and exonic sequences of this gene are enriched in the nucleus and cytoplasm, respectively (fig. S10A). Transcribed intronic sequences, however, are not always found to be enriched in the nucleus. Serine (or cysteine) proteinase inhibitor, clade D (heparin cofactor) (*21*), member 1 on chromosome 22 is an example of a gene in which the intronic transcription detected in intron 4 is enriched in the cytosol, although other intron sequences for this gene are enriched in the nucleus (fig. S10B).

On a chromosomal scale, maps identifying the locations of transcription of poly A+ and A– transcripts found in the nucleus and cytosol provide a set of interesting contrasts (Fig. 4). Paired density plots were computed using a 60-kb sliding window for nuclear poly A+ and A– versus cytosolic poly A+ and A– transcribed regions, cytosolic and nuclear poly A+ versus cytosolic and nuclear poly A–, and well-characterized annotations. These maps provide two overriding impressions. First, at the resolution of 60,000 bp, the density of the synthesis sites of poly A+ and A– transcripts found in the nucleus and cytosol generally reflects the annotation density for each of the 10 chromosomes. However, several annotation-dense regions on chromosomes 6, 7, 13, and 21 appear to be more sparsely transcribed in the HepG2 cell line. Second, the annotation densities and detected transcribed regions differ in many positions along each chromosome, which indicates that additional regions of transcription are observed in annotation-dense locations. The chromosomal map positions for poly A+ and A– designated transfrags are shown in table S3.

(iv) The exclusively poly A– and a portion of the bimorphic transcripts found in the nucleus and cytosol would most likely not be identified with customary cDNA cloning approaches. Interestingly, almost half of the exclusive cytosolic poly A– detected transcripts (6.5% of the total detected) and a quarter of the exclusive nuclear poly A– transcripts (31.0% of the total detected) appear to be derived from intergenic regions of the genome. Thus, intergenic noncoding regions of the genome are a rich source of transcripts that are predominantly unannotated and underrepresented in our understanding of the composition of the transcriptome. Evaluation of the protein coding potential of poly A– transcribed sequences awaits efficient methods to copy and clone these types of transcripts.

Conclusions. Recent empirical experiments have provided consistent evidence that a larger percentage of the human, mouse, fly, and *Arabidopsis* genomes are being transcribed than can be accounted for by the current state of genome annotations. These observations were first described in tiling array-based studies that searched large parts or entire genomes for sites of transcription (*3*, *4*, *6*, *22–24*) and then by approaches aimed at isolation and characterization of full-length cDNAs (*25–29*) and of shorter cDNAs (ESTs and serial analysis of gene expression tags) (*19*, *30*, *31*). These studies used primary tissues and cell lines as RNA sources. Collectively, these empirical and computational observations point to several underappreciated characteristics of the human transcriptome.

(i) The human transcriptome is composed of an interlaced network of overlapping transcripts. The use of arrays in combination with 5′ and 3′ RACE reactions indicates that transcripts encoded on both strands often use the same sequences. Such overlapping transcription is observed in almost 50% of the investigated cases (Fig. 2 and figs. S6 and S8). We believe this estimate to be an underrepresentation. Striking examples of this class are pairs of complementary RNA molecules that appear to use both canonical (GT/AG) and complementary to canonical (CT/AC) signals at their splice junctions. The possibility that cDNA clones derived from the complementary transcripts came only from the sense strand was shown to be unlikely, because subsequent strand-specific RT-PCR reactions have produced cDNA products of expected lengths from the noncoding strand.

The existence of such complementary transcripts raises the question of how such transcripts are produced. One possibility is that the human cell-splicing machinery uses complementary sequences as alternative signals. This seems unlikely given the extent to which the consensus signals are missing from the same transcripts. A second possibility is that these transcripts are cRNA copies synthesized by an RNA-dependent RNA polymerase (RdRP). Such activity has been associated with the synthesis of small interfering RNAs that act as trans-acting regulatory molecules in *Arabidopsis* and *C. elegans* (*32*, *33*). Thus, this second possibility predicts that RdRP activities are likely to be found in human cells.

A second implication of the extensive transcription observed in unannotated genomic regions relates to the genotype-phenotype correlations. Such correlation experiments will require extensive analysis of the transcriptional activity of regions mapped as possible loci for genetic mutations.

(ii) Poly A– RNAs potentially comprise almost half of the human transcriptome. A variety of radiolabeling and sequence complexity studies have indicated that, in addition to histone mRNA transcripts, a large class of poly A– transcripts exists in human cells (*11–13*, *34*, *35*). The majority of studies using in vitro translation approaches, however, have not supported the idea of a separate set of protein products derived from the poly A– RNA fraction (*36*). Our results indicate that transcribed sequences exclusively associated with poly A– transcripts are twice as abundant as sequences transcribed exclusively as poly A+.

Of the exclusive poly A– sequences found in nuclear and cytosolic compartments (43.7%

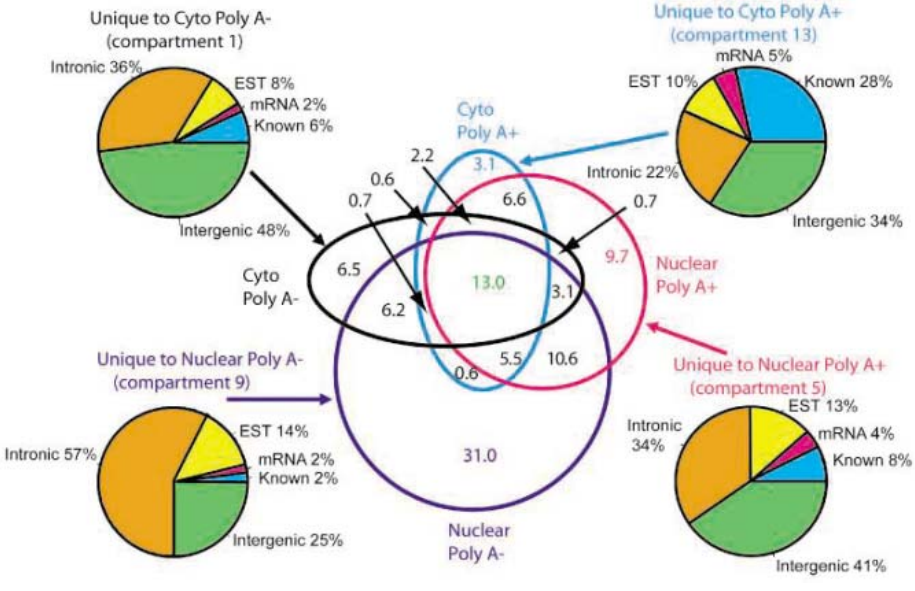

Fig. 3. Distribution of poly A+ and poly A– transcription in the nucleus and cytosol with respect to genome annotations. A four-circle Venn diagram represents proportions of transcribed base pairs in cytosolic poly A+ (cyan), cytosolic poly A– (black), nuclear poly A+ (red), and nuclear poly A– (dark blue). Numbers indicate percentage of total transcription detected in each unique compartment (fig. S9 and Table 1). Pie charts illustrate the distribution of transcribed base pairs detected in each indicated unique compartment among various classes of annotations. The annotations used in this correlation are described in (*15*).

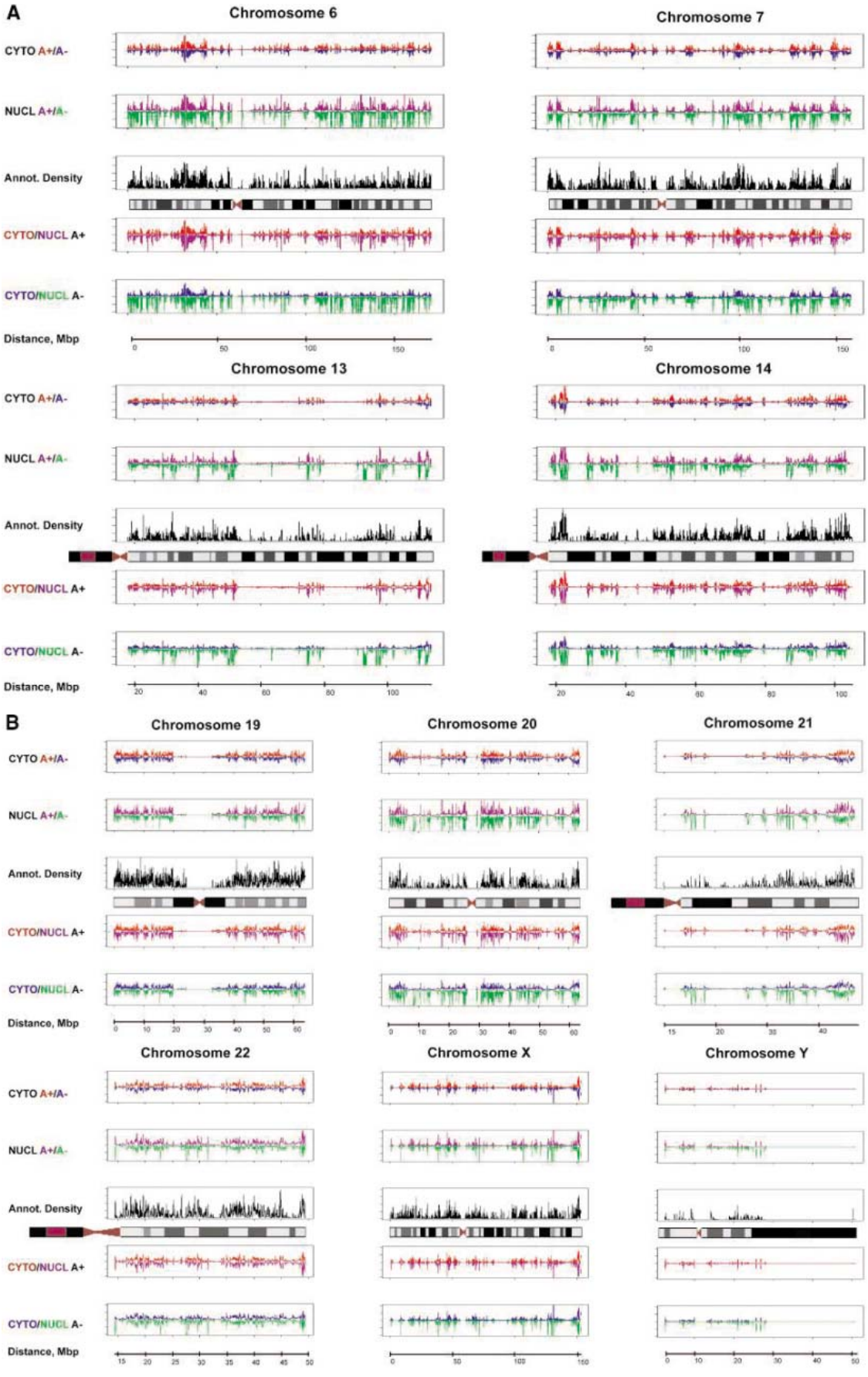

Fig. 4. Density distributions of transcription observed in cytosolic poly A+, poly A–, nuclear poly A+, and poly A– RNA fractions in the 10 human chromosomes. (**A**) Chromosomes 6, 7, 13, and 14. (**B**) Chromosomes 19, 20, 21, 22, X, and Y. The fraction of base pairs found in transfrags is calculated every 6 kb in an overlapping 60-kb window for cytosolic poly A+ (red), poly A– (blue), nuclear poly A+ (mauve), and poly A– RNA (green) and plotted for 10 human chromosomes alongside the base-pair density of exons (black) from Ref Seq, UCSC Known Genes, and GenBank mRNAs. The densities of cytosolic poly A+ versus cytosolic poly A– and nuclear poly A+ versus nuclear poly A– are compared in the top panels, and the densities of cytosolic poly A+ versus nuclear poly A+ and cytosolic poly A– versus nuclear poly A– are compared in the bottom panels for each chromosome.

of all transcription), more than half of nuclear poly A– sequences are derived from intronic regions (Table 1). Clearly, some of these poly A– sequences are introns of spliced coding gene transcripts and may or may not have further biological function once removed from the primary transcripts. However, in the cytosol, the amount of exclusively poly A– sequences is still twice as great as poly A+ sequences (Table 1A), which indicates that there are processed mature poly A– transcripts.

Finally, a total of 36.9% of transcribed sequences are detected as poly A– and poly A+ (Table 1B). These bimorphic sequences are distributed between the two subcellular compartments. It is important to note that detected bimorphic transcribed sequences may be two different transcripts, because transfrags do not identify the strand or specific full-length transcript. However, the presence of such a large proportion of bimorphic transcribed sequences suggests that novel regulatory mechanisms may be involved in the identification of transcripts whose polyadenylation states are altered as a means of regulation. Many of the detected bimorphic sequences are well-characterized coding genes found on the 10 analyzed chromosomes (table S3).

The observations derived from these studies provide some pause as to the state of our understanding concerning where and how the information from the human genome is organized. Many of these and other published observations indicate that our current understanding of the repertoire of transcripts made by the human genome is still evolving. A critical question that applies to both poly A– and poly A+ TUFs centers on the biological functions of these transcripts. Biochemical and genetic experimental approaches are currently being used to answer this question. Until these experiments are completed, systematic identification, mapping, and characterization of as many types of TUFs as possible will assist in understanding and appreciating the complexity of the human transcriptome.

References and Notes

1. E. S. Lander *et al.*, *Nature* **409**, 860 (2001).
2. J. C. Venter *et al.*, *Science* **291**, 1304 (2001).
3. P. Kapranov *et al.*, *Science* **296**, 916 (2002).
4. D. Kampa *et al.*, *Genome Res.* **14**, 331 (2004).
5. S. Cawley *et al.*, *Cell* **116**, 499 (2004).
6. J. L. Rinn *et al.*, *Genes Dev.* **17**, 529 (2003).
7. R. Yelin *et al.*, *Nat. Biotechnol.* **21**, 379 (2003).
8. R. Martone *et al.*, *Proc. Natl. Acad. Sci. U.S.A.* **100**, 12247 (2003).
9. The ENCODE Project Consortium, *Science* **306**, 636 (2004).
10. M. L. Birnstiel, M. Busslinger, K. Strub, *Cell* **41**, 349 (1985).
11. C. Milcarek, R. Price, S. Penman, *Cell* **3**, 1 (1974).
12. M. Salditt-Georgieff, M. M. Harpold, M. C. Wilsone, J. E. Darnell, *Mol. Cell. Biol.* **1**, 177 (1981).
13. P. K. Katinakis, A. Slater, R. H. Burdon, *FEBS Lett.* **116**, 1 (1980).
14. P. Bertone *et al.*, *Science* **306**, 2242 (2004).
15. Materials and methods are available as supporting material on *Science* Online.
16. D. Karolchik *et al.*, *Nucleic Acids Res.* **31**, 51 (2003).
17. W. J. Kent *et al.*, *Genome Res.* **12**, 996 (2002).
18. International Human Genome Sequencing Consortium, *Nature* **431**, 931 (2004).
19. J. Chen *et al.*, *Proc. Natl. Acad. Sci. U.S.A.* **99**, 12257 (2002).
20. Y. Kawabe *et al.*, *J. Biol. Chem.* **276**, 20364 (2001).
21. R. C. Inhorn, D. M. Tollefsen, *Biochem. Biophys. Res. Commun.* **137**, 431 (1986).
22. D. D. Shoemaker *et al.*, *Nature* **409**, 922 (2001).
23. K. Yamada *et al.*, *Science* **302**, 842 (2003).
24. V. Stolc *et al.*, *Science* **306**, 655 (2004).
25. Y. Okazaki *et al.*, *Nature* **420**, 563 (2002).
26. T. Ota *et al.*, *Nat. Genet.* **36**, 40 (2004).
27. The Mammalian Gene Collection Project Team, *Genome Res.* **14**, 2121 (2004).
28. T. Imanishi *et al.*, *PLoS Biol.* **2**, 856 (2004).
29. M. Seki *et al.*, *J. Exp. Bot.* **55**, 213 (2004).
30. S. Saha *et al.*, *Nat. Biotechnol.* **20**, 508 (2002).
31. H. Bono *et al.*, *Genome Res.* **13**, 1318 (2003).
32. A. Peragine, M. Yoshikawa, G. Wu, H. L. Albrecht, R. S. Poethig, *Genes Dev.* **18**, 2368 (2004).
33. F. Vazquez *et al.*, *Mol. Cell* **16**, 69 (2004).
34. M. Edmonds, M. G. Caramela, *J. Biol. Chem.* **244**, 1314 (1969).
35. B. J. Snider, M. Morrison-Bogorad, *Brain Res. Brain Res. Rev.* **17**, 263 (1992).
36. T. E. Geoghegan, G. E. Sonenshein, G. Brawerman, *Biochemistry* **17**, 4200 (1978).

37. The authors thank S. Cawley, C. Schaefer, and J. Manak for helpful discussions; M. Mittmann and D. Le for design of photolithographic masks; D. Bartell for software; R. Wheeler for assistance on the annotation database; H. Caley, H. Gorrell, and B. Wong for database support; J. Stevens for administrative support; and K. Kong for manuscript editing and management assistance. All sequenced transcripts have been submitted to GenBank (accession numbers: AY927468 to AY927642). The supplemental materials, feature intensity (CEL) files, graph file, transfrag, and RACE data are available at http://transcriptome.affymetrix.com/publication/transcriptome_10chromosomes and http://cgap.nci.nih.gov/Info/2005.1. Visual representations of the graph and transfrag data are available at http://genome.ucsc.edu/cgi-bin/hgTracks. This project has been funded in part with federal funds from the National Cancer Institute, National Institutes of Health, under contract N01-C0-12400, and by Affymetrix, Inc. The content of this publication does not necessarily reflect the views or policies of the Department of Health and Human Services, nor does mention of trade names, commercial products, or organizations imply endorsement by the U.S. government.

Supporting Online Material

www.sciencemag.org/cgi/content/full/1108625/DC1
Materials and Methods
Figs. S1 to S10
Tables S1 and S2
References

13 December 2004; accepted 15 March 2005
Published online 24 March 2005;
10.1126/science.1108625
Include this information when citing this paper.

REPORTS

Wet Electrons at the $H_2O/TiO_2(110)$ Surface

Ken Onda,[1] Bin Li,[1] Jin Zhao,[1] Kenneth D. Jordan,[2] Jinlong Yang,[3] Hrvoje Petek[1]*

At interfaces of metal oxide and water, partially hydrated or "wet-electron" states represent the lowest energy pathway for electron transfer. We studied the photoinduced electron transfer at the $H_2O/TiO_2(110)$ interface by means of time-resolved two-photon photoemission spectroscopy and electronic structure theory. At ~1-monolayer coverage of water on partially hydroxylated TiO_2 surfaces, we found an unoccupied electronic state 2.4 electron volts above the Fermi level. Density functional theory shows this to be a wet-electron state analogous to that reported in water clusters and which is distinct from hydrated electrons observed on water-covered metal surfaces. The decay of electrons from the wet-electron state to the conduction band of TiO_2 occurs in ≤15 femtoseconds.

The transport of charge through metal-oxide/hydrous phases is crucial to physical and chemical phenomena in many fields of science and technology, including geochemistry, electrochemistry, corrosion, photocatalysis, sensors, and electronic devices (*1*). When exposed to water vapor, metal oxides are partially hydroxylated and covered with up to several monolayers of H_2O. Interactions of the surface acidic metal and basic O ions, respectively, with the O and H atoms of water impose a two-dimensional (2D) order on the hydrated oxide interface (Fig. 1C). In a redox process, electrons must breach this unique 2D environment before they attain fully 3D hydrated Kevan structure proposed for liquid water, in which six tetrahedrally disposed water molecules point one of their H atoms into the excess electron cloud (*2*, *3*). Similar 2D environments, dubbed "wet-electron" states (*4*), in which the "dangling"—i.e., non–hydrogen bonded—H atoms bind and partially hydrate electrons on surfaces of small water clusters, have recently been predicted by theory and discovered in experiments (*5*–*9*). The electronic structure of wet-electron states at the metal-oxide/water interfaces and the dynamics of charge flow that they mediate have not been explored.

The study of the interfacial charge-transfer dynamics at H_2O/TiO_2 surfaces is of particular interest (*10*–*13*) because photoexcited carriers decompose adsorbed molecules (*14*, *15*), drive photovoltaic cells (*16*), and modify the surface wetting properties (*17*). Photoexcitation of electron-hole pairs across the 3.05-eV band gap of TiO_2 initiates a chain of redox reactions spanning subpicosecond to hour time scales (*18*, *19*). Photocatalysis involves interfacial electron transfer from the Ti^{4+} *d*-electron–derived conduction band to electrophilic molecules, and attack of surface hydroxyls by the O^{2-} *p*-electron–derived valence band holes (*15*). Interfacial electron transfer from photoexcited dye molecules into the conduction band of TiO_2, which is thought to occur on <10-fs time scales, initiates redox cycles in dye-sensitized photovoltaic cells (*10*–*12*, *16*). However, despite the presence of chemisorbed water as reactant or spectator, its role in charge transfer through metal oxide interfaces has not been explored by experiment or theory.

Here, we report a time-resolved two-photon photoemission (TR-2PP; Fig. 1) and density functional theory (DFT) study of wet electrons on H_2O/TiO_2(110) rutile surfaces. A wet-electron state 2.4 ± 0.1 eV above the Fermi level (E_F) is observed by excitation with 3.05-eV light of electrons from partially reduced terminal pentacoordinate $Ti_{5c}^{+4-\delta}$ ion sites only when both OH and H_2O are chemisorbed on TiO_2. Pump-probe measurements give a lifetime of 15 fs for the decay of electrons from the wet-electron surface state to the conduction band of TiO_2.

All experiments were carried out under ultrahigh vacuum (base pressure $<1 \times 10^{-10}$ mbar). The surface electronic structure is explored for the stoichiometric and hydroxylated H_2O/TiO_2 surfaces. Stoichiometric TiO_2(110)-(1×1) surfaces were prepared by cycles of Ar^+ sputtering and annealing in O_2 atmosphere (3×10^{-7} mbar) as described in (*20*). Annealing the stoichiometric surfaces at 900 K in vacuum for 30 min introduces surface bridging O vacancies (Fig. 1B) (*18*, *21*). Thus, reduced surfaces were hydroxylated by exposure to distilled and degassed H_2O at 100 K (*22*–*24*). The sample was excited with 3.05-eV photons delivered in pulses of 10-fs duration and 1.7-nJ energy at 90-MHz repetition rate (*20*). 2PP spectra were measured with a hemispherical electron-energy analyzer (*20*). Interferometric two-pulse correlation (I2PC) measurements of the electron dynamics were recorded for fixed photoelectron energies by scanning the delay between identical pump-probe pulses (*25*).

[1]Department of Physics and Astronomy, [2]Department of Chemistry, University of Pittsburgh, Pittsburgh, PA 15260, USA. [3]Hefei National Laboratory for Physical Sciences at Microscale, University of Science and Technology of China, Hefei, Anhui 230026, China.

*To whom correspondence should be addressed. E-mail: petek@pitt.edu

Typical 2PP spectra of the stoichiometric and reduced TiO_2(110) surfaces before and after exposure to 1.3 Langmuir (1 L = 1.33×10^{-6} mbar·s) of H_2O (Fig. 2), span the range from the work function to the maximum energy (~6.1 eV) given by the two-photon absorption from E_F. The O vacancies introduce excess charge, which is distributed over several Ti_{5c}^{4+} ions to form a broad density of states (DOS) with a maximum 0.9 eV below E_F (*19*, *26*, *27*). With 3.05-eV photons, 2PP was excited exclusively from this $Ti^{+4-\delta}$ DOS even for the nominally stoichiometric surfaces (Fig. 1A). Adsorption of H_2O on the stoi-

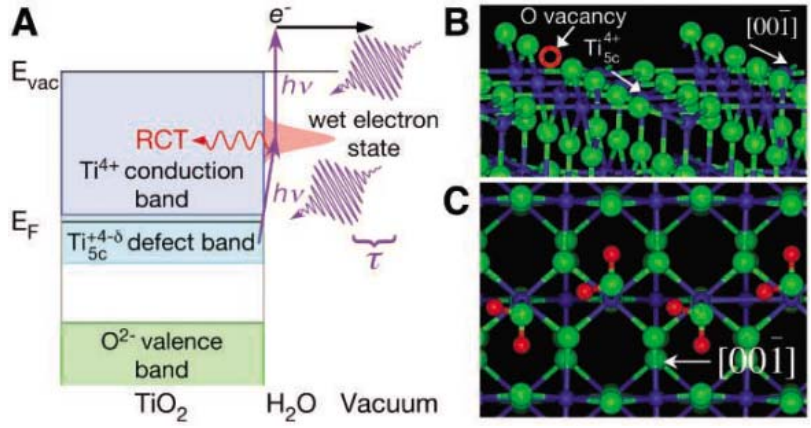

Fig. 1. (**A**) The schematic diagram for the detection of wet-electron states by 2PP spectroscopy. Electrons are excited by two-photon absorption (indicated in purple) from $Ti_{5c}^{+4-\delta}$ defect states to above the work function (E_{vac}). The analysis of photoemitted electron energy with respect to the Fermi level (E_F) yields 2PP spectra representing the density of occupied and unoccupied states. 2PP is resonance enhanced on hydroxylated TiO_2 surfaces by the wet-electron state at 2.4 eV. Measurement of the wet-electron state decay by resonant charge transfer (RCT) is performed by scanning the delay τ between pump and probe excitation pulses (*hν*). (**B**) The calculated structure of the TiO_2(110) surface. Bridging oxygen (green) rows align along the [001] crystallographic direction. The red circle indicates a bridging O vacancy, which is the most common defect on reduced TiO_2(110) surfaces. Acidic pentacoordinate Ti_{5c}^{4+} (blue) sites bind O atoms of water molecules. (**C**) The calculated structure of H_2O/TiO_2 for 1-ML coverage. Hydrogen bonding tilts the bridging O atoms and H_2O toward each other. Red spheres indicate H atoms.

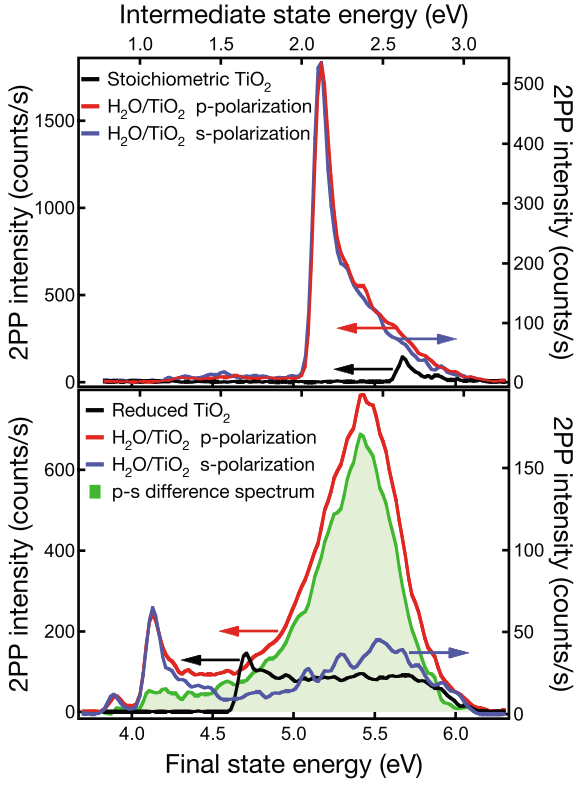

Fig. 2. 2PP spectra of the (**top**) stoichiometric and (**bottom**) reduced TiO_2 surfaces before and after deposition of ~1 ML of H_2O. The H_2O/TiO_2 spectra are taken with s- and p-polarized light. The s-polarized spectra are expanded 3× to normalize the intensities at the work-function edge (horizontal arrows indicate the appropriate axis for each spectrum). The difference between thus normalized p- and s-polarized spectra (green) for the reduced surface isolates the additional DOS of the wet-electron state. The final-state energy is that measured for photoelectrons with respect to E_F, whereas the intermediate-state energy is later reduced by the 3.05-eV photon energy.

chiometric TiO_2 surfaces transfers some charge to the $Ti^{+4-\delta}$ DOS as deduced by the work-function decrease; however, the profiles for the 2PP spectra with p- and s-polarized excitation are identical (Fig. 2, top) (*20*). With the higher O vacancy defect density, the reduced TiO_2 surfaces have a lower work function and higher $Ti^{+4-\delta}$ DOS than the stoichiometric surfaces (*20*). However, when 2PP was excited by p-polarized light, adsorption of H_2O onto reduced surfaces introduces a new band, which was isolated in the difference spectrum in Fig. 2, bottom. Because it appears only in p-polarized 2PP spectra, and not in conventional ultraviolet photoemission spectra (UPS), we attribute this band to an intermediate unoccupied state 2.4 ± 0.1 eV above E_F with the transition moment normal to the surface (*20*, *23*, *25*). On the basis of the chemisorption properties of H_2O and DFT calculations described below, we identified the 2.4-eV band with wet-electron states.

The nature of chemisorption of H_2O on TiO_2 has been studied by temperature-programmed desorption (TPD), vibrational spectroscopy, UPS, and scanning tunneling microscopy (STM). H_2O molecules on reduced surfaces dissociate at bridging O vacancies by a diffusion-limited process at <135 K to form two uncorrelated bridging OH species (*22*–*24*, *26*, *28*). After titrating the vacancies, water adsorbs molecularly at Ti^{4+}_{5c} ion sites between the bridging O rows up to 1-monolayer (ML) coverage (Fig. 1C) (*22*). Because the interaction of H_2O with the amphoteric oxide surface is stronger than with other H_2O molecules, the first monolayer molecules are aligned in a 2D structure (*22*) (Fig. 1C). Beyond the first monolayer, the second monolayer is disordered and the structure of bulk H_2O develops from the third monolayer.

We considered the assignment of the wet-electron state based on its dependence on adsorption of both H_2O and OH. The marked difference between the 2PP spectra of H_2O/TiO_2 in Fig. 2 is caused by a few percent (<5%) of H_2O molecules that dissociate to form OH on reduced surfaces (*29*). The wet electron–state intensity (integrated peak area) also depends on the H_2O exposure (Fig. 3A). The resonance intensity is maximum for 1.35 L of water and saturates at ~25% of its maximum value above 3 L. According to our modeling of the work function change, which is also shown in Fig. 3A, the exposure of 1.35 L corresponds to ~1-ML H_2O coverage (*20*).

To confirm that the wet-electron state attains maximum intensity at 1 ML of H_2O, we measured 2PP spectra for surfaces where H_2O coverage was defined by surface temperature. TPD spectra of H_2O/TiO_2 surfaces, which measure the partial pressure of H_2O as the surface is heated at a constant rate, exhibit peaks at 155 and 270 K, respectively, for the desorption of water from the multilayer and monolayer films. Hydroxyl recombination to form H_2O leads to an additional peak at 500 K for hydroxylated surfaces (*22*, *26*). After dosing 3.7 L of H_2O onto a reduced surface, we measured 2PP spectra at several temperatures, and in Fig. 3B, we plot for each temperature the excess DOS arising from the wet-electron state. The peak intensity increased to a maximum at 180 K after multilayer H_2O present at 100 and 140 K desorbed to expose the first monolayer. The wet-electron DOS was nearly extinguished when the remaining H_2O desorbed at 300 K, confirming that the resonance maximum occurs for ~1-ML coverage. With only OH remaining on the surface at 300 K, a weak feature, which appears to be the low-energy wing of a peak that exists above 3.05 eV, remained. We conclude that the existence of wet-electron state at 2.4 eV requires the cooperative interaction between OH and H_2O on TiO_2.

Finally, we studied the wet-electron lifetimes by recording I2PC scans for reduced TiO_2 surfaces after different exposures to H_2O. In Fig. 4, we plot I2PC scans averaged over the optical phase and their fit to an optical Bloch equation model (*25*). All measurements were only weakly dependent on the intermediate-state energy; however, the adsorption of H_2O noticeably increases the intermediate-state lifetime. The I2PC scan for the bare surface was identical to the pulse autocorrelation, indicating that the 2PP process occurs via virtual intermediate states (*25*). The wet-electron lifetimes increased to 10 ± 1 and 14 ± 1 fs for exposures of 0.7 and 1.6 L of H_2O, respectively, and saturated at ~15 fs for >1-ML coverage. Because their energy relaxation is unlikely to be so fast, wet electrons probably decay by resonant charge transfer into the conduction band of TiO_2. Because the lifetime corresponds to only two periods of O-H stretching vibration, the nuclear motion of H_2O molecules is too slow to stabilize the wet-electron state in a more favorable hydration structure.

To assign the wet-electron state to specific adsorbate structures, we performed plane-wave pseudopotential DFT calculations for associatively chemisorbed H_2O at Ti^{4+}_{5c} sites and H adsorbed on bridging O sites of TiO_2 for various coverages and structures (*30*–*35*). The calculated distribution of orbitals for the lowest energy adsorbate-localized unoccupied states for 1 ML H_2O + 0.5 ML H, and 1-ML H structures, respectively, at 2.4 and 1.5 eV are shown in Fig. 5. The unoccupied states of the adsorbate-covered surfaces are either associated with the Ti^{4+} ions, which form the conduction band of TiO_2, or dangling H atoms on OH and H_2O. For each H_2O and H coverage and structure, we found unoccupied adsorbate-localized states, where the DOS is

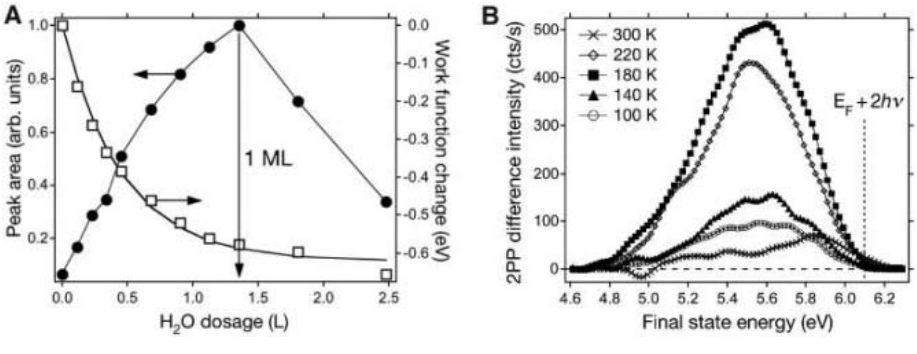

Fig. 3. (**A**) Plot of the wet electron–state peak area from difference spectra such as in Fig. 2, bottom (circles), and work-function change (squares) plotted as a function of water exposure. The solid line is a fit of the work-function change as described in (*20*). The coverage of 1.35 L for the intensity maximum and work-function saturation corresponds to the approximately 1-ML H_2O. The horizontal arrows indicate the appropriate axis for each measurement. (**B**) The difference spectra recorded at different temperatures after exposing the reduced TiO_2 to 3.7 L of H_2O at 100 K. Based on published TPD spectra, 1-ML coverage of H_2O is attained at 180 K where the wet-electron state has maximum intensity. Only OH remains above 300 K (*22*).

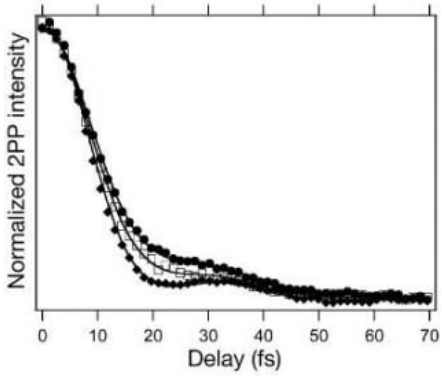

Fig. 4. Phase-averaged I2PC scans for the reduced TiO_2 (solid diamonds), and after exposure to 0.7 (open squares) and 1.6 L (solid circles) of H_2O. The lines represent fits with a three-level optical Bloch equation model with the use of experimentally measured pulse autocorrelation and assuming single exponential decay kinetics for the intermediate state (*25*). The bare surface intermediate-state lifetime is too short to measure, and 10 ± 1 and 14 ± 1 fs for 0.7 and 1.6 L H_2O/TiO_2, respectively.

concentrated on clusters of several dangling H atoms (Fig. 5A). The lowest unoccupied adsorbate-localized state energy correlates with the number of dangling H atoms in each cluster (Fig. 5C).

The association of electrons with the dangling H atoms is well known from the studies of hydrated electrons in water (*3*) and in water clusters (*4*–*9*). Based on the analogy to small water clusters where electrons are partially hydrated on cluster surfaces, we attribute the observed water-induced resonances to the partially hydrated wet-electron states that we calculated for TiO_2 surfaces. The ideal wet-electron structures investigated in Fig. 5 can explain the observed features of the experimentally studied heterogeneous surfaces. Notably, the lowest energy unoccupied state at 1.5 eV for 1 ML of H (Fig. 5B) consists of 1D-delocalized bands on bridging OH groups. When H_2O molecules are added to this structure, hydrogen bonding tilts the OH from surface normal and disrupts the optimal 1D structure. These structural changes reduce the surface dipole and the extent of electron delocalization, thereby increasing the energy of wet-electron states. The most relevant structure to our experiment is 1 ML H_2O + 0.5 ML H in Fig. 5A. For this structure, intervening bridging O atoms hinder orbital overlap between OH species to constrain electron delocalization to clusters involving single OH with two or more H_2O molecules (Fig. 5A). These clusters, which are representative of low-OH (≪0.5 ML) coverage surfaces produced by our methods (*36*), have a calculated unoccupied level at 2.4 eV in good agreement with the experiment. Structures with two or more adjacent OH, which should have lower wet-electron energy, may occur with low probability and could be responsible for the characteristic low-energy tail in the difference spectrum in Fig. 2, bottom. Moreover, the calculated wet electron–state energy of 3.5 eV for 1 ML H_2O explains why the resonance cannot be excited with 3.05-eV light for stoichiometric surfaces. Because H_2O stabilizes the wet-electron state on isolated surface OH species, when H_2O desorbs above 300 K the resonance energy increases above 3 eV. In support of the existence of OH-localized states, in STM experiments, resonant tunneling into OH for bias of ≥+2.5 V leads to the enhanced contrast and desorption of H atoms from TiO_2 (*36*). Above 1-ML coverage, the second-layer H_2O molecules partially consume the dangling H atoms (*22*), thereby reducing the wet-electron DOS.

Hydrated electrons have also been observed on metals (*37*, *38*). However, metals lack the distinct acidic and basic sites present in oxides that could align or even dissociate H_2O to form OH. Therefore, associatively chemisorbed water on metals grows in bilayer structures that occupy the maximum number of H atoms in a hydrogen-bonding network (*38*). There are few preexisting sites that stabilize electrons, and to eject electrons into bilayer structures requires excitation above 3.2 eV into the conduction band of water. The excess energy of these conduction electrons can be used to disrupt the hydrogen-bonding network to form pockets of dangling H atoms. Once trapped at such sites, electrons are stabilized with respect to charge transfer to the metal substrate and undergo further hydration, which is accompanied by a reduction of energy to <2.6 eV, on >100-fs time scales (*37*, *38*).

The existence of wet electrons as excited states on the OH- and H_2O-covered TiO_2 is notable because conditions exist to support similar states on all oxide surfaces in contact with water or humid atmosphere. Depending on specific features of different surfaces, such as structures that promote cooperative interactions, and the acidity of OH species, the energy of the wet electrons could be even lower than calculated for 1 ML OH on TiO_2. For large band gap materials, the wet-electron states could even be occupied. Because they represent the lowest energy pathway for electron transfer at the metal-oxide/aqueous interfaces, wet-electron states may play an important role in photocatalysis and photoelectrochemical energy conversion on TiO_2 and other oxides. For instance, the surface OH impurity formed by the dissociative chemisorption of dye molecules could mediate the astoundingly fast charge injection into TiO_2 by providing conduction pathways through wet-electron states (*10*–*12*). Indeed, interfacial trap states of unknown origin have been invoked to explain the comparable excited state quenching rates of dyes on ZrO_2 as for TiO_2, even though the conduction band of ZrO_2 is not energetically accessible (*13*). Delocalized electron states attributed to Si-OH and Si-H also have been imaged by STM with a bias of +2.6 eV on a hydroxylated Si(100) surface (*39*). Thus, it is likely that wet-electron states perform important but yet unknown functions, for instance, as charge-transfer promoters at transparent metal-oxide electrodes used in organic-molecule–based devices and as electron traps in conventional semiconductor devices.

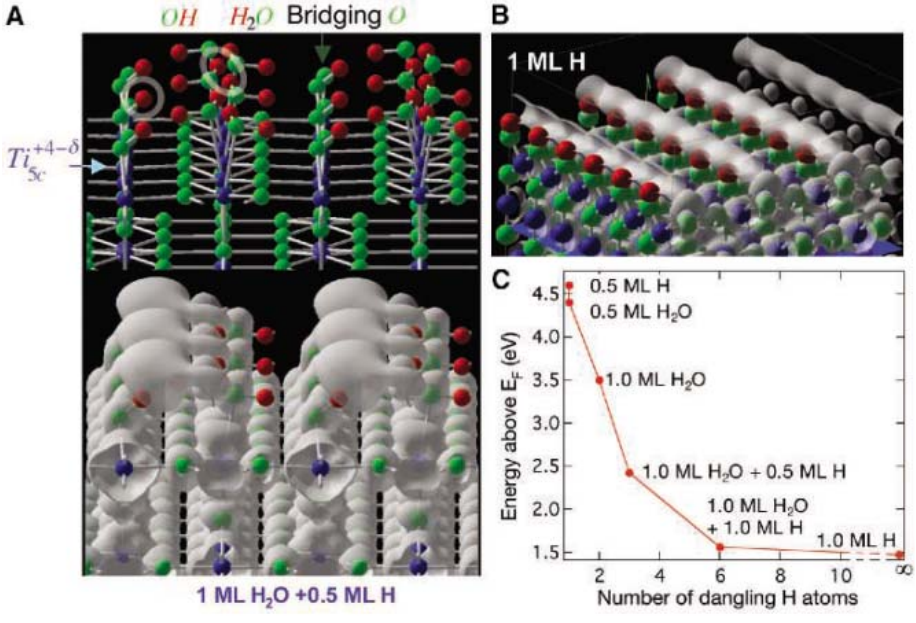

Fig. 5. (**A**) The optimized geometry of a TiO_2 surface covered with 1 ML H_2O + 0.5 ML H. The bottom panel shows the orbital distribution for the same structure at 2.4 eV above E_F. The adsorbate orbitals are delocalized in clusters involving one OH and one H atom each contributed by two adjacent H_2O molecules, which are indicated for a single cluster by white ellipsoids. (**B**) The optimized geometry and orbital distributions at 1.5 eV for 1 ML H on TiO_2. The hybridization of orbitals on H atoms into 1D chains along the bridging O rows makes this the most stable wet-electron state found by theory. (**C**) The correlation of the wet-electron energy for different coverages of H_2O and H adsorbates with the number of dangling H atoms in each hydration cluster. The infinite limit corresponds to the structure in (B). All calculated structures in the experimentally observable energy range are associated with clusters involving both OH and H_2O.

References and Notes

1. G. E. Brown Jr. *et al.*, *Chem. Rev.* **99**, 77 (1999).
2. L. Kevan, *Acc. Chem. Res.* **14**, 138 (1981).
3. J. Schnitker, P. J. Rossky, *J. Chem. Phys.* **86**, 3471 (1987).
4. K. S. Kim *et al.*, *Phys. Rev. Lett.* **76**, 956 (1996).
5. N. I. Hammer *et al.*, *Science* **306**, 675 (2004).
6. A. E. Bragg, J. R. R. Verlet, A. Kammrath, O. Cheshnovsky, D. M. Neumark, *Science* **306**, 669 (2004).
7. J. R. R. Verlet, A. E. Bragg, A. Kammrath, O. Cheshnovsky, D. M. Neumark, *Science* **307**, 93 (2005).
8. D. H. Paik, I.-R. Lee, D.-S. Yang, J. S. Baskin, A. H. Zewail, *Science* **306**, 672 (2004).
9. K. D. Jordan, *Science* **306**, 618 (2004).
10. C. Zimmermann *et al.*, *J. Phys. Chem. B* **105**, 9245 (2001).

11. J. Schnadt *et al.*, *Nature* **418**, 620 (2002).
12. N. A. Anderson and T. Lian, *Annu. Rev. Phys. Chem.* **56**, 491 (2005).
13. R. Huber, S. Spörlein, J. E. Moser, M. Grätzel, J. Wachtveitl, *J. Phys. Chem. B* **104**, 8995 (2000).
14. A. Fujishima, K. Honda, *Nature* **238**, 37 (1972).
15. M. R. Hoffmann, S. T. Martin, W. Choi, D. W. Bahnemann, *Chem. Rev.* **95**, 69 (1995).
16. A. Hagfeldt, M. Grätzel, *Acc. Chem. Res.* **33**, 269 (2000).
17. R. Wang *et al.*, *Nature* **388**, 431 (1997).
18. A. L. Linsebigler, G. Lu, J. T. Yates Jr., *Chem. Rev.* **95**, 735 (1995).
19. S. H. Szczepankiewicz, A. J. Colussi, M. R. Hoffmann, *J. Phys. Chem. B* **104**, 9842 (2000).
20. K. Onda, B. Li, H. Petek, *Phys. Rev. B* **70**, 045415 (2004).
21. U. Diebold, *Surf. Sci. Rep.* **48**, 53 (2003).
22. M. A. Henderson, *Surf. Sci.* **355**, 151 (1996).
23. I. M. Brookes, C. A. Muryn, G. Thornton, *Phys. Rev. Lett.* **87**, 266103 (2001).
24. R. Schaub *et al.*, *Phys. Rev. Lett.* **87**, 266104 (2001).
25. H. Petek, S. Ogawa, *Prog. Surf. Sci.* **56**, 239 (1997).
26. M. A. Henderson, W. S. Epling, C. H. F. Peden, C. L. Perkins, *J. Phys. Chem. B* **107**, 534 (2003).
27. J. Leconte, A. Markovits, M. K. Skalli, C. Minot, A. Belmajdoub, *Surf. Sci.* **497**, 194 (2002).
28. M. A. Henderson, *Surf. Sci. Rep.* **46**, 1 (2002).
29. To confirm that both H_2O molecules and OH are essential, we hydroxylated the stoichiometric surface, which does not exhibit the resonance when exposed to H_2O, with H atoms from a thermal cracking source (*36*). As anticipated, the dissociation of H_2O at bridging O vacancies and the reduction of bridging O atoms by gas phase H atoms (*40*) provide two alternative protocols for the detection of the wet-electron state.
30. The calculations with the Vienna ab Initio Simulation Package code use the generalized gradient approximation with the spin-polarized Perdew-Wang exchange-correlation functional. The oxygen 1*s* and Ti 1*s* to 3*p* are treated as core states. We use the projector augmented-wave (PAW) potential, which is generally more accurate than the ultrasoft pseudopotential. The surface is modeled by periodically repeated slabs containing three Ti layers separated by 10 Å vacuum gaps. A Monhkorst-Pack grid of $(3\times3\times1)$ *k* points is used for the (1×2) surface unit cell. Molecules are adsorbed on both sides of the slab to avoid formation of a dipole moment. The positions of all atoms are allowed to relax until the force acting on each is less than 0.02 eV $Å^{-1}$. We use a 400-eV plane-wave cutoff for the optimization and a 520-eV cutoff for the static calculation of the electronic structure.
31. G. Kresse, J. Hafner, *Phys. Rev. B* **47**, 558 (1993).
32. G. Kresse, J. Hafner, *Phys. Rev. B* **48**, 13115 (1993).
33. G. Kresse, J. Hafner, *Phys. Rev. B* **49**, 14251 (1994).
34. J. P. Perdew, Y. Wang, *Phys. Rev. B* **45**, 13244 (1992).
35. G. Kresse, J. Joubert, *Phys. Rev. B* **59**, 1758 (1999).
36. S. Suzuki, K. Fukui, H. Onishi, Y. Iwasawa, *Phys. Rev. Lett.* **84**, 2156 (2000).
37. C. Gahl, U. Bovensiepen, C. Frischkorn, M. Wolf, *Phys. Rev. Lett.* **89**, 107402 (2002).
38. C. Gahl *et al.*, *Surf. Sci.* **532-535**, 108 (2003).
39. M. Chander, Y. Z. Li, J. C. Patrin, J. H. Weaver, *Phys. Rev. B* **48**, 2493 (1993).
40. B. Li *et al.*, data not shown.

41. This work was supported by the U.S. Department of Defense Multidisciplinary University Research Initiative program under grant DAAD19-01-1-0619, and New Energy Development Organization of Japan "Molecular wire" project. The apparatus for TR-2PP was developed with support from NSF grant DMR-0116034. We thank J. T. Yates Jr. and his group for invaluable discussions.

4 January 2005; accepted 21 March 2005
10.1126/science.1109366

Deterministic Coupling of Single Quantum Dots to Single Nanocavity Modes

Antonio Badolato,[1]* Kevin Hennessy,[1]* Mete Atatüre,[3] Jan Dreiser,[3] Evelyn Hu,[1,2] Pierre M. Petroff,[1,2] Atac Imamoğlu[3]†

We demonstrate a deterministic approach to the implementation of solid-state cavity quantum electrodynamics (QED) systems based on a precise spatial and spectral overlap between a single self-assembled quantum dot and a photonic crystal membrane nanocavity. By fine-tuning nanocavity modes with a high quality factor into resonance with any given quantum dot exciton, we observed clear signatures of cavity QED (such as the Purcell effect) in all fabricated structures. This approach removes the major hindrances that had limited the application of solid-state cavity QED and enables the realization of experiments previously proposed in the context of quantum information processing.

Cavity QED experiments, where single atoms are strongly coupled to single cavity modes, have culminated in the demonstration of conditional quantum dynamics (*1*), quantum nondemolition measurement of photons, and creation of entanglement between three distinguishable quantum systems (*2*). The realization of such systems in the solid state, although challenging, offers several advantages (*3*). Indeed, a monolithically integrated cavity QED system consisting of a self-assembled quantum dot (QD) embedded within a nanocavity could have vanishing uncertainty in the relative location of the emitter with respect to the cavity electric field maxima and could allow for much stronger emitter-cavity coupling because of the ultrasmall cavity volumes. A number of experiments have already demonstrated the potential of QD-based solid-state cavity QED in applications such as single-photon sources (*4–6*). Nonetheless, because it is very difficult to predetermine the exact resonance energy and location of an optically active QD, all of the prior QD-based cavity QED experiments relied on a random spectral and spatial overlap between QDs and cavity modes (*7–9*). The difficulty in tuning the resonance energy of a fabricated nanocavity and the reduced likelihood of spatial overlap for the ultrasmall cavities of interest have so far limited the application of these solid-state cavity QED nanostructures. We demonstrate a deterministic approach to the QD nanocavity coupling based on two crucial components: (i) a positioning technique that allows us to locate a single QD at an electric field maximum of a photonic crystal (PC) nanocavity with 25-nm accuracy, and (ii) a precise spectral tuning of the cavity mode into resonance with any given QD emission line. This deterministic QD cavity coupling yields a spontaneous emission rate enhancement (Purcell effect) of the QD luminescence in all four fabricated devices.

Our basic material was a semiconductor heterostructure (Fig. 1A) grown by molecular beam epitaxy (*10*). The emitter-cavity system comprised free-standing PC membranes fabricated in a 180-nm layer of GaAs (*10*) with coherently embedded QDs. The square-lattice PC pattern with a single missing hole (S1) fabricated in the GaAs membrane can support a nondegenerate donor-type mode with a high quality factor (Q) and an ultrasmall mode volume (*11*).

The first key ingredient of our approach was the active positioning of a QD within the PC defect that eliminated the uncertainty in the relative position of the QD with respect to the cavity mode. We grew six vertically strain-correlated InAs/GaAs QD layers (*12*, *13*) in the GaAs membrane (Fig. 1A, right). The emission energy of the first QD layer (seed QD) was blue-shifted by in situ annealing the QDs when partly capped with GaAs (*14*). Five successive as-grown QD layers (stacked QDs) were stacked up to the surface (*15*), forming a tracer for the seed QD that was detectable by scanning electron microscopy (SEM). By resolving the location of a QD on the surface, we were able to determine the location of the seed QD that was of interest for coupling to a nanocavity. A matrix of gold markers was fabricated on the low-density QD region ($\approx 2 \times 10^5$ cm^{-2}) to map the isolated QDs relative to this matrix. With the use of electron beam lithography, we wrote the S1-PC pattern offset by the appropriate distance from the markers (*16*). The small white dot in Fig. 1B shows the SEM trace of the surface QD in one of our four devices (device I), which was positioned within 25 nm from one of the four

[1]Department of Electrical and Computer Engineering, [2]Materials Department, University of California, Santa Barbara, CA 93106, USA. [3]Institute of Quantum Electronics, ETH-Hönggerberg, CH-8093 Zürich, Switzerland.

*These authors contributed equally to this work.
†To whom correspondence should be addressed. E-mail: imamoglu@phys.ethz.ch

calculated electric field maxima of the S1-PC defect region (Fig. 1C) (*17*).

Before cavity fabrication, we measured the emission spectrum of each targeted seed-stack QD with the use of cryogenic temperature microphotoluminescence (μ-PL) (*10*). This spectrum allowed us to verify that our targeted QDs were truly stacked, as we observed the emission from the excited states of the stacked QDs along with the blue-shifted exciton emission from the seed QD. Likewise, by identifying the exciton lines according to the power dependence of the μ-PL emission intensities, we verified that no unstacked seed QDs had nucleated in close proximity and selected only seed-stack QDs with unambiguous spectra. We then designed our nanocavities (*11*) to ensure that the high-Q cavity mode resonance (M) was near the seed QD exciton energies but remained red-shifted relative to those energies. In this way, we were able to fabricate devices that had cavity resonances with Q values up to 5000 and red-shifted by 13 ± 3 nm with respect to the QD exciton lines. The comparison of the QD-cavity spectrum with the QD spectrum before cavity fabrication allowed us to identify the different modes of the S1-PC. Because test cavities located in regions with no QDs did not show any cavity mode emission, we conclude that in our devices with one seed-stack QD the cavity modes were primarily sustained by excited states of the stacked QDs.

The second key ingredient of our work was the tuning of M through the μ-PL spectrum of the targeted seed QD after PC fabrication. We developed a digital etching (*18*) technique that fine-tuned M by controllably enlarging PC holes and thinning the PC membrane. One etching cycle consisted of selectively removing the native surface oxide of our devices in a solution of citric acid (1 M) and allowing the material to grow a new native oxide layer under atmospheric conditions. Because the entire process is self-limiting, the etched layer thickness per cycle was essentially the same, resulting in a digital (i.e., stepped) etching process (*10*). As shown in Fig. 2A, we obtained blue-shift of M at ~3 nm per cycle without detriment to the Q factor. We emphasize that because of this stepped tuning, we were able to follow the blue-shift of M cycle by cycle—without affecting the QD—and to stop our process as soon as we engaged the QD. With this high tuning accuracy, we could count on blue-shifting (or red-shifting) the QD exciton energy by applying a magnetic field (*19*) (or by increasing the temperature) to reach the exact QD-cavity resonance.

By applying three digital etching cycles to device I, we were able to blue-shift M within 6.6 nm of the charged exciton (X^-) line (red curve in Fig. 2B). Because the linewidth of M is only 0.3 nm ($Q \approx 3000$), it is safe to assume there is no M-X^- coupling for such a detuning, and thus we refer to this stage as off-resonance. After etching for two additional cycles, we observed (at 4.2 K) a reduction of the M-X^- detuning to 0.6 nm together with an enhancement of the X^- intensity by a factor of 11, and an even larger increase in the M line (blue curve in Fig. 2B) (*20*). This striking change in the QD spectrum is direct evidence of a nontrivial cavity QED effect; namely, the QD-cavity coupling is strong enough that even for a finite detuning exceeding the corresponding linewidths, the QD emission intensity and the multi-exciton dynamics are drastically modified.

As we raised the temperature of device I, the X^- line red-shifted more than the M line, thereby achieving resonance at 39 K (Fig. 3A). The bottom curve in Fig. 3A shows that even at a low pump power [0.38 P_{sat}, where P_{sat} (0.59 μW) is defined as the pump power needed to saturate the neutral exciton (X)], the spectrum is dominated by the X^- line on-resonance with an intensity enhancement factor of 43 with respect to the X^- line off-resonance. As shown in Fig. 3B, no M line was detected in the off-resonance case for $P \leq 0.38\ P_{sat}$. As mentioned above, the cavity

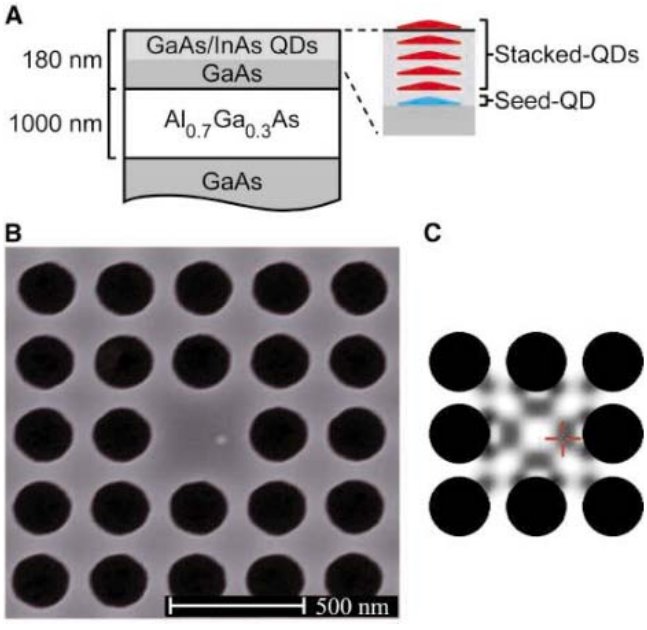

Fig. 1. (**A**) Schematic cross section of the semiconductor heterostructure. (**B**) SEM image of the S1-PC defect region in device I. The small white dot is the top QD of the targeted seed stack. (**C**) Plot of the electric field intensity present in the semiconductor of the S1-PC defect region, calculated by three-dimensional finite-difference time domain (*25*). Cavity-mode maxima correspond to darker gray levels. The red cross indicates the position of the seed stack.

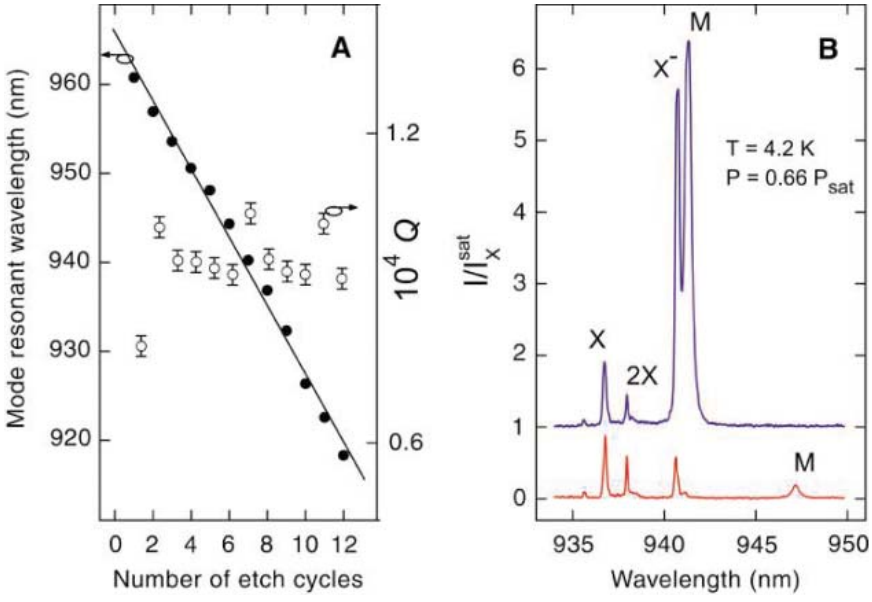

Fig. 2. (**A**) Resonant wavelength of the high-Q mode and Q versus the number of etching cycles for S1-PCs fabricated in the high-density QD region and measured at 4.2 K. The solid line is a guide for the eye. (**B**) Device I μ-PL spectra (*10*) at 4.2 K and pump power of 0.66 P_{sat}. Red curve, spectrum after three digital etching cycles; blue curve (offset for clarity), spectrum after five digital etching cycles. The y axis is normalized to I_X^{sat}, the neutral exciton (X) μ-PL intensity at saturation (*20*).

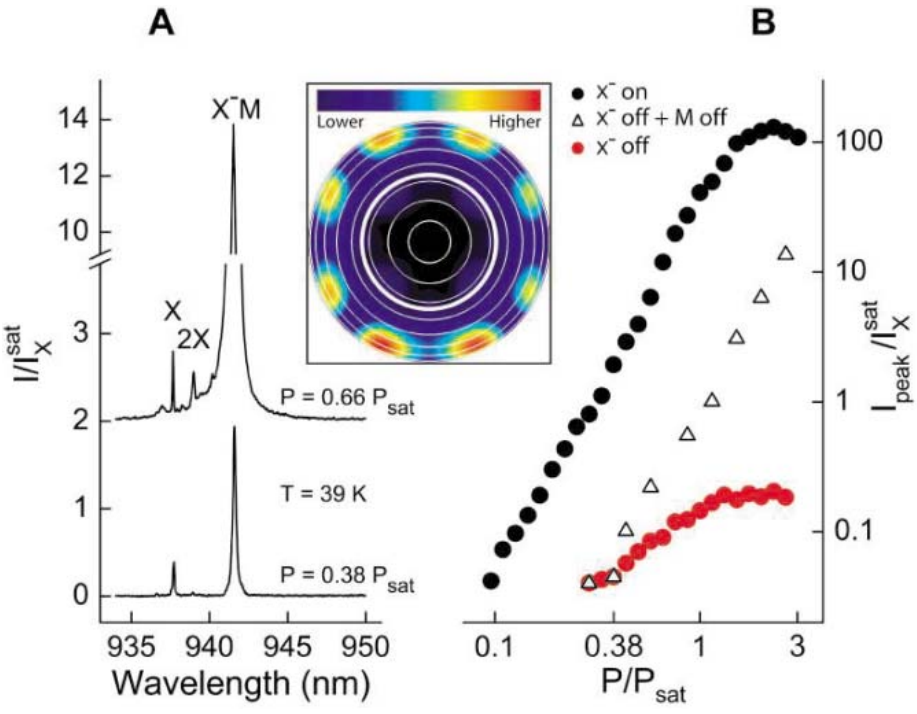

Fig. 3. Device I. (**A**) μ-PL spectra after five digital etching cycles measured at 39 K. The X^- is on-resonance with the cavity mode (X^-M) (*20*). The two curves correspond to different excitation powers: 0.38 P_{sat} (bottom curve) and 0.66 P_{sat} (upper curve, offset for clarity). Inset: Far-field profile of a classical dipole emitting into the PC mode, calculated over a hemisphere of radius 1 m by a fully vectorial algorithm from the near-field dipole fields (*26*). Plotted is $\mathbf{E} \times \mathbf{H}$ normal to the hemisphere surface, where the emission angle is shown in 10° increments with white circles. The thicker white circle corresponds to the numerical aperture (0.55) of our objective. (**B**) Peak maximum intensities versus pump power (log-log scale) of X^- off-resonance (solid red dots), sum of X^- and M both off-resonance (open triangles), and X^- on-resonance (solid black dots). The *x* axis is normalized to the X saturation pump power and the *y* axis to the X saturation intensity (*20*).

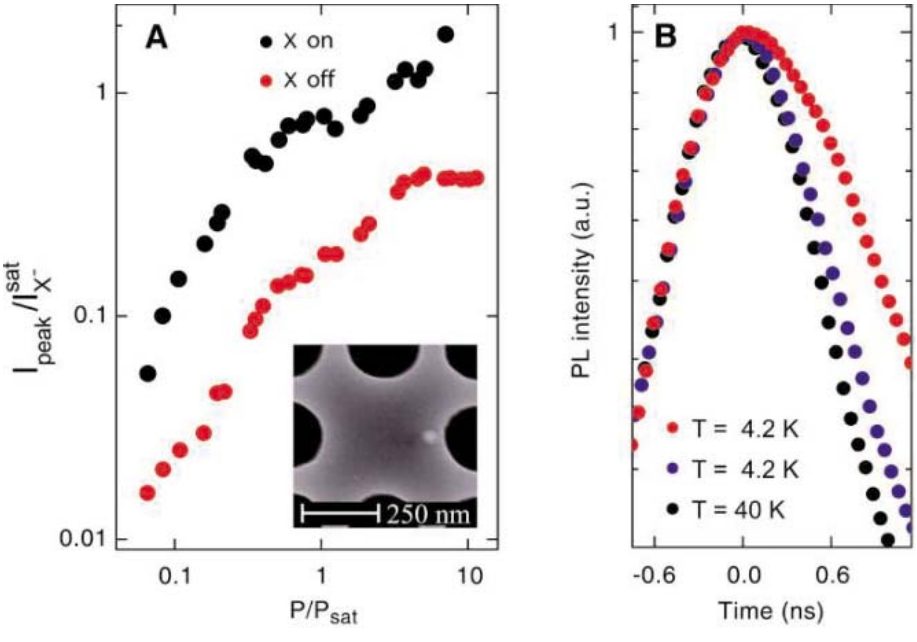

Fig. 4. Device II. (**A**) Peak maximum intensity versus pump power (log-log scale) of X off-resonance (solid red dots) and X on-resonance (solid black dots). Because the X^- at saturation remained independent of the M-X detuning, the *x* axis is normalized to the X^- saturation pump power and the *y* axis to the X^- saturation intensity. (Inset) SEM image of the S1-PC defect region. The small white dot is the top QD of the targeted seed stack. (**B**) Lifetime, as measured by TCSPC, of the X line off-resonance at 4.2 K (solid red dots), near-resonance at 4.2 K (solid blue dots), and on-resonance at 40 K (solid black dots).

modes off-resonance are sustained by the excited states of the stacked QDs, and we consider this background contribution to the X^-M peak intensity as a constant factor independent of the QD-cavity detuning. Therefore, the actual resonant cavity enhancement of QD emission can be obtained by subtracting this constant factor from the total peak intensity. The remarkable enhancement of X^- peak intensity, ranging from a factor of ~20 at $P = 0.29\ P_{sat}$ to a factor of ~700 at $P = 2.3\ P_{sat}$, directly proves the resonant coupling between the seed QD and the PC cavity. We note that in contrast to other solid-state cavities, the S1-PC tends to diffract the far-field radiation (Fig. 3, inset) away from the collection cone of an objective having the optical axis orthogonal to the PC membrane. Consequently, we argue that the large increase of the X^- peak intensity above saturation indicates a substantial Purcell enhancement of the QD radiative decay rate. In device I, time-correlated single photon counting (TCSPC) measurements (*10*) showed resolution-limited lifetimes (<0.7 ns) of X^- both near- and on-resonance. Hence, we were not able to infer the reduction in emission time by directly measuring the decay time.

In device II, after first tuning the M and X lines with the use of digital etching and then temperature tuning (40 K), we observed at low pump powers only a factor of 5 enhancement of the X intensity from off- to on-resonance (Fig. 4A). This weaker coupling was predicted, as the position of the surface QD in the SEM image (Fig. 4A, inset) showed a reduced spatial overlap with the simulated electric field maxima of the S1-PC defect region (*21*, *22*). In this case, we were able to observe directly the effect of QD-cavity spectral resonance on the X lifetime (τ), which continually decreased from off- to near-resonance, reaching the resolution limit of our TCSPC setup at the exact resonance (Fig. 4B). By deconvolving the TCSPC response function, we extracted a lifetime on-resonance (τ_{on}) of 0.2 ± 0.1 ns (at 40 K), near-resonance of 0.6 ns (at 4.2 K), and off-resonance (τ_{off}) of 1 ns (at 4.2 K). These results not only directly prove that we can achieve enhancement of radiative decay rate by a factor of ~5 even in devices with less precise positioning, but also corroborate our calculation-based claims that the enhancement of the exciton μ-PL intensity in the S1-PC is predominantly due to the Purcell effect.

Careful examination of the seed-QD multi-exciton dynamics shows that the physics unveiled by our experiments goes beyond the well-known Purcell effect. In device I (Figs. 2B and 3A), by comparing the bi-exciton (2X) μ-PL intensity at the same pump power (0.66 P_{sat}) for M-X^- off-, near-, and on-resonance, we observed a clear decrease of the 2X intensity (relative to the X intensity) as X^- reached the resonance. This reduction may be

explained in terms of sequential carrier capture by the QD: If electron capture in our QDs is more likely than hole capture, the creation of the 2X state requires that a QD in state X^- capture an additional hole. Yet if the X^- emission rate increases because of a large Purcell effect, the 2X emission will be reduced because the QD is less likely to capture the second hole before the X^- recombines. On the basis of this observation, we conclude that a systematic study of the QD-cavity system, only feasible within a deterministic approach, can give new insights into the carrier capture and multi-exciton dynamics of the QDs.

The QD-cavity coupling coefficient (g) that we extract for our device I, using the data for the off- and near-resonance cases (Fig. 2B) and assuming a cavity enhancement of the collection efficiency by a factor of 20 (*23*), is $g \approx 80$ μeV. This value is only half the theoretical maximum for our cavity structure. The value of g as well as its insensitivity to positioning can be improved by using other PC-cavity designs that also exhibit higher Q values and higher fabrication defect tolerance.

By achieving a deterministic spatial and spectral overlap between a QD exciton line and a PC nanocavity mode, we have demonstrated the realization of a truly tunable solid-state cavity QED system and established a framework for the realization of a new set of cavity QED experiments previously implemented only in atomic systems. The broad implication of this research, however, can have some immediate application in several appealing directions, such as cavity-assisted QD spin-flip Raman transition for generation of indistinguishable single photons (*24*), coupling of two QDs to a single common cavity mode (*25*), and simultaneous coupling of a cavity mode to both X and 2X lines of a single QD.

References and Notes

1. Q. A. Turchette, C. J. Hood, W. Lange, H. Mabuchi, H. J. Kimble, *Phys. Rev. Lett.* **75**, 4710 (1995).
2. J. M. Raimond, M. Brune, S. Haroche, *Rev. Mod. Phys.* **73**, 565 (2001).
3. J. M. Gérard, in *Single Quantum Dots: Fundamentals, Application and New Concepts*, P. Michler, Ed., vol. 90 of *Springer Series in Topics in Applied Physics* (Springer, Berlin, 2003), pp. 269–314.
4. P. Michler *et al.*, *Science* **290**, 2282 (2000).
5. E. Moreau *et al.*, *Appl. Phys. Lett.* **79**, 2865 (2001).
6. C. Santori, D. Fattal, J. Vuckovic, G. S. Solomon, Y. Yamamoto, *Nature* **419**, 594 (2002).
7. J. P. Reithmaier *et al.*, *Nature* **432**, 197 (2004).
8. T. Yoshie *et al.*, *Nature* **432**, 200 (2004).
9. E. Peter *et al.*, in preparation (available at http://xxx.lanl.gov/abs/quant-ph/0411076).
10. Fabrication and characterization details are available as supporting material on *Science* Online.
11. K. Hennessy *et al.*, *Appl. Phys. Lett.* **83**, 3650 (2003).
12. Q. H. Xie, A. Madhukar, P. Chen, N. P. Kobayashi, *Phys. Rev. Lett.* **75**, 2542 (1995).
13. D. M. Bruls *et al.*, *Appl. Phys. Lett.* **82**, 3758 (2003).
14. P. M. Petroff, A. Lorke, A. Imamoglu, *Phys. Today* **54**, 46 (2001).
15. The seed QD layer was grown 64 nm below the top surface of the membrane; successive stacked QD layers were spaced by 12 nm of GaAs.
16. K. Hennessy, A. Badolato, P. M. Petroff, E. Hu, *Photonics Nanostruct. Fund. Appl.* **2**, 65 (2004).
17. In the broad field of QD nanosystems, our positioning technique can provide enough accuracy to implement functional devices such as QDs coupled to nanoelectromechanical systems and electrical addressing of single QDs.
18. G. C. DeSalvo *et al.*, *J. Electrochem. Soc.* **143**, 3652 (1996).
19. C. Schulhauser *et al.*, *Phys. Rev. B* **66**, 193303 (2002).
20. Because the X μ-PL intensity at saturation (I_X^{sat}) remained independent of the M-X^- detuning, we compare spectra at different tuning stages by normalizing them to I_X^{sat}. In this way, we rule out potential variations in optical alignment and laser power.
21. The distance between the QD on the surface and the closest hole surface was ~50 nm, which was large enough to keep the seed QD from interacting with the surface states as described in (*22*).
22. C. F. Wang *et al.*, *Appl. Phys. Lett.* **85**, 3423 (2004).
23. This value is derived from a comparison of the on- and off-resonance μ-PL peak intensity for the lowest measured pump power 0.29 P_{sat} (Fig. 3B).
24. A. Kiraz, M. Atature, A. Imamoglu, *Phys. Rev. A* **69**, 032305 (2004).
25. A. Imamoglu *et al.*, *Phys. Rev. Lett.* **83**, 4204 (1999).
26. These simulations were done with commercially available software from Lumerical Solutions.

27. Supported by NSF Nanoscale Interdisciplinary Research Team grant 0304678 (A.B. and P.M.P.), Binational Science Foundation grant 2000233 (A.B. and P.M.P.), NSF Integrative Graduate Education and Research Traineeship grant 9987618 (K.H. and E.H.), and internal grants from ETH Zürich (M.A., J.D., and A.I.). We thank Lumerical Solutions for detailed assistance with the far-field calculations.

Supporting Online Material

www.sciencemag.org/cgi/content/full/308/5725/1158/DC1

Materials and Methods

14 January 2005; accepted 30 March 2005

10.1126/science.1109815

The Highland Mangabey *Lophocebus kipunji*: A New Species of African Monkey

Trevor Jones,[1]* Carolyn L. Ehardt,[2] Thomas M. Butynski,[3] Tim R. B. Davenport,[4] Noah E. Mpunga,[4] Sophy J. Machaga,[4] Daniela W. De Luca[4]

A distinct species of mangabey was independently found at two sites 370 kilometers apart in southern Tanzania (Mount Rungwe and Livingstone in the Southern Highlands and Ndundulu in the Udzungwa Mountains). This new species is described here and given the name "highland mangabey" *Lophocebus kipunji* sp. nov. We place this monkey in *Lophocebus*, because it possesses noncontrasting black eyelids and is arboreal. *L. kipunji* is distinguished from other mangabeys by the color of its pelage; long, upright crest; off-white tail and ventrum; and loud call. This find has implications for primate evolution, African biogeography, and forest conservation.

The most recently discovered species of monkey in Africa was the sun-tailed monkey, *Cercopithecus solatus*, found in Gabon in 1984 (*1*). Here, we report on the discovery of a new species of mangabey in Tanzania. This discovery was made almost simultaneously by independent field-workers on different mountain ranges in southern Tanzania. We relate the circumstances of discovery in the two sites, describe and name the new species, and discuss its conservation status.

Southern Highlands population. The Southern Highlands of southwest Tanzania (Fig. 1) rise to 2961 m above sea level (asl) and comprise mountain ranges capped by forest-grassland mosaic. The Highlands receive rainfall via convectional uplift from Lake Nyasa of up to 2900 mm a year, the highest in Tanzania.

Within the Southern Highlands, the Tanzanian government is presently gazetting the Kitulo Plateau and adjacent Livingstone Forest as the Kitulo National Park (412 km^2, 09°00′S to 09°16′S and 33°43′E to 34°03′E) (*2*). Mount Rungwe Forest Reserve (150 km^2, 09°03′S to 09°12′ S and 33°35′E to 33°45′E) supports montane and upper montane forest, bamboo, and plateau grassland. The montane forests of Mount Rungwe and Livingstone (Rungwe-Livingstone) are joined only by a narrow corridor of degraded forest. Until now, eight species of primate were known from the Southern Highlands, including a probable new species of dwarf galago, *Galagoides* sp. (*3*).

During interviews in January 2003 in villages around Mount Rungwe, we heard rumors about a shy and atypical monkey known as *Kipunji* (kip-oon-jee). The local Wanyakyusa have a strong oral tradition based on both real and mythical forest animals, and validation of these rumors was protracted. We first observed an unusual primate during biodiversity surveys on Mount Rungwe in May 2003, but

[1]Udzungwa Mountains National Park, Box 99, Mang'ula, Tanzania. [2]Department of Anthropology, University of Georgia, Athens, GA 30602–1619, USA. [3]Conservation International, Post Office Box 68200, City Square 00200, Nairobi, Kenya. [4]Wildlife Conservation Society, Southern Highlands Conservation Programme, Post Office Box 1475, Mbeya, Tanzania.

*To whom correspondence should be addressed. E-mail: tembomkubwa@gmail.com

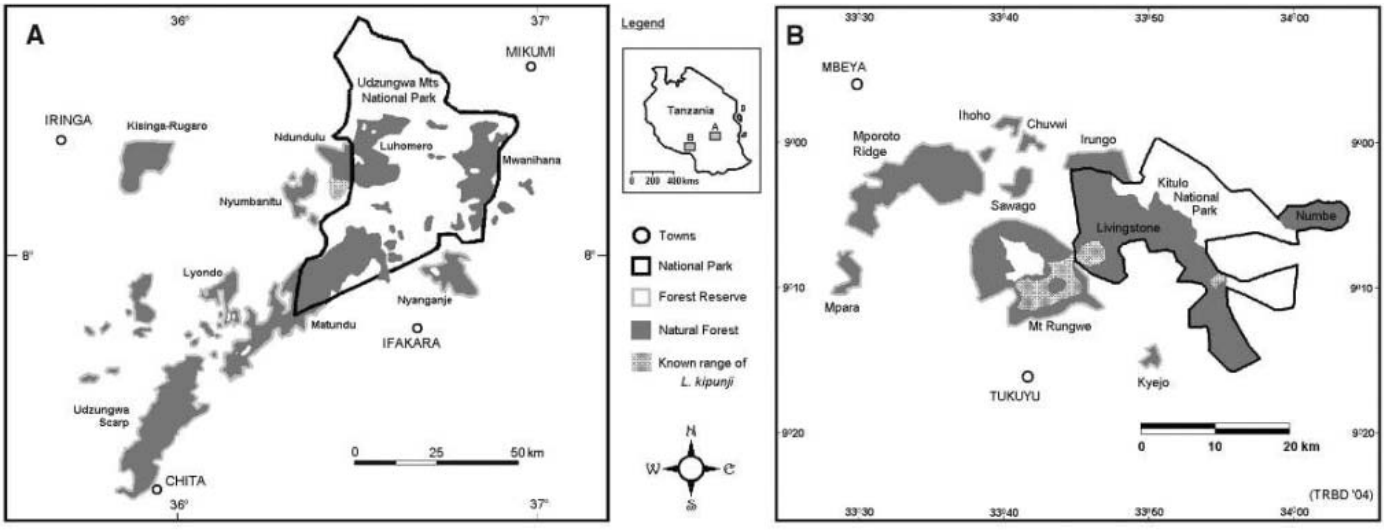

Fig. 1. Maps of Tanzania's Udzungwa Mountains (**A**) and Southern Highlands (**B**) showing the known range of the highland mangabey *Lophocebus kipunji*.

because of the terrain, thick secondary forest, and the animal's cryptic nature, sightings were infrequent and poor. It was not until December 2003, during work in the contiguous Livingstone Forest, that the monkey was clearly observed and recognized as a new species of mangabey.

Ndundulu population. The Udzungwa Mountains (Udzungwas: 10,000 km^2, 07°40′S to 08°40′S and 35°10′E to 36°50′E) lie 350 km to the northeast of Rungwe-Livingstone (*4*, *5*). Supporting circa (ca.) 1017 km^2 of fragmented forest (*6*), the Udzungwas receive a maximum annual rainfall of roughly 2200 mm and were previously thought to hold 10 primate species (*7*), including the endemic Sanje mangabey, *Cercocebus sanjei*, discovered in 1979 (*8*).

Two populations of the Sanje mangabey are known from the Udzungwas (*7*, *9*). During visits from 1991 to 2000, ornithologists working in the Ndundulu Forest Reserve (Fig. 1) reported a third population of the Sanje mangabey (*10*). Subsequent surveys failed to confirm the presence of this species in Ndundulu (*7*, *9*, *11*) and led to our intensified surveys in July and September 2004. During these surveys, Sanje mangabeys were not encountered or heard. However, on 7 July 2004, the new species of mangabey was discovered. It now seems certain that the ornithologists had misidentified the new species of mangabey as the Sanje mangabey.

The researchers working on each of these two new populations of mangabeys did not become aware that a second population was known until October 2004.

Lophocebus kipunji Ehardt, Butynski, Jones, and Davenport sp. nov.

Holotype. Adult male in photograph (Fig. 2). Photograph taken in the type locality at 9°07′S 33°44′E (*12*). The number of individuals in each of the two populations of this species is undoubtedly very small; no live individual should be collected at this time to serve as the holotype. The Rungwe-Livingstone population is designated the source population for physical specimens in support of the holotype.

Fig. 2. Holotype: adult male highland mangabey *Lophocebus kipunji* in the type locality, Rungwe-Livingstone, Tanzania. [Photograph by T.R.B. Davenport]

Paratype. Adult in photograph (Fig. 3). Sex not known. Photograph taken in Ndundulu Forest Reserve (07°48′45″S 36°31′05″E), Udzungwa Mountains, Tanzania.

Type locality. Rungwe-Livingstone (09°07′S to 09°11′S and 33°40′E to 33°55′E), Southern Highlands, Tanzania.

Diagnosis. Pelage of dorsum light to medium brown, center of ventrum and distal half of tail off-white. Crown with very long, broad, erect crest of hair. Eyelids black, not contrasting with color of face. Adults emit a distinctive, loud, low-pitched ''honk-bark'' (Fig. 4). Arboreal. Found only at high altitudes (1300 m up to 2450 m asl) and low-temperature tolerant; temperatures in Rungwe-Livingstone drop to at least –3°C.

Fig. 3. Paratype: adult highland mangabey *Lophocebus kipunji*, Ndundulu Forest Reserve, Tanzania. [Photograph by T. Jones]

Description. A primarily brown, medium-sized, long-tailed, arboreal monkey. Muzzle elongated. Facial skin, including eyelids, black. Suborbital fossae ''tear line'' pronounced. Eyes brown. Pelage light to rufous brown except as follows: center of ventrum and distal half of tail, white to off-white; hands and feet, black; lower forelimbs, dark brown to black. Cheek whiskers long. Crown with very long, broad, stiff, upright crest of hair. Shoulder cape present in some individuals, although there is variation in length and color. White of ventrum sharply offset from brown in at least

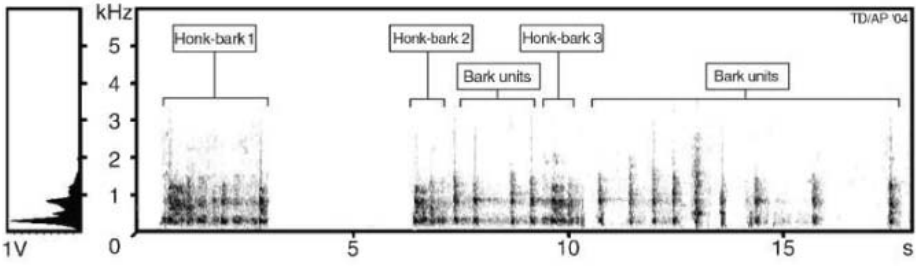

Fig. 4. Sonogram of three honk-bark calls given by adult *L. kipunji* from the type locality, with two series of barks. Honk-barks, which appear to play a role in intergroup spacing, are given singly or in series and may, as in this example, be interspersed with barks. Honk-barks are short discrete phrases, composed of a variable number of units. The first honk-bark shown here has six units. Honk-barks are frequency modulated with formants or emphasized harmonics. In the honk-bark, the first harmonic or "fundamental frequency" is that part of the call with the lowest frequency and often the greatest amplitude, and is thus the farthest traveling element. The fundamental frequency of the honk-bark is 0.28 kHz (n = 3), the frequency range is 0.180 to 0.304 kHz, and the mean unit interval is 0.076 s (n = 3). This call is thus qualitatively and quantifiably different from the type I and type II calls of other studied mangabey species (*20*, *21*). [Call recorded by N. E. Mpunga. Sonogram prepared and interpreted by A. Perkin.]

some Ndundulu animals. Ventrum lighter than rest of body in Rungwe-Livingstone animals but not sharply offset. Small patch of off-white hair between neck and sternum in Rungwe-Livingstone animals. Individual hairs appear to be straight and devoid of bands or speckling. Tail pelage smooth, not shaggy or lax. Tail carried loosely and parallel to or below plane of the back, curving downward to feet level during locomotion. Tail not held strongly arched over back when standing, nor held vertically, except as a semi-prehensile support. No sexual dimorphism in color of adult pelage. Ischial callosities pink: fused in the male, unfused in the female. Genital swelling in oestrus females.

Measurements. None available. Head-body length of adult males in the Rungwe-Livingstone population estimated at 85 to 90 cm. Tail about equal in length to head and body. Adult male body weight estimated at 10 to 16 kg.

Etymology. The specific name acknowledges the Kinyakyusa name for this monkey in Rungwe-Livingstone.

Distribution. Known to occur in ca. 70 km^2 of Rungwe-Livingstone in the Southern Highlands, Tanzania, from 1750 up to 2450 m asl (possibly up to 2600 m asl), and from ca. 3 km^2 of Ndundulu Forest Reserve, Tanzania, from 1300 up to 1750 m asl.

Habitat. From pristine submontane forest in Ndundulu to degraded montane and upper montane forest in Rungwe-Livingstone.

Mangabeys are medium-sized monkeys confined to the forests of equatorial Africa (*13*). Taxonomically controversial, there are currently from five to nine species (and from five to 11 subspecies) recognized in two genera (*Lophocebus* and *Cercocebus*) (*14*, *15*). The mangabeys are diphyletic, as revealed by molecular studies and supported by anatomical and behavioral characteristics. *Cercocebus* spp. are most closely related to mandrills and drills (*Mandrillus* spp.), have pink or white eyelids that contrast with the color of the face, and are semiterrestrial. *Lophocebus* spp. are most closely related to baboons, *Papio* spp., and the gelada, *Theropithecus gelada*; have black eyelids that do not contrast with the color of the face; and are arboreal (*14*, *16*–*18*). We place this new species in the genus *Lophocebus* on the basis of the combination of its noncontrasting black eyelids and arboreality. *L. kipunji* is isolated from the nearest other species of *Lophocebus* (*L. albigena*) by about 800 km.

The other two species of *Lophocebus* (*15*) differ from *L. kipunji* as follows:

Gray-cheeked mangabey *L. albigena*: Body and tail blackish-brown. Cheek whiskers gray. Crown with short tuft (or tufts) of hair (*14*). Frequently holds tail vertical or arched over back. ''Whoop-gobble'' loud call. Mainly occurs below 1600 m (*13*), except Nyungwe, Rwanda, and Kahuzi-Biega, Democratic Republic of Congo, where it occurs up to ca. 2350 m (*19*).

Black mangabey *L. aterrimus*: Entire body black. Crown with tall, thin, central tuft of hair. Cheek whiskers thick and gray (*14*). Whoop-gobble loud call. Not known to occur above 450 m asl.

All mangabey species studied to date possess a loud call, emitted by adult males to coordinate intergroup spacing (*20*, *21*). The characteristic whoop-gobble loud call of other *Lophocebus* species has not been detected in *L. kipunji*. Adult males in Rungwe-Livingstone do give a distinctive honk-bark (Fig. 4), which is most evident when conspecific groups meet.

In Rungwe-Livingstone, we have identified 10 groups of *L. kipunji*: five in the southern section of Mount Rungwe, four in the northern section of Livingstone, and one in the southern section of Livingstone 20 km to the east (Fig. 1). We estimate the total population of *L. kipunji* in Rungwe-Livingstone to be 250 to 500 animals.

L. kipunji are known from only 3 km^2 of Ndundulu Forest. Previous research in the area (*7*, *11*, *22*, *23*) and lack of independent knowledge of the species among local villagers indicate that this monkey is absent from large parts of this forest. We estimate the geographic range for this population to be 3 to 50 km^2. Only three groups have so far been located in Ndundulu, and it seems unlikely that this population exceeds 500 animals.

Once the degree of threat status is formally assessed for the *IUCN Red List of Threatened Animals*, we expect that *L. kipunji* will be classified as a critically endangered species (*24*).

The presence of a third threatened species of monkey makes the Udzungwas arguably the most important single site in Africa for the conservation of primate biodiversity. The presence of *L. kipunji* in both sites also supports the hypothesis that the Southern Highlands are zoologically more aligned to the Eastern Arc Mountains than has usually been thought (*25*).

The threats to *L. kipunji* are considerable. The Rungwe-Livingstone forests are severely degraded. Logging, charcoal making, poaching, and unmanaged resource extraction are common. The narrow forest corridors linking Mount Rungwe to Livingstone and joining the northern and southern sections of Livingstone are almost completely encroached upon. Without immediate conservation intervention, these forests will be fragmented, resulting in three isolated subpopulations of *L. kipunji*; indeed, the easternmost animals may already be isolated. Gazettement of Kitulo National Park should help protect the smaller Livingstone Forest population. However, swift and effective action is imperative, both in the new park and especially within Mount Rungwe Forest Reserve.

Although the submontane forest of Ndundulu is in excellent condition and no signs of recent hunting have been observed in the area from which *L. kipunji* is known, this monkey is present in low numbers. If this small population is to be protected in perpetuity, the Udzungwa Mountains National Park needs to be extended to include the Ndundulu Forest.

References and Notes

1. M. J. S. Harrison, *J. Zool.* **215**, 561 (1988).
2. T. R. B. Davenport, *Oryx* **36**, 224 (2002).
3. A. Perkin, personal communication.
4. N. Myers, R. A. Mittermeier, C. G. Mittermeier, G. A. B. da Fonseca, J. Kent, *Nature* **403**, 853 (2000).
5. T. M. Brooks *et al.*, *Conserv. Biol.* **16**, 909 (2002).
6. N. D. Burgess, J. Fjeldså, R. Botterweg, *J. East Afr. Nat. Hist.* **87**, 37 (1998).
7. C. L. Ehardt, *Afr. Primates* **4**, 15 (2001).
8. K. M. Homewood, W. A. Rodgers, *Int. J. Primatol.* **2**, 47 (1981).
9. C. L. Ehardt, T. Jones, T. M. Butynski, *Int. J. Primatol.* **26**, 557 (2005).
10. L. Dinesen, T. Lehmberg, M. C. Rahner, J. Fjeldså, *Biol. Conserv.* **99**, 223 (2001).
11. C. L. Ehardt, T. T. Struhsaker, T. M. Butynski, "Conservation of the Endangered Primates of the Udzungwa Mountains, Tanzania: Surveys, Habitat Assessment, and Long-Term Monitoring" (Margot Marsh Biodiversity

Foundation, Great Falls, VA, and Conservation International, Washington, DC, 1999).
12. A. Wakeham-Dawson, S. Morris, P. Tubbs, *Bull. Zool. Nomencl.* **59**, 18 (2002).
13. J. Kingdon, *The Kingdon Field Guide to African Mammals* (Academic Press, London, 1997).
14. C. P. Groves, *Primate Taxonomy* (Smithsonian, Washington, DC, 2001).
15. P. Grubb *et al.*, *Int. J. Primatol.* **24**, 1301 (2003).
16. C. P. Groves, *Primates* **19**, 1 (1978).
17. E. E. Harris, T. R. Disotell, *Mol. Biol. Evol.* **15**, 892 (1998).
18. J. G. Fleagle, S. W. McGraw, *Proc. Natl. Acad. Sci. U.S.A.* **96**, 1157 (1999).
19. R. J. Dowsett, F. Dowsett-Lemaire, in *Survey of the Fauna and Flora of Nyungwe Forest, Rwanda*, R. J. Dowsett, Ed. (Tauraco, Ely, UK, 1990), pp. 111–121.
20. P. M. Waser, in *Primate Communication*, T. Snowdon, C. H. Brown, M. R. Peterson, Eds. (Cambridge Univ. Press, Cambridge, 1982), pp. 117–144.
21. F. Range, J. Fischer, *Ethology* **110**, 301 (2004).
22. K. Z. Doody, K. M. Howell, E. Fanning, Eds., "West Kilombero Scarp Forest Reserve zoological report" (Udzungwa Mountains Forest Management and Biodiversity Conservation Project, Matumizi Endelevu ya Misitu ya Asili, Iringa, Tanzania, 2001).
23. A. R. Marshall, J. E. Topp-Jorgensen, H. Brink, E. Fanning, *Int. J. Primatol.* **26**, 127 (2005).
24. *IUCN Red List Categories and Criteria: Version 3.1* (IUCN–The World Conservation Union Species Survival Commission, IUCN, Gland, Switzerland, 2001).
25. T. R. B. Davenport, *Soc. Conserv. Biol. Abst.* **48**, 20 (2004).
26. C.L.E. (Sanje Mangabey Research Project, SMRP) and T.R.B.D. (Southern Highlands Conservation Programme, SHCP) directed the projects that produced the discoveries. T.J. located and observed the Ndundulu population. T.J., C.L.E., and T.M.B. contributed data for the Ndundulu population; T.R.B.D., N.E.M., S.J.M., and D.W.D. located, observed, and contributed data for the Rungwe-Livingstone population; T.J., C.L.E., T.M.B., and T.R.B.D. wrote the paper with editorial input from N.E.M., S.J.M., and D.W.D. Fieldwork in Rungwe-Livingstone was funded by the Wildlife Conservation Society (WCS) through the SHCP with the generosity of E. McBean, G. Fink, Nikon Incorporated, and an anonymous donor. We thank SHCP staff, R. Ngindale, G. Patterson, Rungwe District Council, P. Chibwaye, Tanzania National Parks (TANAPA), W. Mwakilema, Z. Tweve, J. Maher, and B. Stanley. Fieldwork in Ndundulu (SMRP) was supported by WCS, Primate Society of Great Britain, Critical Ecosystem Partnership Fund, Conservation International, Primate Action Fund, the Margot Marsh Biodiversity Foundation, the University of Georgia Research Foundation, and Primate Conservation, Incorporated. We thank A. Alchard, R. Laizzer, A. Mndeme, Tanzanian Wildlife Research Institute, Tanazania Commission for Science and Technology, TANAPA, Iringa District Council, J. Massao, I. Chahe, J. Mudanga, Q. Luke, and the two anonymous reviewers of the manuscript. Particular thanks to L. Dinesen, T. Lehmberg, and A. Marshall for locational information on Ndundulu; A. Perkin for preparing the sonogram; and A. Polaszek for expert advice on behalf of the International Commission on Zoological Nomenclature.

27 December 2004; accepted 3 March 2005
10.1126/science.1109191

Functional Genomic Analysis of RNA Interference in *C. elegans*

John K. Kim,[1,2]* Harrison W. Gabel,[1,2]* Ravi S. Kamath,[1,2]*† Muneesh Tewari,[2,3,4,5] Amy Pasquinelli,[1,2]‡ Jean-François Rual,[2,3] Scott Kennedy,[1,2]§ Michael Dybbs,[1,2] Nicolas Bertin,[2,3,5] Joshua M. Kaplan,[1,2] Marc Vidal,[2,3,5] Gary Ruvkun[1,2]‖

RNA interference (RNAi) of target genes is triggered by double-stranded RNAs (dsRNAs) processed by conserved nucleases and accessory factors. To identify the genetic components required for RNAi, we performed a genome-wide screen using an engineered RNAi sensor strain of *Caenorhabditis elegans*. The RNAi screen identified 90 genes. These included Piwi/PAZ proteins, DEAH helicases, RNA binding/processing factors, chromatin-associated factors, DNA recombination proteins, nuclear import/export factors, and 11 known components of the RNAi machinery. We demonstrate that some of these genes are also required for germline and somatic transgene silencing. Moreover, the physical interactions among these potential RNAi factors suggest links to other RNA-dependent gene regulatory pathways.

Posttranscriptional gene silencing by RNAi is a conserved process by which dsRNA triggers the destruction of homologous target mRNAs (*1*). RNAi-related mechanisms also mediate heterochromatin formation, silencing of transposable elements, antiviral defense, genome rearrangements, cell proliferation, cell differentiation, cell death, and developmental timing and patterning (*2*–*5*).

Although genetic and biochemical studies have identified components of RNAi, including the dsRNA processing enzyme Dicer (DCR-1) and the effector complexes RISC (RNA induced silencing complex) and RITS [RNA-induced initiation of transcriptional gene silencing (TGS)] (*1*, *2*), a comprehensive genomic analysis by RNAi should in principle identify the complete pathway. Using RNAi to identify RNAi factors has been demonstrated previously (*6*). In addition, the production of non-null phenotypes by RNAi enables the study by RNAi of essential genes, such as *dcr-1*, the only *C. elegans* Dicer. In this study, we have used a genome-wide approach to identify an extensive set of genes required for RNAi in *C. elegans*.

To monitor RNAi in vivo, we designed an "RNAi sensor" strain (GR1401) that expresses both a *gfp* (green fluorescence protein) dsRNA hairpin and a *gfp* reporter gene in *C. elegans* epithelial seam cells (Fig. 1A). In wild-type animals, *gfp* dsRNA targets the *gfp* mRNA for degradation, abrogating GFP expression. Feeding the *C. elegans* RNAi sensor strain bacteria that express dsRNA corresponding to genes previously implicated in RNAi robustly restored GFP expression, whereas control dsRNA did not (Fig. 1B).

We screened a library of bacterial clones expressing dsRNAs designed to individually inactivate 94% of the ~19,000 predicted genes in the worm genome (*7*, *8*) [table S1 (*9*)]. L1-stage larvae of the RNAi sensor strain were fed each bacterial clone, and GFP fluorescence was monitored in their progeny. For the 945 genes annotated as embryonic lethal (*7*), L1-stage animals were fed the bacterial clone and GFP fluorescence was monitored in the later larval or adult stage of the same generation. All experiments were scored on a GFP intensity and penetrance scale of 0 (no GFP expression) to 4 (highly penetrant, strong GFP expression), and those that scored an average of ~2 or greater were designated candidate RNAi genes (Table 1). All candidate clones were retested no fewer than five independent times in triplicate.

Screening of the genome-wide RNAi library identified 90 clones (0.5%) that reproducibly disrupt RNAi. Eleven of these correspond to loci known to be required for RNAi, including the core RNAi machinery such as *dcr-1*, *rde-1*, and *rde-4* (Table 1 and table S2). Fifty-four of the new genes are essential for viability, and one-third of the viable 25 new genes exhibit reduced brood sizes ($P < 0.01$, Student's *t* test) (table S3); 85% of the new genes have human homologs, suggesting conserved functions (Table 1 and table S4). It is possible that some of the identified factors could be nonspecific; for example, inactivation of a factor (e.g., *dpy-20*) could inhibit the expression from one epidermal promoter of the RNAi sensor strain but not the other. However, because a large majority of the RNAi clones tested also affect transgene silencing in a variety of other tissues (see below), most are likely to act in the RNAi pathway.

To verify that genes uncovered in our screen are required for RNAi of endogenous

[1]Department of Molecular Biology, Massachusetts General Hospital, Boston, MA 02114, USA. [2]Department of Genetics, Harvard Medical School, Boston, MA 02114, USA. [3]Center for Cancer Systems Biology, [4]Department of Medical Oncology, [5]Department of Cancer Biology, Dana-Farber Cancer Institute, Boston, MA 02115, USA.

*These authors contributed equally to this work.
†Present address: Department of Medicine, Brigham and Women's Hospital, Boston, MA 02115, USA.
‡Present address: Molecular Biology Section, Division of Biology, University of California, San Diego, La Jolla, CA 92093–0349, USA.
§Present address: Department of Pharmacology, University of Wisconsin, Madison, WI 53706, USA.
‖To whom correspondence should be addressed. E-mail: ruvkun@molbio.mgh.harvard.edu

genes, we coinjected animals with dsRNA of each candidate RNAi gene together with dsRNA of *mom-2*, a gene essential for viability (fig. S1) (*6*). The survival of progeny indicates that inactivation of the candidate gene renders animals resistant to the lethality of *mom-2* RNAi. Because the coinjection assay relies on detecting a phenotype in the progeny of injected worms, only the 36 RNAi genes that are not essential for viability were examined (Table 1 and fig. S1). Inactivation of 10 newly identified and 11 known RNAi genes rescued the lethality associated with injection of *mom-2* dsRNA (>45% viability, $P < 0.05$), compared to coinjection with dsRNAs targeting genes dispensable for RNAi [fig. S1 (*9*)] or injection of *mom-2* dsRNA alone.

Among the new RNAi candidates, we identified six proteins with domains found in known RNAi factors: Two proteins contain either a PIWI domain (C04F12.1) or both PIWI and PAZ (K12B6.1) domains found in Argonaute and the RNAi factor RDE-1; F22D6.6 possesses a Tudor RNA binding domain identified in the TSN micrococcal nuclease of RISC; and Y38A10A.6, F56D2.6, and C06E1.10 have DEAD/DEAH-box motifs found in Dicer, MUT-14, DRH-1, and DRH-2 (*1*).

RNA binding and processing factors constitute the largest class of new RNAi factors identified and suggest new steps in the RNAi pathway as well as overlap with other RNA-mediated gene regulatory pathways (Table 1). We identified components of the pre-mRNA cleavage and polyadenylation complex that functions in the formation of mRNA 3′ ends (*10*), including *F09G2.4*, *cpf-2*, and *F43G9.5*, key components of the cleavage and polyadenylation specificity factor (CPSF/F09G2.4), the cleavage stimulation factor (CstF/CPF-2), and the cleavage factor I (CF I_m/F43G9.5), respectively. A mutation in a predicted polyadenylate [poly(A)] polymerase component exhibits an Rde phenotype in *C. elegans* (*11*), whereas poly(A) polymerase (Cid12) associates with the RITS complex in *Schizosaccharomyces pombe* (*12*).

We also identified the nonsense-mediated decay (NMD) gene *smg-2*, as well as three genes predicted to function in NMD—*T25G3.3*, *paa-1*, and *F26A3.2*—as modulators of RNAi, consistent with previous observations implicating *smg-2* and, to a lesser degree, *smg-5* and *smg-6*, in RNAi (*13*). dsRNA processing and initial degradation of the target mRNA are unaffected in *smg* (−) mutants, suggesting that the NMD factors act downstream of siRNA production and initial target cleavage (*13*).

We identified factors required for nuclear import and export, including the Ran GTPase (guanosine triphosphatase) exchange factor RCC1 (*ran-3*), the Ran GTPase binding protein 1 (*npp-9*), and nucleoporins (*npp-1* and *npp-16*) (*14*). In addition, the identification of nuclear import receptors of the importin-α and -β families (*imb-2*, *imb-5*, and *ima-3*) (*15*) suggest a mechanism whereby siRNAs generated in the cytoplasm may subsequently be reimported into the nucleus for TGS.

dsRNAs targeting a genomic locus are known to recruit heterochromatin factors and drive heterochromatin formation and TGS in an RNAi-dependent manner (*2*). A number of RNAi genes encode predicted chromatin factors that may mediate TGS in response to dsRNAs. We identified two Polycomb-related components, MES-4 and T23B12.1, consistent with the finding that TGS requires Polycomb in *Drosophila* and germline transgene silencing requires MES-4 in *C. elegans* (*2*, *16*) (fig. S2). In addition, we identified Sin3 and histone deacetylase complex (HDAC) genes *hda-3*, *pqn-28*, and *rba-1*. Components of Polycomb and HDAC, in addition to the RNAi machinery and RITS, are all required for heterochromatin formation (*2*, *6*). The finding that these chromatin factors are also essential for RNAi implicates the Polycomb and HDAC complexes in an RNAi-mediated gene silencing mechanism and strongly suggests a TGS component to *C. elegans* RNAi.

Other classes of factors that regulate RNAi include the DNA repair factor RuvB and the mitogen-activated protein (MAP) kinase pathway factors ZC449.3 and MTK-1. The DNA repair and recombination factors suggest that the RNA replication or TGS steps in RNAi may include checkpoints and control mechanisms related to those used in DNA replication and recombination. The established role of the ancient p38/MAP kinase pathway in the innate immune response to pathogens suggests that RNAi mechanisms may also be coupled to these stress and pathogen sensing pathways (*17*). A group of genes of unknown function includes the new *rde-5* gene identified by forward genetics (*18*). Five members of this group have orthologs in humans, suggesting conserved functions (Table 1 and table S4).

Transgene silencing in *C. elegans* is mechanistically related to RNAi. A subset of genes required for RNAi are essential for transgene silencing in the germ line, including *dcr-1*, *mut-7*, and *mut-16* (*19*, *20*). However, other genes, including *rde-1* and *rde-4*, are essential for RNAi but dispensable for germline silencing (fig. S2) (*19*), demonstrating that germline gene silencing and RNAi may require distinct, possibly paralogous, sets of genes.

We tested the roles of the new RNAi factors in germline transgene silencing using *let-858p::gfp* (PD7271), which is silenced in the germ line but is expressed in somatic tissues (*21*). Expression of *let-858p::gfp* in the germ

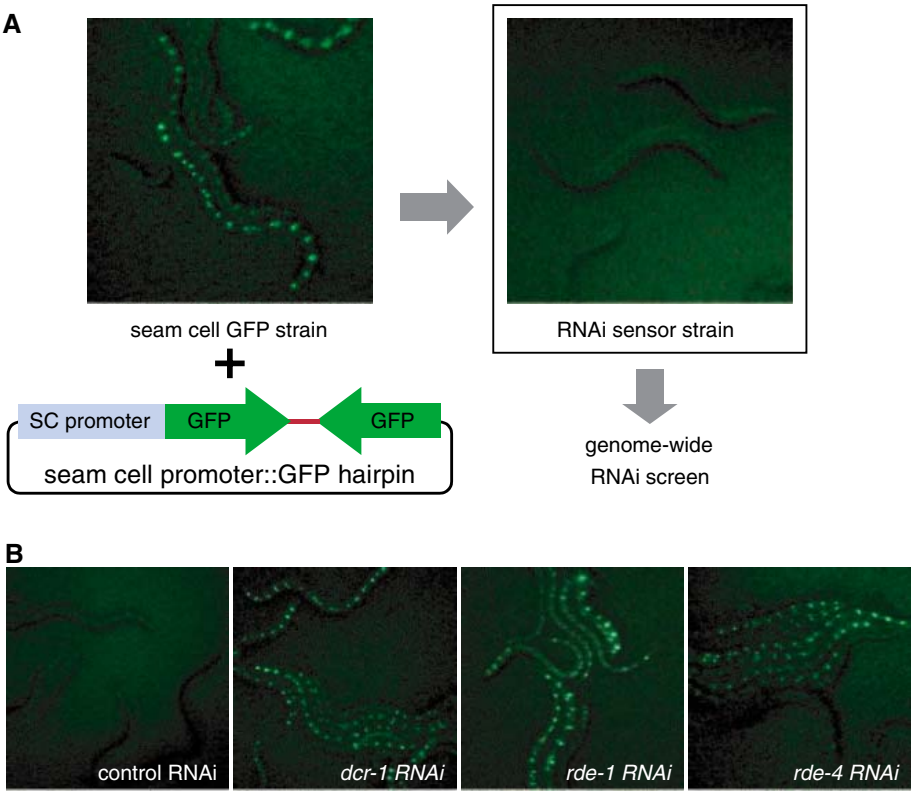

Fig. 1. A scheme for the genome-wide screen to identify factors required for RNAi. (**A**) The RNAi sensor strain (GR1401) is composed of a dsRNA GFP hairpin that silences the GFP reporter expression in the seam cells by RNAi. (**B**) Inhibiting the RNAi pathway by feeding the RNAi sensor strain *Escherichia coli* that expresses dsRNA corresponding to the core RNAi genes *dcr-1*, *rde-1*, and *rde-4* (but not control vector) restores the reporter GFP expression in the seam cells.

line is restored when RNAi of *dcr-1*, *mut-7*, or *mut-16* is sustained for two generations (fig. S2). We assayed expression of *let858p::gfp* in the germ line after inactivation of the 36 RNAi candidates that are viable for multiple generations. Inactivation of 14 of these genes abrogates germline gene silencing, including 9 newly identified RNAi genes (fig. S2 and Table 1). These findings demonstrate a substantial overlap between factors required for RNAi and germline silencing.

To monitor transgene silencing in somatic cells, we developed an assay based on the observation that the seam-cell GFP transgene (in the absence of a transgene expressing GFP dsRNA) is completely silenced in the *eri-1* enhanced RNAi background (*22*). Inactivation of 87 of the 90 genes identified in our screen restored expression of the seam-cell GFP transgene (fig. S3A and Table 1). In addition, expression of a second ubiquitously expressed reporter, *sur-5::gfp* (*23*), which is also silenced by *eri-1*, was restored in nonneuronal tissues in most of the gene inactivations tested (fig. S3B and Table 1). Similar results were observed using another enhanced RNAi strain, *rrf-3* (*24*) (table S3). These findings indicate a near-complete functional overlap of factors required for RNAi and somatic transgene silencing and strongly suggest that the factors identified do not simply affect the epidermal promoters used in the RNAi sensor strain. Silencing in the germ line may use paralogs of

Viable Clones

Gene Targeted	Locus	Description	Homology Hs	Mm	Dm	Sp	GFP Score	Co-injection	Germline Silencing	Transgene Silencing scm	sur-5
Known RNAi											
B0379.3	*mut-16*	Novel nematode protein					4.0	+	+	+	+
K12H4.8	*dcr-1*	DICER RNase III					4.0	+	+	+	+
T20G5.11	*rde-4*	dsRNA binding protein					4.0	+	-	+	+
F15B10.2	*drh-1*	DEAD/DEAH box helicase					2.4	+	+	+	+
M04B2.3	*gfl-1*	Chromatin associated protein					2.3	+	-	+	+
K08H10.7	*rde-1*	Piwi and PAZ domain protein					4.0	+	-	+	+
Y2H9A.1	*mes-4*	SET domain nuclear protein					4.0	+	+	+	+
F52G2.2	*rsd-2*	Required for siRNA spreading					4.0	+	-	+	+
Y48G8AL.6	*smg-2*	NMD protein; RNAi persistance					2.4	+	-	+	-
ZK1098.8	*mut-7*	3'-5' exonuclease domain					2.5	+	+	+	+
F54F2.2	*zfp-1*	Chromatin-associated protein					3.2	+	-	+	+
Chromatin factors											
F02E9.4	*pqn-28*	SIN3 component					2.8	-	-	+	+
R06C1.1	*hda-3*	Histone deacetylase					2.5	+	+	+	+
M03C11.3		Chromatin associated protein					3.6	-	+	+	+
T23B12.1		Polycomb-like PHD Zn-finger					2.3	-	-	-	-
Nuclear import/export											
Y56A3A.17	*npp-16*	Nuclear pore complex component					2.2	-	-	+	+
Other											
F37B12.4		Ubiquitin carboxyl-terminal hydrolase					2.3	-	-	+	-
Piwi/Paz, Tudor, or DEAD/DEAH helicase domains											
C04F12.1		Piwi domain protein					4.0	+	-	+	+
K12B6.1		Piwi and PAZ domain protein					2.5	-	-	+	-
F22D6.6		Tudor domain					2.3	-	+	+	+
Y38A10A.6		DEAD/DEAH-box RNA helicase					2.9	+	-	+	+
RNA binding & processing											
F43G9.5		Pre-mRNA cleavage factor subunit					3.5	-	+	+	-
ZK112.2	*ncl-1*	B-box Zn-finger protein					2.7	+	-	+	+
K08D10.4	*rnp-2*	Spliceosomal protein					2.9	-	+	+	+
W05H7.4		Zn-finger protein					2.3	+	-	+	-
T19B10.4	*pqn-70*	mRNP component					2.3	-	-	+	+
Y71G10AL.1		S.c H/ACA snoRNP homolog					2.4	+	-	+	+
C12D8.1		KH domain protein					2.1	+	-	+	-
Signaling											
B0414.7	*mtk-1*	MAPKKK; ortholog of H.s. MEKK4					3.0	+	-	+	+
ZC449.3		MAPKK; homolog of H.s. MKK4					3.0	-	-	-	+
Transcription											
R03D7.4		RNA pol II elongation factor					2.8	+	+	+	+
ZK1127.6,9¶		Transcription elongation factor CA150					3.5	-	+	+	+
T22B3.1	*dpy-20*	BED zinc finger DNA-binding protein					2.5	-	-	+	+
Unknown											
T01C3.8	*rde-5*	New rde gene *(18)*					3.9	-	+	+	-
T19B4.5							2.5	+	-	+	+
ZK1127.3							2.7	-	+	+	+
None/vector							0.1	-	-	-	-

Lethal Clones

Gene Targeted	Locus	Description	Homology Hs	Mm	Dm	Sp	GFP Score	Transgene Silencing
Chromatin factors								
C26D10.1	*ran-3*	GTPase exchange factor RCC1					3.1	+
K07A1.11	*rba-1*	Rb-binding protein; RbAp48, CAF-1-like					2.7	+
D2096.8		Nucleosome assembly protein					3.3	+
T08G11.4		Methyltransferase domain					2.9	+
ZK1127.7		DNA topoisomerase type II					2.3	+
DNA damage repair								
C27H6.2		RuvB-like 1					2.4	+
T22D1.10		RuvB-like 2					2.7	+
ZK1127.4		BRCA2 interacting protein					3.2	+
Nuclear import/export								
F32E10.4	*ima-3*	Importin-α family					4.0	+
R06A4.4	*imb-2*	Importin-β family					1.9	+
Y48G1A.5	*imb-5*	Importin-β family					3.8	+
K07F5.13	*npp-1*	Nuclear pore protein					2.6	+
F59A2.1	*npp-9*	Ran GTPase-binding protein					3.0	+
C07E3.2		Nuclear export of pre-ribosomes					3.7	+
Other								
F54H12.1	*aco-2*	Mitochondrial aconitase homolog					2.5	+
T09A5.10	*lin-5*	Spindle apparatus component					2.3	+
F46A9.5	*skr-1*	SCF ubiquitin ligase					3.0	+
F56A3.4	*spd-5*	Mitotic spindle assembly					2.8	+
Y38F2AL.3	*vha-11*	Vacuolar H+-ATPase V1 sector					2.3	+
F43G9.1		Mitochondrial isocitrate dehydrogenase					2.6	+
F43G9.10		Microfibrillar-associated protein MFAP1					2.3	+
W04C9.1	*haf-4*	ABC transporter					3.0	+
DEAD/DEAH helicase domains								
C06E1.10		DEAD/DEAH-box RNA helicase					3.0	+
F56D2.6		DEAD/DEAH-box RNA helicase					2.9	+
Protein synthesis								
C15F1.4	*ppp-1*	Translation initiation factor eIF2B subunit					2.2	+
F52B5.6	*rpl-25.2*	60S ribosomal subunit L23a protein					3.7	+
F59A3.3		KOW motif found in ribosomal proteins					2.8	+
Y61A9LA.10		GTP-binding protein AARP2					2.6	+
RNA binding & processing								
R06F6.1	*cdl-1*	Cell Death Lethal-1					1.9	+
F56A8.6	*cpf-2*	mRNA cleavage stimulation factor					2.1	+
F48E8.5	*paa-1*	PP2A subunit A; binds SMG-5					1.9	+
W07E6.4	*prp-21*	PRP splicing factor related protein					2.8	+
D2089.1	*rsp-7*	Splicing factor, arginine/serine-rich					2.5	+
Y71F9B.4	*snr-7*	Small nuclear ribonucleoprotein G					3.3	+
E02H1.1		Ribosomal RNA adenine dimethylase					3.0	+
F09G2.4		mRNA cleavage and polyA factor					2.9	+
F26A3.2		Nuclear cap-binding protein complex					2.8	+
F49D11.1		Pre-mRNA splicing factor PRP17					2.0	+
T25G3.3		Upf1p-interacting protein in yeast					3.5	+
ZK1127.5		RNA 3'-terminal phosphate cyclase					3.3	+
Signaling								
T01G9.6	*kin-10*	Casein kinase II, beta subunit					3.8	+
Transcription								
W10C8.2	*pop-1*	Transcription factor TCF-4					3.8	+
C16A3.4		C2H2-type Zn-finger domain					2.9	+
C55B7.5		Prefoldin chaperone domain					2.4	+
F43G9.12		Transcriptional regulator					2.2	+
T12D8.1		Transcriptional regulator					2.3	+
W06E11.1		RNA polymerase III subunit					2.2	+
Unknown								
C06A5.1							2.7	+
C29E4.2							2.3	+
F26E4.4		Predicted nuclear localization					3.3	+
K12H4.5							2.2	-
T23D8.3							3.2	+
W04A4.5							2.3	+
Y110A7A.19		Contains TPR-like domain					3.0	+
None/vector							0.1	-

Table 1. Best reciprocal BLASTP matches (dark gray box) or homologs (light gray box) with BLASTP *e*-value $\leq 10^{-6}$ in human (*Hs*), mouse (*Mm*), fly (*Dm*), and fission yeast (*Sp*) are indicated. Also indicated: GFP score from the screen, rescue (+) from *mom-2* dsRNA lethality by coinjection of dsRNA of each candidate RNAi gene, germline transgene silencing assay, and somatic transgene silencing using the seam-cell marker (scm) GFP (for viable and lethal clones) or the *sur-5::gfp* (sur-5) reporters (viable clones only). See text and (*9*). ¶ One clone targets two genes, *ZK1127.6* (top cell) and *ZK1127.9* (bottom cell) (BLASTP *e*-value 80% of protein).

these somatic factors or other, unrelated layers of gene regulation.

The microRNA pathway and RNAi share an overall mechanistic framework. However, to date, DCR-1 is the only identified component shared between the two related small-RNA pathways. Inactivation by RNAi of each of the 90 RNAi candidates did not affect precursor microRNA processing (*25*), underscoring the lack of overlap between RNAi and the microRNA pathways at this step. We also examined phenotypes associated with defects in the heterochronic pathway controlled by the *let-7* microRNA (*5*). Mutations in *let-7* cause supernumerary (>16) seam cells (*26*). Of the 90 RNAi factors, inactivation of six genes, including *dcr-1*, caused an increased number of seam cells and, of those, only three (*dcr-1*, *pop-1*, and *kin-10*) also significantly enhanced the weak *let-7* protruding vulva phenotype (tables S3 and S5); furthermore, *pop-1* RNAi may cause cell fate transformations rather than microRNA defects. These findings indicate little molecular overlap between the new RNAi factors and factors required for the microRNA pathway.

Protein-protein interaction maps ("interactomes") can facilitate the identification of complex molecular networks. Interrogating the Worm Interactome map (WI5) (*27*) and our screening of four additional factors provided protein interaction data for 42 of the 90 RNAi factors, giving a total of 161 interactions (table S6). We then tested and found that 21 of these interactors not identified by the initial RNAi screen were nonetheless required for transgene silencing, thus supporting the validity of many of the interactions for the RNAi pathway (fig. S4). The interaction map provides a useful tool from which to postulate connections among the new RNAi factors that were not predicted a priori. For example, the interactome map links the NMD factor, SMG-2, with T25G3.3; the known RNAi factors, RSD-2 and RSD-6 (*28*); and a cleavage and polyadenylation component, F56A8.6 (CPF-2).

The new factors we have identified suggest new steps in dsRNA-triggered gene silencing, including nuclear import/export and downstream stages that use NMD and mRNA polyadenylation/cleavage factors. We also found a near-complete overlap among factors required for RNAi and those required for transgene silencing in somatic tissues. Further, we showed that many of these factors are required for silencing in the germ line, possibly contributing to the maintenance of germ line–soma distinctions, genome integrity, and protection from parasitic genetic elements. Overall, these findings provide a global view of how the machinery of RNAi is integrated into RNA-mediated cellular processes.

References and Notes

1. G. Meister, T. Tuschl, *Nature* **431**, 343 (2004).
2. M. A. Matzke, J. A. Birchler, *Nat. Rev. Genet.* **6**, 24 (2005).
3. D. Baulcombe, *Nature* **431**, 356 (2004).
4. N. L. Vastenhouw, R. H. Plasterk, *Trends Genet.* **20**, 314 (2004).
5. V. Ambros, *Nature* **431**, 350 (2004).
6. N. R. Dudley, J. C. Labbe, B. Goldstein, *Proc. Natl. Acad. Sci. U.S.A.* **99**, 4191 (2002).
7. R. S. Kamath *et al.*, *Nature* **421**, 231 (2003).
8. J. F. Rual *et al.*, *Genome Res.* **14**, 2162 (2004).
9. Supporting online material is available on *Science* Online.
10. N. Proudfoot, *Curr. Opin. Cell Biol.* **16**, 272 (2004).
11. C. G. Chen *et al.*, *Curr. Biol.* **15**, 378 (2005).
12. M. R. Motamedi *et al.*, *Cell* **119**, 789 (2004).
13. M. E. Domeier *et al.*, *Science* **289**, 1928 (2000).
14. B. B. Quimby, M. Dasso, *Curr. Opin. Cell Biol.* **15**, 338 (2003).
15. A. Harel, D. J. Forbes, *Mol. Cell* **16**, 319 (2004).
16. V. Pirrotta, *Cell* **110**, 661 (2002).
17. D. H. Kim *et al.*, *Science* **297**, 623 (2002).
18. C. C. Mello, personal communication.
19. A. Grishok, C. C. Mello, *Adv. Genet.* **46**, 339 (2002).
20. T. Sijen, R. H. Plasterk, *Nature* **426**, 310 (2003).
21. W. G. Kelly, S. Xu, M. K. Montgomery, A. Fire, *Genetics* **146**, 227 (1997).
22. S. Kennedy, D. Wang, G. Ruvkun, *Nature* **427**, 645 (2004).
23. J. Yochem, T. Gu, M. Han, *Genetics* **149**, 1323 (1998).
24. F. Simmer *et al.*, *Curr. Biol.* **12**, 1317 (2002).
25. J. K. Kim *et al.*, data not shown.
26. B. J. Reinhart *et al.*, *Nature* **403**, 901 (2000).
27. S. Li *et al.*, *Science* **303**, 540 (2004).
28. M. Tijsterman, R. C. May, F. Simmer, K. L. Okihara, R. H. Plasterk, *Curr. Biol.* **14**, 111 (2004).
29. We thank C. C. Mello for sharing unpublished data regarding *rde-5*. We also thank J. S. Ahn, D. E. Hill, and T. Hirozane-Kishikawa for technical assistance; H. Y. Mak for the ttx-3::RFP plasmid; W. Kelly for providing the PD7271 strain; A. Frand for extensive comments on the manuscript; and P. Hu, B. Reinhardt, S. Fischer, D. Kim, S. Curran, and D. Parry for helpful discussions. We are grateful to W. Wong and J. Suen for pouring all of the RNAi plates used in this study. This research was supported by a Helen Hay Whitney Postdoctoral Fellowship (tJ.K.K.); a Damon-Runyon Postdoctoral Fellowship, a Howard Hughes Medical Institute Fellowship, and NIH grant K08-AG21613 (tM.T.); and NIH grant GM44619 (tG.R.).

Supporting Online Material

www.sciencemag.org/cgi/content/full/1109267/DC1
Materials and Methods
Figs. S1 to S4
Tables S1 to S6
References

30 December 2004; accepted 15 March 2005
Published online 24 March 2005;
10.1126/science.1109267
Include this information when citing this paper.

Mutations in *Col4a1* Cause Perinatal Cerebral Hemorrhage and Porencephaly

Douglas B. Gould,[1,2] F. Campbell Phalan,[1,2] Guido J. Breedveld,[3] Saskia E. van Mil,[4] Richard S. Smith,[1,2] John C. Schimenti,[2]* Umberto Aguglia,[5] Marjo S. van der Knaap,[6] Peter Heutink,[4] Simon W. M. John[1,2,7]†

Porencephaly is a rare neurological disease, typically manifest in infants, which is characterized by the existence of degenerative cavities in the brain. To investigate the molecular pathogenesis of porencephaly, we studied a mouse mutant that develops porencephaly secondary to focal disruptions of vascular basement membranes. Half of the mutant mice died with cerebral hemorrhage within a day of birth, and ~18% of survivors had porencephaly. We show that vascular defects are caused by a semidominant mutation in the procollagen type IV α 1 gene (*Col4a1*) in mice, which inhibits the secretion of mutant and normal type IV collagen. We also show that *COL4A1* mutations segregate with porencephaly in human families. Because not all mutant mice develop porencephaly, we propose that *Col4a1* mutations conspire with environmental trauma in causing the disease.

Porencephaly [Online Mendelian Inheritance in Man (OMIM) record 175780] is a rare central nervous system disease usually diagnosed in infants. Type I or encephaloclastic porencephaly is characterized by cerebral white-matter lesions and degenerative cavities. Severe cases have drastic consequences, including profound disability and death. Infants who survive are often diagnosed with poor or absent speech development, epilepsy, hydrocephalus, seizures, mental retardation, and cerebral palsy. It has been suggested that porencephalic cavities in humans result from focal cerebral degeneration involving hemorrhages (*1*). Association studies suggest that clotting-factor genes may contribute to genetic susceptibility by predisposing to thrombophilia (*2*). Despite these associations, the genetic and environmental etiology of familial cases is not established (*3–10*), and it seems reasonable that a distinct mechanism involving primary defects of vasculature could predispose to hemorrhage and porencephaly.

To advance the understanding of porencephaly, we have identified and characterized a new mouse mutant (generated by random mutagenesis) with severe perinatal cerebral hemorrhage. In addition to cerebral hemorrhage, mutant mice are smaller than control littermates

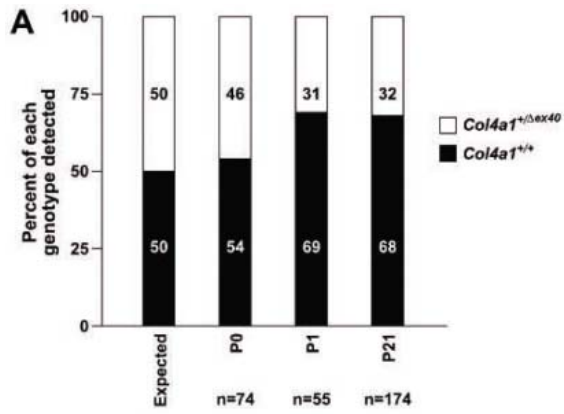

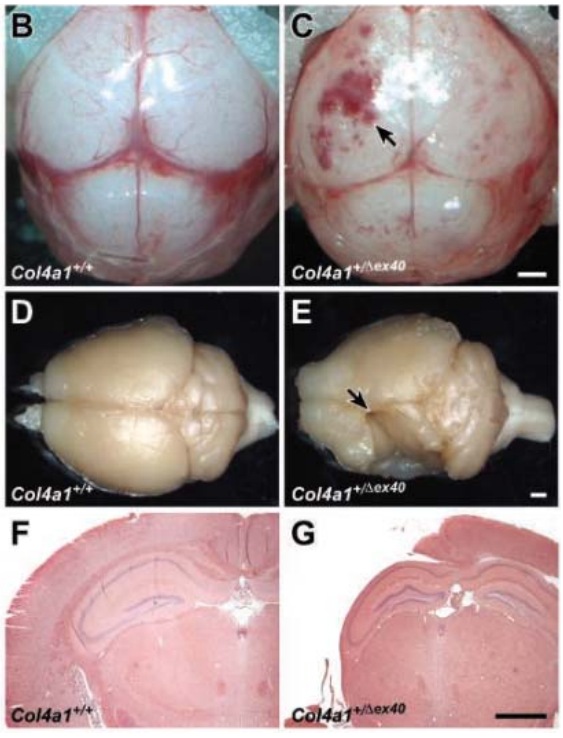

Fig. 1. Mutant mice have cerebral hemorrhage, reduced viability, and porencephaly. (**A**) Mutant mice (*Col4a1*$^{+/\Delta ex40}$, see Fig. 2) have reduced perinatal viability. *Col4a1*$^{+/\Delta ex40}$ mice were bred to wild-type C57BL/6J mice, and the expected proportion of *Col4a1*$^{+/\Delta ex40}$ progeny was 50%. *Col4a1*$^{+/\Delta ex40}$ pups were present at the expected frequency on the day of birth (P0). By weaning age (P21), over 50% of the mutants were missing ($P < 0.001$). Almost all of the missing pups died within a day of birth, suggesting that stress associated with parturition may be an important factor in their deaths. *n*, number of mice. (**B** and **C**) After birth, cerebral hemorrhages are evident in mutant [(C), arrow] but not control (B) pups. (**D** to **G**) Porencephalic cavities [(E), arrow] and (G) were observed in adult mutant, but not age-matched control [(D) and (F)], mice. (G) is from the same brain shown in (E) and demonstrates the absence of the left cerebral cortex (*22*). All scale bars, 1 mm.

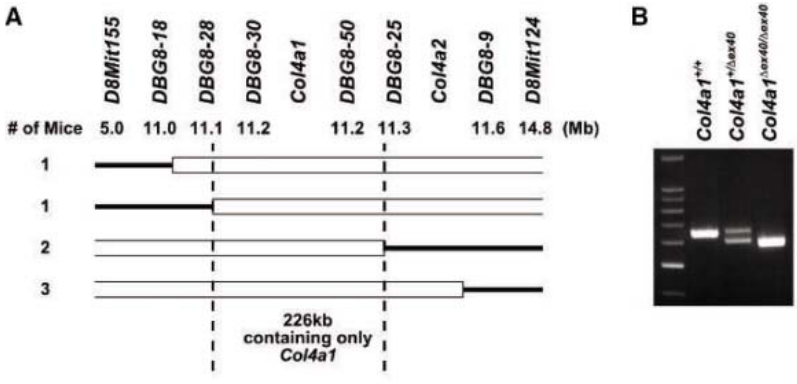

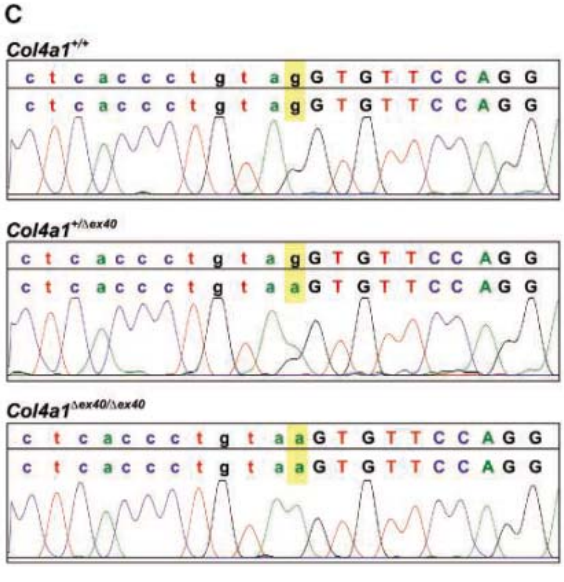

Fig. 2. The mutant mice have a mutation in the *Col4a1* gene. (**A**) Map of critical interval. More than 2000 mice were analyzed, and key recombinant chromosomes are shown (*22*). The thin lines indicate the chromosomal region excluded by recombination. Numbers of mice with each type of chromosome are indicated on the left. Phenotypes of critical recombinants were confirmed by progeny testing. Physical locations for all markers are in megabases (Mb) from the centromere [National Center for Biotechnology Information (NCBI) mouse build 33]. (**B**) Reverse-transcription polymerase chain reaction of exons 35 to 41 of *Col4a1* revealed a smaller amplicon (transcript) in mutant embryos as compared with controls. The mutant transcript lacks exon 40. (**C**) Sequence analysis of genomic DNA revealed a G-to-A transition in the splice acceptor site of exon 40. The intron sequence is shown in lowercase and the exon 40 sequence is shown in uppercase.

and can have multiple pleiotropic phenotypes (including ocular abnormalities, mild renal abnormalities, and reduced fertility) that appear to be influenced by genetic context (*11*). Homozygous mutant mice are not viable after mid-embryogenesis, and about 50% of heterozygous mice die within a day of birth (Fig. 1A). Reduced viability may be explained by variability in the severity and/or location of cerebral hemorrhages that are externally visible in most mutant pups. Detailed analysis of a subset of postnatal day 0 (P0) pups identified cerebral hemorrhages in 12 out of 12 mutant pups but in 0 out of 9 littermate controls (Fig. 1, B and C). About 18% of adult heterozygous mutant mice had obvious porencephalic lesions (6 out of 33) that were not observed in wild-type controls (0 out of 17, Fig. 1, D to G).

We mapped the causative gene to a 226-kilobase region on chromosome 8 that contains

[1]The Howard Hughes Medical Institute, Bar Harbor, ME 04609, USA. [2]The Jackson Laboratory, 600 Maine Street, Bar Harbor, ME 04609 USA. [3]Department of Clinical Genetics, Erasmus Medical Center, 3000 DR, Rotterdam, Netherlands. [4]Department of Human Genetics, Section of Medical Genomics, VU University Medical Center, and Center for Neurogenomics and Cognitive Research, VU University and VU University Medical Center, 1081 BT, Amsterdam, Netherlands. [5]Regional Epilepsy Center, University of Catanzaro, 89100, Reggio Calabria, Italy. [6]Department of Child Neurology, VU University Medical Center, 1081 BT, Amsterdam, Netherlands. [7]Department of Ophthalmology, Tufts University School of Medicine, Boston, MA 02111, USA.

*Present address: Department of Biomedical Sciences, Cornell University, Ithaca, NY, 14853, USA.
†To whom correspondence should be addressed. E-mail: swmj@jax.org

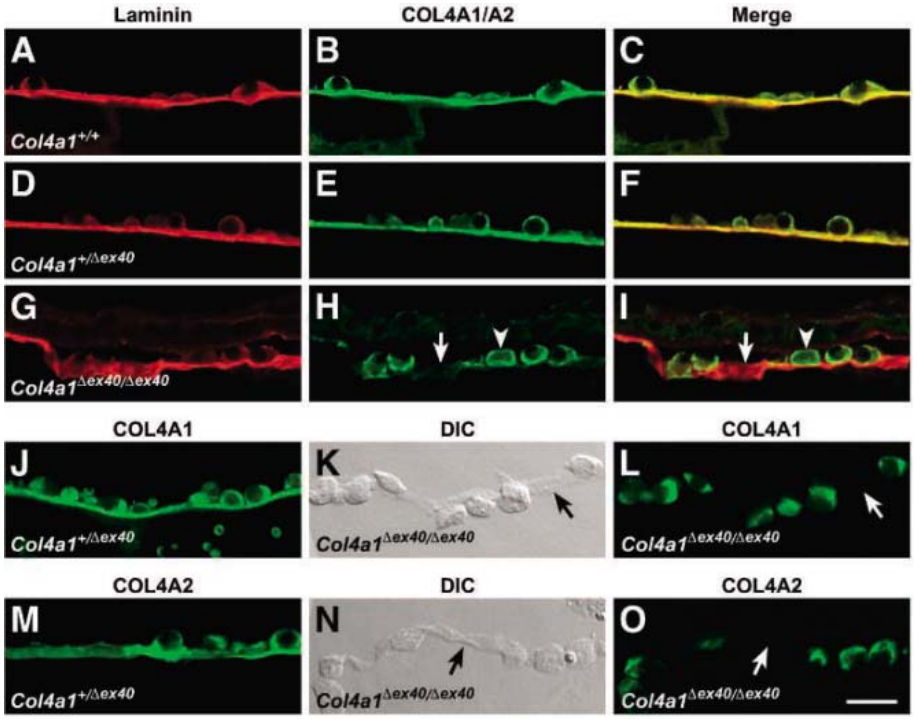

Fig. 3. The COL4A1 mutant inhibits collagen secretion into the BMs. (**A** to **C**) *Col4a1*$^{+/+}$, (**D** to **F**, **J**, and **M**) *Col4a1*$^{+/\Delta ex40}$, and (**G** to **I**, **K**, **L**, **N**, and **O**) *Col4a1*$^{\Delta ex40/\Delta ex40}$ mice are shown. In (A), (D), and (G), immunolabeling for laminin demonstrates the presence of RMs in embryos of each genotype (*22*). In (B) and (E), an antibody that recognizes both COL4A1 and COL4A2 shows the presence of these proteins in RMs of *Col4a1*$^{+/+}$ (B) and *Col4a1*$^{+/\Delta ex40}$ (E) embryos, which is confirmed by colocalization with laminin, shown in (C) and (F), respectively. (G) to (I) show that in contrast, *Col4a1*$^{\Delta ex40/\Delta ex40}$ embryos do not have collagen staining in the RM (arrow) and instead show nonsecreted mutant protein in the parietal endoderm cells (arrowheads). In (J) and (M), specific monoclonal antibodies show that COL4A1 (J) and COL4A2 (M) are present in both the parietal endoderm cells and the RM of *Col4a1*$^{+/\Delta ex40}$ embryos. (L) and (O) show that in contrast, no COL4A1 or COL4A2 is present in the RM of *Col4a1*$^{\Delta ex40/\Delta ex40}$ embryos (arrows). Differential interference contrast (DIC) images showing RMs are shown in (K) and (N). Scale bar, 0.2 μm.

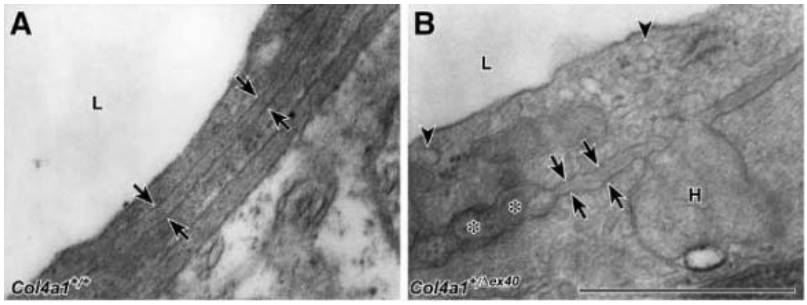

Fig. 4. *Col4a1*$^{+/\Delta ex40}$ mutant mice have structural defects in the cerebral vasculature. Electron micrographs of cerebral vessels of mice of the indicated genotypes are shown (*22*). (**A**) The vascular BMs of all analyzed *Col4a1*$^{+/+}$ mice had well-defined edges, uniform density, and consistent thickness (between arrows). (**B**) In contrast, the vascular BMs of *Col4a1*$^{+/\Delta ex40}$ mice often had uneven edges, inconsistent density, and highly variable thickness (between arrows). Focal disruption (asterisks) and herniation (H) of BMs were specific to mutant mice and probably represent damage due to a weaker BM. Disruptions were observed in about 20% of vessels, whereas qualitative differences such as variable thickness and inconsistent and rough edges existed in all mutant vascular BMs analyzed. Mutant endothelial cells appear enlarged with an accumulation of vesicles, a characteristic of deficient secretion (arrowheads). Further analysis of phenotypes observed in noncerebral tissue reveals that BM defects are not restricted to the brain (*11*). L indicates vessel lumen. Scale bar, 0.5 μm.

a single gene encoding procollagen type IV α 1 (*Col4a1*) (Fig. 2A and fig. S1). It has previously been suggested that a large undefined region including this locus contains a gene involved in cerebral hemorrhage in mice (*12*). Control and mutant embryos expressed *Col4a1* transcripts of distinct size (Fig. 2B). In mutant transcripts (hereafter called *Col4a1*$^{\Delta ex40}$), exon 39 was spliced directly to exon 41 because of a mutation in the splice-acceptor site of exon 40 (Fig. 2C).

Type IV collagens are basement membrane (BM) proteins (*13*–*15*) that are expressed in all tissues, including the vasculature (*16*). COL4A1 and COL4A2 are the most abundant type IV collagens. COL4A1 and COL4A2 form heterotrimers with a 2:1 stoichiometry, respectively (*17*, *18*). Assembly of the heterotrimers is initiated by the C-terminal noncollagenous domains, and the heterotrimer forms a triple helix along the length of the collagenous domains (fig. S2B). The skipped exon in *Col4a1*$^{\Delta ex40}$ mice is in the triple helix–forming domain and codes for exactly 17 amino acids. One mechanistic hypothesis is that after normal heterotrimer initiation, the mutant proteins alter triple helix formation or structure and thus inhibit heterotrimer secretion into the BM. The triple helix domain consists of long stretches of Gly-Xaa-Yaa repeats (where Xaa and Yaa are amino acids), with frequent interruptions in the repeats. These interruptions are thought to be important for the flexibility of BM collagens (*19*–*21*). Because the skipped exon contains a repeat imperfection whose position is highly conserved across species (*19*, *20*), an alternative hypothesis is that the mutant protein is assembled and secreted, but its structural properties in the vascular BMs are altered.

To distinguish between these hypotheses, we assessed the effect of the mutation on the secretion of COL4A1 and COL4A2 into BMs. Because *Col4a1*$^{\Delta ex40/\Delta ex40}$ embryos are not viable after mid-gestation, we assayed for COL4A1 and COL4A2 expression in the Reichert's membrane (RM, a BM of embryonic origin) by immunolabeling embryonic day 9.5 (E9.5) embryos. *Col4a1*$^{+/+}$ embryos showed robust labeling of COL4A1 and COL4A2 in the RM (Fig. 3B). Similarly, both secreted and intracellular COL4A1 and COL4A2 were present in *Col4a1*$^{+/\Delta ex40}$ embryos (Fig. 3, E, J, and M). In contrast, although the RM of *Col4a1*$^{\Delta ex40/\Delta ex40}$ embryos labeled robustly for laminin (Fig. 3G), there was no evidence of COL4A1/A2 heterotrimer secretion into this BM (Fig. 3, H, L, and O). Instead, the proteins appeared to accumulate within the parietal endoderm cells. These findings are consistent with the hypothesis that heterotrimers form but are not secreted (*22*). Similar to our results, a mutation of the nematode *Caenorhabditis elegans* ortholog of *Col4a1* (*emb-9*) results in the impaired secretion and intracellular accumulation of the products of both *emb-9* and the *Col4a2* ortholog *let-2* (*23*).

In further support for a dominant role of the mutant collagen in pathogenesis, mice heterozygous for null alleles of *Col4a1* and *Col4a2*

are normal (*24*). Presumably, these heterozygous mice produce fewer COL4A1/2 heterotrimers than do control mice, but all of the heterotrimers should have normal structure and be secreted. Although *Col4a1*$^{+/\Delta ex40}$ mice may secrete even less normal collagen [possibly only 25% (fig. S2)], the absence of a phenotype in mice with a null allele is consistent with a requirement for mutant proteins to induce disease. Analysis of mutations in the *C. elegans Col4a2* ortholog *let-2* supports this notion (*25*). Consistent with a potential pathogenic role of nonsecreted proteins, we observed swollen vascular endothelial cells with prominent vesicles in *Col4a1*$^{+/\Delta ex40}$ mice (Fig. 4).

COL4A1 and COL4A2 give strength to BMs (*24*, *26*). Mouse embryos homozygous for null alleles of both *Col4a1* and *Col4a2* (*24*), or for null alleles of type IV collagen–processing enzymes (*26*, *27*), die around mid-gestation with disrupted embryonic BMs. Similarly, BMs are weak in *C. elegans* type IV collagen mutants (*23*, *28*). To investigate whether the inhibition of heterotrimer secretion in *Col4a1*$^{+/\Delta ex40}$ mice compromises the structural integrity of the vascular BMs, we assessed the BMs of cerebral vessels by electron microscopy. Compared with controls, *Col4a1*$^{+/\Delta ex40}$ mice had uneven BMs with inconsistent density and focal disruptions (Fig. 4). Although detailed studies are needed, we found that BMs in other tissues also were affected. However, the major site of hemorrhage was the brain. This may be explained by tissue-specific compositional differences in the vascular BMs or the vascular wall (*16*). Alternatively or additionally, the mutant BMs may greatly predispose to hemorrhage at times of stress. Substantial stress on the head during birth could explain the substantial cerebral hemorrhage.

To determine whether *COL4A1* mutations in humans also cause porencephaly, we assessed two families with autosomal dominant porencephaly (*6*, *10*) for mutations in *COL4A1* (GenBank accession number 000013) on chromosome 13q34 (Fig. 5). The first family (*6*) has a Gly^{1236} to Arg^{1236} (G1236R) mutation that segregates with the porencephaly but was not present in 192 ethnically and geographically matched Dutch control chromosomes. The second family (*10*) has a Gly^{749} to Ser^{749} (G749S) mutation that also segregates with the phenotype but was not present in 192 ethnically and geographically matched Italian control chromosomes. Both mutations change conserved Gly residues within Gly-Xaa-Yaa repeats in the triple helix domain (fig. S2). Glycine has a single hydrogen-atom side chain, and there is little tolerance for amino acids with larger side chains that likely disrupt the triple helix during collagen assembly (*29*). Gly-to-Arg and Gly-to-Ser mutations have been shown to be pathogenic in the *C. elegans Col4a1* ortholog (*23*, *25*) and in human *COL4A5*, respectively (*30*).

We have shown that mutations in *Col4a1* can lead to perinatal cerebral hemorrhage and can predispose to porencephaly. Because not all mice of a defined genetic background develop porencephaly, the *COL4A1* mutations in humans may conspire with environmental factors (for example, birth trauma) to cause the disease. In addition to having porencephaly, one adult patient from family 1 suffered from recurrent hemorrhagic strokes, which were caused by his weakened vessels (fig. S3). Thus, it is possible that mutations in *COL4A1* could contribute to hemorrhagic stroke in the absence of porencephaly. In addition to *COL4A1*, alleles of *COL4A2* or other genes encoding BM or BM-associated proteins (including laminins, entactin/nidogen, perlecan, and integrins) also may be important predisposing factors for cerebral hemorrhage with or without porencephaly.

Our findings may have important implications for disease prevention in families with porencephaly resulting from vascular defects caused by mutations in *COL4A1* or other BM genes. For at-risk individuals, preemptive measures could be taken to reduce stress on the abnormal cerebral vessels that may in turn reduce the neurological deficits. For example, cesarean delivery of at-risk babies may increase the likelihood of survival and the possibility of a healthy life by decreasing the severity of cerebral hemorrhage and its sequelae.

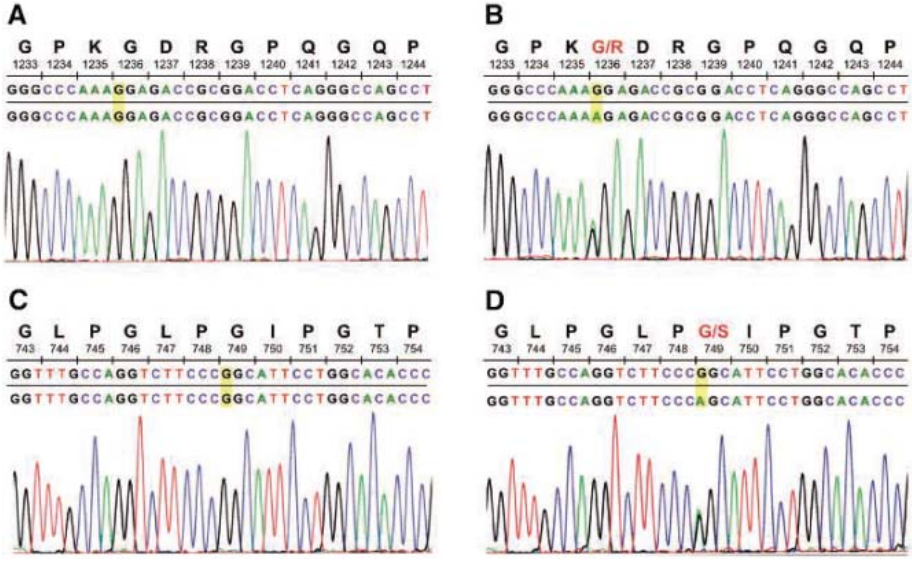

Fig. 5. *COL4A1* mutations in two human families with porencephaly. (**A** and **C**) Sequence chromatograms for unaffected members from family 1 and family 2, respectively. (**B**) Chromatogram for an affected patient from family 1, showing the G3706A transition mutation. (**D**) Chromatogram for an affected patient from family 2, showing the G2245A transition mutation.

References and Notes

1. J. F. Pasternak, J. F. Mantovani, J. J. Volpe, *Am. J. Dis. Child.* **134**, 673 (1980).
2. O. M. Debus, A. Kosch, R. Strater, R. Rossi, U. Nowak-Gottl, *Ann. Neurol.* **56**, 287 (2004).
3. G. M. Mancini, I. F. de Coo, M. H. Lequin, W. F. Arts, *Eur. J. Paediatr. Neurol.* **8**, 45 (2004).
4. R. A. Berg, K. A. Aleck, A. M. Kaplan, *Arch. Neurol.* **40**, 567 (1983).
5. F. Haar, P. Dyken, *Neurology* **27**, 849 (1977).
6. L. M. Smit, P. G. Barth, J. Valk, C. Njiokiktjien, *Brain Dev.* **6**, 54 (1984).
7. J. Zonana, B. T. Adornato, S. T. Glass, M. J. Webb, *J. Pediatr.* **109**, 671 (1986).
8. A. Sensi, S. Cerruti, E. Calzolari, F. Vesce, *Clin. Genet.* **38**, 396 (1990).
9. C. Vilain, N. Van Regemorter, A. Verloes, P. David, P. Van Bogaert, *Am. J. Med. Genet.* **112**, 198 (2002).
10. U. Aguglia *et al.*, *Neurology* **62**, 1613 (2004).
11. D. B. Gould *et al.*, unpublished data.
12. B. M. Cattanach *et al.*, *Mouse Genome* **91**, 853 (1993).
13. N. A. Kefalides, *Biochem. Biophys. Res. Commun.* **45**, 226 (1971).
14. R. Timpl, *Eur. J. Biochem.* **180**, 487 (1989).
15. P. D. Yurchenco, P. S. Amenta, B. L. Patton, *Matrix Biol.* **22**, 521 (2004).
16. N. Urabe *et al.*, *Arch. Histol. Cytol.* **65**, 133 (2002).
17. R. Mayne *et al.*, *J. Cell Biol.* **98**, 1637 (1984).
18. B. Trueb, B. Grobli, M. Spiess, B. F. Odermatt, K. H. Winterhalter, *J. Biol. Chem.* **257**, 5239 (1982).
19. G. Muthukumaran, B. Blumberg, M. Kurkinen, *J. Biol. Chem.* **264**, 6310 (1989).
20. B. Blumberg *et al.*, *J. Biol. Chem.* **262**, 5947 (1987).
21. D. Schuppan, R. Timpl, R. W. Glanville, *FEBS Lett.* **115**, 297 (1980).
22. Materials and methods are available as supporting material on *Science* Online.
23. M. C. Gupta, P. L. Graham, J. M. Kramer, *J. Cell Biol.* **137**, 1185 (1997).
24. E. Poschl *et al.*, *Development* (2004).
25. M. H. Sibley, P. L. Graham, N. von Mende, J. M. Kramer, *EMBO J.* **13**, 3278 (1994).
26. N. Nagai *et al.*, *J. Cell Biol.* **150**, 1499 (2000).
27. K. Rautavuoma *et al.*, *Proc. Natl. Acad. Sci. U.S.A.* **101**, 14120 (2004).
28. K. R. Norman, D. G. Moerman, *Dev. Biol.* **227**, 690 (2000).
29. J. Engel, D. J. Prockop, *Annu. Rev. Biophys. Biophys. Chem.* **20**, 137 (1991).
30. A. Renieri *et al.*, *Nephron* **67**, 444 (1994).

31. All experiments were conducted in compliance with institutional animal care and use committee guidelines. We thank R. Libby and V. Lindner for helpful discussions; Y. Ninomiya and Y. Sado for H12 and H22 antibodies; J. Sanes for R23 antibody; R. Burgess, T. Gridley, R. Libby, and J. Miner for critical review of the manuscript; O. Savinova for assistance; and J. Torrance and S. Williamson for work on the figures. Supported

by the Canadian Stroke Network's Focus on Stroke Program (D.B.G.), the Centre for Medical Systems Biology in the Netherlands (P.H.), and grant EY11721 (S.W.M.J.). Scientific services were subsidized by grant CA34196. S.W.M.J. is an Investigator of the Howard Hughes Medical Institute.

Supporting Online Material
www.sciencemag.org/cgi/content/full/308/5725/1167/DC1
Materials and Methods
SOM Text
Figs. S1 to S3
Table S1
References and Notes

5 January 2005; accepted 14 March 2005
10.1126/science.1109418

Clonal Dominance of Hematopoietic Stem Cells Triggered by Retroviral Gene Marking

Olga Kustikova,[1]* Boris Fehse,[1]* Ute Modlich,[3] Min Yang,[3] Jochen Düllmann,[2] Kenji Kamino,[4] Nils von Neuhoff,[4] Brigitte Schlegelberger,[4] Zhixiong Li,[3]† Christopher Baum[3,5]†

Gene marking with replication-defective retroviral vectors has been used for more than 20 years to track the in vivo fate of cell clones. We demonstrate that retroviral integrations themselves may trigger nonmalignant clonal expansion in murine long-term hematopoiesis. All 29 insertions recovered from clones dominating in serially transplanted recipients affected loci with an established or potential role in the self-renewal or survival of hematopoietic stem cells. Transcriptional dysregulation occurred in all 12 insertion sites analyzed. These findings have major implications for diagnostic gene marking and the discovery of genes regulating stem cell turnover.

Because of their unspecific insertion properties, replication-defective retroviral vectors represent unique tools for genetic marking studies, enabling the numbers and progeny of transplanted (stem) cells to be determined (*1*, *2*). However, retrovirally marked cells can only be expected to behave normally if vector insertion itself does not confer a selective advantage or disadvantage.

Most marking studies published to date have used vectors based on murine leukemia virus (MLV), which is a simple gammaretrovirus with strong enhancer-promoters in the long terminal repeats (LTRs). In replication-competent retroviruses, these sequences may trigger up-regulation of randomly hit proto-oncogenes (*3*, *4*). Given the multistep nature of oncogenesis (*5*), the accumulation of several such events in single cells potentially results in malignant transformation (*3*). Retrovirally marked genes that have been repeatedly associated with experimentally induced murine tumors have been summarized in a database of ~300 common insertion sites (CISs), representing proposed or established cellular proto-oncogenes (*4*). Besides these, there may be many other genes with the potential to influence stem cell kinetics when up-regulated or disrupted. The identification of such genes is of great interest for regenerative medicine, as exemplified by the powerful effect of *Hoxb4* on the self-renewal of hematopoietic stem cells (HSCs) (*6*).

In light of the recent demonstration that MLV vectors preferentially target the promoter regions of active genes (*7*), proto-oncogene activation might be more frequent (>1% of all insertions) than previously anticipated (*8*). However, in the numerous studies performed with retroviral vectors in human subjects, nonhuman primates, dogs, and mice (*9*), few cases have been identified in which malignant complications were caused by insertional mutagenesis. We previously observed an acute myeloid leukemia after insertion of a vector expressing an engineered low-affinity nerve growth factor receptor (dLNGFR) into the *Evi1* proto-oncogene (*10*). **Evi1** encodes a transcription factor with a role in both self-renewal and transformation of HSCs (*11*). Because dLNGFR was not associated with side effects in other studies (*12*), it remained unclear whether vector insertion into *Evi1* was sufficient for leukemogenesis in mice. Similarly, unusual lymphatic leukemias occurred after insertional up-regulation of the *LMO2* proto-oncogene by a vector expressing the interleukin-2 receptor common γ-chain, in a clinical trial performed to correct inborn severe combined immunodeficiency (*13*). We have also shown that leukemias reproducibly evolve in mice if vector insertions occur in independent proto-oncogenes of a single clone (*14*), consistent with the hypothesis that at least two collaborating signal alterations are required for leukemogenesis (*15*).

To examine the effect of retroviral gene hits in normal HSCs, we analyzed cohorts of healthy mice in which a single or very few clones dominated hematopoiesis after serial bone marrow transplantation (BMT) (*16*, *17*) (Fig. 1A). The vectors expressed either a signal-deficient variant of human CD34 (tCD34) or its full-length variant (flCD34); there was no evidence of a selective advantage related to transgene expression (*16*, *18*). Using ligation-mediated polymerase chain reaction (LM-PCR), which introduces a bias for dominant clones (*19*, *20*), we detected several clones contributing to hematopoiesis in each transplant recipient of the first cohort (after 28 weeks observation) (Fig. 1B). We mapped 22 different insertions in the six primary recipients of flCD34-marked cells (mice fl1 to fl6) and 19 insertions in the six primary recipients of tCD34-marked cells (mice t1 to t6) (Table 1 and table S1).

In the tCD34 primary cohort, we observed four insertions in CIS/proto-oncogenes (Table 1), three of which occurred in *Evi1* (Fig. 2A). We have seen a similar incidence of *Evi1* insertions in primary recipients after retroviral expression of the human multidrug resistance 1 (MDR1) cDNA (*14*). Such a recovery of independent hits in identical loci, or pathways, strongly suggested in vivo selection (*4*). Another hit was located between *Hoxb5* and *Hoxb4* (Fig. 2B), marking a clone that we could detect even in two independent primary recipients by locus-specific PCR (Table 1 and table S2).

In the flCD34 primary cohort, LM-PCR showed no insertions in CIS/proto-oncogenes and also fewer insertions within or close to signaling genes (Table 1 and table S1). Among the latter, *Map3k5* is highly related to *Map3k14* detected in primary tCD34 recipients, and both *Stxbp4* (flCD34) and *Igfbp4* (tCD34) map to insulin pathways. Even in this small set of dominant clones from primary flCD34 recipients, we found two hits belonging to the same growth factor pathway (*Vegfa*, *Shb*) (*21*). Vascular/endothelial growth factor encoded by *Vegfa* enhances HSC self-renewal (*22*), and again, the affected clone was detected in two independent primary recipients (Table 1).

To further determine the fate of marked clones, we examined 16 secondary recipients (11 for tCD34, 5 for flCD34) observed for 22 weeks after receiving bone marrow cells pooled from the primary recipients (Fig. 1A). This analysis thus focused on true HSCs, charac-

[1]Bone Marrow Transplantation, [2]Institute for Anatomy II: Experimental Morphology, University Hospital Eppendorf, Martinistraße 52, 20251 Hamburg, Germany. [3]Department of Hematology, Hemostaseology, and Oncology, [4]Institute of Cellular and Molecular Pathology, Hannover Medical School, Carl-Neuberg-Straße 1, 30625 Hannover, Germany. [5]Division of Experimental Hematology, Cincinnati Children's Hospital Medical Center, Cincinnati, OH 45229–3039, USA.

*These authors contributed equally to this work.
†To whom correspondence should be addressed: E-mail: baum.christopher@mh-hannover.de (C.B.); li.zhixiong@mh-hannover.de (Z.L.)

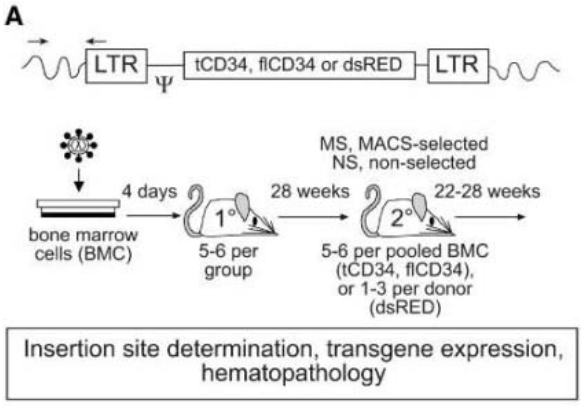

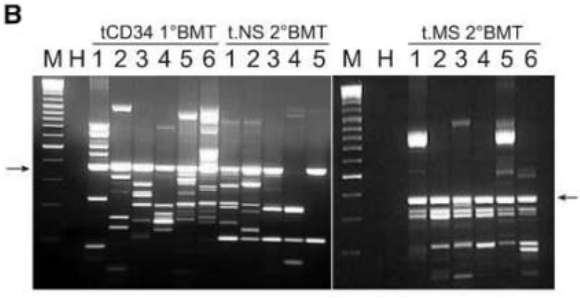

Fig. 1. Gene marking studies and LM-PCR. (**A**) Retroviral vectors expressed tCD34, flCD34, or dsRED. Waves indicate flanking chromosomal DNA, and arrows represent LM-PCR primers. Mice were observed during serial BMT, with detailed analysis of transgene expression and histopathology. ψ, retroviral packaging signal; MACS, magnetic cell sorting. (**B**) LM-PCR gel showing insertions recovered from primary (1°) and secondary (2°) recipients of cells marked with tCD34. Arrows indicate internal control bands. M, molecular weight marker; H, H_2O control.

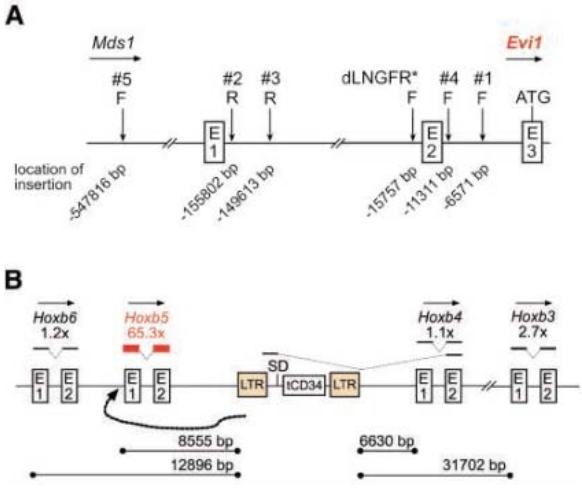

Fig. 2. Selected insertion sites. (**A**) Distribution of *Evi1* insertions. F and R represent forward and reverse orientations of the vector, respectively; E1 to E3 represent exons 1 to 3. Insertion coordinates are given based on the first start codon (ATG) of the NCBI database (June 2004). Exon definition follows the ENSEMBL database (April 2005). The asterisk indicates an insertion from the leukemia associated with the use of a dLNGFR vector; in 2002, this insertion was annotated to exon 1 according to GenBank record M64494 (*10*). bp, base pairs. (**B**) Insertion within the *Hoxb* cluster. Schematic representation of the retroviral vector insertion in the *Hoxb* cluster, with distance to the transcriptional start sites of neighboring *Hoxb* genes. Transcripts and their expression levels are indicated above the scheme of the locus. SD, splice donor.

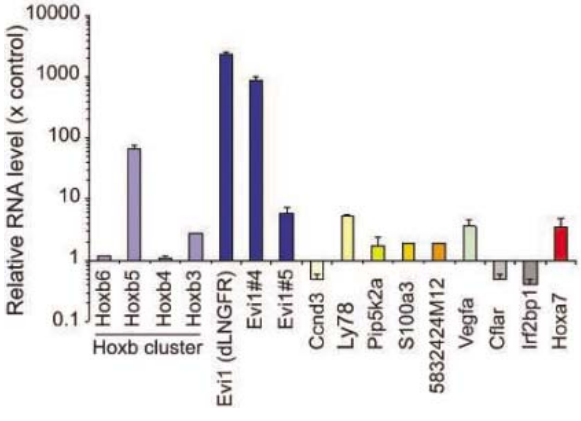

Fig. 3. Transcriptional dysregulation of targeted loci. Real-time RT-PCR shows dysregulation of targeted alleles in selected recipients. Each analysis was performed in triplicate. Error bars indicate standard deviations between independent determinations. RNA from normal hematopoietic cells served as controls (RNA level = 1). With the exception of the dLNGFR leukemia (*Evi1* dLNGFR), RNAs were from uncloned cells, potentially underreporting transcriptional changes.

terized by serial repopulation activity. Two of the three secondary groups received cells after magnetic sorting (MS) for expression of vector-encoded tCD34 or flCD34, resulting in a high frequency of transgene expression in vivo (*16*). Table S2 summarizes transgene expression and clonal distribution over serial BMT.

In the tCD34 MS group (t.MS), we detected only five clones by Southern blot (*16*). LM-PCR, a more sensitive method (*19*), detected six distinct insertions (Fig. 1B). All animals harbored the clone with the insertion between *Hoxb5* and *Hoxb4* (Table 1 and table S2). To date, *Hoxb4* is the best investigated of the transcription factors that, when up-regulated, promote self-renewal of HSCs without malignant transformation (*6*). *Hoxb5* is closely related but differently regulated by enhancer elements located between these two genes (*23*). Although we detected a fusion transcript between the upstream LTR and the second exon of *Hoxb4* (*17*), real-time reverse transcription (RT)–PCR revealed no substantial change of wild-type *Hoxb4* transcripts (Figs. 2B and 3). The upstream primer of this real-time RT-PCR was located in the first (coding) exon, thus ignoring the fusion transcript. When examining neighboring genes of the *Hoxb* cluster, we found that *Hoxb5* was up-regulated by 65.3 times and there was a mild induction of *Hoxb3* (Figs. 2B and 3) (*17*).

All remaining insertions obtained from secondary recipients of tCD34-transduced cells also affected potential growth-regulatory genes (Table 1 and table S1). One dominant clone in this group showed another insertion into *Evi1 (Evi1#4)*, strongly (by 876.1 times) up-regulating the transcript (Figs. 2A and 3). As the RNA used for RT-PCR studies was not prepared from recloned cells, *Evi1#4* and the cloned dLNGFR-associated leukemia showed similar high levels of up-regulation (Fig. 3). In contrast, the three clones with different *Evi1* insertions detected in primary recipients were counterselected in serially transplanted animals (Table 1) (*17*). Like *Evi1#4*, a clone with an insertion in *Ccnd3* (Table 1) also showed delayed dominance. Because this insertion was located in the first intron with reverse orientation, it was no surprise to find the transcript between exons 1 and 2 down-regulated (Fig. 3). Repression of *Ccnd3*, one of the D cyclins that are essential for hematopoiesis, may occur in leukemias (*24*, *25*). The other loci recovered from secondary recipients of tCD34-marked cells were all up-regulated (*Ly78*, *Pip5k2a*, *S100a3*, and *5832424M12*) (Fig. 3).

Southern blot data of the five recipients of MS cells expressing flCD34 (fl.MS) revealed only six different clones (*16*). As in the tCD34 cohorts, one clone with delayed dominance had an *Evi1* insertion, *Evi1#5* (Table 1). This

occurred in the neighboring *Mds1* locus and thus as far as 548 kb upstream of *Evi1*'s first exon, nevertheless resulting in its up-regulation (by 5.8 times) (Figs. 2A and 3) (*17*). In all secondary mice, we recovered the clone with the *Vegfa* insertion (Table 1), also associated with up-regulation (by 3.6 times) (Fig. 3) (*17*). As in the primary recipients, this was associated with a hit upstream of *Map3k5*, suggesting clonal linkage (Table 1 and table S2). Furthermore, two additional clones had insertions in signaling genes, *Cflar=c-Flip* and *Irf2bp1* (Table 1 and table S2). RT-PCR indicated down-regulation of these loci, which in the case of *Cflar* was consistent with its proapoptotic function (Fig. 3).

In all, using LM-PCR to analyze long-term repopulating hematopoietic cells marked with vectors encoding tCD34 or flCD34 (Table 1), we identified 48 different insertions that matched the murine genome, 41 in primary recipients and 7 additional hits only in secondaries. All of the 12 hits recovered from secondary recipients identified CIS/proto-oncogenes

Table 1. Insertion sites recovered by LM-PCR from long-term repopulated primary and secondary recipients. Twenty-two other insertion sites were from other or unknown gene classes (table S1). Genome hits and sequence codes (Gene ID) are according to the National Center for Biotechnology Information (NCBI) mouse genome database (frozen December 2004). Underlined loci recovered from secondary recipients are listed in an HSC transcriptome database (*26*). Insertions are defined with respect to the transcriptional start sites (TSS, the mRNA start according to NCBI) of neighboring genes. In total, we analyzed 69 locus insertions. Six of the 25 insertions for tCD34, 1 of the 23 insertions for flCD34, and 10 of the 21 insertions for dsRed were newly detected in secondary recipients. t1 to t6 represent tCD34-marked primary mice 1 to 6; fl1 to fl6, flCD34-marked primary mice 1 to 6; r1 to r4, dsRED-marked primary mice 1 to 4; t.MS1 to t.MS6, tCD34-marked secondary recipients 1 to 6 of magnetically sorted cells; t.NS1 to t.NS5, tCD34-marked secondary recipients 1 to 5 of nonselected cells; fl.MS1 to fl.MS5, flCD34-marked secondary recipients 1 to 5 of magnetically sorted cells; r1.1, r1.2, etc., secondary recipients of r1, etc. (*17*); F, forward (with respect to the gene's transcriptional direction); R, reverse. TF, transcription factor; ND, not detected (below the sensitivity of LM-PCR); GF, growth factor; Znf, Zinc finger. Refer to the NCBI database for gene name abbreviations.

Locus	Gene ID	Chromosome	Definition or (proposed) function	Position to TSS (intron)	Orientation	Recipients	
						1° BMT	2° BMT
			CIS/proto-oncogenes (n = *13*)				
Ccnd3	12445	17B4	cyclin D3, protein kinase activity	1629(1)	R	ND	t.MS1–t.MS6
Elk4	13714	1E3-G	ELK4, TF of ETS family	–1669	F	t6	ND
Evi1 (hit *#1*)	14013	3A3	Znf TF, murine and human leukemia	-6571	F	t1	ND
Evi1 (hit *#2*)	14013	3A3	Znf TF, murine and human leukemia	–155802	R	t5	ND
Evi1 (hit *#3*)	14013	3A3	Znf TF, murine and human leukemia	–149613	R	t6	ND
Evi1 (hit *#4*)	14013	3A3	Znf TF, murine and human leukemia	–11311	F	ND	t.NS1–t.NS5
Evi1 (hit *#5*)	14013	3A3	Znf TF, murine and human leukemia	–547816	F	ND	fl.MS1
Bcl11a	14025	11A3.2	Znf TF essential for lymphopoiesis	167714	F	r3	r3.1
BC031781/*Lefty2*	208768	1H4	unknown function/morphogen	–1388/–44275	R/R	ND	r1.2
Hoxa7	15404	6B3	homeobox A7 TF	–986	R	ND	r2.1, r2.2
Pdcd1lg1	60533	19C2	programmed cell death 1 ligand 1	34046	R	r3	ND
Runx2	12393	17B3	runt TF, essential for hematopoiesis	141712(4)	R	r3	ND
Scl=Tal1	21349	4D1	Ebox TF, essential for hematopoiesis	–2012	F	ND	r4.1, r4.2
			Signaling genes (n = *34*)				
Atf6	22664	1H3	activating TF 6	136053(21)	R	t5	ND
Ccl27	20301	4A5	chemokine ligand 27, cytokine	3688	R	t6	ND
Cnn2	12798	10C1	calponin 2, calmodulin binding	373(1)	R	t1	ND
Map3k14	53859	11E1	mitogen-activating protein kinase 14	20716(6)	R	t5	ND
Igfbp4	16010	11D	insulin-like GF binding protein 4	–1010	R	t2	ND
LOC381899	381899	7E1	similar to adaptor molecule Gab2	–1365	F	t6	ND
Socs5	56468	17E4	suppressor of cytokine signaling 5	87655	R	t3	ND
Srebf2	20788	15E1	sterol regulating element binding factor 2	7652(1)	F	t3	ND
Hoxb5/*Hoxb4*	15413	11D	homeobox B5 and B4 TF	8555/–6630	F/F	t6	t.NS1, t.MS2–t.MS6
Ly78	17079	13D1	lymphocyte antigen 78, receptor	–26986	F	ND	t.MS1–t.MS6
Pip5k2a	18718	2A3	PI-4-phosphate 5-kinase, II alfa	46080(1)	R	ND	t.MS3
S100a3 cluster	20197	3F1	S100 calcium binding protein A3	–13251	F	ND	t.MS1, t.MS5
5832424M12	218503	13D1	hypothetical cell cycle–associated protein	6242(1)	R	ND	t.NS3, t.NS4, t.MS6
Dapk1	69635	13B2	death-associated protein kinase 1	71753(1)	F	fl5	ND
Shb	230126	4B1	Src homology 2 adaptor protein B	43028(2)	F	fl1	ND
Stxbp4	20913	11C	insulin receptor signaling pathway	84916(11)	R	fl4	ND
Irf2bp1	272359	7A2	interferon regulating factor 2 binding	–1335	R	fl2	fl.MS1
Cflar=c-Flip	12633	1C1.3	CASP8/FADD-like apoptosis regulation	–15374	R	fl5	fl.MS2
Map3k5 locus	26408	10A3	mitogen-activated protein kinase 5	4122(1)	F	fl2, fl6	fl.MS1–fl.MS5
Vegfa	22339	17B3	vascular endothelial growth factor A	–14963	F	fl2, fl6	fl.MS1–fl.MS5
Abr	109934	11B5	active BCR-related	28918(2)	R	ND	r3.1
Btd	26363	14A3	biotinidase, involved in proliferation	27328	F	r4	r4.1, r4.2
Crsp6	234959	9A3	cofactor for TF Sp1	–25697	R	r1, r4	r4.1, r4.3
Depdc2	76135	1A3	DEP domain–containing 2	18431(1)	R	ND	r1.1
Dlx2	13392	2C3	distal-less homeobox TF	–116230	R	ND	r4.2
Ifnb1	15977	4C4	interferon beta 1; cytokine	72106	R	r2	r2.1, r2.2
Ing1	26356	8A2	inhibitor of growth protein 1, TF	–1143	F	ND	r1.2, r4.2
LOC433959	433959	5	transcriptional domain-associated	–100466	R	ND	r3.1
Mybbp1a	18432	11B4	Myb-binding protein	46577	R	r1, r4	r1.1, r4.1, r4.3
Phemx	27027	7F5	absence enhances T cell proliferation	2431(2)	F	r3	ND
Rtn4r	65079	16	nogo (reticulon 4) receptor	34527	R	ND	r1.2
Slfn2	20556	11C	schlafen 2, negative regulation of proliferation	13391	R	r4	r4.2
Stk38	106504	17A3.3	serine/threonine kinase 38	55555	F	r2	r2.1, r2.2
2410075D05Rik	73681	10A4	methyltransferase activity	–650	R	ND	r1.2, r4.1, r4.2

or other (predicted) signaling genes. While there were several clones with insertions in (and dysregulation of) *Evi1* (Fig. 2A and table S3), none of the 21 clones with hits in nonsignaling genes or gene-free regions (51% of all insertions detected in tCD34 and flCD34 primary animals) (table S2) dominated in secondary recipients.

To test whether the vector-encoded transgenes derived from human CD34 were required for insertional selection, we examined cohorts of mice that received cells marked with a related vector expressing the dsRED fluorescent protein (Fig. 1A and Table 1). The results were similar. All insertions of clones dominating secondary recipients affected CIS/proto-oncogenes (*Bcl11a*, *Hoxa7*, *BC031781*, and *Scl=Tal1*) or other signaling genes. In a leukemic clone associated with the use of a retroviral vector encoding MDR1, we recently identified very similar insertions in *Hoxa7* and *Bcl11a* (*14*). We chose *Hoxa7* for RT-PCR analysis and verified transcriptional induction (by 3.5 times) (Fig. 3). *Hoxa7* as well as 20 of the other 28 genes marked in secondary recipients of all cohorts (72.4%) are also found in a transcriptome database of highly enriched mouse HSCs (Table 1) (*26*, *27*). This database also contains numerous nonsignaling genes that were not marked by vector insertions in dominant clones.

Although we would not question that the transgene product might be involved in the selection process (*10*, *14*), it is safe to conclude that insertional mutagenesis gives rise to clonal imbalance in the context of different transgenes. Clonal dominance after retroviral gene marking of hematopoietic cells has been observed since the beginning of such studies in the mouse model (*1*, *27*). Our exploration of the associated insertion sites strongly suggests a selection process in which preferential survival of long-term repopulating clones is triggered by insertional dysregulation of genes that enhance their "fitness," without necessarily resulting in malignant transformation (*17*). Similar insertional effects may have contributed to the sequential activation of cell clones noted in earlier marking studies. Thus, clonal succession (*1*, *27*) may not necessarily reflect a normal hematopoietic property.

Related marking studies performed in nonhuman primates so far have provided little evidence of clonal dominance, despite hits in potential or established growth-regulatory genes (*28*). This may reflect experimental and/or genetic differences. The latter may affect cell cycle regulation, apoptosis, and senescence, all known to be more complexly regulated in primates (*5*). Our mouse model may represent a situation of accelerated stress hematopoiesis that is not expected to occur in the majority of clinical applications of retroviral gene transfer. Thus, the insertional bias of replication-defective retroviral vectors for actively transcribed genes (*7*) may be exploited to literally mark genes and entire pathways involved in developmental decisions of defined cell populations, depending on a specific milieu. Consequently, we would suggest the use of vectors lacking strong enhancer-promoter elements for future clonal tracking studies.

References and Notes

1. I. R. Lemischka, C. T. Jordan, *Nat. Immunol.* **2**, 11 (2001).
2. M. K. Brenner, H. E. Heslop, *Cytotherapy* **5**, 190 (2003).
3. H. Mikkers, A. Berns, *Adv. Cancer Res.* **88**, 53 (2003).
4. K. Akagi, T. Suzuki, R. M. Stephens, N. A. Jenkins, N. G. Copeland, *Nucleic Acids Res.* **32**, D523 (2004).
5. A. Rangarajan, R. A. Weinberg, *Nat. Rev. Cancer* **3**, 952 (2003).
6. J. Antonchuk, G. Sauvageau, R. K. Humphries, *Cell* **109**, 39 (2002).
7. X. Wu, Y. Li, B. Crise, S. M. Burgess, *Science* **300**, 1749 (2003).
8. C. Baum *et al.*, *Blood* **101**, 2099 (2003).
9. D. Kohn *et al.*, *Mol. Ther.* **8**, 180 (2003).
10. Z. Li *et al.*, *Science* **296**, 497 (2002).
11. S. Buonamici *et al.*, *J. Clin. Invest.* **114**, 713 (2004).
12. C. Bonini *et al.*, *Nat. Med.* **9**, 367 (2003).
13. S. Hacein-Bey-Abina *et al.*, *Science* **302**, 415 (2003).
14. U. Modlich *et al.*, *Blood* **11**, 4235 (2005); published online 15 February 2005 (10.1182/blood-2004-11-4535).
15. D. Gilliland, M. Tallman, *Cancer Cell* **1**, 417 (2002).
16. Z. Li *et al.*, *Leukemia* **16**, 1655 (2002).
17. Materials and methods are available as supporting material on *Science* Online.
18. B. Fehse *et al.*, *Mol. Ther.* **1**, 448 (2000).
19. M. Schmidt *et al.*, *Hum. Gene Ther.* **12**, 743 (2001).
20. M. Schmidt *et al.*, *Blood* **100**, 2737 (2002).
21. K. Holmqvist *et al.*, *J. Biol. Chem.* **279**, 22267 (2004).
22. H. P. Gerber *et al.*, *Nature* **417**, 954 (2002).
23. J. Sharpe, S. Nonchev, A. Gould, J. Whiting, R. Krumlauf, *EMBO J.* **17**, 1788 (1998).
24. K. Kozar *et al.*, *Cell* **118**, 477 (2004).
25. M. Yan *et al.*, *Proc. Natl. Acad. Sci. U.S.A.* **101**, 17186 (2004).
26. N. B. Ivanova *et al.*, *Science* **298**, 601 (2002).
27. I. R. Lemischka, D. H. Raulet, R. C. Mulligan, *Cell* **45**, 917 (1986).
28. P. Hematti *et al.*, *PLoS Biol.* **2**, e423 (2004).

29. We thank T. Kirsch, J. Skokowa, and D. Lan for assistance with RT-PCR and M. Rhein for preparation of DNA. Supported by the Deutsche Forschungsgemeinschaft (grant nos. KFO 110-A1 and FE 568/5-1), the Bioprofile program of the Bundesministerium für Bildung und Forschung, and the European Union (grant nos. QLRT-2001-00427, LSHB-CT-2004-005242, and QLK3-2001-01265).

Supporting Online Material

www.sciencemag.org/cgi/content/full/308/5725/1171/DC1
Materials and Methods
SOM Text
Fig. S1
Tables S1 to S3
References and Notes

9 September 2004; accepted 8 March 2005
10.1126/science.1105063

The Intracellular Fate of *Salmonella* Depends on the Recruitment of Kinesin

Emmanuel Boucrot,[1] Thomas Henry,[1] Jean-Paul Borg,[2] Jean-Pierre Gorvel,[1] Stéphane Méresse[1]*

Salmonella enterica causes a variety of diseases, including gastroenteritis and typhoid fever. The success of this pathogen depends on its capacity to proliferate within host cells in a membrane-bound compartment. We found that the _Salmonella_-containing vacuole recruited the plus-end–directed motor kinesin. Bacterial effector proteins translocated into the host cell by a type III secretion system antagonistically regulated this event. Among these effectors, SifA targeted SKIP, a host protein that down-regulated the recruitment of kinesin on the bacterial vacuole and, in turn, controlled vacuolar membrane dynamics.

Intracellular replication of *Salmonella enterica* serovar Typhimurium (*S. typhimurium*) takes place in a membrane-bound compartment, the *Salmonella*-containing vacuole (SCV) and requires the type III secretion system (TTSS) encoded by the *Salmonella* pathogenicity island 2 (SPI-2) (*1*). The SPI-2 TTSS is activated intracellularly and mediates the translocation of bacterial proteins into host cells. SifA is encoded outside of SPI-2 but is tightly controlled by the SPI-2 regulatory system SsrAB, and SifA is delivered into host cells via the SPI-2 TTSS (*2*, *3*). SifA is required for the formation of *Salmonella*-induced filaments (Sifs) (*4*, *5*) and is necessary to maintain the integrity of the SCV (*6*). A *sifA*$^-$ mutant is strongly attenuated in virulence in mice, indicating that the control of vacuolar membrane dynamics is a key aspect of the *Salmonella* virulence process (*7*).

[1]Centre d'Immunologie de Marseille-Luminy, CNRS-INSERM-Université de la Méditerranée, Parc Scientifique de Luminy, Case 906-13288 Marseille Cedex 9, France. [2]Molecular Pharmacology, UMR 599 INSERM, and Institut Paoli-Calmettes, 27 Boulevard Leï Roure, 13009 Marseille, France.

*To whom correspondence should be addressed. E-mail: meresse@ciml.univ-mrs.fr

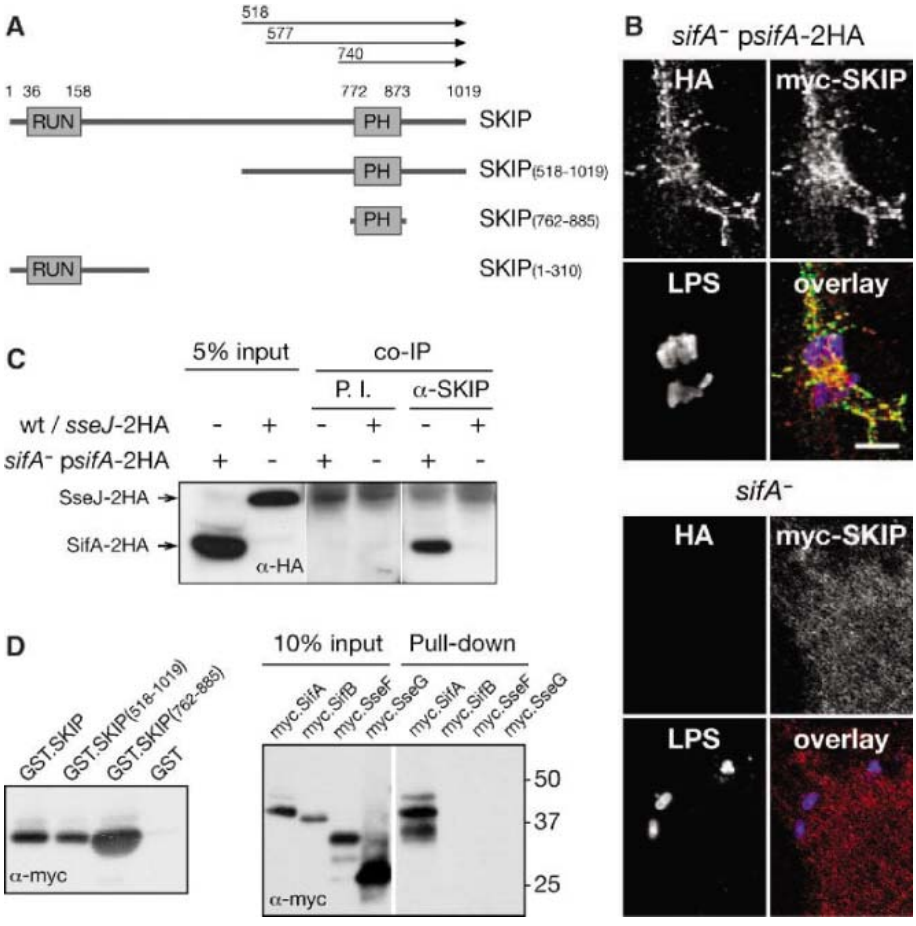

Fig. 1. SifA interacts with SKIP. (**A**) Schematic representation of native SKIP and derived polypeptides. Arrows indicate the regions corresponding to the cDNAs cloned in a two-hybrid screen. The first and last amino acid residue numbers of truncated polypeptides are shown in parentheses. (**B**) SifA recruits myc-SKIP on SCVs and Sifs. HeLa cells expressing moderate levels of myc-SKIP (5 to 10 times greater than the endogenous level) were infected for 14 hours with either a *S. typhimurium* strain secreting SifA-2HA (*sifA*⁻p*sifA*-2HA) or the *sifA*⁻ mutant strain, and were immunostained for HA (green), myc (red), and lipopolysaccharide (LPS) (blue). Scale bar, 5 μm. (**C**) SKIP immunoprecipitates SifA but not SseJ. HeLa cells were infected with *Salmonella* strains secreting SifA-2HA or SseJ-2HA for 14 hours. Cell lysates were incubated with a rabbit antibody to SKIP or the corresponding preimmune serum (P.I.), precipitated using Protein-A beads (co-IP) and immunoblotted with an antibody to HA. The background at the top of the gels corresponds to rabbit immunoglobulin G heavy chains. (**D**) Pull-down experiments with various myc-tagged SPI-2 TTSS effector proteins with GST.SKIP-derived polypeptides. Extracts of HeLa cells expressing SPI-2 effector proteins were incubated with either GST or GST.SKIP-derived polypeptides immobilized on beads. Bound proteins were immunoblotted with an antibody to myc. GST.SKIP(762-885) encoding the PH motif is sufficient to pull down SifA (left panel). GST.SKIP(518-1019) specifically pulls down SifA (right panel). The positions of molecular mass markers are indicated.

The molecular mechanisms underlying the formation of Sifs and the maintenance of SCV integrity are still unresolved, and host proteins with which SifA interacts are unknown. We performed a yeast two-hybrid screen of a human mammary gland cDNA library using SifAΔ6 (*8*) as bait. We isolated three independent cDNA clones, all encoding the C-terminal region of a protein identical to KIAA 0842 (*9*) (Fig. 1A). *Kiaa 0842* encodes a 113-kD ubiquitously expressed polypeptide of unknown function that we have named SKIP (for SifA and kinesin–interacting protein). SKIP contains an N-terminal RPIP8, UNC-14, and NESCA (RUN) motif (*10*) and a C-terminal pleckstrin homology (PH) motif (*11*) (Fig. 1A).

We analyzed whether SifA interacted with SKIP in cultured cells. In HeLa cells, SKIP was essentially a cytosolic protein, and it was partially recruited to membranes upon ectopic expression of SifA (fig. S1). In *S. typhimurium* 12023–infected cells, secreted double hemagglutinin (HA) epitope–tagged SifA (SifA-2HA) was present on SCVs and Sifs (*3*), and overexpressed myc-SKIP was recruited on these *Salmonella*-induced membranous structures (Fig. 1B). However, myc-SKIP remained evenly distributed in HeLa cells infected with a *sifA*⁻ mutant and could not be detected on

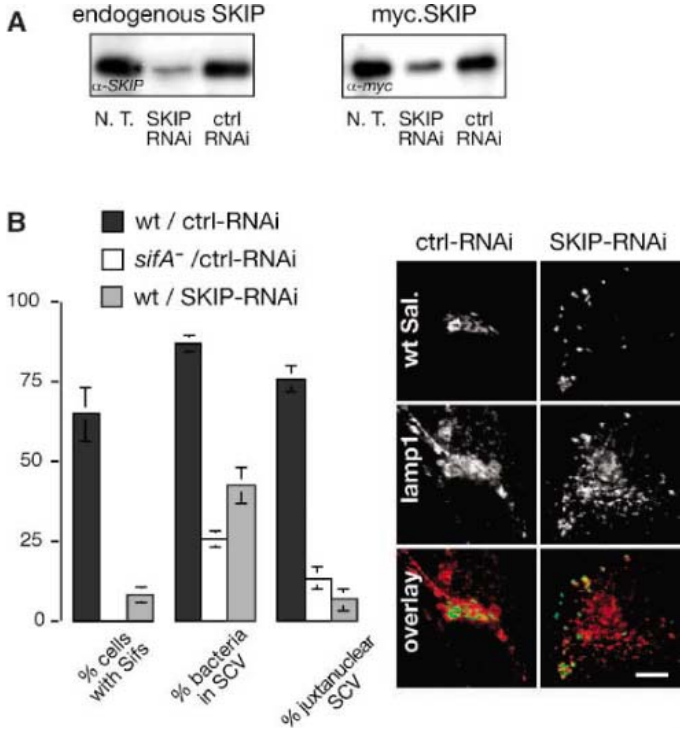

Fig. 2. SifA functions are mediated by its interaction with SKIP. (**A**) Transfection of HeLa cells with siRNA directed against SKIP leads to a strong decrease in endogenous or overexpressed SKIP levels. HeLa cells were either not transfected (N.T.) or transfected with siRNAs directed against SKIP (SKIP-RNAi) or a corresponding scrambled RNA (ctrl-RNAi) for 48 hours and then transfected or not with a plasmid encoding myc.SKIP for 24 hours. 40 μg of total proteins were loaded per lane and were immunoblotted with appropriate antibodies. (**B**) Depletion of SKIP and absence of *sifA* result in the same phenotype in *Salmonella*-infected cells. RNAi-treated HeLa cells were infected with GFP-expressing wild-type (wt) or *sifA*⁻ mutant *Salmonella* for 14 hours, fixed, and immunostained for the SCV marker lamp1. Sifs, bacteria in SCVs, and the position of SCVs were scored (*23*). Representative confocal microscopy images of SKIP-depleted or control cells infected with wild-type *Salmonella* are shown. Scale bar, 10 μm.

bacterial vacuoles (Fig. 1B). The SifA-SKIP interaction was investigated by coimmunoprecipitation analysis of infected HeLa cell lysates. *S. typhimurium* strains secreting SifA-2HA or SseJ-2HA, another SPI-2 effector protein, were used. SifA was specifically detected in SKIP immunoprecipitates (Fig. 1C). Thus, SKIP was recruited to SCVs and Sifs in a SifA-dependent manner. We further analyzed the interaction between SifA and SKIP in vitro and showed that purified glutathione *S*-transferase (GST).SKIP, but not GST, pulled down SifA (Fig. 1D). Various fragments of SKIP were tested to localize the SifA-binding site. The PH motif (amino acid residues 762 to 885) was sufficient for the interaction with SifA (Fig. 1D). None of the other SPI-2 effector proteins tested interacted with SKIP (Fig. 1D). Thus SKIP, through its PH motif, interacts specifically with SifA.

The physiological relevance of the SKIP-SifA interaction was studied by examining the functional consequences of RNA interference (RNAi) depletion of SKIP on SifA-dependent phenotypes. Transfection of HeLa cells with a small interfering (si) RNA directed against SKIP (SKIP-RNAi) reduced the expression of endogenous SKIP or overexpressed myc.SKIP to about 20% of control levels (Fig. 2A). RNAi-treated HeLa cells were infected with wild-type *S. typhimurium* or a *sifA*$^-$ mutant for 14 hours, and SifA-dependent phenotypes were scored. The ability of wild-type *S. typhimurium* to induce the formation of Sifs was strongly reduced in SKIP-RNAi cells as compared to cells transfected with a control oligoribonucleotide (ctrl-RNAi). In addition, depletion of SKIP decreased the stability of SCVs, resulting in the release of wild-type bacteria into the cytosol, phenocopying the effect of the *sifA*$^-$ mutation (Fig. 2B). We then tested whether SKIP was required for intracellular replication of *Salmonella* in MelJuSo human melanoma cells. We found that wild-type *Salmonella* displayed a replication defect in SKIP-depleted cells, which was comparable to that of the *sifA*$^-$ mutant in control cells (fig. S2). Thus SKIP-depleted cells are unresponsive to SifA, and SKIP acts as an essential mediator of SifA functions.

Although most wild-type SCVs had a juxtanuclear localization in control cells, we found SCVs scattered throughout SKIP-depleted cells (Fig. 2B). Scattering of SCVs was also observed in control cells infected with the *sifA*$^-$ mutant (Figs. 2B and 3A), indicating that SifA via SKIP may also control the intracellular positioning of SCVs. These and other findings (*12*–*14*) suggest the importance of the intracellular positioning and of microtubule motors in SCV membrane dynamics. We investigated the role of SifA and SKIP in the regulation of SCV-associated molecular motor activities. Conventional kinesin and dynein are the major plus-end–directed and minus-end–directed microtubule motors, respectively. We analyzed their distribution during the course of a *Salmonella* infection. Dynein was equally distributed on wild-type and *sifA*$^-$ SCVs (fig. S3). Conversely, most *sifA*$^-$ SCVs were strongly decorated by an antibody to kinesin beyond 6 hours of infection, whereas wild-type SCVs displayed a limited association with kinesin (Fig. 3A). We examined the kinetics of kinesin acquisition. As early as 4 hours after invasion, kinesin started to be associated with *sifA*$^-$ SCVs and continued to accumulate, so that 86 ± 6% of SCVs labeled positively for kinesin at 14 hours after invasion (Fig. 3B). Selective accumulation of kinesin on *sifA*$^-$ SCVs was also observed in MelJuSo cells, as well as in mouse bone marrow–derived macrophages (Fig. 3C). The wild-type phenotype was rescued by introducing a plasmid encoding the *sifA* allele into the mutant strain (Fig. 3B). Thus, recruitment of kinesin to SCVs is specifically associated with the absence of SifA. Vacuoles enclosing a *ssaV*$^-$ mutant, which is defective for the secretion of all SPI-2 effector proteins, were seldom positive for kinesin (Fig. 3B), thereby indicating that the absence of SifA per se is not sufficient to induce the recruitment of kinesin. Rather, this phenomenon requires the translocation of other effector proteins via the SPI-2 TTSS. Thus, the formation of the kinesin coat on SCVs requires a functional SPI-2 secretion system and is negatively regulated by SifA.

We next explored whether the SifA-mediated recruitment of SKIP promotes the negative regulation of kinesin recruitment on SCVs. The infection of SKIP-depleted HeLa cells with wild-type *S. typhimurium* for 14 hours resulted in 61 ± 7% SCVs coated with kinesin, compared to 18 ± 4% in control cells (Fig. 4A). Thus, the depletion of SKIP, like the absence of SifA, leads to an accumulation of kinesin on SCVs. We next investigated the impact of high kinesin motor activity on SifA/SKIP-dependent phenotypes. Overexpression of the tetratricopeptide repeat (TPR) cargo-binding domain of the mouse kinesin light chain 2 exerts a dominant negative effect on kinesin motor functions (*15*). In *sifA*$^-$ infected cells, overexpression of a green fluo-

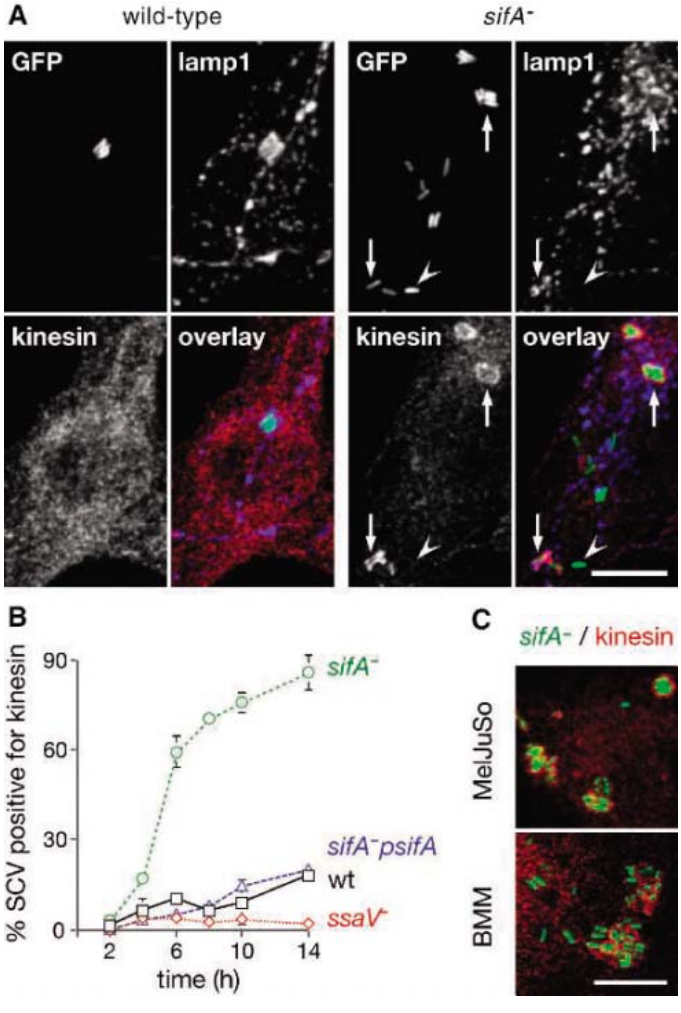

Fig. 3. Vacuoles containing the *sifA*$^-$ mutant accumulate kinesin during the course of an infection. (**A**) HeLa cells were infected with GFP-expressing wild-type or *sifA*$^-$ *Salmonella* (green) for 10 hours, fixed, and immunostained for lamp1 (blue) and kinesin (red) and observed by confocal microscopy. Wild-type SCVs are enriched in lamp1 but seldom positive for kinesin. Most *sifA*$^-$ bacteria are present in the cytosol (arrowhead) as shown by the absence of surrounding lamp1. *sifA*$^-$ mutants still present in vacuoles are associated with kinesin (arrows). Scale bar, 10 μm. (**B**) The percentage of kinesin-positive SCVs at different time points of an infection of HeLa cells was scored (*23*) for wild-type *Salmonella* (squares) and *ssaV*$^-$ (diamonds), *sifA*$^-$ (circles), and *sifA*$^-$p*sifA* (triangles) mutants. (**C**) *sifA*$^-$ SCVs accumulate kinesin in various cell types. MelJuSo cells and mouse bone marrow–derived macrophages (BMM) were infected with *sifA*$^-$ mutant bacteria (green) for 10 hours, fixed, and immunolabeled for kinesin (red). Scale bar, 10 μm.

rescent protein (GFP)–tagged TPR domain (GFP.TPR) was sufficient to relocalize SCVs to the juxtanuclear area and to preserve the integrity of vacuoles (*13*) (fig. S4). Thus, in infected cells, SKIP is an inhibitor of kinesin recruitment, and its activity is required for the positioning and maintenance of the SCV.

Conventional kinesin is involved in the transport of vesicles, organelles, chromosomes (*16*), and intermediate filaments (*17*) and in maintaining the structure and position of the Golgi apparatus (*18*). To test whether SKIP also functions as a kinesin regulator in the context of uninfected cells, we analyzed the fate of the Golgi apparatus in RNAi-treated HeLa cells. Depletion of SKIP induced a scattering of the giantin labeling, whereas control cells presented a regular stacked Golgi (Fig. 4B). An ongoing tug of war between dynein and kinesin occurs at the Golgi level. Golgi scattering has been observed upon disruption of dynein function, presumably because the plus-end–directed motor is still active (*19*). In contrast, the disruption of kinesin function causes the collapse of the Golgi apparatus (*18*, *20*). Thus, scattering of the giantin labeling in absence of SKIP is consistent with elevated kinesin motor activity associated with the Golgi apparatus. To confirm this hypothesis, we inhibited kinesin motor activity by expressing HA.TPR in SKIP-depleted cells. Expression of HA.TPR but not GFP restored the stacked Golgi apparatus (Fig. 4B). Thus, SKIP acts as a down-regulator of kinesin.

Little is known about how kinesin interacts with its cargos and how this process is regulated. Several proteins mediating the binding of kinesin onto cargos have been identified (*21*). Among them are kinectin, the amyloid precursor protein, and JNK-interacting proteins (JIP-1, JIP-2, and JIP-3). The latter are scaffolding proteins that may assemble linkers and regulatory proteins. We investigated the possibility that SKIP may form a complex with kinesin in such a regulatory complex of proteins. We tested the capacity of recombinant SKIP fragments to pull down kinesin from HeLa cellular extracts. SKIP and its N-terminal domain, but not its C-terminal domain, pulled down kinesin (Fig. 4C). Thus, the RUN-containing N-terminal domain of SKIP interacts with kinesin.

We observed an inverse correlation between the recruitment of SKIP and the recruitment of kinesin, thereby ruling out the possibility of a sole direct interaction between both molecules. Because the recruitment of SKIP on membranes displaces kinesin in vivo and because SKIP pulls down kinesin in vitro, we propose a model in which the RUN-containing domain of SKIP binds kinesin in a regulatory complex of proteins (fig. S5). Thus, kinesin displacement would result from the interaction of SKIP with accessory proteins. The RUN motif–containing region of UNC-14 interacts with UNC-16, the *Caenorhabditis elegans* JIP-3 (*22*). UNC-14 also binds kinesin and regulates synaptic vesicle transport (*22*). Thus, RUN motifs may have a role in the regulation of the dynamics of cargo/kinesin interactions.

A dynamic process of kinesin recruitment in *Salmonella*-infected cells is mediated by the secretion of unidentified SPI-2 TTSS effectors and is down-regulated by the SifA-mediated recruitment of SKIP on membranes. *S. typhimurium* is thereby able to fine-tune the SCV-associated kinesin motor activity by regulating the secretion of its own effector proteins. The consequences of an increased kinesin motor activity associated with SCVs may be an excessive formation of outgoing tubules and vesicles, eventually leading to SCV disruption. The identification of SKIP as a SifA interactor and the demonstration that it acts as a negative regulator of kinesin motor activity provide a key to understanding the molecular mechanism of SifA action.

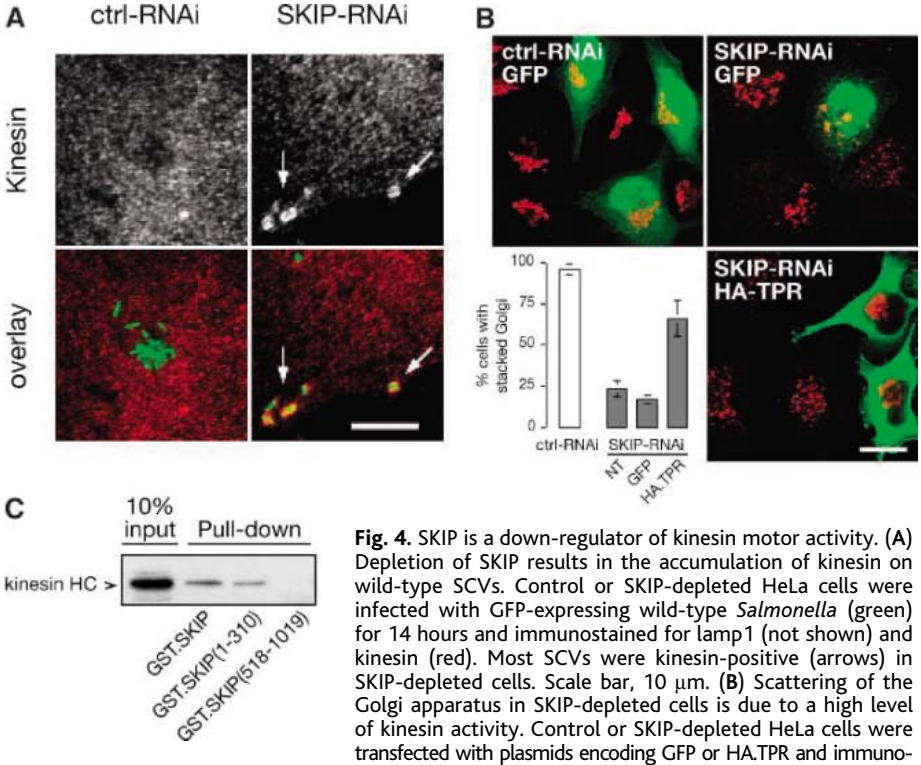

Fig. 4. SKIP is a down-regulator of kinesin motor activity. (**A**) Depletion of SKIP results in the accumulation of kinesin on wild-type SCVs. Control or SKIP-depleted HeLa cells were infected with GFP-expressing wild-type *Salmonella* (green) for 14 hours and immunostained for lamp1 (not shown) and kinesin (red). Most SCVs were kinesin-positive (arrows) in SKIP-depleted cells. Scale bar, 10 μm. (**B**) Scattering of the Golgi apparatus in SKIP-depleted cells is due to a high level of kinesin activity. Control or SKIP-depleted HeLa cells were transfected with plasmids encoding GFP or HA.TPR and immunostained for the Golgi marker giantin (red) and possibly for HA.TPR (green). Nontransfected (NT) and GFP- or HA.TPR-expressing cells were scored (*23*) for the presence of a stacked Golgi apparatus. Representative confocal microscopy images of SKIP-depleted or control cells are shown. Scale bar, 20 μm. (**C**) SKIP pulls down kinesin. An extract from HeLa cells was incubated with GST.SKIP-derived polypeptides immobilized on beads. Bound proteins were immunoblotted with an anti-kinesin heavy chain (HC). SKIP and SKIP(1-310), but not SKIP(518-1019), pulled down kinesin.

References and Notes

1. M. Hensel *et al.*, *Science* **269**, 400 (1995).
2. E. A. Miao, S. I. Miller, *Proc. Natl. Acad. Sci. U.S.A.* **97**, 7539 (2000).
3. J. H. Brumell, D. L. Goosney, B. B. Finlay, *Traffic* **3**, 407 (2002).
4. F. Garcia-del Portillo, M. B. Zwick, K. Y. Leung, B. B. Finlay, *Proc. Natl. Acad. Sci. U.S.A.* **90**, 10544 (1993).
5. M. A. Stein, K. Y. Leung, M. Zwick, F. Garcia-del Portillo, B. B. Finlay, *Mol. Microbiol.* **20**, 151 (1996).
6. C. R. Beuzon *et al.*, *EMBO J.* **19**, 3235 (2000).
7. C. R. Beuzon, S. P. Salcedo, D. W. Holden, *Microbiol.* **148**, 2705 (2002).
8. E. Boucrot, C. R. Beuzon, D. W. Holden, J. P. Gorvel, S. Meresse, *J. Biol. Chem.* **278**, 14196 (2003).
9. T. Nagase *et al.*, *DNA Res.* **5**, 355 (1998).
10. I. Callebaut, J. de Gunzburg, B. Goud, J. P. Mornon, *Trends Biochem. Sci.* **26**, 79 (2001).
11. M. J. Rebecchi, S. Scarlata, *Annu. Rev. Biophys. Biomol. Struct.* **27**, 503 (1998).
12. S. P. Salcedo, D. W. Holden, *EMBO J.* **22**, 5003 (2003).
13. J. Guignot *et al.*, *J. Cell Sci.* **117**, 1033 (2004).
14. M. Marsman, I. Jordens, C. Kuijl, L. Janssen, J. Neefjes, *Mol. Biol. Cell* **15**, 2954 (2004).
15. J. Rietdorf *et al.*, *Nat. Cell Biol.* **3**, 992 (2001).
16. L. S. Goldstein, A. V. Philp, *Annu. Rev. Cell Dev. Biol.* **15**, 141 (1999).
17. E. J. Clarke, V. Allan, *Curr. Biol.* **12**, R596 (2002).
18. V. J. Allan, H. M. Thompson, M. A. McNiven, *Nat. Cell Biol.* **4**, E236 (2002).
19. J. K. Burkhardt, C. J. Echeverri, T. Nilsson, R. B. Vallee, *J. Cell Biol.* **139**, 469 (1997).
20. F. Feiguin, A. Ferreira, K. S. Kosik, A. Caceres, *J. Cell Biol.* **127**, 1021 (1994).
21. R. L. Karcher, S. W. Deacon, V. I. Gelfand, *Trends Cell Biol.* **12**, 21 (2002).
22. R. Sakamoto *et al.*, *Mol. Biol. Cell* **16**, 483 (2005).
23. Values represent the means ± SD of three independent experiments, n >100 events for each experiment.
24. We thank D. Holden for bacterial strains, R. Vale for the anti-kinesin HC (PCP42), M. Way for the pGFP-KLC2-TPR, V. Ollendorf for the $pBTM_{116}$ and $pBTM_{116}$-lamin vectors, and the Kazusa DNA Research Institut for the cDNA encoding full-length KIAA 0842.

We are grateful to J. Deiwick, A. Dumont, and C.-L. Ku for DNA constructs and to C. de Chastellier, J. Ewbank, S. Garvis, N. Lapaque, and S. Salcedo for critical review of this manuscript. E.B. and T.H. were recipients of fellowships from the French Ministry of Research, Association pour la Recherche sur le Cancer and Fondation pour la Recherche Médicale. This work was supported by institutional grants from CNRS and INSERM and the Microban EU network grant MRTN-CT-2003-504227.

Supporting Online Material
www.sciencemag.org/cgi/content/full/308/5725/1174/DC1
Materials and Methods
Figs. S1 to S5
References

25 January 2005; accepted 28 February 2005
10.1126/science.1110225

An Active Role for tRNA in Decoding Beyond Codon:Anticodon Pairing

Luisa Cochella and Rachel Green*

During transfer RNA (tRNA) selection, a cognate codon:anticodon interaction triggers a series of events that ultimately results in the acceptance of that tRNA into the ribosome for peptide-bond formation. High-fidelity discrimination between the cognate tRNA and near- and noncognate ones depends both on their differential dissociation rates from the ribosome and on specific acceleration of forward rate constants by cognate species. Here we show that a mutant $tRNA^{Trp}$ carrying a single substitution in its D-arm achieves elevated levels of miscoding by accelerating these forward rate constants independent of codon:anticodon pairing in the decoding center. These data provide evidence for a direct role for tRNA in signaling its own acceptance during decoding and support its fundamental role during the evolution of protein synthesis.

Selection of cognate aminoacyl-tRNAs (aa-tRNAs) is accomplished by the translation machinery with high accuracy and speed by means of kinetic proofreading (*1*, *2*) and induced-fit (*3*, *4*) mechanisms (Fig. 1). Kinetic proofreading is facilitated by the action of the guanosine triphosphatase (GTPase) elongation factor Tu (EF-Tu) in ternary complex with aa-tRNA and GTP. The GTPase activity of this complex effectively separates selection into two stages, initial selection and proofreading, which allow multiple opportunities for the rejection of incorrect tRNAs. Induced fit further increases fidelity by selectively accelerating the forward rates of two steps in the selection process—activation of EF-Tu for GTP hydrolysis (rate constant k_3) and accommodation of aa-tRNA into the A site (k_5)—for cognate relative to near-cognate aa-tRNAs (*4*, *5*). This induced fit results from cognate codon:anticodon interactions somehow accelerating rate-limiting conformational changes required for GTP hydrolysis and peptidyl transfer. These changes likely originate in the decoding center of the small ribosomal subunit where the codon:anticodon interaction is "read" and are then transmitted to remote regions of the large ribosomal subunit involved in GTP hydrolysis and accommodation. Such conformational changes in the decoding center resulting from cognate (but not near-cognate) interactions have been documented in x-ray structures (*6*). Communication between the decoding center and the large subunit could proceed through intersubunit bridges affected by "closure" of the small subunit upon cognate tRNA binding (*7*–*9*) or through the tRNA itself (*10*). Here we show that the tRNA body acts as a direct functional link between the decoding center and remote regions of the ribosome that promote GTP hydrolysis and accommodation.

The contribution of tRNA to decoding was studied by using the Hirsh suppressor (*11*), a $tRNA^{Trp}$ variant that recognizes both the tryptophan (UGG) and UGA stop codons. Rather than carrying an anticodon mutation, this tRNA carries a G24A substitution in the D-arm, changing the U11:G24 base pair to U11:A24. This mutation could cause miscoding in two distinct ways: It could slow dissociation (rejection) from the ribosome [as previously argued (*12*)] or it could accelerate forward rate constants in tRNA selection. To distinguish between these possibilities, we first measured rate constants for two forward steps, GTPase activation (k_3) and accommodation (k_5), for wild-type and mutant tRNAs. Second, we addressed the effect of this mutation on dissociation of these tRNAs from the ribosome by measuring both rejection rates during proofreading (k_7) and the equilibrium dissociation constant ($k_{-2}\ k_{-1}/k_2k_1$). The pre–steady-state kinetic analysis presented here is modeled on earlier studies of Rodnina and colleagues (*4*, *5*). Although kinetic details of $tRNA^{Trp}$ show some variance from those previously obtained for $tRNA^{Phe}$ and $tRNA^{Leu}$, the overall view of tRNA selection that emerges is notably consistent.

We first determined rate constants for GTPase activation with wild-type and G24A $tRNA^{Trp}$ on ribosome complexes programmed with mRNAs containing cognate (UGG) or near-cognate (UGA) codons in the A site. The GTPase activation rate (k_3) was measured by following GTP hydrolysis, because activation is rate-limiting for this event (*4*). Rates for single-turnover GTP hydrolysis were measured by mixing programmed ribosomes with a purified ternary complex composed of EF-Tu, [γ-^{32}P]GTP, and either wild-type or variant Trp-$tRNA^{Trp}$ (Fig. 2A, top panel). GTP hydrolysis rates were measured at increasing ribo-

Howard Hughes Medical Institute, Department of Molecular Biology and Genetics, Johns Hopkins University School of Medicine, Baltimore, MD 21205, USA.

*To whom correspondence should be addressed. E-mail: ragreen@jhmi.edu

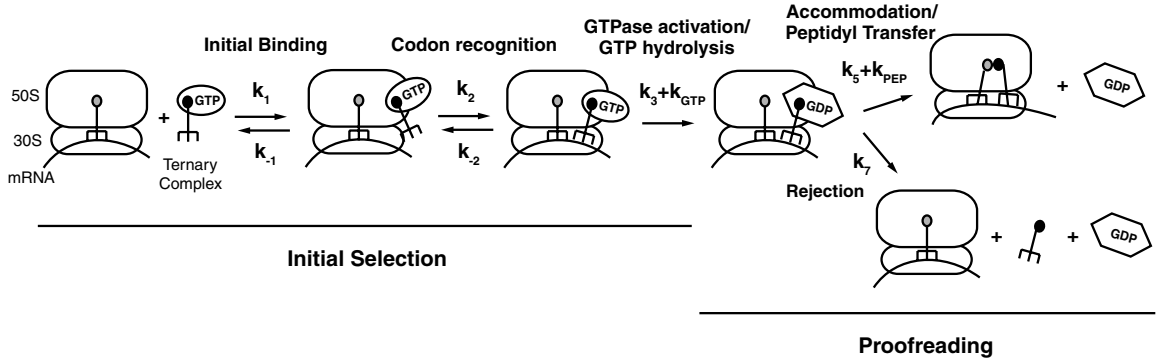

Fig. 1. Kinetic scheme for tRNA selection on the ribosome identifying the two stages of initial selection and proofreading. The scheme includes the relevant kinetically resolved steps (*4*). EF-Tu is shown in different conformations in the GTP- and GDP-bound form.

some concentrations, and pseudo–first-order rate constants were calculated from the extrapolation of hyperbolic fits to saturation (Fig. 2A, middle panel). Although both wild-type and G24A tRNA^{Trp} activate GTP hydrolysis to the same extent on the cognate codon (k_3 = 80 s^{-1}), the mutant tRNA increases this rate constant from ~5 to ~45 s^{-1} on the near-cognate codon (Fig. 2A, bottom panel, and Table 1).

These data establish that the G24A substitution in the D-arm of tRNA^{Trp} bypasses the otherwise strict requirement for cognate codon:anticodon interactions to activate GTP hydrolysis. To rule out that the observed rate increase was specific for the UGA near-cognate codon, we examined whether G24A tRNA^{Trp} had similar effects on additional mRNAs [as suggested by earlier in vitro studies with UGU codons (*13*)]. We measured rate constants for GTPase activation (k_3) on other third- (UGU and UGC) and first-position (CGG) near-cognate codons. Although the rate constants for GTPase activation are considerably lower on first-position near-cognate codons, the relative increase in k_3 seen for G24A tRNA^{Trp} is similar to that observed on the third-position mismatch UGA (Fig. 2A and Table 1). Similar results were also obtained for the third-position mismatched codons UGU and UGC (*14*). Finally, we used a truncated mRNA to determine whether GTPase activation by mutant tRNA^{Trp} is enhanced relative to that of the wild type in the complete absence of an A-site codon. Again, G24A tRNA^{Trp} stimulates GTP hydrolysis by ~4-fold relative to that of the wild type (from 0.01 ± 0.005 to 0.04 ± 0.004 s^{-1}, at 5 μM ribosomes) (*14*). The uniform stimulation of k_3 by the G24A substitution, independent of codon:anticodon interaction, indicates that this miscoding tRNA variant autonomously stimulates downstream events. Moreover, it seems unlikely that the G24A substitution also overcomes deficits in the stability of the codon:anticodon interaction for such distinct mismatches, arguing against effects on k_{-2}.

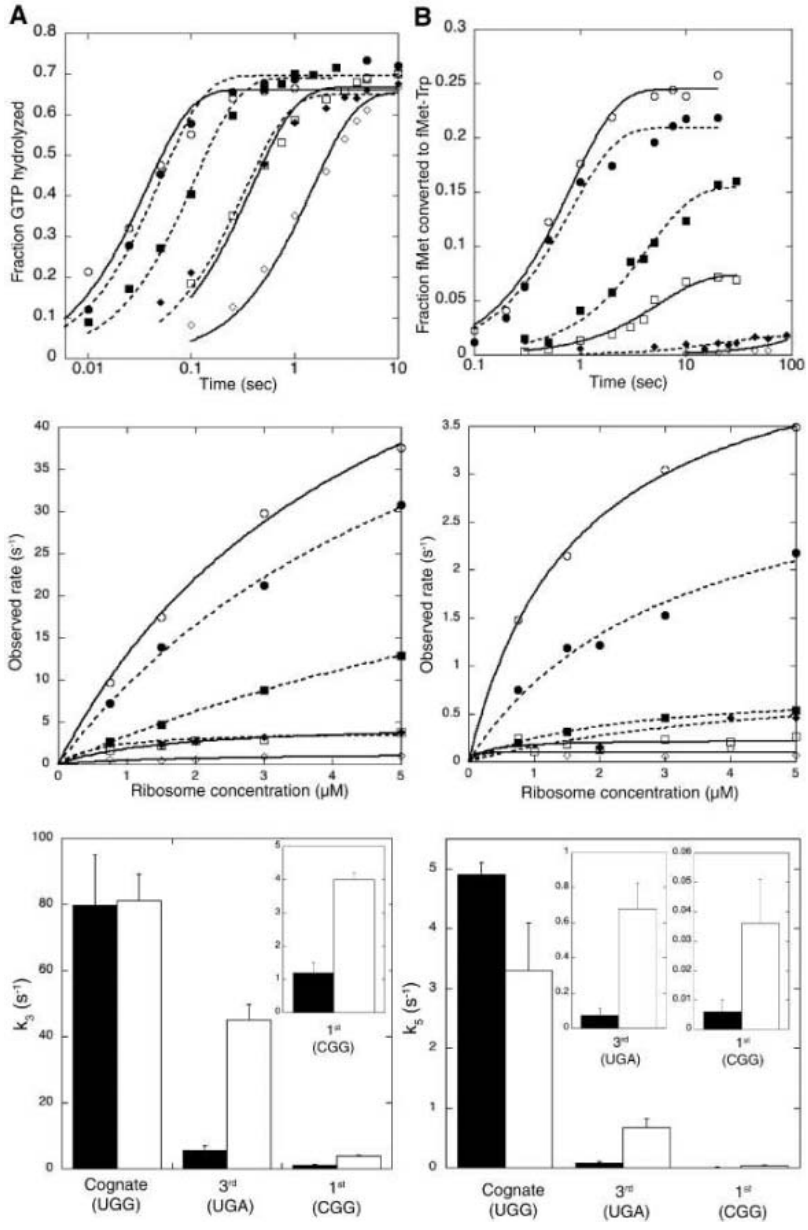

Fig. 2. G24A tRNA^{Trp} variant accelerates forward rates of (**A**) GTPase activation and (**B**) accommodation on near-cognate codons. The top panels show representative time courses (at 2 μM ribosomes) of GTP hydrolysis and dipeptide formation for wild-type (solid lines, open symbols) and G24A (dashed lines, solid symbols) tRNA^{Trp} on cognate (circles), UGA (squares), or CGG (diamonds) programmed ribosomes. The middle panels show ribosome titrations and fits for rate-constant calculations. The bottom panels show calculated rate constants for wild-type (black) and G24A (white) tRNA^{Trp}. Each bar represents the average of two to four ribosome titration experiments and the error bars represent their standard deviations.

We next determined rate constants for another forward step, tRNA accommodation (k_5), for wild-type and G24A tRNA^{Trp} on ribosome complexes containing cognate (UGG) or two different near-cognate (UGA and CGG) mRNAs. Here we followed peptide bond formation, because its rate (k_{pep}) was limited by accommodation (k_5) (*4*). After the mixing of programmed ribosomes containing f-[^{35}S]-Met-tRNA^{fMet} in the P site with wild-type and mutant Trp-tRNA^{Trp} ternary complex, the amount of fMet-Trp dipeptide formed over time was quantitated (Fig. 2B, top panel). Because accommodation (k_5) is at a branch point in the kinetic pathway (Fig. 1), the observed rate constants (k_{obs}) obtained from ribosome titrations (Fig. 2B, middle panel) represent the sum of the individual rate constants of accommodation and rejection ($k_{obs} = k_5 + k_7$). For cognate interactions, rejection is negligible (*4*, *5*), and thus the observed rate constant simply represents accommodation ($k_{obs} = k_5$). For near-cognate interactions, the extent of dipeptide formation is substantially reduced (Fig. 2B, top panel), indicating that a fraction of bound tRNA proceeds through the productive pathway, whereas the rest is irreversibly rejected [fraction = $k_5/(k_5 + k_7)$]. Because accommodation is rate-limiting, we can calculate individual rate constants (k_5 and k_7) for near-cognate complexes. As observed for k_3, rate constants for accommodation (k_5) are similar for wild-type and mutant tRNA^{Trp} on the cognate codon. On near-cognate codons, however, G24A tRNA^{Trp} increases accommodation rates by six- to ninefold relative to wild type (Fig. 2B, bottom panel and Table 1). Thus, variant tRNA^{Trp} promotes general miscoding by accelerating the other forward step, k_5, in tRNA selection.

The observed stimulation of forward rate constants (k_3 and k_5) by G24A tRNA^{Trp} establishes that miscoding is promoted by kinetic contributions to induced fit. To investigate

Table 1. Rate and dissociation constants of wild-type and mutant $tRNA^{Trp}$ on cognate and near-cognate codons. l.d., limit of detection; wt, wild type.

	k_3 (s^{-1})		k_5 (s^{-1})		k_7 (s^{-1})		K_d (nM)	
	wt	G24A	wt	G24A	wt	G24A	wt	G24A
UGG (cognate)	79.7 ± 15.2	81.2 ± 8.0	4.9 ± 0.2	3.3 ± 0.8	< l.d.	< l.d.	1.2 ± 0.7	0.6 ± 0.3
UGA (3rd)	5.6 ± 1.4	45.1 ± 4.7	0.07 ± 0.04	0.68 ± 0.14	0.12 ± 0.08	0.19 ± 0.23	19.9 ± 3.5	25.7 ± 3.9
CGG (1st)	1.2 ± 0.3	4.0 ± 0.2	0.006 ± 0.004	0.036 ± 0.015	0.09 ± 0.06	0.41 ± 0.17	20.3 ± 4.8	19.3 ± 3.4

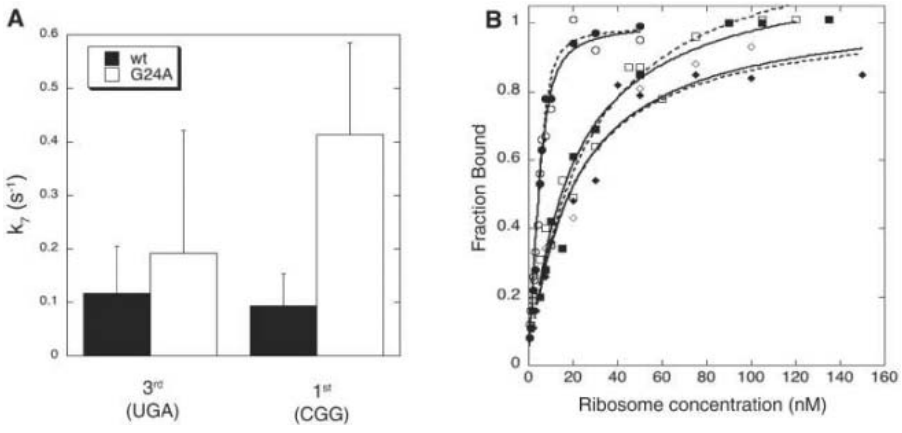

Fig. 3. G24A $tRNA^{Trp}$ variant does not increase miscoding levels by slowing rejection from the ribosome. (**A**) Rate constants of rejection during proofreading (k_7) were calculated from the rate and extent of dipeptide formation for wild-type (wt) (black) and G24A (white) $tRNA^{Trp}$. Errors were calculated by standard error propagation. (**B**) Equilibrium dissociation constants (K_d's) were measured by filter-binding for wild-type (solid lines, open symbols) and G24A tRNA (dashed lines, solid symbols) on cognate (circles), UGA (squares), or CGG (diamonds) programmed ribosomes.

whether this mutation also increases miscoding by slowing dissociation, we examined rate constants of rejection during proofreading (k_7) (Fig. 3A and Table 1). The rejection rate for G24A $tRNA^{Trp}$ is equal to or higher than that for the wild type, indicating that increased residence time on the ribosome of the variant tRNA does not contribute to its miscoding capacity.

To examine the other dissociation step, k_{-2}, we measured equilibrium dissociation constants ($K_d = k_{-1}k_{-2}/k_1k_2$) between tRNAs in ternary complexes with a GTPase-deficient EF-Tu variant (*15*) and cognate- or near-cognate programmed ribosomes. The K_d's measured by filter binding were similar for wild-type and G24A $tRNA^{Trp}$ ternary complexes on each programmed ribosome (Fig. 3B and Table 1). This observation implies that the dissociation rate constant, k_{-2}, is unaffected by the G24A substitution in $tRNA^{Trp}$, because otherwise changes in k_{-2} would need to be exactly compensated by changes in the other rate constants (k_1, k_2, and k_{-1}). Because k_1, k_{-1}, and k_2 are indistinguishable for different tRNA species on various cognate and near-cognate codons (*4*, *5*), this compensation seems unlikely.

Our data establish that the D-arm substitution stimulates miscoding through acceleration of forward selection rates. Thus, the miscoding tRNA variant takes advantage of the induced-fit mechanism for tRNA selection, and in doing so, triggers downstream events, bypassing normally required signals from the decoding center. The two rate constants, k_3 and k_5, are similarly affected, suggesting that a common property of tRNA is central to the mechanism of both steps. These results do not preclude a role for the ribosome itself in the signaling process.

The D-arm substitution likely has a direct effect on tRNA deformability, somehow facilitating required conformational changes during decoding. Altered flexibility of G24A $tRNA^{Trp}$ is supported by earlier work, showing that variant $tRNA^{Trp}$ exhibits slower rates of intramolecular cross-linking (*16*). The cross-linked G24A $tRNA^{Trp}$ no longer suppresses UGA stop codons but is still otherwise functional (*17*). These observations suggest that flexibility in tRNA plays a critical role in decoding.

Cryo–electron microscopy studies provide a view of tRNA in a pre-accommodated state (*18*) that reveals a "kink" between the anticodon- and D-stems, close to position G24 of tRNA, providing evidence that tRNA structural conformers are relevant intermediates in decoding. Alterations of tRNA in this region might affect its capacity to assume this kinked conformation and thus promote downstream events (*19*). It also is possible that G24A $tRNA^{Trp}$ interacts differently with nearby ribosomal elements including helix 69, the sarcin-ricin loop, and the GTPase associated center, all candidates for participating in signal transmission during tRNA selection (*18*, *20*, *21*).

Our studies suggest that conformational changes in tRNA are the physical basis for induced fit, which is an essential contributor to high-fidelity tRNA selection (*5*). Protein synthesis is widely thought to have evolved in an RNA-dominated world where, in the absence of sophisticated factors like EF-Tu, the earliest translational machinery must have relied on active contributions from tRNA. Our results mesh well with recent studies detailing an active role for tRNA in peptidyl transfer (*22*). The recognition of tRNA as an active player in translation (*23*) will replace the historical view of tRNA as a static "adaptor" as more specific roles for tRNA are uncovered.

References and Notes

1. J. Ninio, *Biochimie* **57**, 587 (1975).
2. J. J. Hopfield, *Proc. Natl. Acad. Sci. U.S.A.* **71**, 4135 (1974).
3. D. E. Koshland, *Proc. Natl. Acad. Sci. U.S.A.* **44**, 98 (1958).
4. T. Pape, W. Wintermeyer, M. V. Rodnina, *EMBO J.* **18**, 3800 (1999).
5. K. B. Gromadski, M. V. Rodnina, *Mol. Cell* **13**, 191 (2004).
6. J. M. Ogle *et al.*, *Science* **292**, 897 (2001).
7. J. M. Ogle, F. V. Murphy, M. J. Tarry, V. Ramakrishnan, *Cell* **111**, 721 (2002).
8. I. S. Gabashvili *et al.*, *Cell* **100**, 537 (2000).
9. M. M. Yusupov *et al.*, *Science* **292**, 883 (2001).
10. O. Piepenburg *et al.*, *Biochemistry* **39**, 1734 (2000).
11. D. Hirsh, *J. Mol. Biol.* **58**, 439 (1971).
12. D. Smith, M. Yarus, *J. Mol. Biol.* **206**, 489 (1989).
13. R. H. Buckingham, C. G. Kurland, *Proc. Natl. Acad. Sci. U.S.A.* **74**, 5496 (1977).
14. L. Cochella, R. Green, unpublished data.
15. T. Daviter, H. J. Wieden, M. V. Rodnina, *J. Mol. Biol.* **332**, 689 (2003).
16. A. Favre, R. Buchingham, G. Thomas, *Nucleic Acids Res.* **2**, 1421 (1975).
17. J. Vacher, R. H. Buckingham, *J. Mol. Biol.* **129**, 287 (1979).
18. M. Valle *et al.*, *Nat. Struct. Biol.* **10**, 899 (2003).
19. J. M. Ogle, V. Ramakrishnan, *Annu. Rev. Biochem.* 10.1146/annurev.biochem.74.061903.155440 (2004).
20. D. Moazed, J. M. Robertson, H. F. Noller, *Nature* **334**, 362 (1988).
21. H. Stark *et al.*, *Nat. Struct. Biol.* **9**, 849 (2002).
22. J. S. Weinger, K. M. Parnell, S. Dorner, R. Green, S. A. Strobel, *Nat. Struct. Mol. Biol.* **11**, 1101 (2004).
23. C. R. Woese, *RNA* **7**, 1055 (2001).
24. We thank M. Rodnina for advice; O. Uhlenbeck and M. Yarus for reagents; and J. Lorsch, C. Merryman, and R. Reed for comments. R.G. is an investigator of the Howard Hughes Medical Institute. This work was supported by NIH grant R01GM059425.

Supporting Online Material

www.sciencemag.org/cgi/content/full/308/5725/1178/DC1
Materials and Methods
References

23 February 2005; accepted 4 April 2005
10.1126/science.1111408

Functional Interaction Between β-Catenin and FOXO in Oxidative Stress Signaling

Marieke A. G. Essers,[1] Lydia M. M. de Vries-Smits,[1] Nick Barker,[2] Paulien E. Polderman,[1] Boudewijn M. T. Burgering,[1]* Hendrik C. Korswagen[2]*

β-Catenin is a multifunctional protein that mediates Wnt signaling by binding to members of the T cell factor (TCF) family of transcription factors. Here, we report an evolutionarily conserved interaction of β-catenin with FOXO transcription factors, which are regulated by insulin and oxidative stress signaling. β-Catenin binds directly to FOXO and enhances FOXO transcriptional activity in mammalian cells. In *Caenorhabditis elegans*, loss of the β-catenin BAR-1 reduces the activity of the FOXO ortholog DAF-16 in dauer formation and life span. Association of β-catenin with FOXO was enhanced in cells exposed to oxidative stress. Furthermore, BAR-1 was required for the oxidative stress–induced expression of the DAF-16 target gene *sod-3* and for resistance to oxidative damage. These results demonstrate a role for β-catenin in regulating FOXO function that is particularly important under conditions of oxidative stress.

Forkhead box O (FOXO) transcription factors are negatively regulated by the insulin signaling pathway through phosphoinositide 3-kinase (PI 3-kinase) and protein kinase B (PKB, also called c-Akt). Phosphorylation by PKB leads to nuclear exclusion of FOXO, and as a result, its function as a transcriptional activator is inhibited (*1*). In *C. elegans*, an insulin-like signaling pathway controls entry into the dauer diapause, an alternative larval stage that is induced by starvation, a dauer pheromone, or high temperature. Under dauer-inducing conditions, the FOXO homolog DAF-16 is activated, and dauer development is initiated (*2*). We observed that animals containing a null mutation in the β-catenin gene *bar-1* (*3*) are defective in starvation-induced dauer development. To investigate whether BAR-1 is required for DAF-16–dependent dauer formation, we activated DAF-16 with a temperature-sensitive loss-of-function allele of the insulin receptor–like gene *daf-2* (*4*–*6*), then, we compared dauer induction in the presence and absence of *bar-1*. At the restrictive temperature (25°C), both *daf-2* and *daf-2*; *bar-1* double mutants showed 100% dauer induction (n = >200), demonstrating that BAR-1 is not required for the execution of dauer development. At intermediate temperatures, when DAF-16 signaling was not fully activated, there was a significantly lower induction of dauer larvae in the absence of *bar-1* (Fig. 1A). This shows that BAR-1 is required for DAF-16 function when DAF-16 activity is limiting. Overexpression of BAR-1 enhanced the *daf-2*–induced formation of dauer larvae (Fig. 1A). Reduced expression of *daf-16* by RNA interference (RNAi) inhibited the dauer-inducing effect of overexpressed BAR-1 (Fig. 1B), which indicates that BAR-1 may increase dauer formation by enhancing DAF-16 activity. In addition to controlling dauer development, DAF-16 also influences longevity (*6*). Because *daf-16* null mutants show a shorter average life span, we tested whether BAR-1 was also required for normal longevity. *bar-1* mutants had a shorter life span, one that was similar to that of *daf-16* mutants (Fig. 1C). Taken together, these results show that BAR-1 is required for DAF-16 signaling in dauer induction and life-span regulation.

To investigate whether β-catenin is required for FOXO function in mammalian cells, we analyzed FOXO activity in cells that have no detectable β-catenin expression (IIAI.6 cells) (*7*, *8*). In these cells, expression of FOXO4 induced transcription of several different FOXO reporters (Fig. 2A) (*9*), and transcriptional activity was enhanced when β-catenin was also expressed. Cytoplasmic abundance of β-catenin is controlled by glycogen synthase kinase–3β (GSK-3β), a component of the β-catenin destruction complex. Stabilization of endogenous β-catenin in A14 cells (*10*) by treatment with the GSK-3β inhibitor LiCl enhanced FOXO4 activity (Fig. 2B). This effect of LiCl appeared to be

[1]Department of Physiological Chemistry and Center for Biomedical Genetics, University Medical Center, Universiteitsweg 100, 3584 CG Utrecht, Netherlands. [2]Hubrecht Laboratory and Center for Biomedical Genetics, Uppsalalaan 8, 3584 CT Utrecht, Netherlands.

*To whom correspondence should be addressed. E-mail: b.m.t.burgering@med.uu.nl and rkors@niob.knaw.nl

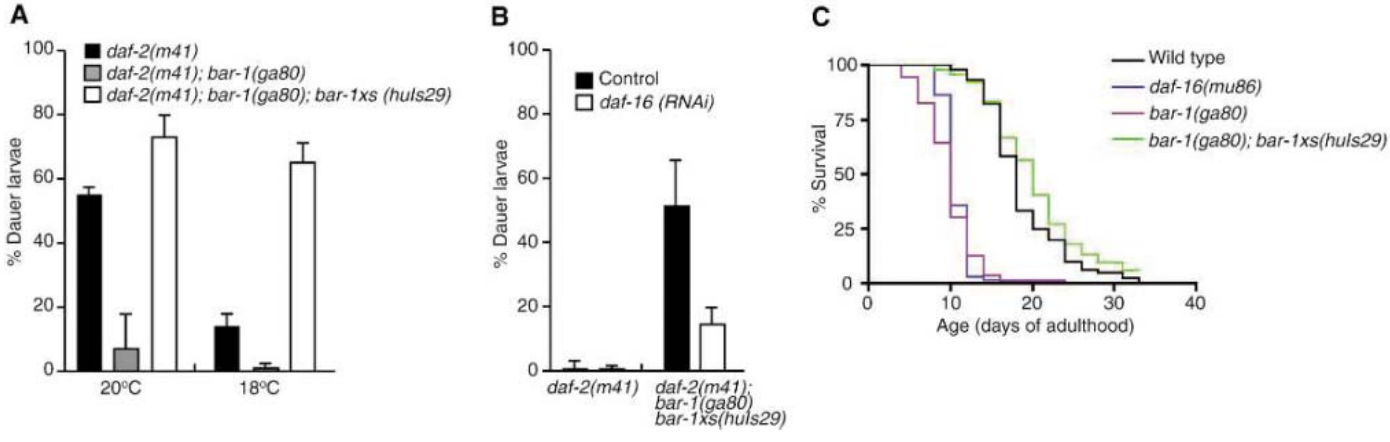

Fig. 1. Genetic interaction between *bar-1* and *daf-16* in dauer induction and life-span regulation. (**A**) Dauer larvae formation induced by *daf-2* was reduced in the absence of *bar-1* ($P < 0.01$, one-way ANOVA with Bonferroni correction), but was enhanced when BAR-1 was overexpressed (*bar-1xs*) ($P < 0.01$ at 18°C). Data are presented as means ± SD and represent the average of four independent experiments. Note that overexpression of BAR-1 did not induce dauer formation in wild-type animals (n = >1000). (**B**) The dauer-inducing effect of BAR-1 overexpression was reduced when DAF-16 function was inhibited by RNAi ($P < 0.01$). Data are presented as means ± SD and represent the average of five independent experiments. (**C**) Loss of *bar-1* reduces life span. Survival curves show that *bar-1* and *daf-16* mutants have a shorter mean life span (10 days, n = 100) than wild-type animals (18 days, n = 100) ($P < 0.01$, Kaplan-Meier survival analysis).

specific to β-catenin stabilization, because LiCl treatment in IIA6.I cells, which lack β-catenin, did not affect FOXO reporter activity (Fig. 2B). Ectopic expression of FOXO results in increased expression of the cell cycle inhibitor p27Kip1 and a consequent arrest in G_1 (*11*). Consistent with the reporter assays, β-catenin overexpression enhanced the expression of endogenous p27Kip1 (Fig. 2C) and the FOXO-induced arrest in G_1 (Fig. 2D). To further investigate the requirement for endogenous β-catenin in FOXO signaling, we used LS174 colon carcinoma cells, which express a β-catenin–specific small interfering RNA (siRNA) under the control of a tetracycline-inducible promoter (*12*). LS174 cells express a mutant form of β-catenin that is insensitive to degradation by the β-catenin destruction complex. As a consequence, T cell factor (TCF)–dependent transcription is increased. Expression of β-catenin–specific siRNA inhibited TCF reporter activity (Fig. 2E). Note that reduction of β-catenin expression also inhibited FOXO-dependent signaling. Transcription induced by FOXO4 overexpression or by activation of endogenous FOXO in cells treated with the PI 3-kinase inhibitor LY294002 was reduced after expression of β-catenin–specific siRNA (Fig. 2E). These experiments show that β-catenin is required for FOXO activity.

In a yeast two-hybrid assay, β-catenin interacted with FOXO1 and FOXO3a (table S1). The interaction required armadillo repeats 1 to 8 of β-catenin and the C-terminal half of FOXO (starting at the DNA binding domain). Binding of FOXO to the armadillo repeats of β-catenin appears to be specific, as FOXO did not bind to the armadillo repeats of APC1 or APC2 proteins. When FOXO4 tagged with

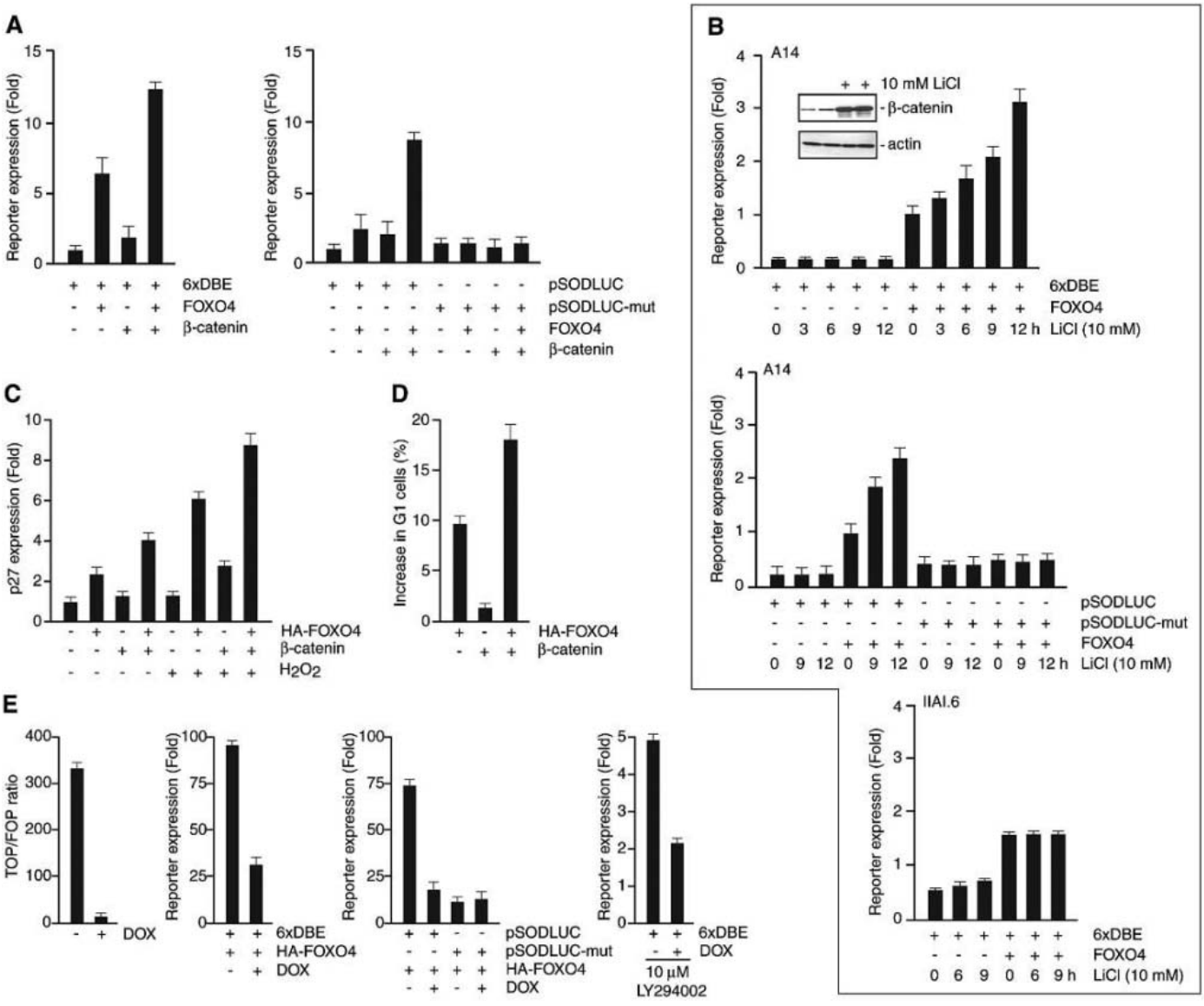

Fig. 2. Enhancement of FOXO transcriptional activity by β-catenin. FOXO activity was measured by using the reporter 6xDBE-luciferase, which contains six canonical FOXO-binding sites, or pSODLUC-3340, which contains the FOXO-binding sites of the SOD promoter. pSODLUC-3340 mutant, which has point mutations in the first and second FOXO-binding sites, was used as a control. Data are presented as means ± SD and represent three independent experiments performed in triplicate. (**A**) In IIAI.6 cells, which lack detectable β-catenin expression, coexpression of β-catenin enhanced FOXO transcriptional activity. (**B**) Stabilization of β-catenin by LiCl treatment enhanced FOXO transcriptional activity in A14 cells, but not in IIAI.6 cells. Inset shows LiCl-induced accumulation of β-catenin. (**C**) Cotransfection of β-catenin in A14 cells enhanced FOXO-induced p27Kip1 gene expression, as measured by quantitative polymerase chain reaction. Cells were treated for 16 hours with 100 μM H_2O_2 (+) or were left untreated (–). (**D**) Cotransfection of β-catenin in A14 cells enhanced the FOXO-induced arrest at G_1. (**E**) Induction of β-catenin–specific siRNA expression in LS174T cells reduced TCF and FOXO transcriptional activity. Cells were treated for 48 hours with doxycycline (DOX) to induce β-catenin siRNA expression. LY294002 treatment was for the last 16 hours. TCF reporter activity was measured by using TOP, which contains optimal TCF binding sites, and the negative control FOP.

hemagglutinin (HA) and β-catenin tagged with the Flag epitope were expressed in human embryonic kidney (HEK293T) cells, Flag–β-catenin could be coimmunoprecipitated with HA-FOXO4 and vice versa (Fig. 3A; fig. S1). In DLD-1 cells, which endogenously express β-catenin and FOXO3a, both proteins were immunoprecipitated together as well (Fig. 3B). Thus, β-catenin and FOXO physically interact in mammalian cells. This binding is likely to be direct, as the two proteins can interact in yeast. Coimmunoprecipitation experiments with BAR-1 tagged with vesicular stomatitis virus glycoprotein (VSV) and Flag–DAF-16 expressed in HEK293T cells showed a detectable interaction between BAR-1 and DAF-16 (Fig. 3C). DAF-16 did not interact with HMP-2 or WRM-1, two β-catenin–like proteins that function in adhesion and noncanonical Wnt signaling, respectively (Fig. 3D) (*9*, *13*). Thus, the interaction between β-catenin and FOXO appears to be evolutionarily conserved.

In *C. elegans*, as well as in mammalian cells, oxidative stress activates FOXO signaling by stimulating its relocation from the cytoplasm to the nucleus (*4*, *14*, *15*). We therefore investigated whether oxidative stress influences the binding between FOXO and β-catenin. Treatment of cells with 200 μM hydrogen peroxide resulted in enhanced binding between ectopically expressed β-catenin and FOXO4 (Fig. 3A), whereas treatment of cells with insulin, which reduces FOXO activity, did not affect the binding (*9*). A small increase in binding (about twofold) in response to oxidative stress was also observed between the endogenously expressed proteins in DLD-1 cells (Fig. 3B). The interaction between exogenous BAR-1 and DAF-16 expressed in HEK293T cells was increased in response to oxidative stress as well (Fig. 3C). We tested whether BAR-1 is required for oxidative stress–induced DAF-16 activity in *C. elegans*. One FOXO target gene that undergoes increased expression after oxidative stress is manganese superoxide dismutase (MnSOD) (*16*). We examined expression of the MnSOD homolog *sod-3* (*17*) in transgenic animals using a green fluorescent protein (GFP)–based reporter (*sod-3::gfp*). There was a strong increase in *sod-3* expression when animals were grown in the presence of 0.25 mM paraquat, a herbicide that induces the formation of reactive oxygen species (*18*) (Fig. 4A). This effect appeared to be DAF-16 dependent, as there was no increase in *sod-3* expression levels in *daf-16* mutants. The paraquat-induced expression of *sod-3* was also reduced in *bar-1* mutants, a defect that was rescued by overexpression of wild-type BAR-1 (Fig. 4B). This shows that BAR-1 is required for oxidative stress–induced DAF-16 signaling. Indeed, overexpression of BAR-1 (in a wild-type *bar-1* background) led to a modest, *daf-16*–

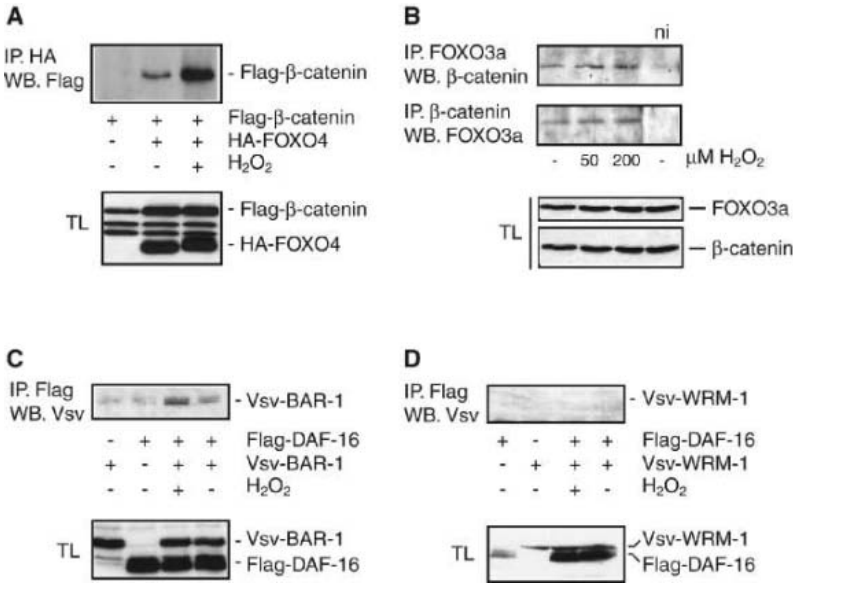

Fig. 3. Binding of β-catenin to FOXO transcription factors. (**A**) Coimmunoprecipitation between transfected Flag–β-catenin and HA-FOXO4 in HEK293T cells. The bottom panel shows expression of the transfected constructs (TL, total cell lysate). (**B**) Coimmunoprecipitation between endogenous β-catenin and FOXO3a in DLD1 human colon carcinoma cells. (**C**) Coimmunoprecipitation between transfected VSV–BAR-1 and Flag–DAF-16 in HEK293T cells. (**D**) VSV–WRM-1 and Flag–DAF-16 do not bind in HEK293T cells. In (A, C, and D), HEK293T cells were treated for 1 hour with 200 μM H_2O_2 (+) or were left untreated (–).

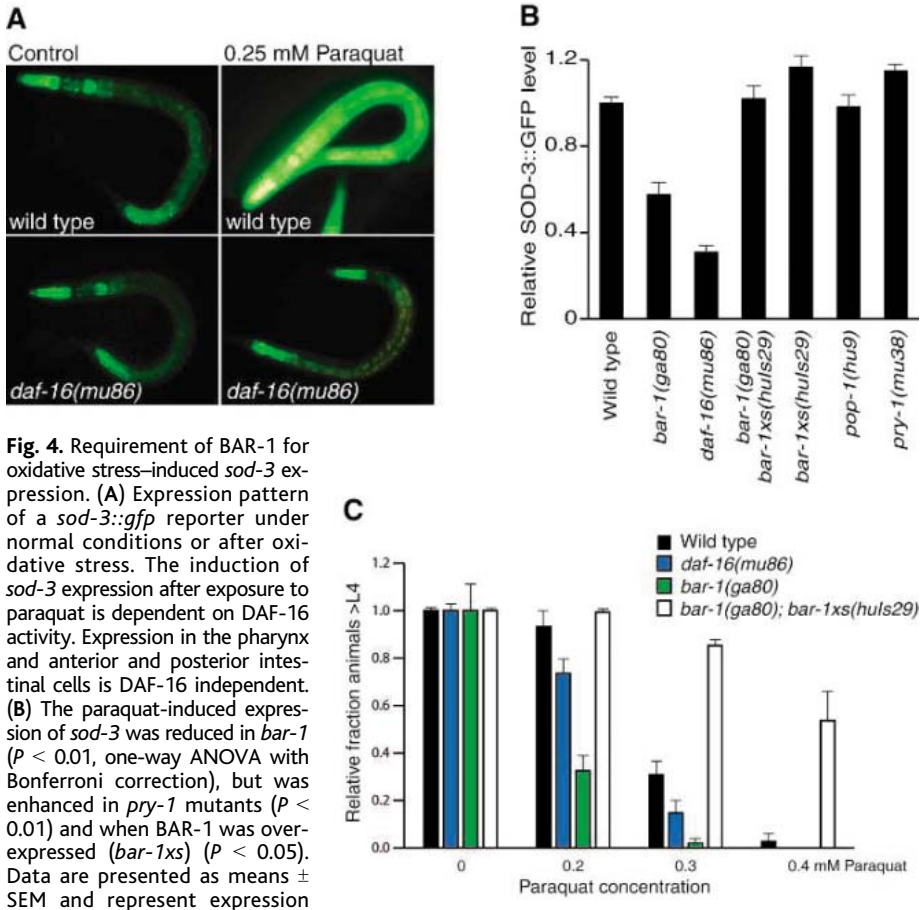

Fig. 4. Requirement of BAR-1 for oxidative stress–induced *sod-3* expression. (**A**) Expression pattern of a *sod-3::gfp* reporter under normal conditions or after oxidative stress. The induction of *sod-3* expression after exposure to paraquat is dependent on DAF-16 activity. Expression in the pharynx and anterior and posterior intestinal cells is DAF-16 independent. (**B**) The paraquat-induced expression of *sod-3* was reduced in *bar-1* ($P < 0.01$, one-way ANOVA with Bonferroni correction), but was enhanced in *pry-1* mutants ($P < 0.01$) and when BAR-1 was overexpressed (*bar-1xs*) ($P < 0.05$). Data are presented as means ± SEM and represent expression levels measured in >20 animals. (**C**) *bar-1* and *daf-16* mutants were more sensitive to paraquat-induced oxidative stress, whereas animals that overexpress BAR-1 were more resistant. The relative fraction of animals that have reached the L4 stage is indicated. Data are presented as means ± SD and represent the average of three independent experiments.

dependent increase in *sod-3* expression (Fig. 4B; fig. S2). A similar increase in *sod-3* expression was observed in the absence of PRY-1, a negative regulator of BAR-1 (*19*). To exclude the possibility that BAR-1 might affect *sod-3* expression through an interaction with the TCF homolog POP-1, we investigated *pop-1(hu9)*, which contains a mutation that specifically disrupts the function of POP-1 in canonical Wnt signaling (*19*), to find out whether it has an effect on paraquat–induced *sod-3* expression. There was no difference in *sod-3* expression between the wild type and *pop-1* mutants, demonstrating that this function of BAR-1 does not require TCF signaling. Because MnSOD is required for the detoxification of reactive oxygen species, we tested whether *bar-1* mutants were more sensitive to oxidative stress. *daf-16* and *bar-1* mutants were more sensitive to paraquat than wild-type animals (Fig. 4C). Furthermore, overexpression of BAR-1 resulted in resistance to oxidative stress. Taken together, these results show that BAR-1 is required for the DAF-16–mediated response to oxidative stress. This is consistent with our finding that the expression of the FOXO target gene, the gene for p27Kip1, is enhanced when β-catenin is overexpressed in the presence of oxidative stress (Fig. 2C).

Our results reveal an evolutionarily conserved function of β-catenin that is independent of TCF signaling. We have previously shown that FOXO transcription factors inhibit cell cycle progression (*11*, *20*), and here we show that this function is enhanced by β-catenin. In contrast, the β-catenin–TCF interaction stimulates cell cycle progression, and deregulated β-catenin–TCF signaling has a major role in the development of cancer. Thus, β-catenin appears to fulfill a critical function in balancing positive (through TCF) and negative (through FOXO) regulation of cell cycle progression. Different modes of signaling input, including insulin signaling and oxidative stress, may shift the balance between FOXO and TCF. In *C. elegans*, there is a strong correlation between DAF-16 function, the response to oxidative damage, and life span. Consistent with this, we find that loss of *bar-1* negatively affects both stress resistance and longevity. Given the known role of β-catenin in the development of cancer, our results suggest that a shift in β-catenin regulating FOXO and TCF signaling could link aging, the response to oxidative stress, and the development of certain types of cancer.

References and Notes

1. B. M. T. Burgering, G. J. Kops, *Trends Biochem. Sci.* **27**, 352 (2002).
2. H. A. Tissenbaum, L. Guarente, *Dev. Cell* **2**, 9 (2002).
3. D. M. Eisenmann, J. N. Maloof, J. S. Simske, C. Kenyon, S. K. Kim, *Development* **125**, 3667 (1998).
4. S. T. Henderson, T. E. Johnson, *Curr. Biol.* **11**, 1975 (2001).
5. R. Y. Lee, J. Hench, G. Ruvkun, *Curr. Biol.* **11**, 1950 (2001).
6. K. Lin, H. Hsin, N. Libina, C. Kenyon, *Nat. Genet.* **28**, 139 (2001).
7. V. Korinek, *Science* **275**, 1784 (1997).
8. M. van de Wetering *et al.*, *Cell* **88**, 789 (1997).
9. M. A. Essers, B. M. T. Burgering, unpublished data.
10. B. M. Burgering, P. J. Coffer, *Nature* **376**, 599 (1995).
11. R. H. Medema, G. J. Kops, J. L. Bos, B. M. Burgering, *Nature* **404**, 782 (2000).
12. M. van de Wetering, *EMBO Rep.* **4**, 609 (2003).
13. H. C. Korswagen, M. A. Herman, H. Clevers, *Nature* **406**, 527 (2000).
14. A. Brunet *et al.*, *Science* **303**, 2011 (2004).
15. M. A. Essers *et al.*, *EMBO J.* **23**, 4802 (2004).
16. G. J. Kops *et al.*, *Nature* **419**, 316 (2002).
17. Y. Honda, S. Honda, *FASEB J.* **13**, 1385 (1999).
18. N. Ishii *et al.*, *Mutat. Res.* **237**, 165 (1990).
19. H. C. Korswagen *et al.*, *Genes Dev.* **16**, 1291 (2002).
20. G. J. Kops *et al.*, *Mol. Cell. Biol.* **22**, 2025 (2002).

21. We thank H. Bos, H. Clevers, F. Zwartkruis, and R. Plasterk for critical reading of the manuscript; M. Alexander-Bridges, R. Medema, L. Tertoolen, M. van de Wetering, and D. Weinkove for advice and reagents; the *C. elegans* Genetics Center (University of Minnesota, Minneapolis) for strains; and the Dutch Cancer Foundation (M.A.G.E.) and the Center for Biomedical Genetics (H.C.K.) for financial support. Molecular interaction data have been deposited in the Bimolecular Interaction Network Database (BIND) with accession codes 258460 to 258463.

Supporting Online Material

www.sciencemag.org/cgi/content/full/308/5725/1181/DC1
Materials and Methods
Figs. S1 and S2
Table S1
References and Notes

23 December 2004; accepted 31 March 2005
10.1126/science.1109083

Small-Scale Cross-Flow Filtration System

The AKTAcrossflow is a fully automated small-scale cross-flow filtration system designed to simplify membrane selection and process development at the research scale. AKTAcrossflow links the chromatography and membrane filtration steps, eliminates the need to perform multiple manual operations during process development, and therefore increases workflow efficiency. It simulates large-scale conditions from cell separation to final concentration and diafiltration with no cell or protein disruptions. Designed to handle sample volumes from milliliters to liters, the system includes hardware, software, and membrane devices.

GE Healthcare For information 732-457-8149 www.gehealthcare.com

Free Mounting System

The Free Mounting System is an integrated solution for optimization of protein crystals in the collection of X-ray crystallographic data. Used in real-time conjunction with an X-ray diffractor system, a protein crystal is mounted in a cryo-loop at room temperature and positioned in the center of a stream of gas for which the humidity and temperature are precisely controlled and adjustable. With this system, it is possible to manipulate the crystal in different ways and simultaneously analyze diffraction behavior so as to optimize the crystal for the best possible diffraction resolution.

Rigaku/MSC and Proteros Biostructures For information 281-363-1033 www.RigakuMSC.com

Mass Spectrometer System

The HCTultra is a top-of-the-line high capacity trap (HCT) mass spectrometer (MS) system. The HCTultra provides outstanding ion trap performance in terms of sensitivity, speed, and mass accuracy, resulting in superb proteomics and metabolomics data quality, as well as enhanced information gain per unit of time in liquid chromatography/MS/MS applications in pharmaceutical, biotechnology, and academic research. Its high ion capacity and dynamic range make it suitable for quantitative proteomics, as well as for quantitative small molecule applications. The system's full-scan MS sensitivity is a major benefit for data-dependent experiments, enabling intelligent real-time decisions even on low-abundance precursor ions prior to ultra-sensitive MS/MS fragment analysis. The system increases the quality and information content of MS/MS through new smart precursor ion selection strategies. For example, for the analysis of post-translational modifications, the new PhosphoScan can detect phosphopeptides on-the-fly in a single run; in the same experiment the unique PeptideScan allows the selection of multiply charged precursor ions for information-rich MS/MS without time-consuming charge state determination precursor scans.

Bruker Daltonics For information 978-663-3660 www.bdal.com

X-Ray Detector

The Vantec-2000 is a high-performance two-dimensional X-ray detector based on patented MikroGap technology for demanding X-ray diffraction applications in advanced materials research. The Vantec-2000's proprietary MikroGap technology achieves an impressive 14 by 14 cm^2 active area, with spatial resolution of 70 μm and a dynamic range of 10^8. The instrument combines the advantages of gaseous detectors with those of solid-state detectors. With its real-time data display and true photon-counting capabilities, it is suitable for non-destructive nanotechnology investigations by X-ray diffraction. It improves data quality in applications such as small-angle X-ray scattering, thin film investigations, and micro X-ray diffraction analysis, for example in demanding applications in which the scattered X-ray signal is weak, a high dynamic range needs to be covered, and high resolution is critical.

Bruker AXS For information 800-234-XRAY www.bruker-axs.com

Rabbit Monoclonal Antibodies

Epitomics has developed a proprietary method for making monoclonal antibodies using rabbits. Rabbit monoclonal antibodies offer advantages including more diverse epitope recognition, improved response to less immunogenic antigens, and improved response to rodent proteins. Antibodies for key proteins involved in various cell signaling pathways, including apoptosis, cell cycle control, and cytokine signaling, and many phospho-specific proteins are available in 100-μl quantities.

Epitomics For information 877-772-2622 www.epitomics.com

Luminescent Label

Type 2 EviTag is a second-generation luminescent label. It features a proprietary natural coating that provides increased flexibility, easier use, and wider applications in biological assays and other types of life science research. EviTags are biologically inert, conjugation-ready fluorescent labels built around a base of the company's EviDot quantum dots, which are semiconductor nanocrystals coated with a variety of patented, water-stabilizing surface treatments appropriate for a range of applications. Type 1 EviTags feature robust and stable synthetic materials that help withstand the rigors of testing. Type 2 EviTags offer additional benefits because of their natural surface coating, brighter fluorescence and smaller size, which make them more suitable for fluorescent resonance energy transfer work, live animal or in vivo imaging, and molecular targeting.

Evident Technologies
For information 518-273-6266 www.evidenttech.com

Literature

Vector Laboratories 2005/2006 Catalog offers labeling and detection systems for nucleic acids, proteins, and carbohydrates, including the new ImmPRESS peroxidase polymer, biotin- and avidin-based reagents, lectins, mouse and rabbit monoclonal primary antibodies, immunohistochemical reagents and related products, and affinity gels and antibodies for isolating or detecting fusion proteins.

Vector Laboratories For information 650-697-3600 www.vectorlabs.com

Newly offered instrumentation, apparatus, and laboratory materials of interest to researchers in all disciplines in academic, industrial, and government organizations are featured in this space. Emphasis is given to purpose, chief characteristics, and availability of products and materials. Endorsement by *Science* or AAAS of any products or materials mentioned is not implied. Additional information may be obtained from the manufacturer or supplier by visiting www.science.labvelocity.com on the Web, where you can request that the information be sent to you by e-mail, fax, mail, or telephone.

ScienceCareers.org

Classified Advertising

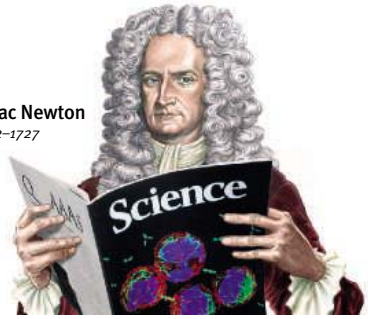

Isaac Newton
1642–1727

For full advertising details, go to **www.sciencecareers.org** and click on **How to Advertise,** or call one of our representatives.

United States & Canada

E-mail: advertise@sciencecareers.org
Fax: 202-289-6742

JILL DOWNING
(CT, DE, DC, FL, GA, MD, ME, MA, NH, NJ, NY, NC, PA, RI, SC, VT, VA)
Phone: 631-580-2445

KRISTINE VON ZEDLITZ
(AK, AZ, CA, CO, HI, ID, IA, KS, MT, NE, NV, NM, ND, OR, SD, TX, UT, WA, WY)
Phone: 415-956-2531

KATHLEEN CLARK
Employment: AR, IL, LA, MN, MO, OK, WI, Canada; Graduate Programs; Meetings & Announcements (U.S., Canada, Caribbean, Central and South America)
Phone: 510-271-8349

EMNET TESFAYE
(Display Ads: AL, IN, KY, MI, MS, OH, TN, WV; Line Ads)
Phone: 202-326-6740

BETH DWYER
(Internet Sales Manager)
Phone: 202-326-6534

Europe & International

E-mail: ads@science-int.co.uk
Fax: +44 (0) 1223-326-532

TRACY HOLMES
Phone: +44 (0) 1223-326-525

HELEN MORONEY
Phone: +44 (0) 1223-326-528

CHRISTINA HARRISON
Phone: +44 (0) 1223-326-510

JASON HANNAFORD
Phone: +81 (0) 52-789-1860

To subscribe to *Science*:
In U.S./Canada call 202-326-6417 or 1-800-731-4939
In the rest of the world call +44 (0) 1223-326-515

Science makes every effort to screen its ads for offensive and/or discriminatory language in accordance with U.S. and non-U.S. law. Since we are an international journal, you may see ads from non-U.S. countries that request applications from specific demographic groups. Since U.S. law does not apply to other countries we try to accommodate recruiting practices of other countries. However, we encourage our readers to alert us to any ads that they feel are discriminatory or offensive.

ScienceCareers.org
We know science AAAS

Immunology and Infectious Disease Careers

A *Science* Advertising Supplement

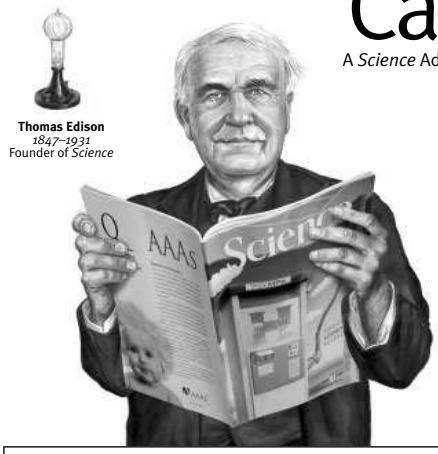

Thomas Edison
1847–1931
Founder of *Science*

Issue date 15 July
Reserve ad space by 28 June

Science's qualified circulation of 129,590[1] plus our pass-along readers brings total global weekly readership to over 710,000.[2]

1 *Science* June 2004 BPA Publisher's Statement. 2 *Science* June 2004 circulation as applied to 14 January 2000 Harvey Readership Survey and 2002 Harvey Cumulative Report, publisher's own data.

Don't forget — if you post your job online, it is also searchable on these websites:

- Biocompare
- National Postdoctoral Association (NPA)
- Stanford University School of Medicine
- *Science*'s Signal Transduction Knowledge Environment (STKE)
- *Science*'s Aging Knowledge Environment (SAGE)
- *Science*'s Next Wave

To advertise contact:

U.S. Daryl Anderson
Phone: (202) 326-6543
E-mail: advertise@sciencecareers.org

Europe and International
Tracy Holmes
Phone: +44 (0) 1223 326 500
E-mail: ads@science-int.co.uk

Japan Jason Hannaford
Phone: +81 (0) 52 789-1860
E-mail: jhannaford@sciencemag.jp

ScienceCareers.org
We know science AAAS

Biochemistry A SCIENTIFIC UMBRELLA

THE EMERGENCE OF GENOMICS AND PROTEOMICS HAS PUT FRESH EMPHASIS ON BIOCHEMISTRY, THE FIELD THAT INCORPORATES THOSE SUBDISCIPLINES. TO GAIN SUCCESS IN THEIR BURGEONING ARENA, BIOCHEMISTS NEED BOTH A BROAD UNDERSTANDING OF SCIENCE AND A GRASP OF SUCH NONSCIENTIFIC SKILLS AS COLLEGIALITY AND COMMUNICATIONS. BY PETER GWYNNE

- **Ambion, Inc.** http://www.ambion.com
- **United States Food and Drug Administration** http://www.fda.gov
- **Wake Forest University School of Medicine** http://www.wfubmc.edu

Bringing together key aspects of biology and chemistry, biochemistry lies at the center of modern research in life science. The field has expanded significantly in recent years with the emergence of such pursuits as genomics and proteomics. But the discipline's ability to integrate chemical and biological principles in the effort to understand the nature and function of cells remains unchanged. There is one difference: Modern biochemists must work hard to understand the fresh advances enabled by those two subfields and to apply them to fundamental understanding.

What do employers and academic supervisors expect of biochemists today? In this survey, representatives of academic, governmental, and industrial organizations outline their specific needs. They have two common themes: Scientifically, applicants for jobs and high-level training in biochemistry need a good publication record. And beyond the lab, would-be professionals in biochemistry must show a mastery of communication skills, both oral and written.

Toby Hardister

LESLIE POOLE

The Action End

How does biochemistry differ from emerging fields such as genomics and proteomics? "I think of genomics and proteomics as descriptive disciplines, but they don't tell you much about how things happen; they identify possible correlations," says Emily Shacter, chief of the division of therapeutic proteins in the U.S. Food and Drug Administration's (FDA's) Center for Drug Evaluation and Research. "Biochemistry looks at the action end of our medicine and biology and our cells. It involves deciding which of a list of, say, 50 proteins make a difference in the clinical situations that we look at." Leslie Poole, associate professor of biochemistry at Wake Forest University School of Medicine, takes a similar view. "I see biochemistry as the umbrella," she explains. "In my opinion, both genomics and proteomics are biochemistry. But if you relied on just those two pieces, you would leave a lot of biochemical questions unanswered." Matthew Winkler, CEO and chief scientific officer of RNA company Ambion, defines the field more pithily. "A biochemist," he asserts, "understands the subtleties of how a cell functions."

Those definitions don't imply that new subdisciplines don't have much impact on biochemistry. The field has gained significant benefit from them. "The importance of biochemistry decreased in the 1980s and 1990s," Winkler says. "But it's now enjoying something of a renaissance. People are taking a renewed interest in the tools of biochemistry to get a more fundamental understanding of what's happening."

Certainly the new subdisciplines have helped to make life somewhat easier for traditional biochemists. "The major point is that we don't spend as much time having to sequence genes and proteins ourselves," Poole points out. "The information is already out there in the databases. One still has to carry out biochemical functional characterizations on representative genes and proteins, but not all of them." The pursuits have also helped to expand the reach of traditional biochemistry. "Genomics has given us another avenue to identify disease targets," Shacter says. "It has also given us information on the spectrum of proteins we should be looking at. Mostly it's about helping us to keep our eye on the ball of disease targets."

Wide Range of Activities

For Shacter's group at the FDA, that effort covers a wide range of activities. "We regulate biotechnology products. We look at proteins to be used for therapeutics; we need to understand their action and bio-

Biochemistry

A SCIENTIFIC UMBRELLA


EMILY SHACTER

chemistry so that we can identify and predict safety concerns," she explains. As an example she notes that, because proteins are multifunctional, biochemists need to look into possible unintended consequences when they are used for therapeutic purposes. "You have to be able to characterize the protein to know what it is and what changes its activity and pharmacokinetics," Shacter continues. "We need to understand the relationship between the structure of the protein and how it works. We also need to be able to understand manufacturing processes and their impact."

Biochemists at Ambion focus more on the research laboratory. "A large amount of our work is centered around developing new assays and making existing assays more robust," Winkler explains. "In a sense, that facilitates the research of our academic and industrial colleagues. Biochemistry is one of the major disciplines underlying the work we do. Anyone developing assays should have a biochemistry background."

The 27 faculty members in Wake Forest Medical School's biochemistry department carry out research in a range of topics, including structural biology, cancer, the genetic and molecular bases of disease, and cell signaling. Poole, whose own research focuses on antioxidant enzyme systems, flavoprotein structure-function relationships, and redox-active cysteinyl centers, points out that the department continually seeks to expand its research interests. "Just over three years ago I was in charge of a search committee for an X-ray crystallographic initiative," she recalls. "We had outstanding candidates and hired our top two choices. So now we have a very strong crystallography group."

That success came as no surprise. "We've been very successful in our recruitment of faculty," Poole says. "We offer a very supportive environment. And we have very low attrition." Attracting graduate students has proven more elusive. "We're always looking for high quality postdocs and Ph.D. students, but also recognize that we're in a very competitive environment for attracting applicants to Ph.D. programs," Poole says.

Strict Requirements

Poole's department has strict requirements for Ph.D. and postdoc applicants. "Research experience is not absolutely essential but it is an important factor; it shows that the candidates know what they're getting into," Poole says. "And we weigh letters of reference pretty heavily. In addition to their academic qualifications, we make an effort to assess the motivational level of the applicants as well. That is the deciding feature that determines whether or not they'll be successful in our program."

At the FDA's Center for Drug Evaluation and Research, Shacter says, "We need some more protein chemists on board to study structure-function relationships. The Center also has occasional vacancies for scientists outside the laboratory, managing files for regulatory submissions for therapeutic protein projects and working as consumer safety officers. "It's helpful if they understand biochemistry," Shacter continues, "although often a Master's degree is sufficient."

Ambion also hires scientists with various types of training for its biochemical work. "We worry less about disciplines and more about how good a scientist a candidate is," Winkler says. "We advertise for senior scientists who have Ph.D.s and several years of postdoctoral experience, whom we expect to function as independent investigators. We also hire at the more junior levels for various research positions."

The company seeks self-starters. "We want what we call 'strong senior scientists' who are entrepreneurial and visionary," Winkler says. As an example, he notes the company's early involvement with RNA interference, a subdiscipline that has blossomed in the past three years. "Our scientists had the vision to jump into it before management told them," he recalls.

Characteristics that aren't specifically associated with scientific training, such as collegiality and communications skills, play important roles in all selection decisions. "For our regulatory work in particular we have to work as a team. A group makes the decision as to whether clinical trials will go forward," Shacter explains. "We have to be able to communicate with our team members and with biotechnology companies. In addition, FDA people have to be able to multitask. They have to have a strong interest in public health, by looking at molecules in relation to medicine. And we need creative thinkers and scientists who will take the initiative. At the ground level we're looking for potential."


MATTHEW WINKLER

Early Development

Biochemists need to develop those general abilities early in their training. "Oral and written communications skills are arguably some of the most important things we look for in applications for our Ph.D. program and postdoctoral fellowships," Poole says.

Would-be postdocs and faculty applicants need one more item on their CVs. "We look for a strong publication record," Poole continues. "We look at the quality of the journals in which the publications have appeared." Winkler echoes that point. "The single most beneficial thing our applicants can do is demonstrate their productivity by publishing good papers in which they are the first or second authors," he says. "That assures us that, when they get here, they'll have the confidence to develop new technologies."

Shacter strikes a similar theme. "We look for people who have demonstrated both accomplishment and motivation," she says. "Motivation is really one of the most important criteria. The more biochemists can demonstrate that to us, the better."

A former science editor of Newsweek, *Peter Gwynne (pgwynne767@aol.com) covers science and technology from his base on Cape Cod, Massachusetts, U.S.A.*

Join us in Juncos, Puerto Rico, at our state-of-the-art biotechnology facilities for fill & finish/bulk manufacturing. For more than a decade, Amgen has achieved an outstanding quality and compliance record, as well as standard-setting manufacturing processes. And we are investing $1.2 billion to grow to 1 million square feet. The new site will include manufacturing for key biologics, expanded full-testing quality and analytical labs, additional syringe fill and freeze-drying capability, and warehouses. There will also be process development facilities, administrative and training buildings, and such amenities as a cafeteria, child care center and an excellent on-site gym. And with Puerto Rico's gorgeous beaches, exciting night life, golf courses, and restaurants, we promise you the bio-adventure of your life. • As an EEO/AA employer, Amgen values a diverse combination of perspectives and cultures. M/F/D/V.

SOME OF THE OPPORTUNITIES WE ARE HIRING FOR IN PUERTO RICO INCLUDE:

Quality
Manager of Regulatory Compliance (Job# amge-00008938)
Supplier Quality Management - Manager QA (Job# amge-00009828)
Molecular/Cell Biology/Electrophoresis - QAL Associate III (Job# amge-00009543)
Microbiology - QAL Associate III (Job# amge-00010412)
Sample Management – Supervisor QAL (Job# amge-00010298)

Process Development
Analytical Sciences - Glycoprotein
Associate Director (Job# amge-00009563)
Scientist (Job# amge-00009714)

Cell Sciences & Purification
Scientist (Job# amge-00008675)
Scientist (Job# amge-00008677)

Process Engineering
Engineer III (Job# amge-00008680)
Engineer III (Job# amge-00009493)

Amgen also has opportunities available in **Manufacturing, Operations** and **Engineering**. Please visit our website at www.amgen.com/careers for more details.

AMGEN®

Dramatically Improving People's Lives

www.amgen.com/careers

★ Juncos, PR, Amgen's fill & finish / bulk manufacturing location

CAREERS IN BIOCHEMISTRY

POSITIONS OPEN

dkfz.

Deutsches Krebsforschungszentrum
Stiftung des öffentlichen Rechts
in der Helmholtz-Gemeinschaft

Universität Heidelberg

Am Deutschen Krebsforschungszentrum (DKFZ) ist gemeinsam mit der Medizinischen Fakultät der Universität Heidelberg eine

Professur (W3)

für

Epigenetik

zu besetzen. Mit dieser Stelle ist die Leitung einer Abteilung am DKFZ verbunden.

Bewerber sollten international herausragende Forschungsleistungen auf dem Gebiet der epigenetischen Genregulation erbracht haben. Erwartet wird die Fähigkeit, auf der Basis epigenetischer Grundlagen neue Konzepte für die Krebsdiagnostik und -therapie zu entwickeln und in Kooperation mit der Klinik umzusetzen. Darüber hinaus müssen erfolgreiche Bewerber in der Lage sein, kompetitive Drittmittel-finanzierte Forschungsprogramme zu etablieren.

Die Stelle steht unbefristet zur Verfügung. Bei der ersten Berufung in ein Professorenamt ist das Dienstverhältnis gemäß § 67 Abs. I UG grundsätzlich zu befristen. Ausnahmen sind insbesondere möglich, wenn Bewerberinnen/Bewerber aus dem Ausland oder aus dem Bereich außerhalb der Hochschulen sonst nicht gewonnen werden können. Soll das Dienstverhältnis nach Fristablauf fortgesetzt werden, bedarf es nicht der erneuten Durchführung eines Berufungsverfahrens.

Das Deutsche Krebsforschungszentrum und die Universität Heidelberg streben eine Erhöhung des Anteils der Frauen am wissenschaftlichen Personal an und fordern qualifizierte Frauen nachdrücklich auf, sich zu bewerben. Schwerbehinderte werden bei gleicher Qualifikation bevorzugt eingestellt.

Bitte richten Sie Ihre Bewerbung bis spätestens 20.06.2005 an Herrn Prof. Dr. O. D. Wiestler, Wissenschaftlicher Stiftungsvorstand des Deutschen Krebsforschungszentrums, Im Neuenheimer Feld 280, 69120 Heidelberg und Herrn Prof. Dr. C. R. Bartram, Dekan der Medizinischen Fakultät Heidelberg, Im Neuenheimer Feld 346, 69120 Heidelberg. Ihre Bewerbungsunterlagen sollen den Kriterien entsprechen, welche Sie unter http://med.uni-hd.de/berufungen_hinweise_bewerber.html einsehen können.

Positions @ NIH
THE NATIONAL INSTITUTES OF HEALTH

Scientific Projects Director
Scientific Projects Manager
(2 positions)

The Office of the Director of the National Cancer Institute (NCI), National Institutes of Health (NIH), Department of Health and Human Services (DHHS) invites applications for a Scientific Projects Director, GS-601-15 and a Scientific Projects Manager, GS-601-14 in the Office of Cancer Genomics. These are key positions responsible for providing leadership, management, and oversight of a wide range of projects associated with the activities of the office. NCI has developed a number of genomics based initiatives such as the Cancer Genome Anatomy Project and the trans-NIH Mammalian Gene Collection. NCI is continuing to use genomics to identify and catalog mutations that are found in various cancer types and subtypes by initiating a pilot project together with the Human Genome Institute (NHGRI). The program will integrate with new NCI technology infrastructure programs in cancer bioinformatics, clinical databases and genomics. Please visit the OCG website at htpp://www3.cancer.gov/ocg/ for further information about our programs. The individuals selected for the positions will possess an M.D. or Ph.D. degree with independent research experience and some administrative training. Publication and public presentation record is a strong asset. In addition, the individuals will have knowledge and experience in the fields of cancer biology and genomics. Salary is commensurate with research experience and accomplishments, and a full Civil Service package of benefits (including retirement, health, life and long-term care insurance, Thrift Savings Plan participation, etc.) is available. Relocation expenses may be paid.

The NCI vacancy announcements for these positions contain complete application procedures and list all mandatory information which you must submit with your application. Both announcements will be available on **May 17, 2005.** To obtain the vacancy announcement for the Scientific Projects Director, GS-601-15, see announcement number NCI-05-69139; and, for the Scientific Projects Manager, GS-601-14, see announcement number NCI-05-69134. You may visit the NIH Career website at: **http://careerhere.nih.gov OR you can have it faxed to you by calling 1-800-728-JOBS (for local calls, 301-594-2953). Applications must be received by June 17, 2005.**

Cognitive Neuroscience and Brain Imaging Postdoctoral Fellow

The National Institute on Drug Abuse (NIDA), Intramural Research Program (IRP), a major research component of the National Institutes of Health (NIH), Department of Health and Human Services (DHHS), is recruiting for individuals interested in joining an interdisciplinary team of scientists studying the cognitive and affective processes underlying human drug abuse and their alterations during addiction and withdrawal. fMRI is used to study the sites and mechanisms of action of nicotine, cocaine, marijuana and other abused drugs; their effects on cognitive (e.g. attention, working memory, central executive processes, reward, decision making, learning) and affective processes (e.g., mechanisms and consequences of craving and interactions with emotional processes); and how their (dys) function(s) may be a factor in human drug addiction.

A Ph.D. and/or M.D. and background in cognitive neuroscience, drug abuse pharmacology and/or functional imaging is desirable. A 3 Tesla MRI scanner is available for full-time research. Candidates must be U.S. citizens or permanent resident. Send a CV with bibliography, a statement of research background and interests, and a copy of doctoral degree to: **Elliot A. Stein, Ph.D., Chief, Neuroimaging Research Branch, IRP/NIDA, 5500 Nathan Shock Drive, Building C, Room 381, Baltimore, MD 21224. Email: estein@intra.nida.nih.gov.** Applications from women and minorities are encouraged.

Center for Cancer Research
Chief, Medical Oncology Branch

The National Cancer Institute (NCI) is seeking an outstanding physician scientist to serve as Chief of the newly formed Medical Oncology Branch. The Chief of Medical Oncology will oversee medical oncology efforts across the Center for Cancer Research (CCR), NCI; will be responsible for establishing priorities for clinical studies in Medical Oncology; will oversee a large group of investigators dedicated to novel investigator-initiated molecular targets research; and will be responsible for developing and implementing a strong identity for medical oncology within the intramural research program of the NCI.. The Chief of the Medical Oncology Branch will also oversee a large clinical infrastructure which provides all intramural investigators interested in bringing discoveries to clinical trials and the infrastructure for performing such work. The Chief must excel at fostering collaboration between basic researchers and clinical investigators and facilitating the development and execution of translational research. The Chief will report directly to the Scientific Director for Clinical Sciences.

The CCR is the largest component of the intramural biomedical research effort at NIH and a major user of the NIH Clinical Center, which in April 2005 opened its new state-of-the-art hospital. The CCR has major ongoing efforts in molecular targets development that allow for discovery and clinical application of novel inhibitors and bioprobes. Preclinical models development is another area of major activity. The Molecular Oncology Center consists of major initiatives in clinical proteomics and genomics, advanced tumor imaging, molecular diagnosis, and interfaces directly with the medical oncology clinical infrastructure that is led by the Chief of Medical Oncology.

The CCR provides an environment in which interdisciplinary and multidisciplinary translational research is encouraged and supported and uses a disease-based, translational research matrix to identify the intersection of research areas and particular cancers to identify programmatic efforts. These specific program areas will enhance and enable collaborations, interdisciplinary and multidisciplinary research, and a dynamic translational research process in which discovery, development, and delivery flow seamlessly.

The successful candidate must have an M.D. degree, be board certified in medical oncology, have an established record in the development of targeted agents and delivery into clinical trials, and have an in-depth knowledge of, and interest in, the application of genomics, proteomics, imaging, and molecular diagnostics in the clinical setting. Salary is commensurate with experience. All applicants should submit a letter indicating interest in the position; a statement of research interests; a career synopsis and brief bibliography; current curriculum vitae and complete bibliography; and the names and addresses of five references. **Applications should be sent to: Steven Rosenberg, M.D., Ph.D., c/o Julie Cummings, 31 Center Drive, Suite 3A19, Bethesda, Maryland 20892.**

WWW.NIH.GOV

National Institutes of Health

Virtual Career Center

at the tip of your mouse

www.training.nih.gov/careers

-EXPLORE CAREER OPTIONS
-CONTINUE YOUR EDUCATION
-SEARCH FOR A JOB

Careers in science, medicine, and beyond at the college, postbaccalaureate, graduate, and postdoctoral levels

Office of Intramural Training and Education
(800) 445-8283

Hire the World's Best Scientists

Advertise your positions to the more than 3800 doctoral scientists and clinicians who are in training at the National Institutes of Health

Reach scientists who are at the forefront of their fields

Access a population large enough to guarantee interest in your position

Post new positions with a click of your mouse

Visit the NIH Virtual Job Fair @ www.training.nih.gov/careers

Office of Intramural Training and Education

University of California Riverside

Glial⇔Neuronal Interaction Position (open search)

The Department of Cell Biology and Neuroscience (**http://cbns.ucr.edu**) at the University of California, Riverside, is strengthening its faculty in the area of glial-neuronal interactions, and plans hiring a cluster of several new faculty with primary research interests in this area over the next two years. A new laboratory building, the Biological Sciences Building now under construction, will be available in early/mid 2006 to house these new faculty as well as most of those in the current department. In this initial search for one position, we are inviting applicants at all ranks from assistant professor to professor who have primary research interests in interactions between glia and neurons. It is expected that this hire would become an integral member of the Center for Glial⇔Neuronal Interactions at UC Riverside, and participate in the ongoing Health Sciences initiative (including stem cell initiatives) on the campus. Additionally, this person could further strengthen our links with the Center for Nanoscale Science and Engineering. Opportunities for graduate student training are available through participation in several interdepartmental graduate programs, including the Neuroscience Program (**http://neuro.ucr.edu/**) and the Cellular, Molecular and Developmental Biology Program (**http://www.cell.ucr.edu/**). Other teaching responsibilities would be at the undergraduate level.

Send applications, including Curriculum Vitae and complete contact information for at least three references to: **Chair, GNI Search Committee, Department of Cell Biology and Neuroscience at the University of California, Riverside, CA 92521 USA**. Review of applications will begin **July 1, 2005** and will continue until the position is filled.

The University of California is an Equal Opportunity/ Affirmative Action Employer.

NORTHWESTERN UNIVERSITY

CHAIR

DEPARTMENT OF MICROBIOLOGY-IMMUNOLOGY THE FEINBERG SCHOOL OF MEDICINE

Northwestern University's Feinberg School of Medicine in Chicago is searching for a new Chair to lead a major expansion of its Microbiology-Immunology Department. The Department presently has 19 primary research faculty members with active programs in Molecular Virology, Immunology, or Microbial Pathogenesis (**http://bugs.mimnet.northwestern.edu/labs/**). The new department chair should have an MD, PhD or combined MD/PhD degree and is expected to have exceptional leadership skills as well as an outstanding, internationally recognized and well-funded research program. The Chair will have the opportunity to build upon a strong base and expand the department in new directions. The Chair will also be responsible for promoting the research programs and teaching efforts of the departmental faculty as well as fostering school-wide programs in related areas. The position is full-time with salary and starting date negotiable.

Interested candidates should submit a letter of intent, curriculum vitae, and contact information for at least three references to: **Prof. Gary Borisy, PhD, Chair of the Microbiology/ Immunology Search Committee, c/o Sheri Carney, Recruitment Coordinator, 303 E. Chicago Avenue, 4-161 CHW125, Chicago, IL 60611**. Electronic applications (Word file or PDF) are preferred and should be sent to **microsearch@northwestern.edu**. To ensure consideration, applications should be received by **August 1, 2005**.

Northwestern University is an Affirmative Action/Equal Opportunity Employer. Hiring is contingent upon eligibility to work in the United States. Women and minorities are encouraged to apply.

TEXAS AGRICULTURAL EXPERIMENT STATION

Associate Vice Chancellor and Deputy Director

The Associate Vice Chancellor and Deputy Director provides state-wide management and oversight of the Texas Agricultural Experiment Station (TAES) and all associated research activities. The individual serves as the Chief Operating Officer and provides leadership in the development of programmatic goals and objectives, in coordination of Experiment Station resources to ensure research excellence and fiscal accountability, and in promoting research outcomes and values to all stakeholders. In a leadership capacity, the Associate Vice Chancellor and Deputy Director will ensure growth in the stature and financial support for discovery and translational research necessary for improving the welfare of Texans and in providing economic and environmental benefits to the agriculture, urban, and natural resource sectors of the state. The Associate Vice Chancellor and Deputy Director is a member of the Vice-Chancellor's cabinet in developing and advancing the goals and objectives of the Agriculture Program.

We encourage applications from accomplished and notable scientists appreciative of discovery and translational research, and who possess a doctoral degree in the life sciences, agriculture or related fields of science or engineering. Experiences should include competence in appropriation, budgeting and human resources procedures relevant to academic institutions and government agencies; and demonstrated ability to work with diverse audiences and constituencies in support of the goals of the Texas Agricultural Experiment Station.

Salary will be competitive and commensurate with experience and qualifications. This position is headquartered in College Station, Texas, on the campus of Texas A&M University. College Station is also the headquarters for the Agriculture Program and The Texas A&M University System.

Applications and nominations will be accepted until June 15, 2005 or until a suitable applicant is identified. Candidates should submit a letter of intent, resume, and the names, physical and email addresses, and telephone numbers of five references electronically to **Dr. Kevin M. Heinz, Search Advisory Committee Chair**, at **KMHeinz@tamu.edu** or mail to: **Chair, Search Advisory Committee, Kevin M. Heinz, Professor and Head, Department of Entomology, Minnie Belle Heep Bldg., Room 412, 2475 TAMU, College Station, TX 77843-2475**

For additional information regarding this position, please contact Dr. Kevin Heinz at **KMHeinz@tamu.edu** or 979-845-2510, and see **http://TAESDeputyDirector.tamu.edu.**

The Agriculture Program is an equal opportunity employer

SCOTT & WHITE

College of Medicine
The Texas A&M University System Health Science Center

Pediatric Hematology-Oncologist

The Section of Pediatric Hematology/Oncology at **Scott and White Clinic** and the **Texas A&M University System Health Science Center College of Medicine** (TAMUS HSC-COM) are seeking a clinician scientist with current research grants for a faculty position in a rapidly growing program. The candidate should be BE/BC in pediatric oncology and committed to an academic career. The successful candidates will join and enhance ongoing efforts in basic and translational research, with an institutional commitment to building a world-class experimental therapeutics program. An outstanding start-up package includes high quality laboratory space, excellent benefits and competitive salaries commensurate with academic qualifications. The position guarantees 75% protected time for research activities.

Scott & White Clinic is a 500+ physician directed multi-specialty group practice that is the leading provider of cancer care in Central Texas. Scott and White Clinic and the 486 bed tertiary Scott & White Memorial Hospital is the main clinical teaching facility for TAMUS HSC-COM. Outstanding clinical practice and laboratory facilities on campus that perform state of the art molecular and cellular biology research, flow cytometry, genomics and biostatistics are in place to support the research effort.

Please contact: **Don Wilson, M.D. Professor and Chairman, Department of Pediatrics, Scott & White, 2401 S. 31st, Temple, TX 76508. (800)725-3627 dwilson@swmail.sw.org Fax (254) 724-4974.**

For more information about Scott & White, please visit www.sw.org For Texas A&M www.tamhsc.edu. Scott & White is an equal opportunity employer.

Health Research in a Changing World

Fighting Diseases and Improving Lives

ScienceCareers.org

DIRECTOR, DIVISION OF INTRAMURAL RESEARCH
National Institute of Allergy & Infectious Diseases
National Institutes of Health
Department of Health & Human Services

The National Institute of Allergy & Infectious Diseases (NIAID) is seeking a Director for the Division of Intramural Research (DIR).

The DIR conducts basic and clinical research in immunology, allergy, virology, parasitology, bacteriology, including emerging infections and pathogens that may involve biodefense efforts and includes clinical and translational research such as development of vaccines and therapeutics for immunologic and infectious diseases. In addition to conducting research, the DIR also provides many laboratory and clinical research training opportunities.

The DIR is comprised of approximately 1300 scientific and administrative staff. More than 120 investigators lead the research in laboratories located in Bethesda, Rockville and Frederick, Maryland as well as in Hamilton, Montana.

The Director, DIR, reports to the Director, NIAID and provides overall executive direction and scientific leadership for the DIR. Specifically, develops, directs and coordinates research programs; manages resource allocations to include staff, physical and financial resources; maintains staff through recruitment and training efforts and ensures effective day-to-day program operations. In addition, the successful candidate will serve as an advisor to the Director, NIAID on scientific affairs involving DIR research programs. Also, will serve as Executive Secretary of the NIAID Board of Scientific Counselors and represent NIAID on the NIH Board of Scientific Directors and on other NIAID and NIH committees and boards as assigned. Preference will be given to accomplished scientists with expertise in areas consistent with the mission of the NIAID and with a documented record as a senior scientific administrator.

APPLICATION PROCESS: Applicants must be U.S. citizens or permanent residents. Salary commensurate with experience. Curriculum vitae & bibliography to: Ms. Lisa Poindexter-Steed, Office of Administrative Management & Operations, NIAID, Building 31, Room 7A18; 31 Center Drive, MSC 2520, Bethesda, Maryland, 20892-2520 and reference announcement number **SDDIR-05-01**. The application review process will begin **June 30, 2005**. Direct inquiries to: Ms. Poindexter-Steed via email: lsteed@niaid.nih.gov or at 301-594-3964. Further information on this position is available on our website at http://healthresearch.niaid.nih.gov Information about the Division of Intramural Research is available at www.niaid.nih.gov/dir/. All information provided by applicants will remain confidential and will only be reviewed by authorized officials of the NIAID.

DHHS and NIH are Equal Opportunity Employers

Department of Health and Human Services
National Institutes of Health
National Institute of Allergy and Infectious Diseases
Proud to be Equal Opportunity Employers

University of California Office of the President

Director, Research Compliance

The Office of Research, located at the University of California Office of the President, invites applications and nominations for the position of Director, Research Compliance. Serving the ten campuses and three national laboratories, the Director will implement the strategic plan for systemwide research compliance and will serve as the primary point of contact on research compliance issues.

SUMMARY OF RESPONSIBILITIES: Coordinate the creation of compliance standards, policies, procedures, communication and training programs to assist the university with its research compliance efforts. Serve as an information resource on pending regulatory issues and changes. Work with campus representatives to ensure mechanisms are in place to enforce research compliance standards. Establish and convene a systemwide compliance committee whose charge includes reviewing current research compliance standards, practices, and education and training materials. Work with the Research Compliance Oversight Committee consisting of the senior management of the University of California.

QUALIFICATIONS: The applicant must have knowledge of current federal and state laws and regulations relating to the conduct of research. Extensive experience in regulatory and statutory interpretation. Experience and understanding of research compliance in an academic research environment. Must possess the ability to draft clear, concise and logical reports, correspondence, and summaries. Work as a leader in a collaborative environment. Ability to work independently and as a team member maintaining cooperative working relationships with others. Experience developing training resources appropriate to target audiences. Education equivalent to a B.A./B.S. and an advanced degree in an area relevant to research regulatory compliance, and at least 6 years of professional experience with state and federal regulatory compliance in an academic research environment, or an equivalent combination of education and experience.

TO APPLY: For a complete job description or to apply for this position, please visit the University of California Office of the President employment website at http://jobs.ucop.edu and reference Job Number 2318-05. The closing date for this position is June 2, 2005. EEO/AA

UK UNIVERSITY OF KENTUCKY

Department of Internal Medicine

Chief of the Division of Endocrinology & Chief of the Division of Infectious Diseases

The Department of Internal Medicine at the University of Kentucky is seeking candidates for the positions of Chief of the Division of Endocrinology and Chief of the Division of Infectious Diseases. The tenure or tenure track positions will be at the rank of Associate Professor or Full Professor. As part of the healthcare enterprise, individuals will oversee and may participate in teaching, clinical activities and research within the University of Kentucky Chandler Medical Center. Both Divisions are financially viable and have major growth potential under the appropriate leadership. Successful applicants will be board certified in Internal Medicine and specialty.

Interested individuals should send a CV and names of three references to:

Frederick C. de Beer, M.D.
Chairman, Department of Internal Medicine
University of Kentucky, College of Medicine
740 S. Limestone Street, J524 Kentucky Clinic
Lexington, KY 40536-0284
Email: fcdebe1@uky.edu

Electronic submission of CVs and references is encouraged.

The University of Kentucky is an equal opportunity employer and encourages applications from minorities and women.

www.uky.edu

NRDC
THE EARTH'S BEST DEFENSE

Science Center

The Natural Resources Defense Council (NRDC), a leading environmental advocacy organization, announces the establishment of its new Science Center, an expansion of the organization designed to increase the role of technical information and scientific principles in environmental and public health decision-making. There are three immediate openings:

Deputy Director: A permanent position in Washington, D.C. to provide technical capacity in one area of scientific expertise, manage technical resource needs across the organization, interact frequently with the scientific community, and supervise a group of rotating Science Fellows. Candidates must have a Ph.D. or equivalent in a relevant field and 5+ years of experience applying technical information to policy decision-making.

Conservation Genetics Fellow: A two-year, full-time fellowship in Washington, D.C. to work on genetic analysis and conservation of rare/endangered plants/animals and determine the proper role of genetic studies in conservation matters. **Requirements:** Ph.D. in conservation/evolutionary genetics; excellent scientific/technical background; strong interest in applying science to policy decision-making.

Ocean Protection Fellow: A two-year, full-time, fellowship in NYC or San Francisco to work on ecosystem-based management for ocean protection. **Requirements:** Ph.D. or equivalent in marine ecology; excellent scientific/technical background; strong interest in applying science to policy decision-making.

We offer salary commensurate with experience, an excellent benefits package, and a pleasant, fast-paced work environment. Please email resume, writing sample, and letter of interest indicating qualifications and what issues most interest the candidate to **hr_dc@nrdc.org**. If necessary, mail materials to: **Monique Waples, NRDC, 1200 New York Ave, NW, Ste 400, Washington, DC 20005**. Fellows should indicate the desired effects of fellowship on their career in the letter of interest. Deadline: **June 15, 2005**.

To learn more about NRDC, visit **www.nrdc.org**.

EOE

Clinical Cytogeneticist

The Department of Hematopathology at **The University of Texas M. D. Anderson Cancer Center** is seeking a candidate for the position of Clinical Cytogeneticist for the Clinical Cytogenetics Laboratory. Candidates must possess a Ph.D. and/or M.D. degree and must be board-eligible/certified by the ABMG in Clinical Cytogenetics.

The successful applicant will have a strong commitment to diagnostic cancer cytogenetics and clinical research. Primary responsibilities will include review of cytogenetic cases and reports, and development and monitoring of test protocols. Opportunities for clinical research within the department and throughout the institution are numerous, and the applicant will be expected to interact closely with the clinical faculty and staff. Additional responsibilities will include teaching residents, fellows, and undergraduate students in the Allied Health Science programs. The salary, title and level of appointment will be dependent on academic qualifications and experience.

Interested applicants should submit a current C.V. and the names of three references to:

Lynne Abruzzo, M.D., Ph.D.
The University of Texas M. D. Anderson Cancer Center
Department of Hematopathology
1515 Holcombe, Box 072
Houston, TX. 77030
Fax: 713-745-0736
E-mail: labruzzo@mdanderson.org

THE UNIVERSITY OF TEXAS
MD ANDERSON
CANCER CENTER
Making Cancer History®

M. D. Anderson Cancer Center is an equal opportunity employer and does not discriminate on the basis of race, color, national origin, gender, sexual orientation, age, religion, disability or veteran status except where such distinction is required by law. All positions at The University of Texas M. D. Anderson Cancer Center are security sensitive and subject to examination of criminal history record information. Smoke-free and drug-free environment.

European Science Foundation (ESF)

Position Announcement

Head of Unit/Scientific Secretary of the Standing Committee for Life, Earth and Environmental Sciences (LESC)

ESF is inviting applications for the position of Head of the LESC Unit. The LESC Unit is one of five science Units dealing with the various domains of science in ESF. The European Science Foundation, established in 1974, is an association of 78 member organisations in 30 European countries, located in Strasbourg, France. It is devoted to the coordination, implementation, networking and science policy development in the basic sciences.

Profile and recruitment

The successful candidate should have:

- Proven experience at senior level in the field of the Earth and Life Sciences (encompassing Biology, Biotechnology, Agriculture, Earth Sciences, Climate Research, Glaciology, Oceanography, Meteorology, Environmental Studies): in scientific research (in depth knowledge in a specific domain gained through personal research, plus a broad overview of science in the LESC field), in science policy, and in the management of grants schemes
- Good knowledge of European and international research structures and institutions, in particular in the field of LESC, as well as of national funding organisations
- Proven management experience with strong interpersonal and communications skills, a team work attitude and the ability to work in a multicultural environment
- Excellent spoken and written English. Working knowledge of French and other European languages would be an advantage

Tasks and responsibilities

The Head of Unit reports to the Director of Science and Strategy. The principal tasks include:

- Acting as the Secretary to the Standing Committee for Life, Earth and Environmental Sciences of the ESF
- Developing proposals for new LESC activities, including new science policies, strategic frameworks for the LESC domain, scientific activities and interdisciplinary initiatives with other science domains
- Implementing the policies of LESC within the ESF context
- Responsibility for peer review processes
- Managing the staff and the budget of the LESC Unit
- Membership of the ESF Management Group, including support for strategic ESF activities and management of the interfaces with other ESF Committees
- Liaison with ESF Member Organisations, ESF Committees (ESF Marine Board, European Polar Board, European Space Science Committee), COST Technical Committees and external bodies relevant to the LESC domain

Employment conditions

- The fulltime position is offered for a three year term, with the possibility of a prolongation of two years, preferably starting 1st September 2005.
- The place of work is Strasbourg and the job will involve a significant amount of travel
- The salary level will be based on experience and qualifications of the successful candidate and will follow ESF terms and conditions

Contact persons: Dr John Marks / Dr Martina Hilger-Hildebrandt

For further information about ESF see ***www.esf.org***

Applications by **20 June 2005** to:
ESF, Human Resources Unit, 1 quai Lezay-Marnésia, BP 90015, F-67080 Strasbourg cedex or *jobs@esf.org*

PHYSICIAN OR SCIENCE ADMINISTRATOR
Respiratory Sciences/Genetics
($62,886 to $114,882)

The Department of Health and Human Services and the National Institutes of Health are seeking to hire a person with expertise in molecular and/or population genetics to complement and further develop genetically oriented extramural pulmonary basic and clinical research. The candidate would serve as a member of the Division of Lung Diseases' (DLD) Extramural Program and as a resource to work closely with the National Heart, Lung, and Blood Institute (NHLBI) staff and to develop programs in clinical and molecular genetics.

The DLD's primary focus is on research related to the lungs and its associated diseases and sleep. It supports basic research, clinical and applied studies, including cohort studies, case-control studies and randomized trials. Understanding genetic determinants of susceptibility to diseases can provide new and exciting opportunities to develop strategies to uncover the underlying patho-physiologic process and provide new prevention and treatment opportunities. Expertise in modern genetic approaches is critical to fully elucidating mechanisms underlying complex diseases, such as asthma, chronic obstructive pulmonary disease, pulmonary hypertension, and sarcoidosis. In addition, clinical investigations to dissect how gene variations in conjunction with environmental factors influence or modify clinical phenotypes and outcomes require the combined effects of experts in molecular genetics, genomics, proteomics and clinical medicine. The DLD seeks a scientist with strong genetic/genomic expertise to guide the development of basic and clinical investigations to discover genes important to etiology and progression of lung disease, correlate genotype with phenotype, and identify genetic predictors and markers of subclinical and overt disease. Such an individual would guide the development of new programs focused on deciphering the genetic basis of diseases and linking genes to function. Such an individual would be responsible for the planning, development, direction and coordination of genetically focused basic and clinical research relevant to the DLD. An individual with knowledge of molecular genetics, population genetics, genomics, proteomics and pulmonary diseases would complement a number of activities focused in critical disease areas as well as facilitate charting novel areas in which new information on genetic contribution of diseases will become available.

Selective Factors: Scientific knowledge and research expertise in genetics, molecular genetics/genomics, statistical genetics/genomics, proteomics, population genetics, biology, physiology, or related discipline, with an emphasis on understanding application to human pulmonary disease. U.S. citizenship is required. For the basic qualification requirements, refer to the NIH guidance for Health Scientist Administrators or Medical Officers.
http://www.nhlbi.nih.gov/about/jobs/hsaguide.htm
www.opm.gov/qualifications/SEC-IV/B/GS0600/0602.HTM

Benefits: Appointment will be made at GS-12/13/14 grade level depending on qualifications. A Physician Comparability Allowance may be paid up to $30,000 per year. In addition, a recruitment bonus may also be considered. Excellent health, life, investment, and personal leave benefits.

Position requirements and detailed application procedures are provided in two separate vacancy announcements. Please access **www.usajobs.opm.gov** and refer to **NHLBI-05-69395** for Science Administrators and **NHLBI-05-69399** for Physicians. How to Apply: Submit a resume, c.v./bibliography or other format to: Kathryn Osbourn, Human Resources Specialist, Two Democracy Plaza, Suite 901, 6707 Democracy Blvd., Bethesda, MD 20817-2157. All applications must be postmarked by the closing date **07/15/05**. For additional information contact Kathryn Osbourn at (301) 402-8031.

DHHS and NIH are Equal Opportunity Employers

POSITIONS OPEN

MEDICAL COLLEGE OF WISCONSIN

FACULTY POSITIONS NEUROPHARMACOLOGY Medical College of Wisconsin

The Department of Pharmacology and Toxicology is expanding its program in the area of neuropharmacology. Outstanding candidates in promising and emerging areas of neurobiology are sought. Preference will be given to applicants studying neuronal plasticity or drug abuse using molecular, electrophysiological, morphological, or behavioral approaches. Facilities are modern and include core laboratories for generation of transgenic mice; flow cytometry; electron and confocal microscopy; microarray, peptide/DNA synthesis and analysis, mass spectrometry, electron spin resonance, and functional magnetic resonance imaging. Tenure-track appointments can be made at **ASSISTANT** or **ASSOCIATE PROFESSOR** ranks. Applicants for Assistant Professor must have a doctoral degree in a relevant area and a minimum of two years of postdoctoral experience. They should have a strong record of research accomplishments, be committed to developing an independent, extramurally funded research program, and be willing to participate in graduate and medical teaching. Applicants for Associate Professor are expected to have an established, productive, and NIH-funded research program. Competitive salaries, space, and startup funds are available. Applicants should send curriculum vitae, statement of research interest and plans, three relevant publications, and names of three references to:

Neuropharmacology Search Committee
Department of Pharmacology and Toxicology
Medical College of Wisconsin
8701 Watertown Plank Road
Milwaukee, WI 53226
E-mail: neurosearch@mcw.edu
Website: http://www.mcw.edu/pharm/

The Medical College of Wisconsin is an Equal Opportunity/Affirmative Action Employer.

ASSISTANT PROFESSOR, BIOCHEMISTRY PLANT BIOCHEMICAL GENETICS University of Nebraska-Lincoln

A joint, tenure-track Assistant Professor position is currently available in the Plant Science Initiative and Department of Biochemistry at the University of Nebraska-Lincoln (UNL). The position is 80 percent research and 20 percent teaching. As part of a newly emerging Nutritional Genomics Center, the successful candidate is expected to maintain a vigorous research program focused on biochemical genetics of plants. Research may include plant secondary metabolism, metabolic profiling, nutritional genomics, and genetic regulation of plant metabolism. Teaching responsibilities include teaching one graduate- or undergraduate-level course annually in a relevant area, and mentoring students. A Ph.D. and postdoctoral experience in plant genetics, biochemistry, or related field is required. Salary is commensurate with qualifications and experience. Review of applications will begin June 15, 2005, and continue until the position is filled or the search is closed. Applicants should go to **website: http://employment.unl.edu/** and complete the Faculty/Administrative Information form and then send complete application file, consisting of a statement of research interests, curriculum vitae, and arrange for three letters of recommendation to be sent to: **Search Committee Chair, Assistant Professor Biochemical Genetics, N300 Beadle Center for Genetics Research, University of Nebraska-Lincoln 68588-0660.** We assure reasonable accommodation under the Americans with Disabilities Act. Contact: **Dr. Sally Mackenzie** at **telephone: 402-472-6997** or **e-mail: smackenzie2@unl.edu** for assistance. *UNL is committed to a pluralistic campus community through Affirmative Action and Equal Opportunity and is responsive to the needs of dual career couples.*

Berea College, Biology Department invites applications for a two-year **POSTDOCTORAL TEACHING FELLOWSHIP,** beginning fall 2005. Position designed for recent Ph.D.s or research postdoctoral fellows desiring to gain significant teaching and supervisory classroom experience, teaching laboratory and undergraduate research laboratory, with goal of obtaining a tenure-track appointment at a similar undergraduate liberal arts institution. Department Faculty and Berea College Learning Center Associates will mentor fellows in their teaching. Fellows will also participate in all teaching-learning events, new faculty seminars and workshops, and other professional growth opportunities during the academic year. Teaching responsibilities would include introductory biology (laboratory course; nonmajors), natural science (general education science course; nonmajors), and a special topics course in area of specialty (upper-division; majors). Fellows are eligible to apply for college-supported Undergraduate Research and Creative Projects Grants to fund summer research projects actively involving undergraduate students. Berea College has a rich tradition of teaching excellence in the classroom, the laboratory, and beyond. The College is committed in its mission to provide a quality college education to high ability students of limited economic means, to foster interracial and intercultural education, and to serve the Appalachian region. Interested applicants should send curriculum vitae, graduate and undergraduate academic transcripts, a statement of teaching philosophy, and two letters of recommendation to:

Dr. Dawn J. Anderson
Chair, Department of Biology
Berea College, CPO 1683
Berea, KY 40404

Consideration of applicants will begin Wednesday, 1 June 2005, and will be accepted until the position is filled.

Minority candidates are especially encouraged to apply.

POSTDOCTORAL POSITIONS: Department of Physiology and Functional Genomics University of Florida

Two Postdoctoral positions are available immediately to investigate mechanisms of neural control of cardiovascular functions. One position requires experience in molecular biology, cloning, and viral vector-mediated gene transfer. The second position involves electrophysiological and signal transduction studies and experience in patch clamp electrophysiological recordings from neuronal cells in culture and/or brain slices is required. Ph.D. or equivalent required. An understanding of the physiology of the cardiovascular system is desirable. Full description of both positions is posted at our **website: http://www.med.ufl.edu/phy/raizada.** Send curriculum vitae with names of three references via **e-mail: mraizada@phys.med.ufl.edu** or mail to: **Dr. Mohan K. Raizada, Professor, Physiology and Functional Genomics, University of Florida, P.O. Box 100274, Gainesville, FL 32610.** *Equal Employment Institution.*

RESEARCH ASSISTANT PROFESSOR: Nontenure-track, full-time research faculty position available in the Department of Medicine, Division of Gastroenterology and Hepatology at the University of Alabama at Birmingham (UAB). Applicant should have molecular biology experience with HIV-1 and cytomegalovirus and cellular transport mechanisms. Experience in mucosal immunology, particularly working with dendritic cells, is preferred.

Contact: **Phillip D. Smith, M.D., Division of Gastroenterology and Hepatology, Department of Medicine, University of Alabama at Birmingham, 703 19th Street South, ZRB 633, Birmingham, AL 35294. Fax: 205-934-8493; e-mail: pdsmith@uab.edu.**

Applicants must comply with the Immigration and Control Act. *UAB is an Equal Opportunity/Affirmative Action University.*

USDA ARS Agricultural Research Service
www.ars.usda.gov

POSTDOCTORAL POSITION Molecular Biologist/Microbiologist, GS-11 Starting Salary $50,541

The U.S. Department of Agriculture (USDA), Agricultural Research Service (ARS), National Center for Agricultural Utilization Research (NCAUR), Peoria, Illinois, is seeking a postdoctoral Molecular Biologist/Microbiologist, GS-11 for two years. Extension of the position beyond two years depends upon the availability of future funding. The successful candidate will join a functional genomics laboratory contributing directed enzyme evolution research for enhanced microbial stress tolerance. A recent Ph.D., within the last four years, is required. Applicants should have knowledge and experience in library creation, gene cloning, polymerase chain reaction, and enzyme-linked immunosorbent-based assays. Knowledge in bioinformatics is beneficial. The candidate should be self-motivated and able to work both independently and as a team member. Salary starts at $50,541 and benefits package is available. *Citizenship restrictions apply. For non-U.S. citizens, please refer to* **website: http://www.opm.gov/employ/html/Citizen.htm** *for information on the circumstances under which non-citizens may be employed.* For details and application directions, see **website: http://www.afm.ars.usda.gov/hrd/jobs/index.htm.** Please send applications, including a detailed curriculum vitae and contact information for three references, to: **Dr. Z. Lewis Liu** at **e-mail: liuzl@ncaur.usda.gov** or by mail to: **NCAUR, U.S. Department of Agriculture, 1815 N. University Street, Peoria, IL 61604.** *USDA/ARS is an Equal Opportunity Employer and Provider.*

ASSISTANT/ASSOCIATE PROFESSOR MICROBIOLOGY Job #05-22

Kansas City University of Medicine and Biosciences (KCUMB) has a long history of educational innovation and progressive leadership and invites applicants for the position of Assistant or Associate Professor of microbiology. The successful candidate must have a Ph.D. in microbiology or related discipline and demonstrated record of educational scholarly activities. Experience in teaching fully integrated systems-based curriculum is a plus. Responsibilities will include teaching virology and immunology to medical students and effectively contributing to an innovative curriculum. We are looking for an outstanding educator with exemplary professional characteristics. For additional information contact: **Nehad El-Sawi, Ph.D., Senior Associate Dean, Professor, and Chair, Microbiology** at **telephone: 1-800-234-4847, extension 2210,** or **telephone: 816-283-2210.**

KCUMB is Missouri's largest medical school and strives to hire outstanding faculty and staff to provide an exemplary medical education for approximately 900 osteopathic medical students. Excellent pay is complemented with an exceptional benefits package. We are located in the historic Northeast part of Kansas City, Missouri, near downtown and collaborating institutions.

To apply, send a letter of interest for job #05-22, curriculum vitae, statement of research, teaching goals and philosophies, and contact information for three references to: **Susan M. Schmidt, Assistant Director of Employment Services, 1750 Independence Avenue, Kansas City, MO 64106-1453. Telephone: 1-800-234-4847, extension 2229** or **telephone: 816-283-2229; e-mail: employment@kcumb.edu** (Word or PDF format only please); or **fax: 816-283-2285.** Pre-employment drug screen and background check required. *Must be authorized to work in the United States.* **Website: http://www.kcumb.edu.** KCUMB is committed to being a key stakeholder and integral part of the Kansas City Area Life Sciences Institute. **Website: http://www.kclifesciences.org.**

Equal Opportunity Employer.

POSITIONS OPEN

RESEARCH ASSOCIATE PROFESSOR, Nontenured–Department of Biology, Temple University anticipates an opening in the Biology Department for a nontenured faculty position at the level of Research Associate Professor to carry out research in the areas of cancer biology, obesity, and novel therapeutics development in the Center for Biotechnology of the College of Science and Technology. This position is not tenure track, but may be renewable for terms up to five years, dependent upon available funding. The requirements for this position are at least 10 years experience as an independent investigator in the relevant research area with at least 20 publications as a senior author, proven record of mentoring postdoctoral fellows and graduate students, evidence of external funding from federal agencies and other sources, national and international recognition of expertise documented by service as grant evaluator, project consultant, and conference leader. Candidates should send resume, letter of interest, three letters of recommendation, and transcript of highest academic degree to: **Dr. Antonio Giordano, Center for Biotechnology, Biology Department, Attn: Faculty Search, Temple University, 1900 N. 12th Street, Biology Life Sciences Building, Philadelphia, PA 19122.** *Applications from women and underrepresented minorities are especially encouraged. Temple University is an Affirmative Action Employer.*

NEUROSCIENCE INSTITUTE
Department of Neurosciences
College of Medicine
Medical University of South Carolina

The Medical University of South Carolina (MUSC) has implemented a strategic plan to expand areas of research and medical education. Competitive startup support, laboratory space, and salary are offered. The Department of Neurosciences invites applications and nominations for the Josephine Tucker Morse Endowed Professorship in Neuropathology. The Morse Professorship is a tenured appointment at the **ASSOCIATE** or **FULL PROFESSOR** level. Applicants must have earned a medical degree in neuropathology and be a recognized leader in the area of neuroscience research. We are seeking applicants who have active research programs in the areas of neurological diseases including Alzheimer's disease, Parkinson's disease, stroke, and/or other neurological disorders. The successful candidate is expected to be externally funded and to establish a strong basic science and/or clinical research program. **Websites: http://neurosciences.musc.edu** and **http://www.musc.edu/neuroscienceinstitute/.**

Applicants should apply online at **website: http://www.musc.edu/hrm/careers/faculty.htm.** Position requisition number is 041546. Applicants should also attach online a cover letter expressing their interest and qualifications along with curriculum vitae and three references addressed to: **Mark S. Kindy, Ph.D., Chair, Search Committee, Neuroscience Institute, Department of Neurosciences, Medical University of South Carolina, 173 Ashley Avenue, BSB 403, Charleston, SC 29425.**

MUSC is an Equal Employment Opportunity/Affirmative Action Employer.

SENIOR SCIENTIST with experience in research on kidney disease progression and tubular atrophy. Send resumes to: **Jeffrey H. Miner, Ph.D., Renal Division, Department of Internal Medical, Washington University School of Medicine, Campus Box 8126, 660 S. Euclid Avenue, St. Louis, MO 63110.** Must reference job code 051160.

POSITIONS OPEN

ASSISTANT OR ASSOCIATE PROFESSOR PATHOLOGY
Ohio University College of Osteopathic Medicine
Biomedical Sciences
Athens, Ohio

College of Osteopathic Medicine invites applications for a tenure-track Assistant or Associate Professor of pathology who will teach pathology in the medical curriculum, supervise graduate students, and maintain an active, externally funded research program. Clinical activities are possible but not a requirement for this faculty appointment. Area of research is open, but candidates who study the pathology of disease and who may interact with diabetes research initiatives at Ohio University are encouraged.

Ohio University, with 20,000 students, is located in a picturesque college town in the rolling foothills of the Appalachian Mountains in rural southeastern Ohio where costs of living are moderate.

A Ph.D. (or equivalent), M.D., or D.O. is required. Salary will be commensurate with experience. Submit a statement of career interests, curriculum vitae, and three letters of recommendation to: **Kenneth J. Goodrum, Ph.D., Biomedical Sciences, 228 Irvine Hall, Ohio University, Athens, OH 45701-2979. E-mail: goodrum@ohio.edu.** Position is available as soon as August 1, 2005. Applications will be reviewed on June 15, 2005; will be accepted until the position is filled. **Website: http://www.ohio.edu/dual.** *Ohio University is an Affirmative Action/Equal Opportunity Employer with a Dual Career Network.*

The Center for Biotechnology of the University of Nebraska-Lincoln (UNL) seeks a **MANAGER** for its Bioinformatics Core Research Facility. The Facility cooperates with the UNL faculty to develop and exploit state-of-the-art bioinformatic tools, e.g., molecular modeling, mining genomic, and proteomic databases, as well as microarray and complex systems data. The Manager will support life sciences research and act as a liaison among UNL computational biology groups in the State to foster bioinformatics program development. Excellent computer laboratory facilities will be available for conducting collaborative extramurally funded research. The manager also has primary responsibility for team-teaching a senior undergraduate/graduate-level laboratory course in bioinformatics and for training and service of existing UNL licensed software including VectorNTI, GCG (SeqLab), Affymetrix software. The manager is also expected to share system administration of the Facility's Linux cluster with an existing staff. A doctoral degree and demonstrated expertise in computational biology and sound, practical knowledge and experience in molecular biology and genomics research, is required. Background in computer science is desirable. We offer a competitive salary plus excellent benefits. Review of applications will begin May 20, 2005. Position will remain open until suitable candidate is found. Complete the faculty/administrative form at the **website: http://employment.unl.edu** then submit curriculum vitae and the names and addresses of three references to: **Search Committee Chair, Bioinformatics Specialist, Center for Biotechnology, University of Nebraska-Lincoln, 1901 Vine Street, Lincoln, NE 68588-0665. Fax: 402-472-3139.**

We assure reasonable accommodation under the Americans with Disabilities Act; contact the Center for Biotechnology at **telephone: 402-472-2635** for assistance. *The University of Nebraska is committed to a pluralistic, campus community through Affirmative Action and Equal Opportunity.*

POSITIONS OPEN

DEPARTMENT OF HEALTH AND HUMAN SERVICES
NATIONAL INSTITUTES OF HEALTH

National Institute of Allergy and Infectious Diseases Experimental Molecular Mechanism in B Cell Development and Lymphomagenesis **POSTDOCTORAL RESEARCH POSITIONS.**

Postdoctoral positions are available with the Laboratory of Immunopathology (LIP), National Institute of Allergy and Infectious Diseases, National Institutes of Health located in Rockville, Maryland. The NIAID is a major research component of the NIH and the Department of Health and Human Services (DHHS).

The LIP is seeking candidates with a Ph.D. or M.D. degree and less than five years postdoctoral experience to study molecular mechanisms of B cell development and lymphomagenesis. A strong background in cellular immunology and molecular biology is required. Applicants with skills in microarray and computational genomics are encouraged to apply. Salary is commensurate with research experience, starting at $38,500 per year. Health benefits are available through NIH.

Please apply electronically by sending letter of interest, curriculum vitae, and names of three references to **e-mail: hmorse@niaid.nih.gov.**

DHHS and NIH are Equal Opportunity Employers.

POSTDOCTORAL POSITION

Postdoctoral position in molecular immunology available immediately to study the immunobiology of gamma/delta T cells during normal homeostasis and during responses against mucosal pathogens using molecular immunological approaches, including global analyses of gene expression. The successful candidate will join a research group of more than 12 research personnel in a new research facility, supported by state-of-the-art flow cytometry, confocal microscopy, and genomics core laboratories, and funded by the NIH, U.S. Department of Agriculture, and U.S. Department of Defense. Required qualifications: (1) Ph.D. in a biomedical discipline, (2) proven ability to design appropriate experiments, and (3) demonstrated ability to work independently and collaboratively. Preferred qualifications: (1) cellular immunology experience, (2) molecular biology experience, (3) infectious disease research experience, and (4) record of excellence as a supervisor. The successful candidate will possess effective communication and writing skills. Salary is competitive and commensurate with experience and training. To apply, send a letter of application and curriculum vitae, and have three letters of reference sent to:

Dr. Mark Jutila, Professor
Veterinary Molecular Biology
Montana State University
Bozeman, MT 59717-3610
Fax: 406-994-4303
E-mail: uvsmj@montana.edu

ADA/Affirmative Action/Equal Opportunity/Veteran's Preference.

POSTDOCTORAL FELLOW

A Postdoctoral position is immediately available for cutting-edge research into genetic mechanisms for cognitive behaviors. The candidate should have a recent Ph.D. or M.D./Ph.D. with experience in one or more of the following disciplines: mouse behaviors, electrophysiology, and molecular biology. *U.S. citizenship or permanent residency is required.* Interested candidates should send curriculum vitae and names of three references (postal and e-mail addresses and telephone numbers) to: **Ya-Ping Tang** at **e-mail: yptang@bsd.uchicago.edu.**

The University of Chicago is an Affirmative Action/Equal Opportunity Employer.

POSITIONS OPEN

POSTDOCTORAL POSITION: Yale University School of Medicine. Seeking a highly motivated Ph.D. or M.D. to study the mechanisms used by the hypothalamus to sense and activate counterregulatory hormone responses during hypoglycemia using a variety of approaches, including: in vivo microinjection, microdialysis, short interfering RNA transfection, as well as basic molecular techniques. Applicants should send a cover letter, their curriculum vitae, and three letters of reference to:

Robert S. Sherwin, M.D.
Yale School of Medicine
Section of Endocrinology
Department of Internal Medicine
P.O. Box 208020
New Haven, CT 06520-8020

Yale University is an Affirmative Action/Equal Opportunity Employer.

Applications from qualified women and members of minority groups are encouraged.

POSTDOCTORAL POSITION
Harvard Medical School

Exciting research on the structure, function, cell biology, and in vivo function of integrins and IgSF adhesion molecules in the context of inflammation, vascular injury, and autoimmunity. The structural basis of integrin activation is studied using a multidisciplinary approach including mouse genetics, biochemistry, molecular and cellular biology, and structural biology. We are particularly interested in candidates in the following two NIH-funded projects: (1) conformational regulation of integrins in vivo, studied by generation of conditional knock-in mice in which conformational signal transmission is manipulated and (2) development of novel integrin anti-inflammatory antagonists through a structure-oriented approach. Candidates with prior experience in gene targeting, mouse disease models, and/or biochemistry are especially encouraged to apply to:

Motomu Shimaoka, M.D., Ph.D.
Assistant Professor
The CBR Institute for Biomedical Research
Harvard Medical School
Boston, MA 02115
E-mail: shimaoka@cbrinstitute.org

See **website: http://cbrinstitute.org/** for further information.

POSTDOCTORAL POSITION

A Postdoctoral position is available to investigate *Staphylococcus aureus* in the population and the environment to better understand the spread of this pathogen between humans and their surroundings. The focus of the laboratory is on understanding the mechanism of bacterial survival and spread at the molecular level. Qualified applicants will have a doctoral degree in microbiology, molecular biology, or a related field preferably with experience in bacterial strain typing and statistics. The opportunity to teach undergraduates exists. Send curriculum vitae and three letters of recommendation to: **Dr. Tammy Domanski, Chemistry Department, United States Naval Academy, 572 Holloway Road, Annapolis, MD 21402. Mailstop 9B. E-mail: domanski@usna.edu.** *U.S. citizenship, green card, or H1-B visa is required. The Naval Academy is an Equal Opportunity Employer and makes reasonable accommodations to individuals with disabilities.*

POSTDOCTORAL/RESEARCH ASSOCIATE
MOLECULAR NEUROSCIENCE

Study transcriptional regulation of neurotransmitter gene expression triggered by stress, nicotine, and estrogens. Ph.D. with experience in molecular biology, quantitative polymerase chain reaction, and microarrays desirable. Competitive salary and benefits. **Dr. Esther Sabban, Department of Biochemistry and Molecular Biology, New York Medical College, Valhalla, NY 10595. E-mail: sabban@nymc.edu.** *Equal Opportunity Employer.*

POSITIONS OPEN

EMORY SCHOOL OF MEDICINE

NEUROSCIENCE FACULTY POSITION

Applications are invited for a faculty position in the Department of Physiology of Emory University. The rank of the position is open. We seek an outstanding investigator to join a strong and established group devoted to basic sensorimotor research with an emphasis on the spinal cord. Research areas of interest include those at the developmental, molecular, cellular, and systems levels and will complement research of the existing faculty. We are particularly interested in candidates who can bridge these levels of analysis.

Extensive collaborative opportunities exist within the Department and the Emory neuroscience community. The successful candidate will be expected to establish an independent research program and participate in the scholarly activities of the neuroscience community.

Interested candidates may submit curriculum vitae, a statement of research and teaching interests, and a list of three to five references to: **Dr. T. Richard Nichols, Department of Physiology, Emory University, Atlanta, GA 30322.** The review of applications will continue until the position is filled. *Emory University is an Equal Opportunity/Affirmative Action Employer and Recruiter. Women and minority candidates are encouraged to apply.*

SYSTEMS and **INTEGRATIVE NEUROSCIENTIST.** The Department of Biomedical Sciences at Colorado State University (**website: http://www.cvmbs.colostate.edu/bms/**) seeks a Systems and Integrative Neuroscientist to be hired at the **ASSOCIATE PROFESSOR/PROFESSOR** level. Candidates should have a vigorous, extramurally funded research program and will be expected to teach in undergraduate, graduate, or professional veterinary programs. Applicants must have a Ph.D., D.V.M., M.D., or equivalent. A letter of application, curriculum vitae, and names of three references should be sent electronically or by post to: **Robert J. Handa, Ph.D., Department of Biomedical Sciences, College of Veterinary Medicine and Biomedical Sciences, Colorado State University, Fort Collins, CO 80523 (e-mail: robert.handa@colostate.edu).** Review of applications will begin July 1, 2005. *Colorado State University is an Equal Employment Opportunity/Affirmative Action Employer.*

NIH-funded **POSTDOCTORAL POSITION (RESEARCH ASSOCIATE)** Job #32798, available at the Liver Research Institute of The University of Arizona College of Medicine for a recent graduate (M.D. or Ph.D.) interested in basic research on topics related to the prevention of toxic liver injury. Strong experience in molecular biology, protein-protein and protein-DNA interactions, or in the biochemical purification of proteins is desirable. Salary is negotiable. For further detail or to apply for this position go to **website: http://www.hr.arizona.edu.** Questions may be asked by **e-mail: rwhalen@u.arizona.edu.** Review of materials begins June 1, 2005, and will continue until position is filled. *The University of Arizona is an Equal Opportunity/Affirmative Action Employer, Minorities, Women, Veterans, Persons with Disabilities.*

Energetic and self-driven **POSTDOCTORAL FELLOWS** are invited to join an exciting laboratory with the following three active research areas: (1) Ty1 transcriptional silencing of *S. cerevisiae* (*Genes Dev.* **16:**467–78, 2002); (2) slow DNA-induced filamentous growth of *S. cerevisiae* (*Mol. Biol. Cell* **14:**5116–24, 2003); (3) novel peptide antibiotics.

Interested persons may send curriculum vitae and three letters of recommendation to: **Yiwei Jiang, Department of Medical Biochemistry and Genetics, Texas A&M University System Health Science Center, 1114 TAMU, College Station, TX 77843-1114. Telephone: 979-845-5058; e-mail: ywjiang@medicine.tamhsc.edu.** *Affirmative Action/Equal Opportunity Employer.*

POSITIONS OPEN

VCU

POSTDOCTORAL POSITION
Department of Biochemistry
Virginia Commonwealth University
School of Medicine

A Postdoctoral position is available in the laboratory of **Dr. Paul Dent,** Massey Cancer Center, Virginia Commonwealth University, Richmond, Virginia, U.S.A. The project involves the use of novel therapeutic agents in cells to manipulate signal transduction pathways and cell survival. The applicant must have a strong work ethic and background in biochemistry and molecular biology and be able to interact with individuals in the laboratory of **Dr. Steven Grant.** Experience in the culture of mammalian cells and in the assessment of cell death is required. Please contact: **Dr. Dent** at **e-mail: pdent@hsc.vcu.edu** with curriculum vitae and the names and addresses of three references. *Virginia Commonwealth University is an Equal Opportunity Employer.*

POSTDOCTORAL POSITIONS

Postdoctoral positions are available to study the mechanisms of DNA damage signal transduction by oxidants (*Am. J. Physiol. Lung Cell Mol. Physiol.* **286:**L87–L97, 2004). Requires Ph.D. in molecular biology, or other related disciplines. Preference will be given to candidates who have demonstrated expertise in biochemistry and molecular biology skills as evidenced by peer-reviewed publications. We offer excellent benefits and competitive salary based on the experience of the candidates. Little Rock is a scenic place situated in the heart of Arkansas. The University of Arkansas for Medical Sciences (UAMS) is the premier medical center and offers a vibrant scientific community (**website: http://www.uams.edu**). Send curriculum vitae, publication record, and names of three references to: **Kumuda C. Das, Ph.D., Associate Professor, Department of Pathology, University of Arkansas for Medical Sciences, 4301 W. Markham Street #845, Little Rock, AR 72205. E-mail: kdas@uams.edu.**

UAMS is an Equal Opportunity Employer, promoting workplace diversity.

SENIOR POSTDOCTORAL ASSOCIATE
University of Southern California

Senior Postdoctoral position available for molecular research on adipogenic transcriptional regulation of hepatic stellate cell differentiation or iron-mediated signaling for NF-kB activation in macrophages. Applicants are required to: (1) *be U.S. citizens or permanent residents* and (2) have completed two to four years of postdoctoral training in cell and molecular research. The position is to be filled between June and August 2005. Send curriculum vitae and names of three references by **e-mail: htsukamo@usc.edu** or mail to: **Professor Hide Tsukamoto, Department of Pathology, Keck School of Medicine of the University of Southern California, 1333 San Pablo Street, MMR 4th Floor, Los Angeles, CA 90033-9141.** *An Equal Opportunity/Affirmative Action Employer.*

POSTDOCTORAL FELLOW: Patch-Slice Electrophysiology. Position available for electrophysiologist with experience in patch-slice recording to join multidisciplinary research group studying molecular bases of spinal cord and nerve injury. Expertise in patch clamp recording, with experience in slice preparations, is essential. Prior work on spinal cord injury and pain is desirable. Excellent opportunity to collaborate with highly productive, multidisciplinary team. Send curriculum vitae, statement of interest, and three letters of reference to: **Bryan Hains, Ph.D., Neuroscience and Regeneration Research Center, VA Connecticut Healthcare, 950 Campbell Avenue, West Haven, CT 06516.** *Women and members of underrepresented minority groups are encouraged to apply. Affirmative Action/Equal Opportunity Employer.*

2005 BUCK INSTITUTE SYMPOSIUM ON AGING

Pharmacology of Lifespan

Thursday–Saturday, October 6–8, 2005

Sessions

- Targets for Interventions in Aging 1—Regulatory mechanisms
- Targets for Interventions in Aging 2—Endocrine targets
- Developing Screens for Anti-Aging Compounds
- Pharmacology and Criteria for Success
- Applications—Aging and Age-related Disease
- Regulatory affairs

Sponsored by
Larry L. Hillblom FOUNDATION

Scientific Program Focus

The Buck Symposium on the *Pharmacology of Lifespan* will bring together investigators from diverse backgrounds to address the current status of the pharmacology of aging and tackle the challenges associated with the discovery of compounds that slow aging.

As genetic interventions have resulted in spectacular progress in our understanding of the aging process, now pharmacological interventions promise to advance it further. The Buck Symposium will focus on targets for interventions in aging, developing screens for anti-aging compounds, applied drug discovery and the criteria for successful pharmacological interventions.

Speakers include

Elizabeth Blackburn, PhD	University of California, San Francisco
Ashley Bush, MD, PhD	University of Melbourne, Australia
Catherine Clarke, PhD	University of California, Los Angeles
Peter S. DiStefano, PhD	Elixir Pharmaceuticals
Monica Driscoll, PhD	University of New Jersey
Laura Dugan, MD	University of California, San Diego
Robert Floyd, PhD	University of Oklahoma
Matthew Gill, PhD	Buck Institute for Age Research
Francine Grodstein, ScD	Harvard Medical School
R. Kiplin Guy, PhD	University of California, San Francisco
Franz Hefti, PhD	Rinat Neuroscience
Robert Hughes, PhD	Buck Institute for Age Research
Donald Ingram, PhD	National Institutes of Health
Thomas Johnson, PhD	University of Colorado at Boulder
Kevin Kregel, PhD	University of Iowa
Richard Miller, MD, PhD	University of Michigan
Nancy Nadon, PhD	National Institute on Aging
Stephen Spindler, PhD	University of California, Riverside
Phyllis Wise, PhD	University of California, Davis
Catherine Wolkow, PhD	National Institutes of Health

Buck Institute Organizers:

Gordon Lithgow, PhD
Simon Melov, PhD
Dale Bredesen, MD

For further information and registration, visit our website at **www.buckinstitute.org**, click on **events**, or contact

symposium@buckinstitute.org

Buck Institute for Age Research

8001 Redwood Blvd.
Novato, CA 94945

"Brilliantly insightful*" new books from Yale

New in paper

Red Sky at Morning

America and the Crisis of the Global Environment

James Gustave Speth

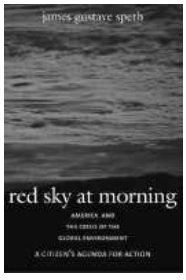

With a new Afterword on climate change

"Brilliantly insightful and extraordinarily useful." —Thomas F. Malone, *American Scientist* *

"The ultimate insider offers **a devastating critique of global environmental efforts."** —*Time*

$16.00 A Yale Nota Bene **paperback**

Climate Change and Biodiversity

Edited by Thomas E. Lovejoy and Lee Hannah

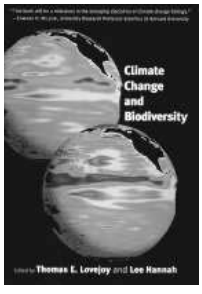

"A milestone in the emerging discipline of climate change biology. No issue is more important for the global environment; the impressive line-up of experts here gives it definitive coverage."—Edward O. Wilson

107 b/w + 11 color illus. $65.00

Forests in Time

The Environmental Consequences of 1,000 Years of Change in New England

Edited by David R. Foster and John D. Aber

"An important and timely addition to a growing literature that documents change and, by implication, underlines our responsibilities to that thing out there that we call 'nature.'" —Michael Williams, *Science*

202 illus. $45.00

Before Darwin

Reconciling God and Nature

Keith Thomson

"A **lively** and detailed account of the two centuries of vigorous arguments about science and religion that preceded the publication of Darwin's ideas in 1859. This account is one that anyone interested in the controversy of natural theology will wish to read." —John Polkinghorne

33 illus. $27.00

How the Earthquake Bird Got Its Name and Other Tales of an Unbalanced Nature

H.H. Shugart

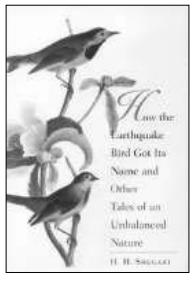

"Shugart enlightens by entertaining, in the hope that we become inspired to become better caretakers of our small, blue marble."—Susan Dworski, *Los Angeles Times*

48 illus. $27.50

Disconnected Rivers

Linking Rivers to Landscapes

Ellen Wohl

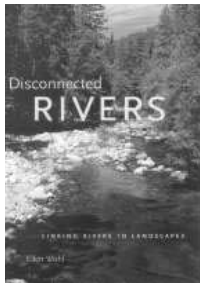

"Wolf explains the rivers of the U.S. as they were and as they have become. . . . **The story is beautifully told**, with diversions into the life stories of river creatures from the alligator to the salamander." —Martin Ince, *New Scientist*

131 illus. $35.00

Doctor Dolittle's Delusion

Animals and the Uniqueness of Human Language

Stephen R. Anderson

With illustrations by Amanda Patrick

"A masterly overview of what is currently known about the communication abilities of a wide range of creatures . . . [that also] outlines what is special about human language. . . . [An] elegant book."—Neil Smith, *Nature*

Winner of the 2004 Professional/Scholarly Publishing Division Annual Award Competition in the Psychology category.

68 halftones & line drawings $35.00

First in Line

Tracing Our Ape Ancestry

Tom Gundling

"Gundling places the history of an important paleoanthropological thread within a straightforward and well-articulated framework. His book is **an original work of sound scholarship."**—Ian Tattersall

12 line illus. + 4 tables $25.00

New in paper

Wider Than the Sky

The Phenomenal Gift of Consciousness

Gerald M. Edelman, M.D., PH.D.

From the Nobel Prize-winning neuroscientist, **"[an] elegant . . . laudable, [and] accessible exploration** of what's happening in neuroscience, biochemistry, and other disciplines."—*San Diego Union-Tribune*

$15.00 A Yale Nota Bene **paperback**

New in paper

Consciousness

A User's Guide

Adam Zeman

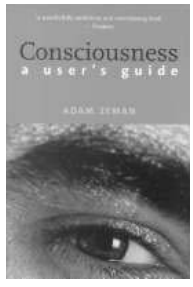

"An articulate . . . neurologist . . . covers many aspects of consciousness for general readers. His treatment of the disorders of knowledge is superb. If you were intrigued with *The Man Who Mistook His Wife for a Hat*, you'll appreciate [the book's] buildup to what Oliver Sacks described in that work. . . . **Approachable and instructive."** —William H. Calvin, *New York Times Book Review*

75 figures $18.00 **paperback**

50 Signs of Mental Illness

A Guide to Understanding Mental Health

James Whitney Hicks, M.D.

"A smart, alphabetically arranged layperson's guide to common symptoms. . . . Fascinating observations abound."—Gregory Mott, *Washington Post Book World*

Yale University Press Health & Wellness $27.50

A Field Guide to North Atlantic Wildlife

Marine Mammals, Seabirds, Fish, and Other Sea Life

Noble S. Proctor and Patrick J. Lynch

"The depth and detail found in this guide is equaled only by the richness of the environment that is its focus. **Don't leave shore without it."**—Pete Dunne

299 maps + color illus. $19.95 **paperback**

Yale University Press yalebooks.com